STRAN S POPRAVKI / ERRATA

Stran z napako	Vrstica z napako	Namesto	Naj bo
Page	Line	Error	Correction

“Blank page.”

BIBLIOGRAPHIC-DOCUMENTALISTIC INFORMATION AND ABSTRACT

UDC: 622.515:624.136.6:531.755(043)
Author: Mateja Klun
Supervisor: Assist. Prof. Andrej Kryžanowski, Ph.D.
Co-Supervisor: Prof. Dejan Zupan, Ph.D.
Title: Analysis of Concrete Gravity Dam Conditions using State-of-the-art Experimental and Numerical Methods
Notes: 159 p., 58 fig., 16 tab., 32 eq.
Keywords: measurements, concrete dam, laser Doppler vibrometry, safety, vibration, structural health monitoring

Abstract:

With monitoring of dynamic properties of dams we can continuously observe the ageing process of the structure, while by vibration monitoring we can estimate the condition of the built-in material. Every structure has unique modal characteristics and its unique vibrational signature that change only in case when the structure's mass, stiffness, or geometry is altered. Therefore, if the structural damage causes a decrease in stiffness, the vibration patterns as well as modal properties of the structure will change. Dams represent an important infrastructure and the ageing of dams and preservation of their structural health is rapidly becoming one of the major challenges of the entire dam engineering community. This research focuses on the analysis of operational loads and their effect on the ageing process of a hydropower dam. Shortly after the construction of the Brežice dam and during the start-up tests of hydro-mechanical equipment, we performed vibration monitoring, using state-of-the-art non-contact measurement techniques in combination with traditional contact technologies. The thesis is divided into two parts. In the first part, the motivation and fundamentals of structural health monitoring, vibration based monitoring, dam surveillance, and Laser Doppler Vibrometry (LDV) are presented, followed by the review of peer literature. Experimental work lies at the core of this research. In the second part of the thesis we present the experimental site, the equipment, the procedure and the numerical models of the powerhouse and its overspilling section. Our research confirmed the susceptibility of the concrete dam structure to the effect of operational loads, which is supported also with numerical results in experimental findings. With the beginning of our work during the construction of the dam we were able to capture the initial reference state of the dam, which will serve as a baseline for future diagnostic work. Furthermore, by adopting a corrective procedure of the LDV output, we are now able to use the LDV during regular operation of the powerhouse, when the instrument is placed inside the structure under observation and excited as well. LDV can be used as part of regular vibration monitoring activities on dams during operation.

"Blank page."

BIBLIOGRAFSKO-DOKUMENTACIJSKA STRAN IN IZVLEČEK

UDK:	622.515:624.136.6:531.755(043)
Avtor:	Mateja Klun
Mentor:	doc. dr. Andrej Kryžanowski
Somentor:	prof. dr. Dejan Zupan
Naslov:	Analiza kondicijskega stanja betonskih težnostnih pregrad z uporabo sodobnih eksperimentalnih in numeričnih metod
Obseg in oprema:	159 str., 58 sl., 16 pregl., 32 en.
Ključne besede:	meritve, pregrada, vibrometrija, nekontaktne metode, spremljanje kondicijskega stanja, varnost, vibracije

Izvleček:

S spremljanjem dinamičnih lastnosti konstrukcije lahko opazujemo tudi proces staranja objekta, saj lahko preko spremljanja vibracij sklepamo na stanje vgrajenega materiala. Vsak objekt ima zanj značilne modalne lastnosti, ki so posledica njegove zasnove in togosti ter se odražajo v načinu, kako se objekt odzove na mehansko vzbujanje. Če se torej zaradi staranja vgrajenega materiala spremeni njegova togost, se bo posledično spremenil tudi odziv konstrukcije in njegove modalne lastnosti. Staranje pregrad trenutno predstavlja enega glavnih izzivov pregradnega inženirstva. S to raziskavo smo se osredotočili na prepoznavanje in analizo obratovalnih obtežb na konstrukcijo pregrade pretočnega tipa, namenjene za proizvodnjo energije. Stalno prisotna obtežba, ki jo povzroča hidro-mehanska oprema, namreč vpliva na pospešeno staranje betonskih konstrukcij. V okviru raziskave smo izvajali meritve vibracij na pregradi Brežice. Z eksperimentom smo pričeli že v času gradnje. Prvi odziv konstrukcije smo zabeležili kmalu po zaključku glavnine konstrukcijskih del, takrat smo izmerili odziv mlade konstrukcije in zabeležili t. i. referenčno stanje, ki predstavlja osnovo za vse nadaljnje spremljanje kondicijskega stanja objekta. Pri meritvah smo uporabljali sodobne nekontaktne metode kot tudi tradicionalne kontaktne merilne tehnike. Naloga je razdeljena v dva dela. V prvem delu predstavimo teoretično ozadje spremljanja kondicijskega stanja konstrukcij, meritve vibracij, opazovanja pregrad in laserske vibrometrije. Eksperimentalno delo predstavlja bistvo te naloge. V drugem delu predstavimo eksperiment, opremo, metode dela in izdelana numerična modela. Obratovalna obtežba ima vpliv na pregrado. Vpliv obratovalnih manevrov smo z meritvami med zagonskimi testi zaznali na vseh eksperimentalnih mestih. Precejšnji del naše pozornosti smo usmerili v uporabo laserske vibrometrije v tako zahtevnem okolju, kot je hidroelektrarna med rednim obratovanjem. Vpeljali smo metodologijo, kjer z izvedbo dodatnih meritev na optični merilni napravi izločimo napako zaradi gibanja stojišča, kar omogoča uporabo vibrometra znotraj elektrarne med njenim rednim obratovanjem.

ABBREVIATIONS/ OKRAJŠAVE

ICOLD	International commission on large dams
SLOCOLD	Slovenski nacionalni komite za velike pregrade
HPP	hydropower plant
LDV	laser Doppler vibrometry
FVT	forced vibration test
AVT	ambient vibration test
NDE	non-destructive evaluation
SHM	structural health monitoring
RC	reinforced concrete
MAC	modal assurance criterion
COMAC	coordinate modal assurance criterion
FRF	frequency response function
FEM	finite element model
HST	hydrostatic-season-time
HTT	hydrostatic-temperature-time
RSM	response surface method
LDA	laser Doppler anemometry
RMS	root mean square
PG	concrete gravity dam
TE	earthfill embankment
ER	rockfill embankment
AAR	alkali-aggregate reaction
FIB	International federation on structural concrete
LNEC	Laboratório nacional de Engenharia Civil
USBR	US Bureau of Reclamation
ACI	American Concrete Institute
DAQ	data acquisition
DC	direct current
AC	alternating current
IIR	infinite impulse response
FFT	Fast Fourier transform
EM	electro magnetic
HEA, IPE	type of steel profiles
FSI	fluid-structure-interaction
LF	lastna frekvenca (eigenfrequency)

GCIS	Gornji Cirnik station
BNC, PVC	type of plug-in connector

“Blank page.”

ZAHVALA

Zahvaljujem se družbi Hidroelektrarne na Spodnji Savi, d.o.o., ki je dovolila izvajanje eksperimentalnega dela in uporabo njihovih podatkov za to raziskavo. Zahvala gre ekipi, ki je izvajala zagonske teste na HE Brežice in me je prijazno vključila v svoj delovni proces. Hvala Matjažu Hauptmanu, vodji testov, ki je imel izjemen posluh za moje delo. Zahvaljujem se gospodu Branku Belingarju za pomoč pri iskanju vzroka za šum v meritvah ter za vse nasvete.

Posebna zahvala gre dr. Alešu Bardorferju, ki mi je v številnih razpravah in s svojim izjemnim znanjem o signalih in merilni tehniki pomagal pregristi se prek izzivov in najti pot do konca.

Iskreno se zahvaljujem družini, za vso podporo in razumevanje. Zahvaljujem se prijateljem, ki v tem času niso pozabili name, me podpirali in razumeli. Hvala vam tudi za vso posojeno opremo; brez nje bi bil eksperiment zelo okrnjen. Hvaležna sem za vse prijetne trenutke z vami in hvala, da ste mi pomagali skozi temačne dneve, ko se mi je zdelo, da se svet podira name. Hvala tebi Aleš, v svojem prostem času si z menoj obiskal več pregrad, kot bi jih kadar koli bilo treba videti povprečnemu Zemljanu.

Hvaležna sem za možnost sodelovanja v tehničnem komiteju za numerične analize pregrad. Hvala Franciscu Lopezu in Loiuisu Hattinghu, ki sta kljub svojemu natrpanemu urniku z zanimanjem spremljala moj napredek in mi vedno znova postavljala zanimiva in kritična vprašanja. Vajino znanje, izkušnje in veselje do pregrad so mi vedno znova v navdih.

Hvala sodelavcem, še posebej Klaudiji Sapač, s katero sva skupaj vstopili na raziskovalno pot. Zahvaljujem se doc. dr. Lopatiču za njegovo sodelovanje pri 3. fazi meritev. Hvala tudi Mojci Vilfan za vse jezikovne popravke, ki so vedno servirani s prijaznim nasmehom.

Zahvala gre tudi Javni agenciji za raziskovalno dejavnost RS, ki je financirala podiplomski študij, ter prof. dr. Mikošu, ki mi je z mestom mlade raziskovalke tega tudi omogočil. To delo je nastajalo pod vodstvom mentorjev, za kar se jima zahvaljujem.

Hvala vsem učiteljem in sošolcem v tisti drugi šoli.

"Blank page."

KAZALO VSEBINE

"Blank page."

KAZALO SLIK

“Blank page.”

KAZALO PREGLEDNIC

"Blank page."

LIST OF FIGURES

LIST OF TABLES

1 INTRODUCTION

When we get ill, it seems completely normal for us to visit a doctor. We are all aware that care for our health is very important, and it is better to prevent than to cure. At the doctor's everyone has their own medical chart where our health history is noted from our first visit to the doctor until our last. The idea that mechanical equipment and appliances need regular maintenance is close to us, we complain about taking the car to the mechanic every year but we still do it. However, large structures or large infrastructure objects are generally considered that they are there built to last forever, while their properties are supposed to remain time-invariant. We tend to forget that large civil engineering structures also need regular maintenance and inspection and that also those structures are subjected to ageing and fatigue even if they seem to be standing still, like there is nothing "disturbing their peace". It is true that some can get very old, e.g. the Great Pyramid of Giza in Egypt was built some 4,500 years ago, but also those are slowly deteriorating over time. As large infrastructures have a great and broad impact on the environment, it is crucial to maintain them in good health, since failure, decommissioning, and out-of-service time have a broad impact and severe consequences. And as we all know, it is better to prevent than to cure. An analogy with medical work can be expanded even further. Doctors use specialised equipment to monitor patients' health and when alarming symptoms are recorded, treatment and if necessary additional tests are prescribed, while symptoms, illness, and treatment procedure are recorded in the patient's chart. A similar approach can be adopted to structures (Aktan et al., 2000).

According to the definition by the International Committee on Large Dams (ICOLD), a large dam is any dam with a structural height of 15 m or more. For the dams with a retaining capacity, this criterion is even stricter, i.e. every dam with a structural height of at least 5 m and a minimum capacity of the reservoir of 3 hm^3 is considered a large dam. There are 42 large dams in Slovenia that fulfil the ICOLD criteria. According to the data from the register of large dams, obtained from Slovenian National Committee on Large Dams (SLOCOLD), most of the large dams were built before 1990. The mean age of all large dams in Slovenia is approximately 43 years, while the mean age with respect to dam type is 32 for embankments and 50 years for concrete dams (VODPREG, 2012). In addition, in our streams, we have over 9,588 small dams, dykes, and other water infrastructure facilities (Sodnik et al., 2014). Dams are strategically a very important infrastructure that brings numerous economic and social benefits to the mankind. At the same time, every dam poses a certain degree of risk in the area of influence (Zhang et al., 2016b). Due to Slovenia's diverse topography and dispersed settlements, many urban areas are located downstream of large dams. Therefore, structural health of large dams should be a national priority.

In Slovenia, we are increasingly faced with the problem of ageing of dam structures. At the same time, we are also faced with changes in the environment, especially with the variability in time-dependent loads and with new patterns of operation on dams used for hydropower, with several starts and stops of turbines happening on a daily basis. These changes can lead to a decrease in structural and operational safety of dams. Dams are built to serve for a long time and require safe and reliable operation. They also play an important role in the society, as they bring about numerous benefits, i.e. besides electrical generation, also water storage, irrigation, and flood control. But in the event of their technical or structural (partial or total) failure they represent a risk to downstream areas (Kryžanowski and Humar, 2014). To ensure their safe operation, it is necessary to establish a system for technical monitoring of dams, where the behaviour of the structure is regularly being monitored (Chang et al., 2003). In Slovenia, such a monitoring system is a legal obligation for all large dams (Kryžanowski and Humar, 2011). As part of regular monitoring, various parameters are logged, but analysis and evaluation of measured data are performed only in exceptional cases, usually after the occurrence of unforeseen events (visible large cracks, partial failure). In this thesis the importance of regular evaluation of the condition of all large dams is emphasised. Implementing regular evaluation of a dam's condition is the key to having a continuous insight into the actual (health) state of the dam.

The accumulation of damage in a structure causes changes of its dynamic properties. Vibration monitoring can be used as a base for structural identification. The main purpose of this thesis is to establish the basic knowledge on the activities involving structural identification, structural health monitoring (SHM), and the role of vibration monitoring on dams. Dam monitoring has a longer tradition than monitoring in other civil engineering fields, however nowadays it is somehow lagging behind in comparison with the monitoring of bridges and buildings, where dynamic testing and damage detection is often used (Bukenya et al., 2014a). The methodology in buildings and bridges cannot be directly applied to dams, vibration patterns of dams are different and additionally complicated by fluid-structure interaction (Humar et al., 2006). Dams are also built to operate for a long period of time, much longer than 50 years. It may be considered that after construction, the structural lifetime is conditioned by the intensity of the load, environmental actions, and maintenance. Furthermore, during the dam's life regulations concerning building construction, dam ownership, and monitoring operators can change (Tekie and Ellingwood, 2003). Our first aim is to establish a solid ground for future work, i.e. to identify the structural properties at a dam's young age and establish a database. The key to extend the lifetime of the already aged and further ageing dam inventory is good diagnostics. It is important to assess the real behaviour of these structures by using on-site tests (Humar et al., 2006). If the appearance of damage is diagnosed early and proper safety measures are adopted, dramatic and life-threatening consequences can be minimised or even prevented, while the cost of repair can be minimised (Mesquita et al., 2016).

1.1 Motivation

Every year about 200 new large dams of different types are built worldwide (Bernstone, 2006); however, the intensity of dam construction was even higher in the past. It can be assumed that most dams that will operate in the 21st century already exist. This means that ageing of dams, preservation of their functionality, and preservation of their structural health are the main challenges of the dam engineering community. The situation is similar in Slovenia, as ageing of dams and variability of time-dependent loads have become the main concern for dam owners. Various load cases, which occur during regular operation with dams, can have a significant impact on the ageing process. In this scope, permanent and temporary dynamic loads can be divided into usual operating loads (manoeuvres when vibrations are caused with the operation of units, hydro-mechanical equipment, and hydrodynamic forces of flowing water) and exceptional operating loads (operational test of hydro-mechanical equipment, induced dynamic effects of the structure due to hydrodynamic processes, such as cavitation or abrasion). Especially the usual operating loads are commonly overlooked in dam design, due to the assumption that the magnitude of operational dynamic effects is much smaller than that of seismic load. As a consequence, seismic load is seriously considered, while other dynamic effects are assumed as trivial. The case of Sayano-Shushenskaya HPP accident in 2008 is one proof that operational loads need serious attention. During regular operation, one of the units was suddenly destroyed and thrown out of its position. At the same time, most of the automatic protective systems were not activated and due to the power loss, the ancillary safety services needed to be manually activated; this resulted in a vast structural damage and death of 75 people (Bryksin et al., 2014). The HPPs on Lower Sava River are designed as run-of-river type of dams that operate in a closed hydro energy scheme. The basic components of such an energy scheme are the headwater reservoir (Mavčiče-Medvode), the re-regulating reservoir (Brežice-Mokrice) at the end, and the number of run-of-river dams in between. The role of the Lower Sava hydro energy scheme and power production patterns has changed as nowadays HPPs no longer operate continuously as provided for in their design, but there are many stops and starts, sometimes even several times a day (providing peak power, production of energy on demand, providing frequency in the system, and sufficient reserves of power). Each HPP operates as a run-of-river system with a limited storage and not as a continuous chain. These changes originate from the changes on the financial and energy markets. Unfortunately, these significant changes in operating patterns were not considered in the design phase, and it is of utmost importance to confirm the integrity of the dams under the new operating conditions. Additionally, during regular inspections, defects such as cracking were discovered at Vrhovo, Blanca, and Krško dams. The main suspicion as to why these defects occurred is the change in the operating patterns on these dams. Due to the extent of structural damage in the Vrhovo HPP powerhouse, in 2000 extensive rehabilitation works were required. Also, the condition of other dams on the Lower Sava River indicates the need for a detailed analysis of the effect of the new dynamic patterns, since they can be a silent threat to the structural safety for all dams operating under these modified conditions. Identification of a significant mechanical response of dams to the induced vibration patterns can improve dam safety in the future. This issue is not confined solely to the Sava River, but to all HPPs in Slovenia and beyond.

The transition from base to peak load operation is common to the majority of dams used for hydropower which were not built in recent years (ICOLD Technical Committee on Dams for Hydroelectric Energy, 2019). Hydropower turbines provide ancillary services for the electrical network: maintenance of system frequency (due to fast and automatic response), fast reserve, reactive power series, and black start capabilities. With the inclusion of more renewable power sources in the grid, which are known to be intermittent, the role of water turbines has even increased and will increase even further since a large portion of non-renewable power plants in EU will be decommissioned before 2030 (Farfan and Breyer, 2017). Most hydropower project were designed to provide primary or base load power generation in the grid. With the inclusion of less flexible and less predictable generation technologies, e.g. thermal, nuclear, solar and wind, the ability of hydro turbines to respond quickly gave hydropower production a new role in power grids to fill the gap between demand and supply. This enables for the optimisation of base load production, i.e. nuclear power plants can operate at a constant level (preferably at the level of their best efficiency) and only with hydropower regulation stochastic contributions from solar and wind power can be covered. Thermal plants provide a certain amount of flexibility, however, they require a considerable amount of time and energy at each start-up, and regulation velocity is limited due to the high thermal inertia. Additionally, frequent start-stop cycles significantly reduce their service life (Chanda and Suparna, 2016). Gas fired thermal plants allow the highest level of flexibility among this kind of power plants. Their regulation capacity is around 75% of rated power, while HPPs still remain the most flexible element in the grid to perform continuous regulation. In the past only a few units were sacrificed to be highly flexible in operation, nowadays, due to changed conditions, practically all hydro units in operation on the grid are continuously regulated and daily operate in transient and unsteady modes. Hydropower turbines serve as primary and secondary reserve; water turbines can run at a zero load while being synchronised to the system and can be connected to the grid in seconds after the demand increases. They can run at as low as 2% of the installed power, the regulation requires minimum energy input, units can also rapidly enter the grid when they are at full stop (non-spinning reserve). In addition, they enable regulation and frequency response, which prevents damage in the grid system and loss of power. The frequency in the system must remain constant at 50 Hz with minimal fluctuations. Whenever the system is not able to respond to a load change, this reflects in a frequency change, and the responsiveness of the hydro units is an enabler to stabilise the system. Furthermore, the rotating mass of the units provides inertia in the system, which is an important stabilising factor. This enables also voltage support as well as black start capabilities. Capabilities of hydropower technologies in the system, in comparison to other technologies, are unparalleled. Due to this, they also react to the profound portion of instabilities in the grid (ICOLD Technical Committee on Dams for Hydroelectric Energy, 2019). Run-of-river hydropower schemes were assumed in the past to contribute to base load generation, offering few of the ancillary benefits; but their role changed since now we know a run-off-river plant can be used for ancillary services. Unfortunately, this has not been taken into account in the design and construction of most Slovenian dams. We find that it is necessary to broaden our knowledge about the behaviour of hydropower dams to improve their operational safety and extend their life expectancy. The knowledge gained during the study on the Lower Sava can be applied also to other run-of-river types of concrete gravity dams.

Before 1990 the majority of hydropower plants were operated locally. The crew consisting of operation, maintenance, and control personnel was present on dams every day. When operation gradually shifted from local to remote, simultaneously also the workforce was reduced. Not only operational workforce; the departments for design, planning and maintenance of civil works have shrunk or were even cancelled. The tasks of structural and civil engineers were shifted to the operational staff, with mainly electrical engineering or sometimes mechanical engineering background. Therefore, the skill and knowledge of civil and structural engineers was partially transferred to the operational staff and also partially lost in transition. Nowadays the personnel on dams, also the personnel dealing with structural maintenance, has electrical engineering background, while civil engineers only have a marginal role. As a consequence, the electrical measuring equipment is excellently maintained, the operation of dams is done according to the state-of-the-art, while concern for structural integrity does not receive the same attention.

We have to underline the fact that many HPP schemes have been in operation for decades. Generations have coexisted with the reservoirs, bringing numerous ecosystem services. The ageing of dams also concerns the reservoir areas, while emptying the reservoirs will have broader environmental impacts.

1.2 Research Hypotheses

This research is founded on three research hypotheses:

- Dynamic loading present throughout regular or exceptional operating regimes has a significant impact on mechanical properties of concrete gravity dams.
- The laser Doppler vibrometer is an appropriate tool for monitoring the dynamic response of dams.
- State-of-the-art experimental techniques can be used for a more efficient monitoring of dam ageing. In this way, we can improve the management and operational safety of dams.

Dynamic loading due to regular or exceptional operating regimes has a significant impact on mechanical properties of concrete gravity dams. The constant exposure to low-amplitude, high-frequency oscillations causes an accelerating growth of micro-cracks present in concrete due to the process of hydration of cement, placement, and curing conditions. Vibration testing is well present in various engineering techniques. Civil engineering and especially dams provide a special challenge for the methods. Nowadays, with the modern technology and knowledge, we believe that non-contact techniques can be of great benefit in dam condition monitoring. Laser technologies have developed substantially. We believe that the laser Doppler vibrometer (LDV) is an appropriate and promising new technology to be implemented in dam monitoring. By enabling non-contact, remote, on-site measurements, linearity in the entire frequency spectrum, and ease of use, LDV provides an excellent alternative to traditional contact type measurements. Its use can help to reduce the cost of vibration monitoring and improve the quality of measurements. Notably, this technology has never been applied to dams and used inside the structure of interest during operation, when the instrument is excited as well.

1.3 Research Goals

The main goals of this research are:

- Identification of the operational loads in the structural response of a hydropower dam.
- Improved understanding of typical behaviour of concrete gravity dams subjected to operational loads.
- Development of a system to perform non-intrusive damage detection and inclusion of the results of regular monitoring into the system for continuous condition-based monitoring of concrete gravity dams.
- Identification of the initial reference condition of a dam in an undamaged state.
- Evaluation of eigenfrequencies of a concrete gravity dam and the structural response to typical dynamic loading.
- Preparation of the proposal on upgrading the monitoring system on run-of-the-river concrete dams on the Sava River.
- Fundamentals for further research and identification of mechanisms causing failure modes associated with operational loads and transfer of research results into practice.
- Application of laser Doppler vibrometry in vibration monitoring on dams.

1.4 Organisation of Work

The thesis is divided into two parts. In the first part, the motivation and theoretical background are presented. We prepared a literature review on structural health monitoring and on the history of dam surveillance, micro-cracking in concrete, the development of laser Doppler vibrometry, and ageing of dams. Chapter 3 presents the fundamentals of structural health monitoring, vibration based monitoring, dam surveillance, and laser Doppler vibrometry. We provide some critical assessment of the relevant papers and conference proceedings and identify the areas where the process of evaluating the dam ageing can be improved.

Experimental work presents the core of this research. In Chapter 5 we describe the experimental site, the equipment, the procedure of our work, and numerical models. At the end of the chapter we present our findings. One of the objectives in this work is the development of a methodology to observe dam ageing using vibration monitoring. In Chapter 6 we prepared a recommendation on the implementation on the run-of-the-river dams used for hydropower purposes. The work is concluded with a brief summary of the research findings and recommendations for future work.

At the end we provide an extended abstract written in Slovenian where the highlights of the work are presented.

In the appendix we provide representative time series and frequency plots, captured during the testing of the hydro-mechanical equipment on the Brežice dam.

2 THEORY BEHIND VIBRATION-BASED TECHNIQUES FOR STRUCTURAL HEALTH MONITORING

2.1 Modal Properties of Structures

By observing the vibration of the structure, we can estimate the condition of the built-in material. We will refer to resonant frequencies, modal damping, and mode shape vectors as the modal properties of a structure. Every structure has unique modal characteristics and its unique vibrational signature, which change only in case when the structure's mass, stiffness, or geometry is altered. Therefore, if the structural damage causes a decrease in stiffness, the vibration patterns and modal "fingerprint" of the structure will change as well. In theory, if we know the response of a system in sound state, by comparing the two states, the observed changes in modal properties are indicators of structural damage. We use this principle in our daily life, for example by knocking on the fruit and listening to its sound we can estimate the ripeness of some types of fruit. Similarly, the sound of glass that is not sharp and clear tells us that this glass is damaged and we can expect it to break soon. Which modal property to use depends on the technology we can use and the desired level of detection. The application's advantages and disadvantages are presented in Chapter 3. For example, by studying the recent studies we can notice that resonant frequencies have less statistical variation and are less prone to error than other modal parameters (Doebling et al., 1998; Farrar and Lieven, 2006).

2.1.1 Vibration

Vibration is a mechanical oscillation around an equilibrium point. Every structure vibrates under the effect of excitation source. Even when the structure is in the "rest state", a certain amount of excitation can always be identified (wind, atmospheric conditions, micro-tremor). Therefore, the structures are never at a completely still state. The structure either vibrates naturally or it is subjected to forced vibration. Vibration-based approaches of structural identification can be divided into two groups:

- forced vibration testing (FVT) or
- ambient vibration testing (AVT).

With forced vibration testing, a structure is excited with an additional external force. This technique is proven to be effective to get an accurate estimation of higher mode shapes. However, it is expensive and time consuming, since it usually causes disturbances to the normal operation or even requires a complete shut-down of the structure, which in most cases also means that special permits are required. During the test, the structure is excited with steady-state or impact forced vibrations, with one or multiple sources of excitation. Different types of actuators can be used: shakers, step relaxation, or impact hammers. Forced excitation tests have usually strong signal-to-noise ratio, where the input force usually dominates above the sources of noise. One of the benefits of this methodology is the possibility of a local deployment; we can excite only part of the structure and not the whole system, while AVT is more appropriate for global application. FVT can also be performed with free vibration testing. Free vibration testing occurs when a structure is moved from its original-stationary position and begins to vibrate in a free vibration decay, i.e. we observe the behaviour of a structure caused by only one sudden release (De Roeck et al., 2000; Hsieh et al., 2006).

We define ambient excitation with the level of excitation of a structure under normal operating conditions. AVT type of testing uses the ambient (micro-tremor) load as an excitation force (wind, seismic activity, traffic, operation, etc.). The main advantages for the use of ambient excitation are: minimal disruption to the operation, it is faster and more economical than FVT, it is non-destructive and requires a lower energy input, and the measured response describes the actual frequency content representative for the structure. The main disadvantage of this methodology is difficulties in measuring the excitation force (input). Accurate measurement of the input is not possible. Whenever possible at least some elements of excitation force are measured, e.g. wind speed, seismic acceleration from the closest seismic observation point. Since the input is not completely known, transfer functions cannot be obtained (i.e. FRF methodology cannot be applied). Ambient excitation is random (unpredictable) and can also have an unfavourable direction, with variable amplitude, frequency content, and duration. Ambient excitation also often limits the frequency range, and environmental changes can also add additional uncertainty, therefore long-term monitoring based on AVT should have an extensive learning period. However, AVT is proven to be good for global assessment (Bukenya et al., 2014a; Rücker et al., 2006).

Trifunac (1972) performed a comparative study between AVT and FVT on a twenty-two storey, steel-frame building and a nine-storey, reinforced concrete building (Jennings et al., 1971; Trifunac, 1970; Jennings and Kuriowa, 1968). In both cases the structures were first tested using the FVT and afterwards using the AVT method. Based on this research, authors conclude the results obtained from AVT and FVT are comparable when the structure is excited in a linear range of response.

Based on the data acquisition method, we distinguish between two possibilities to measure vibration, i.e. in time domain or frequency domain (Fassois and Sakellariou, 2007). According to the control and automation literature, most methods are based on time-series (Balageas et al., 2006). The frequency domain response is usually obtained using the Fourier transformation from time-domain measurements. The transformation reduces the quantity of data and decreases the effect of the random noise by averaging.

Furthermore, we can distinguish between local and global methods. With local methods we cover a small area. Usually, local methods are applied to the investigation of "hot spots", i.e. places where advanced damage is recognised or where structural changes are expected to occur. Local methods are very sensitive and are able to detect very small flaws and changes. Global methods, on the other hand, look at the whole structure and are based on the assumption that local damage affects also the global behaviour, since the reduction of stiffness causes a change in eigenfrequencies, which is a global parameter. Vibration-based methods can be further classified into response-based and model-based methods. Response-based methods provide direct or indirect interpretation of the structural response by knowing the connection between modal parameters in sound and damaged state. Model-based methods use either an analytical or a numerical model to assume a structural behaviour, while any discrepancy provides for damage identification. Models are often used when solving an inverse problem after a large amount of damage is introduced to the system. Another group is data-based methods that are based solely on pattern recognition. The latter techniques are good to detect changes, however, they do not perform well in classification of the change (Kong et al., 2017).

Das et al. (2016) and Kong et al. (2017) present a comprehensive review and critical assessment on the vibration-based detection techniques and the framework of vibration-based detection, identification, and decision making in monitoring of structures. The response-based methods are easily applicable, but do not provide a quantitative assessment of the damage. On the other hand, model-based methods, which are based on a well-correlated numerical model and where we have to have in mind modelling assumptions, introduce an error into the model. The development of a well-correlated model is a challenge and a demanding task. In authors' opinion, the future challenges are: development of the models, which are currently predominantly based on linear theory, identification of ambient factors, minimizing uncertainties in measurements, and development of robust experimental and numerical techniques.

2.1.2 Theoretical Background

The general form of the equation of motion of a system with a finite number of degrees of freedom in a dynamic equilibrium between the external, inertia, damping, and elastic forces can be written as:

$$\mathbf{M}\ddot{\mathbf{x}} + \mathbf{C}\dot{\mathbf{x}} + \mathbf{K}\mathbf{x} = f(t) \tag{2.1}$$

where **M**, **C**, **K** represent mass/inertia, damping, and stiffness matrix, respectively; f(t) represents the external load of the system, and **x** is the displacements vector. **M**, **C**, and **K** are symmetric. The damping matrix **C** describes various mechanisms that dissipate energy in the system. The damping values are usually an assumption, by adopting one of the hypotheses, e.g. Rayleigh damping in Equation (2.2), with corresponding α, β coefficients (Chopra, 2012).

$$\mathbf{C} = \alpha\mathbf{M} + \beta\mathbf{K} \tag{2.2}$$

If we assume an undamped conservative system, free vibration problem can be written as (Chopra, 2012):

$$\mathbf{M}\ddot{\mathbf{x}} + \mathbf{K}\mathbf{x} = \mathbf{0} \tag{2.3}$$

When the system is undamped or only lightly damped, the natural frequencies can be determined from the eigenvalue problem where $\lambda_i = \omega_i^2$.

$$[\mathbf{K} - \omega_i^2\mathbf{M}]\varphi_i = \mathbf{0} \tag{2.4}$$

where ω_i are the circular natural frequencies and φ_i is the corresponding mode shape eigenvector. The above equation has always the trivial solution $\varphi_i = 0$, which we are not interested in, since it means there is no motion (Chopra, 2012). A non-trivial solution is obtained when:

$$det[\mathbf{K} - \omega_i^2\mathbf{M}] = 0 \tag{2.5}$$

The characteristic equation 2.5 has *N* real and positive roots (*i = 1,2,....,N*) since **M** and **K** are symmetric and positive definite. The roots of the characteristic equation are known as eigenvalues. There are *N* independent vectors, φ_i, corresponding to each natural vibration frequency (*N*) known as eigenvectors or natural modes. The term natural is used to emphasise the fact that these values depend solely on the properties of the structure in free vibration, i.e. on their mass and stiffness (Chopra, 2012; Hansteen and Bell, 1979).

For the standard eigenproblem, the corresponding period (T) and frequency of motion (f) can be computed with:

$$\begin{aligned} \lambda_i &= \omega_i^2 = f_i^2 \\ \omega_i T_i &= 2\pi \\ f_i &= \frac{\omega}{2\pi} = \frac{1}{T_i} \end{aligned} \tag{2.6}$$

3 STATE-OF-THE-ART OVERVIEW

Monitoring of structures is, in its basic form, very old. It originates from the time in history when the first structures were built. At first, it started with manual inspections; engineers and architects observed their structures during construction and later. In their wish to gain knowledge and improve the design of the future projects, they were interested in their behaviour, appearance of cracks, and damage. At first, the integrity of civil structures was maintained by means of a system of manual inspection, and later by using conventional measuring and testing equipment, non-destructive evaluation (NDE). Nowadays it is moving towards the use of an integrated system (Salazar et al., 2017).

The drive behind the need for an innovative approach and evolution from structural monitoring to structural health monitoring is partially arising from the need to minimise operational and maintenance costs of the owners of civil structures. SHM can help to minimise out-of-service time by applying an automated and integrated system, to reduce manpower, and to reduce the room for human error. Service disruption due to regular periodic inspection should be reduced, while deterioration caused by normal operation should be detected without obstructing the regular operation. Only inspection following extreme events would demand obstructions to the operation (Chang et al., 2003; Mesquita et al., 2016).

This chapter presents the fundamentals of structural health monitoring, vibration based monitoring, dam surveillance, and laser Doppler vibrometry.

3.1 Structural Health Monitoring

To summarise the words of Professor Ralph Peck, as presented in Bulletin 999 (ICOLD Technical Committee on Dam Surveillance, 2018), Worden et al. (2007), who presented seven fundamental axioms of structural health monitoring, and Karbhari (2005), the following five statements are in authors' opinion the fundamentals of the interdisciplinary field of structural health monitoring (SHM):

- All materials have flaws.
- Sensors cannot measure damage.
- Every sensor installed should be selected and placed to answer a specific question.
- Structural assessment requires a comparison between two system states.
- SHM is the basis for condition-based rather than time-based monitoring.

Structural health monitoring is a multidisciplinary field connecting disciplines of structural vibration analysis, structural control, non-destructive testing and evaluation, material science, signal processing, sensors, and conventional civil and mechanical engineering. This is a relatively new field that developed as such in the final decade of the 20$^{\text{th}}$ century, emerging from the need to systematically address the issues connected with fatigue, system identification, long-term monitoring, and prognosis (Balageas et al., 2006). Research work in this area started to intensify in the late 90s. In 1997 the first International workshop on Structural Health Monitoring (IWSHM) at University of Stanford was organised. In 2002 the first journal specializing in structural health monitoring was published, and the area has developed since (Chang et al., 2002; Mufti, 2011). SHM is a procedure of providing a diagnosis on the state of the structure by monitoring and its analysis. The aim is to observe (monitor) the in-situ behaviour of a structure to determine its condition (health), i.e. to provide an interpretation on the state at every moment during the lifetime of a structure. The condition of the structure must remain within the limits of the designed domain (operational, safe) to provide the optimal use of the structure with minimal halt time due to regular repairs, prevention of failures (or at least prevention of catastrophic failures), and extension of service life. The object under observation is the structure as a whole as well as its individual constituting parts. The state of the structure is a function of ageing phenomena, environment factors, and accidents. SHM is a wide field consisting of installation/integration of sensors, data acquisition and processing, usage monitoring, diagnosis, maintenance, action, prognosis, and knowledge transfer. The conceptual principle of a SHM system is presented in Fig. 3.1. We have to emphasise that in civil engineering, every project is unique and a common general rule for a perfect SHM system does not exist. When talking about SHM, we always need to have the whole system in mind. The object under observation and the sensory system together also form an integrated system, while the monitoring system is only as good as the installation. Every instrument, installed in the system, has a specific role and it should be selected and placed to assist in answering a specific question (ICOLD Technical Committee on Dam Surveillance, 2018). It is not enough to simply install an instrument, wait to get some data, and expect the readings to tell us something eventually. An unfortunately placed instrument will at best provide confusing information. Also each instrument placed on the structure presents a discontinuity and their presence may also alter the measured quantity, while poor placement of the instrument may cause the loss of data and offset in the output. Location, quality of the joint, and number of instruments play a considerable role as well. There must be some redundancy in the system in case of malfunction or failure to have a continuous data set through the life-cycle. We also have to note that in case a fixed instrument has to be replaced, even if the same type of instrument is placed in the same location, the absolute continuation of the measurements is lost. Therefore, at least the redundancy of the crucial quantities has to be ensured. However, at the same time, too much instrumentation does not provide a higher quality of monitoring. All this has to be considered in the design, data collection, and interpretation. A well-organised library for data storage is a the backbone of any SHM system; each step has to be well documented, while interpretation is the most demanding part of the SHM activity. In observations of a complex system, visual inspections performed by a qualified person play an indispensable role. Knowledge transfer and presentation of the results to everyone involved is also a key step. Each step must be handled by a qualified person and a well informed and motivated person will do a better job. Therefore, it is crucial to inform everyone involved about the importance of their job, for instance to tell the person performing manual reading of the piezometer, why these readings are important and, after the synthesis, to also show them what their readings provide, provide interpretation of results, and present how will their readings help us in the maintenance process. Providing feedback and highlighting the workers' role in the process is a simple step to assure the quality of their work. Unfortunately, in reality this step is often missing. The human factor is present at all stages of SHM and the first step in minimizing room for error is to have a clearly defined and transparent methodology, where everyone involved understands the importance of their role. To summarise, SHM represents the integration of a

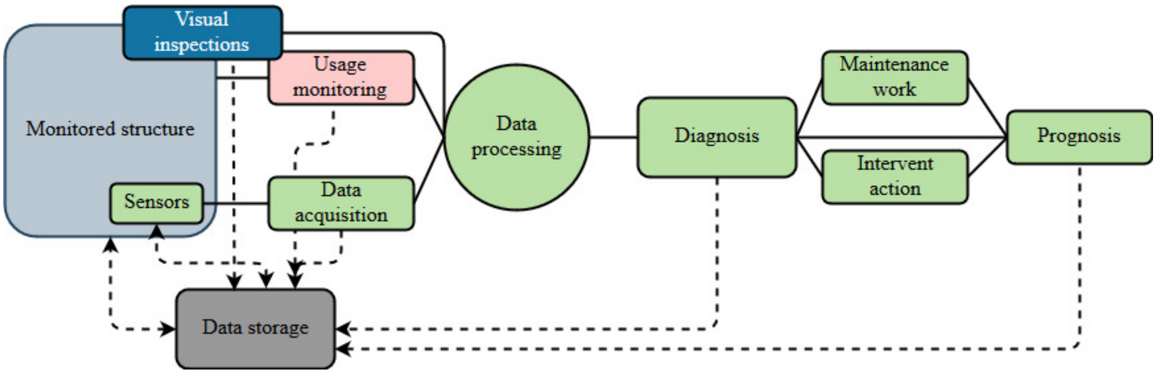

Slika 3.1: Zasnova sistema spremljanja kondicijskega stanja.
Figure 3.1: Principle of a SHM system.

sensory system, a data acquisition system, a data processing system, an archiving system, a communications system, and a damage detection and modelling system to acquire knowledge, either on demand or on a continuous basis, regarding the in-service performance of structures. A truncated form of SHM, only with the implementation of monitoring, has been present on strategically important structures for decades (Balageas et al., 2006).

Visual inspection is the oldest and most widely used inspection method in civil engineering. It is based on engineers' observation (vision, hearing, taste), intuition, measurements, knowledge, experience, and information they have in their possession. Regular visual inspections provide general information on the state and will probably never be completely replaced. We can divide visual inspections into two groups: routine and in-depth inspections. By performing routine inspections we gain a general overview over the state of the structure and can also identify potential warning signs. Visual inspection is indispensable in the form of in-depth inspections when damage occurs and a decision on proper measures has to be taken (see Fig. 3.2). In such case, more than one inspector examines the structure. Local non-destructive tests are used to complement visual inspections: ultrasound, acoustic emission, penetration testing, X-ray (Kong et al., 2017; FIB Task group 5.1, 2003).

Traditional techniques of condition monitoring consist of discrete or continuous data acquisition of strain, corrosion, displacements, temperature, water level, etc. Sensors are permanently

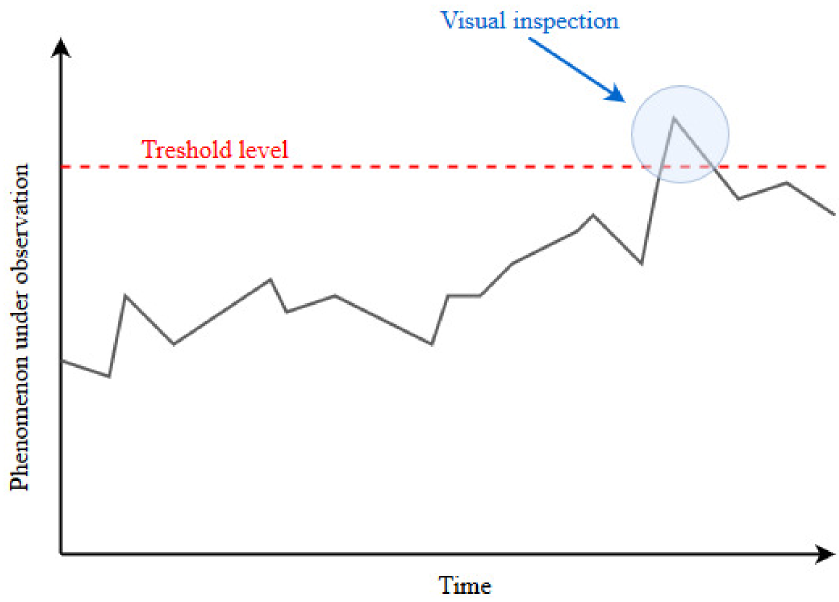

Slika 3.2: Detaljni vizualni pregled konstrukcije zaradi izrednega dogodka. Povzeto po: FIB Task group 5.1 (2003).
Figure 3.2: In-depth visual inspection after a triggering event. Summarised after: FIB Task group 5.1 (2003).

mounted on the structure or a permanent stub enables sensor installation for the time of the measurement. The processing and measurement technology advanced from analogue to digital, with manual or automatic reading. Measurement is taken based on the sensors' physical, electrical or thermodynamic characteristics. Hsieh et al. (2006) present an overview of vibrational SHM and the sensors in use. The origin of the methodology and technology development arises from aerospace and mechanical engineering disciplines. Due to the uniqueness and size of the civil engineering structures, applications in this field are applied with some delay. Robust full-scale vibrational SHM systems include also other monitoring systems working in parallel. Devices and sensors commonly used in vibration measurements are: accelerometers, velocity, displacement, and strain sensors. Accelerometers may be the most used vibration monitoring sensors, since they are small, robust, and have a wide bandwidth. Velocity sensors are used for similar tasks as accelerometers; however, they have a smaller bandwidth. Displacement sensors measure relative displacements, and they can be of contact or of non-contact type (laser, and GPS type, photogrammetry) (Kong et al., 2017).

Modern approaches to SHM based on vibration detection have their origins in the 1970s in the research for offshore platforms, where on-site inspections are difficult, expensive, and dangerous (Vandiver, 1977). Offshore platforms are a demanding environment. Their vibration based monitoring has to satisfy the following criteria: sea and wind are used as an excitation force (ambient excitation), instruments have to withstand a harsh environment, mode shapes are identified solely from the measurements above the sea level, vibration measurements must remain stable over a long period of time, and the methodology applied has to be financially more favourable than the use of divers (Begg et al., 1976). Unfortunately, the majority of the first applications were unsuccessful to fulfil all the criteria and therefore, for the time being, the oil industry has abandoned this path approach after a decade (Doebling et al., 1998).

Besides vibration-based methods, other non-destructive ones can be used to detect damage: acoustic, magnet, radiography, eddy-current, thermal, and optical methods. Optical fibre methods are gaining a lot of attention in the last years (Doebling et al., 1998; Mesquita et al., 2016). Ye et al. (2014) provides a comprehensive review on the use of optical methods in civil infrastructures. In the scope of this work these methods will not be presented further.

Space industry also recognised and applied the benefits of quality control based on modal properties, where it is nowadays practically a routine practice (Juneja et al., 1997). The conventional techniques (X-ray, ultrasonic) require a removal of at least some thermal protective tiles on the Shuttle, whereas with modal inspection this is not necessary (Doebling et al., 1996, 1998). Laboratory vibration tests to identify modal properties of the space shuttle components were conducted by Pappa et al. (1997). A scaled model of the international space station was built for studying the dynamic behaviour and implementation of an on-orbit damage location scheme (Kashangaki, 1991). Similarly, in aviation industry, with increasing civilian and military fleet size, as well as its mean age, benefits of vibration-based SHM have been recognised (Boller, 2001).

There are numerous applications of vibration testing methods for damage detection on model and prototype wind turbine blades. With the evolution of wind turbines, the blades have become larger. Since the blades are the most expensive part, a lot of effort is being put into monitoring the structural integrity and minimizing downtime caused by regular maintenance and damage (Stevanovic et al., 2017; Tang et al., 2016; Niezrecki et al., 2014).

Rotating machinery testing is one of the most extensively researched fields in the non-destructive vibration testing; the work in that field was comprehensively revived by Jardine et al. (2006) and Aiwina et al. (2009). Successful applications exist due to the comprehensive and large amount of data from industrial components, which are available because of a large number of tests, including failure tests (Farrar and Lieven, 2006). However, due to the specific nature of testing on rotating machinery, this field will not be separately reviewed in this thesis.

Salawu (1997) authored a review paper on detection of structural damage through changes in frequency in 1970–1995. The author reviewed 65 papers considering: prestressed structures, continuously supported plates, beams, concrete portal frames, testing on bridges or bridge parts (prestressed concrete stay of a cable-stayed bridge), and dynamic tests on scaled models of different types of bridges (box-girder, prestressed concrete bridge). Doebling et al. (1996), in a review paper, presented applications of SHM according to structural types. Authors summarised published research on concrete beams, metal and miscellaneous beams, trusses, plates, shells and frames, bridges, offshore platforms, aerospace structures, composites, and other large civil engineering structures (wind turbine blades, multi-story frame buildings and steel frames). They presented a report on four research projects on concrete beams where modal testing was performed on reinforced and unreinforced beams in sound state and with defects. The early work focused on simple structural elements or simple scaled structures. Chowdhury and Ramirez (1992) observed changes in the natural frequencies over time while testing 27 beams. Similarly, Slastan and Pietrzko (1993) tested T shaped beams before and after damage; they have detected small but measurable frequency shifts due to damage. There has been a substantial amount of experiments on various types of trusses using natural frequencies and mode shapes for damage detection. Damage detection is possible for those members that have a significant contribution to the strain energy of the measured modes, while the damage is more apparent in the natural frequency changes than in mode shapes (Kashangaki et al., 1992). Research on aluminium plate considering several damage cases revealed that only those damage scenarios that have a global effect are discoverable via modal parameters monitoring (Wolff and Richardson, 1989). Saitoh and Takei (1996) applied a modal investigation technique to investigate welding quality at the end of the production line of car doors. On each door, there is approximately 100 spot welds. Authors performed measurements on 40 door specimens with good and poor welds and discovered that doors with weak welds scatter from sound specimens.

Based on the literature review, dynamic testing is well present on bridges with application of prototype and model testing. Saed Mirza et al. (1990) performed dynamic testing on scaled, one and two box-girder bridges. Gardner-Morse and Huston (1993), with testing on a cable-stayed pedestrian bridge in Vermont, presented that lowering of natural frequencies can be linked with the loss of cable tension in cable-stayed bridges. Kato and Shimada (1986) conducted an investigation on a prestressed concrete bridge during failure by performing vibration tests during static loading cycles. Salawu (1997), based on the review of state-of-the-art at that time, claimed that a 5% change in the natural frequency should be detected in order to be confident a damage in the structure has occurred. However, Chen et al. (1995) claimed that prediction on damage, supported solely by natural frequency drift estimation, is not sufficient, since a drift of less than 10% is already associated with progressive fatigue. The response of the structure should be measured at points where all representative mode shapes and natural frequencies (in the frequency range of interest) are well represented. In order to use dynamic testing as a diagnostic tool, failure mechanisms and the effect of deterioration have to be identified in advance, since not all deterioration effects can be measured using dynamic testing; e.g. testing on long span bridges revealed that local damage does not cause a measurable change of dynamic properties. Shirole and Holt (1991), based on a survey of bridge failures in the United States from 1950 and further, concluded that catastrophic failures (for example the Tacoma Bridge failure) have led to overall bridge design and inspection program modifications. Salane et al. (1981) conducted a full scale in-situ dynamic testing of a three-span highway bridge in order to detect deterioration and fatigue cracks in the girders. Cycling loading tests, by applying a moving mass, provided information on the change of modal properties due to fatigue. Turner and Pretlove (1988) present a methodology for beam-like road bridges, where random traffic load is used as an excitation force for SHM measurements. Testing of a simply supported beam, subjected to a series of moving loads, is analysed both in time and frequency domain. The theoretical model was compared with measurements on a full-scale road bridge. The advantage of the proposed ambient testing methodology is that SHM can be performed without interrupting the bridge operation and the excitation force does not have to be measured. The authors discovered that the response of the bridge under traffic load excitation suffices for determination of the natural frequencies. They conclude that with the monitoring of the frequencies, a 5% change indicates a significant damage on the structure. Mazurek and Dewolf (1991) emphasise the importance of continuous automated monitoring of highway bridges by highlighting some notable failures and near failures; e.g. the Rhode Island bridge where failure was prevented when a pedestrian noticed progressed cracking on a primary girder. With laboratory model testing, Mazurek and Dewolf (1991) also discovered that major structural degradation is reflected in natural frequencies and in mode shapes as well. Modal testing revealed that the greatest change of mode shapes happens in the vicinity of the structural damage. Authors proposed the use of natural frequencies to discover whether structural damage is present and the use of modal shapes for further localisation. Raghavendrachar and Aktan (1992) performed on-site impact tests with the aim of detecting local and hidden damage in contrast to progressed global damage. The object under observation was a 3-span RC bridge. The authors concluded that inclusion of higher modes, although this requires a larger energy input to excite the structure, is required to identify local phenomena. De Roeck et al. (2000) and Peeters et al. (2001), by monitoring vibration and environmental effects (air temperature, humidity, wind speed and direction) of the Z24 bridge in Switzerland with hourly readings over the course of one year, present an experimental case where the effect of ambient temperature on the frequency shifts was determined. Moreover, following an extensive damage testing program, they present the case where corresponding stiffness degradation can be detected if the frequency shifts by more than 1%.

Doebling et al. (1996) summarises research efforts on modal properties of different types of bridge structures performed in the 70s, 80s, and 90s. The motivation for a vast scale of research can be mostly attributed to the several catastrophic failures in that time. Early research focused mainly on damage detection via natural frequency changes. Later work also included modal shapes, while damping has yet not been proven to be a useful indicator on bridge structures. Authors still have a concern while in some cases even with reliable modal data, changes in modal parameters may not be a reliable damage indicator; the use of higher modes is necessary for the detection of damage occurring locally in early stages. Study cases show that in cases when the damage is well developed and information on the sound state is missing, strain is not a good indicator for structural changes (Zhang and Aktan, 1995). Some early researchers also claimed that mode shapes are not sensitive to local damage (Chang et al., 2003). It is important to be able to predict the influence of environmental factors (e.g. humidity, temperature) on dynamic characteristics as well, or at least minimise their input. A limitation for the existing structures is the absence of the information on the pristine dynamic characteristics. The as-built characteristics are usually unavailable and have not been measured until severe or at least visible damage has already occurred. Since engineers require this information in order to be able to asses the current state, SHM is often a process of solving an inverse problem. An unsolved issue at this point is still the consensus on what is the general level of sensitivity of modal parameters to small flaws in a structure; there still is no general rule, only particular cases to support both claims (the parameters are sensitive enough to local damage, or modal parameters are not sufficient). There are many promising techniques presented in the example cases however, their applicability is still to be fully demonstrated.

Sohn et al. (2004), in their review of structural health monitoring literature 1996–2001, provided a technical review of 15 SHM studies focusing on global identification. Authors defined SHM as a statistical pattern recognition paradigm, consisting of 4 steps: operational evaluation, data acquisition, feature extraction, and statistical model development for feature discrimination. Authors emphasise the lack of publications devoted to operational evaluation, while majority of studies are devoted to laboratory tests, and the need for SHM to make a transition to the next level, i.e. in-situ investigations. The area that receives the most attention in the literature is feature extraction. Feature extraction is the name for a process of identifying damage-sensitive properties that enable the distinction of a damaged state from the undamaged. The most applied methodology consists of data compression and finding the link from assumed linear behaviour in an undamaged state to damaged state resulting in time varying behaviour. Authors emphasise disadvantages of using the neural network and machine learning techniques to detect damage. To map the relationship between the measured response and the change of structural parameters, a large training set from damaged and undamaged state is required. The latter is missing in an on-site application and is solely possible in laboratory testing.

In his PhD thesis, Rytter (1993) proposed a classification of SHM methods into four levels; based on the level of the detail the following classification is provided:

- damage identification (level 1);
- damage location (level 2);
- damage characterization (level 3);
- prediction and prognosis (level 4).

Recent advances, after 2000, are summarised in a series of review papers. Chang et al. (2003) focused on the overview of global techniques and recent applications in the USA, Carden and Fanning (2004) reviewed literature from the perspective of feature extraction and structural lifetime predictions. They have divided the methods into groups: natural frequencies, mode shapes (direct comparison of mode shapes, curvature), operational deflection shapes, modal strain energy, dynamically measured flexibility matrix, residual force vector, model updating, FRF (frequency response function), wavelet transform, neural network, genetic algorithm, and statistical methods. Karbhari (2005) focused his review on prognosis and service-life prediction issues. The majority of literature is focused on methods based on natural frequencies and modal properties, since they are easy to interpret in comparison to others, out of which some are more of an abstract nature. Mottershead and Friswell (1993) prepared a review on model updating methods. Overall identification methods can be divided into two groups; model-based or data-based. Model-based methods arise from simple analytical models. Due to the discrepancy between the measured and modelled modal properties, researchers started to develop methods based on observations. The development of finite element (FE) tools laid the foundations for matrix updating methods, which originate and are based on FE model updating, and for establishing a correlation of the FE model with the original state of the structure. Mode shapes can be obtained with multi-point measurements of the response, preferably to excitation in a single point (Pandey et al., 1991). Natural frequencies can be measured more accurately than mode shapes, while mode shape error can even reach 10% or more (Friswell and Penny, 1997). Damage extraction is based on comparison of mode shapes, e.g. a damaged set compared to an undamaged one by evaluating MAC and COMAC values as measures of similarity of two mode shapes (MAC - Modal Assurance criterion, COMAC - Coordinate Modal Assurance criterion (Allemang, 2003)). Modal strain methods are an option in cases where a particular vibration mode stores a large amount of strain energy. Flexibility matrix is the inverse of the stiffness matrix. The resulting structural displacement is related to the applied static force. This methodology is suggested to be used in damage identification of slender structures (for example chimneys) (Li et al., 1999). FRF methods are widely used; the method requires complete data on the excitation force and the system response as well. Wavelet methods perform well in thin metal testing, while in concrete, where different aggregate size and other geometrical inequalities cause too much disturbance and noise, they are not a preferred method. Neural networks, genetic algorithms, and statistical methods are data-based methods where the need for vast training sets with failure cases is a major disadvantage in applicability on life-scale structures. Mesquita et al. (2016), in a global overview on advances in structural health monitoring platforms, present the advances on SHM from its beginnings to 2015, with an emphasis on the recent works. The development went from destructive methods towards non-destructive (NDE) experimental methods. The most innovative work on damage detection is based on vibration analysis. Rytter's method was further extended to a 5-level approach where also structural risk is characterised and summarised for each level. Historic structures are studied as a special case as vulnerable structures with a high societal value. On-site inspections of the historic buildings that possess a high heritage value demand the use of non-destructive and non-invasive technologies. Heritage structures were built in times of different standards and building techniques. Based on the literature review, cracks, humidity damage, and displacements are the three major concerns in structural safety of historic buildings; another issue is preservation of the art work and aesthetic value. Abruzzese et al. (2009) presents a study case of a historical tower subjected to an earthquake. They have identified dynamic properties of the tower by performing accelerometer-based vibration measurements; the data were further used for numerical modelling and after the structure encountered a real earthquake, the measurements showed good correlation with the modelled phenomena. Lima et al. (2008) present the displacement and temperature monitoring system of 19 fiber Bragg displacements and 5 temperature sensors applied to a 16th century church. A pre-survey and numerical modelling was used to identify crucial places to mount the sensors to monitor evolution of natural frequencies due to the damage.

Publications concerning level 1 - damage identification are focused toward NDE and applied on scaled and also real-life structures. The used technologies are based on vibration measurement, system analysis, and expert knowledge, or solely on data collection and manipulation, often with the "black-box" approach. An example of the latter is laboratory failure tests, as for example Bandara et al. (2014) on a case study of a bookshelf structure, where artificial neural network training for undamaged and damaged state is used for damage prediction. The level 2 - damage location research is focusing on improving the possibilities for localisation. It is known that VB techniques perform well on the global level however, on the local level natural frequencies are often not sensitive enough, since higher modes' shapes are more appropriate, but they also require higher energy input, more sensors, and are less accurately measured. Xia et al. (2006) observed the effect of ambient conditions, e.g. temperature and humidity changes on the response of RC slab for the first 4 modes (Xia et al., 2006). After a 2-year extensive laboratory vibration testing of a slab subjected to humidity and temperature changes, no clear correlation of mode shapes with either parameter was established. However, with the increase of ambient humidity the concrete absorbs water and increases the mass, similarly the rise of the temperature has an effect on the modulus of elasticity. Increasing humidity and increasing temperature both cause a decrease in natural frequencies. Nie et al. (2012) proposed a novel methodology; phase space mode shape curvature parameter detection for real-time SHM for local damage detection. They applied the methodology to a scaled steel arch structure. Development of new sensors and smart materials is another thriving field; Alessandro et al. (2015) describe nano-composite cement-based sensors where deformation causes measurable change in electrical resistance. Gillich and Praisach (2014) present a methodology for damage detection in beam-like structures with detection of changes in the first 10 natural frequencies. The method is based on an extensive study regarding the behaviour of damaged and undamaged beams. The response of the beams before and after various types of damage is identified by applying a hammer impulse and accelerometer measurements. Lower vibration modes are used for damage detection. There are numerous successful level 3 - damage characteristics (type, development phase, extent, geometry), level 4 - characterization of structural risk, and level 5 - structural lifetime prediction (under current state, with measures, etc.) applications applied to bridges (De Sousa, 2012). Zhou et al. (2013), in a review of benchmark studies and guidelines for SHM, emphasise the need to objectively evaluate and compare numerous approaches presented in the literature. In the paper they summarised recommendations and lessons learned from worldwide research projects including SAMCO - Structural Assessment, Monitoring and Control (http://www.samco.org/), the European Collaborative Network (Rücker et al., 2006), health monitoring guidelines for major bridges presented by Aktan et al. (2003), and report on monitoring and safety evaluation of existing concrete structures presented by FIB Task group 5.1 (2003).

Damage prognosis is the future of structural health monitoring (Farrar and Lieven, 2006). The multidisciplinary field of damage prognosis is a profound challenge and is now in its initial stages of research and development. Together with the implementation of the decision-making platform applied to real-life infrastructure systems, this field offers a wide variety of challenges on the path to developing robust and applicable methods. There is a lack of real life implementations. Moreover, there are unresolved issues at every level, e.g. how to increase sensitivity to detect small amounts of damage in the very early stages without getting false positives. The advances in detection, sensor, and information technologies provide solid ground to make SHM an indispensable instrument in managing civil infrastructures. An increasing number of large-scale and real-life studies with successful implementation can be found in the literature. An increase in the research interest alongside with the interest of the end-users provide a proper atmosphere to push the SHM field one step further (Karbhari and Ansari, 2009; Das et al., 2016; Kong et al., 2017). Additional challenges in implementation are also compatibility with the existing traditional sensing systems, which are already installed and going one step further, owners should be included as part of SHM systems (Mesquita et al., 2016).

3.2 Dam Surveillance - Towards SHM on Dams

Dam surveillance is recognised as one of the key activities in dam safety. Dam surveillance includes installation of the monitoring equipment, visual inspections, performance monitoring and functional testing, data management, and diagnostics. Surveillance serves both to provide early detection of anomalies and to provide knowledge on long-term trends of the dam behaviour. The aim of dam surveillance should be oriented towards monitoring of the identified potential failure mechanisms for the structure under observation and detection of warning signs linked to the mechanisms leading to failure, identifying potential deterioration, and taking action before they become uncontrollable (or before the remedial work costs rise) (ICOLD Bulletin 138, 2009).

Dam monitoring has a very long tradition, longer than other in civil engineering fields. Traditionally this takes the form of visual inspections, which also nowadays have an indispensable role in dam surveillance activity and should never be completely abandoned (Bukenya et al., 2014a). In the beginning of the 19th century, the measurements on concrete dams were limited to topographic surveys of plan displacements. Similarly on embankments, settlement and movements were measured; the first piezometers used to observe the phreatic line were of open tube type and the first type of settlements gauges were plates, installed at the foundation level. With the evolution of dam shape, increasing height, and decreasing thickness, the need to understand complex behaviour drove the development of new monitoring techniques (ICOLD Bulletin 60, 1988).

Parameters, monitored on dams, are divided into three basic groups: load, response, and integrity parameters, which can be further divided into static (reservoir level, ambient temperature, humidity, crack and joint opening, strains, displacements) or dynamic parameters. Dynamic properties are determined through vibration monitoring, induced by ambient or forced load. Static, cyclic, and dynamic loads of different intensities reflect in response parameters: translations, rotations, vibrations of different intensities, uplift, seepage, and leakage. Cycling loadings are mostly connected with climate; e.g. variation of temperature (daily, seasonal), humidity, and insolation. Seismic load is of major concern when we have dynamic loads in mind. Other sources of dynamic loads on dams are wind, operation of the power plant, operation with outlets, explosions, etc. The effect of dynamic loads is reflected in vibration of the structure. We can distinguish between low-level vibration with amplitudes as low as only several microns or high intensity vibrations with millimetre amplitudes. Special attention should be given to the integrity parameters, in other words to indicators of functionality and performance. By observing the integrity parameters we get information on deterioration processes that affect the elementary function of the structure or its constituent parts (ICOLD Bulletin Preprint 180, 2018; Bukenya et al., 2014a).

Each dam is an individual case. In the design stage, when the desired safety level is established, it is also the appropriate moment to design the monitoring system. The concept of surveillance should be able to answer some plain and simple formulating questions: Which are the potential failure modes? What are the signs of potential deterioration (signs of ageing)? What do we want to see, measure? What is the object under observation? How will monitoring be performed? These questions are the backbone of SHM on dams, regardless the aim of the task is a technical or a scientific one. We monitor the identified failure modes and potential deterioration processes by observing the warning signs linked to the identified mechanisms. The program of monitoring activities follows the life-cycle of the structure (pre-survey, measurements during construction and first filling, measurements during operation, and in decommission). Monitoring on dams produces large amounts of time-dependent data which need to be converted into information. This is a demanding task, sometimes also referred to as "the art of data interpretation" (ICOLD Bulletin 138, 2009; ICOLD Bulletin 60, 1988; ICOLD Bulletin Preprint 180, 2018; ICOLD Bulletin 68, 1989).

After catastrophic dam failures in the 1950 and later, the dam community became aware of the lack of knowledge on the potential failure mechanisms for all type of dams. Early dams were of low heights; with the industrial revolution the height of dams suddenly rose. The dams grew larger and more slender, while the structural behaviour and problems associated with high dams were not even identified and were far from being understood. The answers could not be provided solely with qualitative (visual inspection) and quantitative (instrumented data collection) monitoring. Scaled shaking table tests were used to identify failure modes and to better understand the structural behaviour especially during strong motion earthquakes (Niwa and Clough, 1980). Koyna dam in India is probably one of the most studied dams. The dam severely cracked during a 6.5 magnitude earthquake. At the USBR structural laboratory, a 1:50 scaled model of a monolithic and cracked dam was built and tested on a shaking table (Harris, 2002; Harris and Travers, 2006). Moreover, they launched an extensive program to determine failure modes of concrete gravity dams and representative arch dams with reservoirs subjected to strong motions to determine seismic failure risks. Paine (2002) performed failure tests of a 1:150 scaled arch dams subjected to 14 Hz horizontal sinusoidal excitation where 5 different joint configurations were used. Crack growth in gravity dams is affected by the gravity effect, more than in other types of dams. To properly simulate crack growth on a scaled model, Plizzari et al. (1995) performed centrifuge tests where the gravitational field was multiplied with the factor of geometric scale.

On-site full-scale non-destructive tests are another tool to prevent failure and to learn. During the field tests, static and/or dynamic properties of the structure are monitored. Bukenya et al. (2014a) prepared a state-of-the-art literature review on health monitoring of dams with a focus on in-situ applications, while Salazar et al. (2017) prepared a review of the data-based models to describe dam behaviour. They emphasise there is an increase in publications on the use of advanced data-based tools in dam safety analysis and very few examples where the methodology is also practically integrated into the system. The studies are also mainly focused on the model assessment and not on the interpretation of the behaviour of the dam. Static monitoring is used for decades, statistical and theoretical deterministic models to interpret large amounts of data have been developed as well. Based on observations, Gamse et al. (2018) used a fourth degree polynomial to describe the hydrostatic level in a hydrostatic-season-time (HST) model; seasonal effects were modelled as a sum of trigonometric functions, while deformation is described with a combination of exponential and polynomial functions of time to describe reversible and irreversible behaviour. Léger and Leclerc (2007) described a hydrostatic-temperature-time model (HTT) using frequency domain algorithms of 1D transient heat transfer equation. TADAM - computer program for thermal analysis of concrete dams - was developed and applied to Schlegeis arch dam in Austria. Statistical analysis is commonly used to relate the measured response data to the large series of boundary conditions. Structural identification techniques that involve statistical methods and finite element modelling and enable correlation of structural behaviour with its properties, e.g. change of modulus of elasticity, are used. This procedure is not used as often as statistical analysis, since it is time-consuming and demanding, but its main advantage is that, besides time-based condition monitoring, it also provides a step forward to condition-based observations. Klun et al. (2016) applied the response surface method (RSM) to describe the relationship between the hydrostatic pressure, modulus of elasticity, and crest displacements; the method was used to describe the behaviour of an arch-gravity dam. The hydrostatic pressure values were obtained from a 35-years series of measurements and the modulus of elasticity was obtained using on-site ultrasonic tomography measurements. To get reliable data, long data sets are required. De Sortis and Paoliani (2007) performed a structural identification of 3 buttress dams in Italy with 40 years of monitoring data. Variation in crest movements was correlated with hydrostatic load. A non-dimensional parametric analysis established a correlation between the Young modulus, dam height, water load, and crest displacements. On uniformly distributed data, a discrete Fourier transform can be used to gain information on periodic phenomena (Pytharouli and Stiros, 2005). Principal component analysis, where partially dependent variables are linearly combined into an independent set of principal components, is a promising tool. The methodology was proven to be useful in managing a large amount of data provided by monitoring on dams. For instance, the Three Gorges dam in China has over 8000 sensors already installed (Hong et al., 2010). Multiple linear regression models are used to model the linear behaviour between the dependent and independent variables: a multi-layer perception and artificial neural network is used to detect complex trends, autoregressive models based on multivariate statistics where signal is decomposed in principal component time series and linear, and non-linear principal component analysis are used as well (Pytharouli and Stiros, 2005; Salazar et al., 2017).

Dynamic structural parameters can be obtained numerically with the finite element modelling. However, true values can be only obtained by on-site measurements and testing, whether by FVT or AVT. The first dynamic tests on dams were using FVT where the dams were excited with shakers and the dynamic properties were determined using frequency response functions. Severn et al. (1980) performed FVT on Wimbleball buttress dam, Llyn Brianne rockfill dam, and Baitings concrete gravity dam. The measurements conducted with different levels of water in the reservoir confirmed the reduction of natural frequencies with the rising water level and the decrease in the magnitude of response per unit of force. The test on the rockfill dam disproved the belief that embankment dams are not the most suitable for dynamic testing. The authors concluded that concrete gravity dams of the three tested types provided the most straight forward interpretation of their dynamic behaviour. Deinum et al. (1982), with the research on the Emosson arch dam in Switzerland, concluded the work of Severn et al. (1980) and provided the missing information on the seismic behaviour and dynamic properties for all four major types of dams.

In a research project by Clough et al. (1984), the vibration behaviour of a single-curvature Xiang Hong Dian arch dam in China was measured. The dam was tested while being excited with rotating mass shakers and under ambient effects as well. The measurements were compared with the analytical solutions of the dam-foundation-reservoir system. By analysing FRF curves, 12 natural modes in the range 4–12 Hz were obtained. The study demonstrated that the foundation and reservoir interaction can be measured using FVT. The model (1:60) and the prototype vibration tests of the Pine Flat gravity dam, along with numerical models, were the basis for estimating the dynamic properties of the dam system (Norman and Stone, 1981; Rea et al., 1972). A comparison of scaled and prototype tests revealed a strong agreement between them; the estimated natural frequencies in the numerical model were lower than those obtained with physical tests, since the numerical model did not include the hydrodynamic contribution. Based on the observations from the Kyona and Pine flat dam, through testing Fenves and Chopra (1986) proposed an equation to estimate the fundamental vibration period of a non-overflow concrete gravity monolith on a rigid foundation with an empty reservoir:

$$T_1 = 0.38 \frac{H}{\sqrt{E}} \tag{3.1}$$

where T_1 is the first fundamental vibration period in seconds, H is the height of the dam in meters and E is the Young's modulus of concrete in MPa (Fenves and Chopra, 1986).

Records on ambient vibration testing of dams date back to 1986 with tests on Contra Dam, a 220 m high arch dam in Switzerland (Bukenya et al., 2014a). Loh and Wu (1996) analysed Fei-Tsu arch dam with a relatively large width to height ratio (W/H = 4). The dynamic characteristics of the dam were obtained by seismic and ambient vibration data. Measurements were performed only in the upstream-downstream direction. Dynamic properties; first two eigenfrequencies, mode shapes, and corresponding damping ratios, obtained using both data sets were comparable. Daniell and Taylor (1999) conducted ambient vibration tests on a 56 m high Claerwen concrete gravity dam, as there were no suitable locations to mount mechanical exciters on the dam body. Excitation sources were wind, overspilling water, and operation with the outlet-pipes. The magnitude and distribution of the ambient forces could not be controlled, therefore with AVT it could not be guaranteed that during the test all the desired modes will be excited. The test lasted for two weeks. During the full reservoir condition, the excitation was caused by overspilling, and later by the operation of the pipes at the toe of the dam. Four channels of data were simultaneously sampled with a 128 Hz rate. They encountered a significant electronic drift due to temperature gradients before the equipment warmed up; once equilibrium was established, the drift disappeared. In total, they recorded over 200 hours of data. The authors conclude that measurements of wind speed and directions should be performed simultaneously during AVT. Blocks with 4096 samples in the frame with a 0.0312 Hz frequency resolution were used for frequency analysis. Even though significant noise was present in the data, 6 resonant peaks in the 6–14 Hz range were identified.

The development of the instrumentation and signal processing tools resulted also in evolution of ambient testing on dams. An experimental program of continuous dynamic evaluations of Swiss high altitude large dams launched in the 1990s. Five dams, including the Emosson and Mauvoisin arch dams, were instrumented with strong-motion accelerographs (Proulx et al., 2001; Darbre and Proulx, 2002). The instrumented dams were subjected to similar seasonal loading cycles, e.g. alternating low and high reservoir levels. Results obtained by ambient and forced vibration tests showed the change in natural frequencies of the arch dams with respect to the water rising in the reservoir. The rise in water from the minimal levels in May or June at first causes an increase of the stiffness of the dam, due to the contraction of the structural joints; however, after reaching a certain level the contributing mass of the reservoir causes a drop in the natural frequencies. Darbre and Proulx (2002) conducted a 16-month ambient testing on the Mauvoisin dam, with water levels dropping from 13 m to 127 m below the crest level. Moreover, an automated data acquisition system was established and for a period of 6 months, besides the influence of variable water levels also the influence of temperature variations on the natural frequencies were observed. Horizontal radial motions were captured on 16 locations at a 100 Hz sampling rate. Twice a day, time-series with 8192 samples were captured. 41% of the recorded data had to be rejected due to low signal-to-noise-ratio or malfunction of the recording system.

The sources of noise were identified to be the wind and the operation of the two powerhouses in the proximity. The first 6 eigenfrequencies were identified; the sole effect of the temperature could not be extracted. Authors assume that higher temperature would stiffen the dam in summer and soften it in winter, so the temperature would have the same pattern as the water rise cycle.

Ambient vibration tests on Cabril arch dam, built in 1954 in Portugal, captured 30-minute long time-series sampled with a 200 Hz sample rate. To acquire good frequency resolution, longer time-series were captured. The dam was excited with the operation of the power plant, located at the downstream toe of the dam. During the test, the units were operating on various power levels. One series of the data was captured also when the power plant was not operating. The maximum accelerations were captured when the units were at full operation at about $2{\cdot}10^{-3}g$, while when the units were at full stop, the acceleration amplitudes dropped to $0.05{\cdot}10^{-3}g$ peak value. With the frequency analysis they were able to identify a well defined and narrow peak at 3.57 Hz, which is the rotation frequency of the power units. Furthermore, the FE model confirmed the measured values. A section of the dam had cracked and they represented the cracked part of the dam with the reduced values of the vertical modulus of elasticity of the FEM in the damaged area. The modal analysis revealed that the first 3 modal shapes remained almost constant, while the 4th dropped significantly. This finding again agrees well with the experimental values. The model confirmed that the horizontal cracking of the Cabril arch dam is connected with the modification of the 4th mode shape (Oliveira et al., 2004; Mendes et al., 2004). This work is probably pioneering in output-only techniques in modal testing to monitor the development of the structural damage and establishing a continuous dynamic monitoring on a dam with the influence of the auxiliary structures on the structural response (Mendes, 2006; Mendes and Oliveira, 2009). The research is still ongoing, nowadays several dams in Portugal are included in the LNEC project of seismic structural health monitoring (Oliveira and Alegre, 2019).

Moyo and Oosthuizen (2009) performed ambient vibration testing of Roode Elsberg double-curvature arch dam in South Africa to gain the as-built dynamic characteristic of the dam to have a baseline for the long-term monitoring. Moreover, the in-depth knowledge on the structural dam-foundation and dam building blocks interaction will provide a better interpretation of structural behaviour. Wavelet analysis, due to its sensitivity to non-linear phenomena, was used to perform time-frequency computations. Between 2008–2010 four AVT tests were conducted. Vibration measurements were taken in the radial direction on the dam's crest and in the top and bottom galleries. Each block had one accelerometer mounted in the top crest elevation, while in the galleries, the accelerometers were placed on 10 m intervals. Testing lasted for two days, i.e. on the first day in the crest and in the lower gallery, and on the top gallery on the second day. The data acquisition set-up enabled simultaneous sampling of 8 channels; each sampling lasted for 1–5 minutes, with a 24-bit resolution at a 1000 Hz sample rate. One accelerometer was a stationary-reference accelerometer, while others were moved around the structure. The test enabled identification of the first 5 natural frequencies. The monitoring system on the dam consists of clinometers, stress cells, temperature sensors, pendulum clinometers, and crack gauges, with ambient testing being a part of the surveillance actions on the dam. Bukenya et al. (2014b) performed continuous AVT using 3 three-axial, force balance accelerometers, being in a continuous operation. The data signal is sampled with a 50 Hz sampling frequency and sent to a remote computer where 60-minute time windows are analysed automatically. The developed methodology has been used in ambient testing of Oanob Dam in Namibia, where unexpected behaviour of the dam with missing monitoring data has been observed (Hattingh et al., 2019).

By observing Alto Lindoso concrete dam, Mata et al. (2013) used a short-term Fourier transformation to identify whether the dam responds to short-term daily variations of temperature. A positive linear relation between radial displacements and air temperature of an arch dam was confirmed. Authors propose the methodology to be adopted in a continuous dam monitoring; they suggest that observation of the non-linear behaviour could be a sign of structural damage. Furthermore, a similar approach was applied to a case of Alto Ceira dam, an arch dam where a potential failure mode, failure of the right foundation embankment due to several discontinuities, was identified. A series of instruments to monitor reservoir water level, air and concrete temperature, uplift, discharges, foundation displacement, radial and tangential dam displacement, and relative block movements were installed on the dam and in its proximity. The decision rules concerning the identified failure mode are based on displacements' measurements. The automated system was established already during the construction; together with the numerical model and statistical analysis it is an aid to the dam management (Mata et al., 2014).

Gaftoi et al. (2016) are performing periodic dynamic monitoring of Gura Raului buttress dam in Romania. Their aim is early detection of ageing phenomena. The ambient vibration test is conducted twice a year, at the end of winter and at the end of summer. The measured values are compared to the values obtained during previous tests and with respect to the numerical model of the structure. The discrepancies connected with reservoir level and temperature variations are evaluated using a numerical model. Vibration measurements are performed using piezoelectric accelerometers. The initial measurements captured the response of the maximum height block in non-overflow and overflow sections and in two medium height abutment blocks. All further measurements included an additional maximum height block, so in total 5 blocks. The instruments are placed to capture upstream-downstream and right-left bank direction of vibration. The first phase measurements were conducted in 2013 and 2014 and serve as a baseline to which in later stages mathematical models were calibrated. 5 numerical models were created: for the maximum height block, for the medium height abutment block, maximum height spillway block, entire spillway section, and the model of the entire dam. The reservoir is modelled as added masses on the upstream face. The first 3 eigenfrequencies were evaluated.

Antonovskaya et al. (2017) presented a system to remotely monitor turbine vibration for early detection of hazardous hydrodynamic phenomena. Besides the Sayano-Shushinskaya accident, authors listed 5 other hazardous hydraulic phenomena occurring on Russian dams, connected to shaft beating and to fluctuation of the water column. Based on the analysis on seismic monitoring applied to dams and accidents, authors propose a methodology on how to extend the current practice to improve seismic monitoring and to perform continuous monitoring of turbine vibrations. Dams should be equipped with three-axial seismometers or velocity-meters, data acquisition should be at a rate higher than 50 Hz, the recording must be continuous and not in trigger mode as it is a common practice. An additional seismic observation point should be located in the area within 30 km from the dam with horizontal axis in cardinal directions N-S and E-W. Sensors on dams should have the lateral axis aligned in wise and cross-wise direction or in tangential and radial direction for arch dams. The sensor for turbine vibration monitoring cannot distinguish whether the vibration is connected with turbine malfunction or other sources, e.g. local earthquake, therefore seismologic monitoring should be continuous, and able to detect not only threshold events but also local tremors. A benchmark system is installed on the Chirkey HPP in Russia. The continuous monitoring system consists of seismology sensors installed at a distance of 7 km from the dam site, strong motion and ambient noise sensors in the dam body, and vibration control of turbines to monitor fluid pressure pulsations and turbine vibrations. In total 12 seismometers are installed in the system. GPS is used for time synchronization. Data acquisition is synchronised to $0.1\ \mu$s and processed in real time. Authors present a readout of time histories where a local earthquake and the turbine start occur in a short time interval showing maximum amplitudes of the turbine start to have higher values. Authors conclude that different dynamic events can be distinguished in the readouts, while vibration monitoring can successfully complement seismic monitoring and help with turbine diagnostics.

Dynamic testing offers a valuable insight into dams' behaviour and calibration of numerical models. A drawback of FVT is the need to measure excitation forces. Further development of output-only techniques offers a breakthrough and expansion on the application of dynamic testing. Dynamic monitoring of dams using AVT has been getting more and more attention over the last two decades. Most of the attention is given to arch dams, even though the worldwide population of arch dams is around 5% according to ICOLD World Register of Dams. Structural safety evaluation of dams is moving towards the implementation of new technologies, such as fibre optic or InSar, improving data processing capabilities, and prognosis (Colombo et al., 2016; Cheng and Zheng, 2013). Nevertheless, data pre-processing is commonly overlooked; the reality is that monitoring data are prone to reading errors or missing values, meaning data pre-processing is an essential step (Salazar et al., 2017). Further development should be aiming at improving the DAQ tools, while quantity and quality both play an essential role in successful implementation of dynamic testing as a constituent part of SHM on dams. During the literature review, we found information on how much of the data obtained could be possibly used for further analysis (Darbre and Proulx, 2002). Based on the literature, we could notice the focus of dam professionals gradually shifting from dam design to dam maintenance and to preserving the structural integrity during operation. In the future we will witness vibration monitoring becoming part of automated surveillance systems with partial and comprehensive tests happening as a part of maintenance plan. However, we do not expect the critical evaluation of qualified expert being completely abandoned. At the moment we can highlight two implementations of condition-based motoring on arch dams, i.e. Mauvoisin in Switzerland and Roode Elsberg in South Africa (Darbre and Proulx, 2002; Moyo and Oosthuizen, 2009). In both cases, experts from vibration monitoring on bridges were part of the first research team, while the initial learning phase in both cases was very extensive and lasted for years. This field provides many challenges, while every dam type is a case in itself, where the total of embankment and gravity dams represent approx. 90% of all dam types, acknowledging that the initial studies by Severn et al. (1980) have not yet been put under serious consideration.

3.3 Laser Doppler Vibrometry

The laser technology was invented shortly after 1960. A few years later, laser Doppler anemometry (LDA) as a novel technology to measure fluid velocity was introduced, and finally in the late 1970s, laser Doppler vibrometry (LDV) was invented (Yeh and Cummins, 1964; Vanlanduit and Dirckx, 2017). Both technologies have advanced since then and are nowadays widely used in different areas of applications, e.g. vibration measurements of human middle ear, non-intrusive diagnostic of fresco paintings, performance measurements of under-platform friction dampers for turbine blades (Gladiné et al., 2017; Castellini et al., 1996; Zucca et al., 2012). In a review paper "An International Review of Laser Doppler Vibrometry", the leading authors in this field present a detailed review of the chronological and technological advancement in the field (Rothberg et al., 2017). The basic principle of LDV is the Doppler effect in the laser light. LDV measures the vibration velocity at one single point on the surface of the object. Coherent

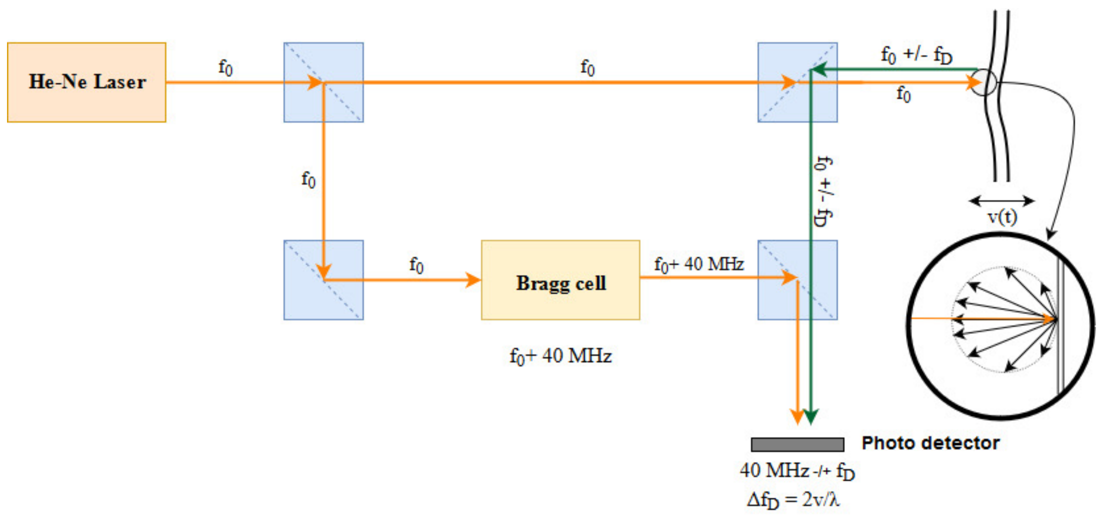

Slika 3.3: Shema delovanja heterodinskega vibrometra. Prirejeno po: Polytec (2016), Donges and Noll (2015) in Dainty (1975).

Figure 3.3: The schematic set-up of the vibrometer (heterodyne interferometer). Adapted after: Polytec (2016), Donges and Noll (2015), and Dainty (1975).

laser light is backscattered from an illuminated surface, while surface velocity is proportional to the Doppler frequency shift of the reflected laser beam. Fig. 3.3 shows the schematic set-up of the vibrometer. The laser beam is split into measuring and reference beam. The measuring beam travels to the vibrating surface, where it is reflected back towards the photo detector. The reference beam is guided to the Bragg cell, where its frequency is shifted by 40 MHz. This enables the distinction between positive and negative Doppler frequencies, since object movement away from the interferometer generates the same modulation pattern as movement towards it. The reference and measuring beam are mixed on the photo detector. When the measured object is at still the output modulation frequency is 40 MHz, if the object moves towards the interferometer, the frequency is increased and decreased when the movement is in the opposite direction. Vibration velocity (v) in the direction of the beam is directly proportional to the Doppler frequency (f_D):

$$f_D = \frac{2v}{\lambda} \tag{3.2}$$

where wavelength λ of HeNe laser light equals 633 nm (Strean et al., 1998). Measurements using LDV are limited to surfaces smooth enough to provide a sufficient amount of the reflected light. Unfortunately, the majority of the surfaces is at least to some extent optically rough with respect to the laser light wavelength. As a result, diffuse reflection speckles are formed. Speckles can be described (observed) as granular light patterns on the illuminated surface. They form when coherent waves of the incident laser beam are de-phased when the surface is optically rough. The reflected rays are still coherent, but since they scatter in all directions they interfere with each other in a constructive and destructive manner (bright and dark speckles are formed). The measurement is possible when a speckle has sufficient intensity to be recognised on the photo detector. The use of a retro-reflective tape helps us to obtain higher intensities of the backscattering. Retro-reflective tape is also optically rough on the scale of laser light, speckle patterns form even when reflective-tape is used (Martin and Rothberg, 2011). The amount of the backscattered light is also affected by atmospheric conditions (humidity, temperature) and laser beam propagation. The maximum stand-off distance is limited by the product limitations, while the actual range is usually smaller than specified, due to the conditions never being completely optimal. The optimal stand-off distances are located within the maximum range at points of visibility maxima. Maximum signal levels are obtained at distances that can be divided with the value of the laser cavity length (138 mm for PDV-100). In practice, the search for visibility maximum is in most cases unnecessary, while the devices are sensitive enough to make the measurement even in the lower visibility conditions.

The laser speckle is classified as a fundamental measuring uncertainty. Laser signal can be the carrier of motion information unrelated to normal surface motion, known under the term pseudo-vibration (Rothberg et al., 1989). Strean et al. (1998) studied the phenomena of speckling and signal drop-out in laser light. Theoretically, the beam diameter should be as small as possible so coherence is maintained over a larger detector aperture. An optimal Doppler signal is obtained if the detector receives only one intense speckle. However, in cases when the relative movement of the illuminated surface is not happening solely in the direction perpendicular to the laser beam, e.g. rotation machinery, when using of continuous laser scanning, this is not always the case. With sideways movements a new area is being illuminated and with time new speckle patterns are formed. This movement produces errors and signal drop-out, at which point the amplitude and phase become random and, in the worst case scenario, the measurement becomes impossible. In this special case the increasing of the laser spot can reduce the error caused by sideways movement, while this may increase the sensitivity to the surface tilt. Signal drop-out is easily recognised in the velocity output as an absolute drop in the time-series towards the zero value of the amplitude axis. This phenomenon is also described as the biased-low condition; when there is a large amount of signal drop-out occurring, this results in an absolute velocity output lower than the signal without drop-outs.

Martin and Rothberg (2008a) studied high-resolution images of partially and fully developed speckle patterns of a backscatter from surfaces with surface roughness from 1/60 to 1.6 of the wavelength of laser light. Retro-reflective tapes were tested as well. Sideways movements were divided in in-plane and tilting motions. Changes of speckle patterns due to in-plane and tilting motions of the surface were observed with respect to different beam diameters. The angular increment of the surface produces speckle translation on the photo detector, while larger diameter beams produce larger translations. Moreover, when the surface tilts the beam, the spot becomes elliptical, which means a new additional part of the surface is illuminated. The test proved this effect to be insignificant to the quality of the measurement. In-plane movement causes translation of the speckle as well as evolution of the pattern. The degree of change is correlated with the ratio between the beam spot diameter and the roughness of the surface. Authors conclude that increasing the beam spot diameter reduces the effect of speckle noise caused by in-plane motion. Martin and Rothberg (2011) further investigated sensitivity of commercial laser vibrometers to pseudo-vibration. Surfaces with different values of arithmetic average roughness parameter R_a from 1 μm to 11 nm and also retro-reflective tape surfaces were used. During the measurement the various surfaces were subjected to transverse and angular movement, and in-plane rotation. Transverse sensitivity has mean levels around 0.03% for smaller beam diameters and around 0.01% for larger diameters. The rougher surfaces are prone to higher traverse sensitivity; for example, Polytec PDV-100 has a transverse sensitivity of 0.03% for rougher surface and 0.009% for smoother ones. Tilt sensitivity has mean levels around 0.03 μms^{-1}/deg s^{-1} for rougher surfaces and 0.005 μms^{-1}/deg s^{-1} for smoother surfaces, while with increasing beam diameter the error increases. In-plane movement provides better results with smaller beam diameters, the error is in a range of 0.4 μms^{-1}/rad s^{-1} (beam diameter 45 μm)–0.9 μms^{-1}/rad s^{-1} (beam diameter 520 μm). By increasing the surface roughness, the sensitivity to error increases as well. When retro-reflective tape is used, sensitivity for transverse movements is decreasing with increasing beam diameter, while angular and in-plane rotation sensitivity increases. The overall performance of retro-reflective tape is comparable with R_a = 1μm roughness surface or smoother. Table 3.1 summarises the mean values (Root Mean Square - RMS is used) of sensitivity for pseudo-vibration phenomena for surfaces equipped with retro-reflective tape, subjected to maximum translational movement of 420 mm RMS, tilt of 0.51°–0.78° RMS, and rotation of a shaft with a 15 mm diameter. The use of retro-reflective tape is beneficial and should always

Preglednica 3.1: Občutljivost meritev na prečno gibanje, nagib in rotacije merjene ploskve ob uporabi odsevnega traku (Martin and Rothberg, 2011).
Table 3.1: Sensitivity to transverse and angular movement and to in-plane rotation when using the retro-reflective tape with respect to beam diameter (Martin and Rothberg, 2011).

Beam spot diameter [μm]	45	60	90	520
Transverse movement [%]	0.033	0.030	0.0245	0.011
Angular movement [μ ms^{-1}/deg s^{-1}]	0.086	0.049	0.0572	0.279
In-plane rotation [μ ms^{-1}/rad s^{-1}]	0.457	0.616	0.53	1.68

be used, unless there is an obvious reason why it cannot be used. For example the in-plane rotation sensitivity reduces even by 20%. The tests were performed on relatively smooth surfaces and have demonstrated that the reflective tape is beneficial also in comparison to surfaces coated with reflective paint. It is safe to assume that the applications in SHM in majority of the cases deal with material with rougher surfaces. Phenomena of pseudo-vibration and speckle noise are even nowadays still not fully investigated and explained. Advanced laser applications will definitively be a subject of further research (Halkon and Rothberg, 2017a). According to the state-of-the-art, laser speckle becomes problematic when the governing periodic target motion (such as rotation) is a source of speckle movement and evolution, while pseudo-vibration also becomes periodic with frequencies close to the fundamental frequency and higher order harmonics. Test sites suffering from non-periodic speckle noise have elevated white noise threshold, while periodic pseudo-vibration affects the data above the random noise threshold, which has to be considered in the interpretation of vibration measurements. The phenomenon was well documented during continuous scanning of rotating machinery (Rothberg et al., 1989). At the moment, the most successful application to break the effect of pseudo-vibration noise is by introducing a small sideways motion to the laser, to break the periodicity of the noise (Halliwell, 1996).

Accelerometers are probably the most commonly used vibration monitoring sensors (Hsieh et al., 2006). However, laser vibrometer can be used as an effective alternative to the traditionally used contact measurements. Cristalli et al. (2006) performed a comparative study between laser vibrometer and accelerometers to be used in an on-line testing to detect mechanical faults of motors at the end of their production line. The authors concluded that displacement measurements using LDV were not an appropriate tool for these tasks, since the displacement amplitudes for higher harmonics, which are indicators of structural damage, were too low. However, velocity measurements using LDV and accelerations from accelerometers are both appropriate. Both measurements are affected by noise; accelerometers are affected by electromagnetic noise and contact flaws during mounting, while the vibrometer is affected by tripod vibrations excited by the operation of the production line. The main advantage of the LDV is its non-contact nature and the simplicity of measurement. The relative nature makes the measurements with LDV susceptible to the vibration of the instrument itself. This issue is being addressed, e.g. Halkon and Rothberg (2018) are investigating the possibility to operate LDV mounted on unmanned aerial vehicles, where corrective measurements using accelerometers are used to remove the input contribution of the instrument movement. Similar is the application of LDV where the object under investigation is hidden from the line of the laser beam, using a glass prism mounted on a vibrating surface. A corrective measurement is performed with the accelerometer mounted on the back side of the glass prism so that the true vibrating response is obtained (Halkon and Rothberg, 2017a).

4 AGEING OF DAMS

Any long-term behaviour that leads to any change in dam properties with the passage of time, and might affect dam safety, is described as dam ageing (Zenz, 2008). Based on ICOLD definition, ageing is defined as a structural deterioration that occurs more than 5 years after the beginning of operation. The deterioration that occurs before is associated with inadequate design and defects during construction or improper operation, where the effect of the exceptional events is excluded (ICOLD Committee on Dam Ageing, 1994). Ageing of dams and preservation of their structural health is rapidly becoming one of the major challenges for the entire dam engineering community.

According to SLOCOLD's data, approximately 60% of Slovenian large dams were built before the 1980. In total, we have 42 large dams (according to ICOLD criteria); three historic dams (Ovčjaške klavže, Belčne klavže, and Putrihove klavže) are over 200 years old. The mean age of modern large dams in Slovenia is 43 years[1]; the oldest modern-age large dam in Slovenia, Završnica, is 105 years old. Brežice dam is the newest large dam, it was constructed in 2017. Fig. 4.1 presents the time dynamic of large dam construction in Slovenia. The golden era of Slovenian dam construction was from 1950 to 1990. Fig. 4.2 presents the number of large dams in Slovenia according to the dam type. The most common dam type is concrete gravity and combined type of dam (concrete gravity and embankments). In total, we have 25 of such dams (18 PG and 7 combined TE/PG)[2], together they represent 60% of Slovenian dam inventory (see Fig. 4.3).

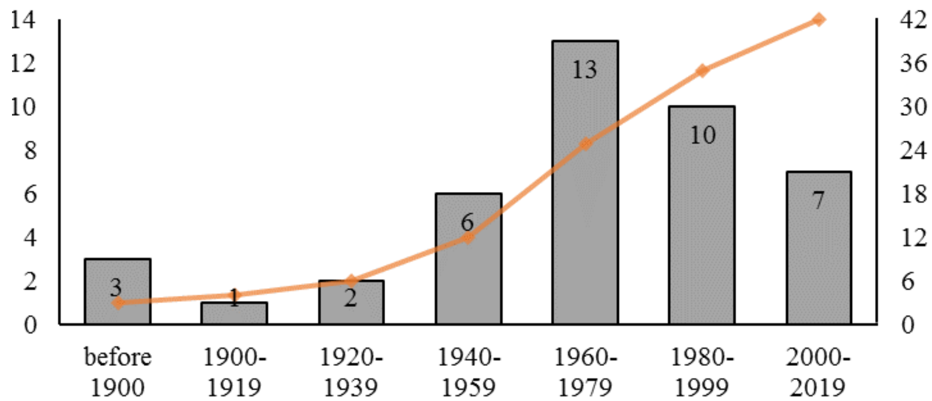

Slika 4.1: Število pregrad, zgrajenih v Sloveniji, razdeljeno v 20-letna okna. Vir podatkov: SLOCOLD.

Figure 4.1: Number of dams in Slovenia built since 1900, divided into 20-year periods. Data source: SLOCOLD.

[1] age data values for year 2019

The mean age of concrete dams is 50 years, the majority of them being built in the period 1954–1986; after 2000 we have built eight large dams (4 TE, 1 PG, 3 TE/PG/TE)[2]. The majority of large dams in Slovenia was built for hydropower purposes, 80% of concrete dams are in hydropower use (Kyžanowski and Humar, 2018).

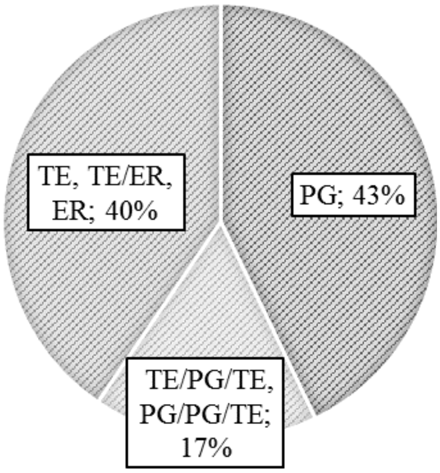

Slika 4.2: Delež pregrad v Sloveniji po tipu[2]. Vir podatkov: SLOCOLD.
Figure 4.2: Number of dams in Slovenia according to dam type[2]. Data source: SLOCOLD.

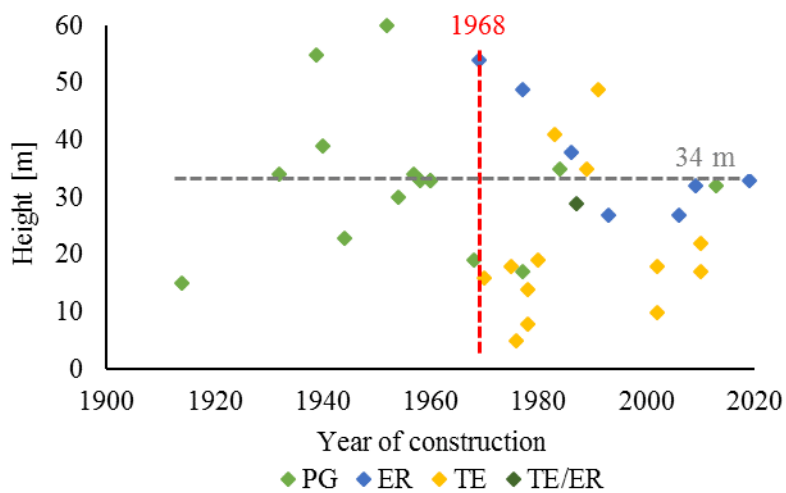

Slika 4.3: Leto izgradnje sodobnih slovenskih pregrad po tipu in glede na konstrukcijsko višino. Rdeča črta označuje leto, ko je bila zgrajena povprečna betonska pregrada, siva črta predstavlja povprečno višino betonskih pregrad. Vir podatkov: SLOCOLD.
Figure 4.3: Construction year of modern dams in Slovenia with respect to the structural height and dam type. Red line represents the mean year of construction of concrete dams and grey line the mean height of concrete dams. Data source: SLOCOLD.

The dam ageing phenomenon is not unique to Slovenia, e.g. in China the majority of dams were built between 1950–1970. According to the United States National Inventory of Dams, more

[2]ICOLD classification of dam types: PG - concrete gravity, TE - earthfill embankment, ER - rockfill embankment.

than 80% of their dams were built before the 1979, similarly in Australia where more than half of their dam inventory was built before 1969 (Su et al., 2013; SLOCOLD, 2018; USBR, 2018; ANCOLD, 2018).

A concrete dam built for hydropower purposes goes through some typical stages: design stage, construction, first filling of the reservoir, operation, repairs, and decommissioning. In the design stage, the characteristics of the dam are specified. The designed structure is a generic, idealised dam, with idealised behaviour. Once the dam is constructed and the reservoir filled, the as-built (real) values of the idealised parameters can be obtained. The first few years of a dam's life are the most critical; the first filling of the reservoir presents a major transition in the local environment, the dam structure and waterways have to adapt to the new load condition while a new equilibrium is established. The longest period in a dam's life cycle is the operation phase, which is occasionally interrupted by regular maintenance periods. The duration of this period is a subject of quality and intensity of the deterioration processes. During this period, regulations concerning building construction, dam ownership, and monitoring operators can change. These changes, to some extent, have a direct or indirect influence on dam ageing (Tekie and Ellingwood, 2003). For example, a hydropower dam built somewhere in the mid-20th century has most likely surpassed transition in operation, due to the reorganisation in the power supply market, which has a consequence on the hydropower dams to operate under less favourable conditions.

Ageing occurs due to time-related phenomena that affect chemical, physical, and mechanical properties of the materials (Smoak, 1996). Concrete gravity dams are especially prone to the following:

- alkali-aggregate reaction;
- chemical attack (chloride, sulphate);
- abrasion and cavitation;
- water seepage;
- concrete expansion and contraction;
- temperature cycles (e.g. freezing-thawing);
- operational loads.

The reason for the alkali-aggregate reaction is the use of reactive aggregates; chemical attack is caused by the acidic water, or sulphates present in water and results in leaching (dissolving of the concrete mix) or expansion. Transport mechanisms, i.e. abrasion, cavitation, and erosion can happen on surfaces in contact with water. Temperature cycles due to daily and seasonal variations of temperature, and also as a side effect of hydropower operation with the exposure to continuous vibrations at relatively low amplitudes, cause ageing. Over time these vibrations can initiate the formation of fatigue cracking, i.e. at first on a microscopic scale and later with further growth, which evolves in exponential manner to the situation of reaching the critical point. The most vulnerable are points of stress concentration, joints, discontinuities, and nonhomogeneities. The severity of the damage caused by the described phenomena can be limited with measures that prevent penetration of the aggressive substance in the concrete (de Wrachien and Mambretti, 2009).

Crack growth after the crack initiation is slow at first due to gradual wear. Under the constant loading-unloading amplitude, the damage is slowly accumulating and eventually evolves into the exponential growth phase where the damage development becomes accelerated. The process is schematically presented in Fig. 4.4. The evolution of damage due to low-amplitude vibration is considered a slow process. Once the crack opens with the initial length l_0 under constant loading conditions, its length remains roughly the same or increases only a little; this stage can last for years or even decades. However, when the fatigue progresses, at one point in time, cracks start to grow exponentially. This phase of progressive fatigue is fast, and crack length can soon reach a critical value, which is defined as the length where instabilities start to occur (not necessarily resulting in structural failure). Higher amplitudes on the other hand, caused by predictable or unpredictable discrete events, are a source of faster accumulation of damage. These events additionally feed the damage supply, which is still driven by gradual damage accumulation mechanism. One example of vibration-caused fatigue on hydropower dams is the operation of turbines for power production. Induced amplitudes are low with relatively high frequencies in comparison to the natural frequencies of the structure. However, the continuous operation provides for high accumulation potential. Regular starts and stops are a case of predictable discrete events and emergency operation manoeuvres account for the unpredictable discrete events (Fritzen, 2006).

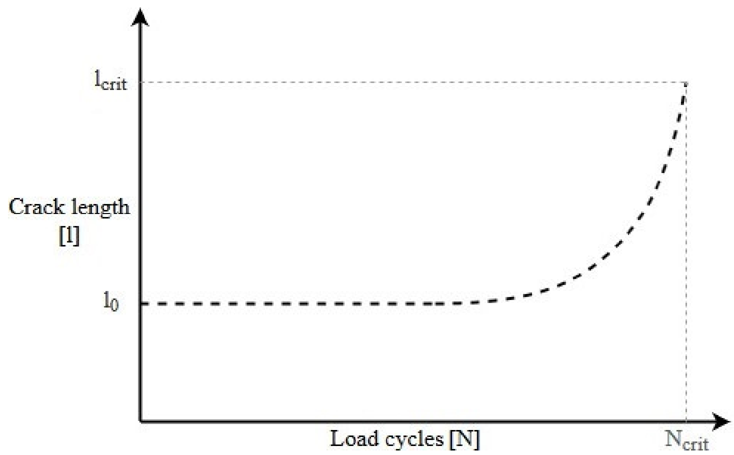

Slika 4.4: Eksponentna rast razpoke zaradi vibracij s stalno amplitudo. Povzeto po: Fritzen (2006).

Figure 4.4: Schematic representation of exponential crack growth under vibration loading with constant amplitude. Adapted after: Fritzen (2006).

4.1 Behaviour of Concrete

Concrete is a composite material consisting of cement, water, aggregate, and admixtures. Properties of the composite depend on the properties of each component, their ratio, curing and placement speed, placement quality, and atmospheric conditions. Mass concrete, used in dam construction, is very specific; the maximum aggregate size is usually larger compared to ordinary concrete, the maximum size is somewhere between 50–80 mm, and aggregates are usually manufactured from rocks obtained near the dam site. Concrete in gravity dams is mainly unreinforced, with the exception of the reinforced concrete near the surface and on critical elements. Due to large volumes of mass concrete being placed, it is important that it has low hydration temperature properties. The concrete body consists of multiple monolith blocks. Homogeneity of the built-in concrete plays a key role. Based on the location in the dam structure, specific performance requirements are preferred, e.g. concrete at the faces of the dam needs to have water-tightness quality, resistance toward freezing-thawing cycles, and abrasion; rock contact concrete has good bonding performance; and structural concrete also has good placing performance. Usual air content in a mixture is between 4–7%, for water tight concrete the standard w/c ratio is 60% or less. The water content in the concrete mix influences the resistance to cycle loading, dry concretes have a higher fatigue strength than concretes with higher water content. Higher water content can be linked to higher values of drying shrinkage and higher initial micro-cracking potential (Japan Society of Civil Engineers, 2007; Lamond and Pielert, 2006; de Wrachien and Mambretti, 2009; ACI Committee 207, 2009).

Even perfectly placed and cured concrete develops a system of micro-cracks as a consequence of internal stresses between the cement paste and aggregates developing during the hardening process. Especially mass dam concretes are subjected to extensive early-age cracking (de Wrachien and Mambretti, 2009). Mihashi and Leite (2004) divide the shrinkage mechanism of early-age concrete into three groups: autogenous, drying, and thermal shrinkage. Autogenous shrinkage is a consequence of the absorption of water while cement hydrates, drying shrinkage is caused by the evaporation of water from the hardened concrete, and thermal shrinkage is caused by the cooling of the concrete. These three mechanisms act at different times, while the majority of early-cracking is considered to develop in the first seven days after the placement, and it is considered that the process ends by the 60th day (Safiuddin et al., 2018). Autogenous and drying shrinkage result in volumetric changes, while autogenous shrinkage results in uniform deformation and it starts just a few hours after the placement and acts until the hydration process is completed. On the other hand, drying shrinkage happens a few days after placement and results in non-homogeneous deformation; the shrinkage initiates at the surface and progresses towards the core. Thermal shrinkage acts as a consequence of heat dissipation generated during the hydration process with respect to the ambient temperature. Additional heat causes the expansion of the concrete during the hydration process. In the later stages, when the concrete cools down, the associated shrinkage causes cracking (Safiuddin et al., 2018; USBR, 1988).

There are three types of micro-cracks in concrete based on the location of their formation: bond cracks on the aggregate-cement interface, mortar, and aggregate cracks; and two types based on their topology: simple (one isolated crack) or combined (multiple cracks growing together) (Sriravindrarajah and Swamy, 1989). The aggregate grains are stiffer than the cement paste, while they limit free shrinkage of the paste during the hydration process and cause formation of bond cracks (Ortiz, 1985). Concrete is a heterogeneous material. When subjected to compressive loading the compressive stresses in the direction of the loading are higher in the aggregate than in the cement paste. Aggregate is assumed as being a linear, elastic, and brittle material, while cement paste as being a non-linear, softening material (Wicke et al., 1999). Derucher (1978) observed with the microscope the development of bond cracks while subjected to compressive loading. He discovered that at approximately 15% of the ultimate compressive strength of concrete, bond cracks start to propagate, and at 30%, individual bond cracks start to bridge between one and another. At approximately 45% of ultimate strength, the bridging is complete and mortar cracks start to develop, and at 75% of ultimate strength, mortar cracks start to join. Mortar cracks grow at an accelerated rate in a direction more or less parallel to the load. When subjected to tension, further development and propagation of cracks starts at approximately 70% of tensile strength of concrete (ACI Committee 224, 2002). When subjected to tension, after the cracking occurs, the deformation localises. The tests show that specimens usually fail with one large crack perpendicular to the applied external load (Plizzari et al., 1997; ACI Committee 207, 2009).

Cracks form differently in concretes of lower and medium strengths than in those of high strength. In low and medium strength concretes, micro-cracking is concentrated in the cement paste and the cement-aggregate interface, while cracks in high strength concretes propagate also through the aggregate grains, which is the case in dam concrete with a larger maximum grain size. The development of micro-cracking in tension and compression is concentrated in a limited region in the composite (Wicke et al., 1999). Crack growth has two distinct stages: initiation and propagation phase. We assume the propagation phase has initiated when cracks grow to the macro-level size. Micro-crack growth is progressive under sustained and cyclic loading. Fatigue represents an irreversible accumulation of damage. Failure occurs when the resistance of concrete against repeated loading is exceeded by the damage accumulation with each load cycle. Accumulation of damage in a material subjected to variable amplitude loading is commonly described by Palmgren-Miner as a damage summation rule (Ciavarella et al., 2018):

$$D = \sum_i \frac{n_{Si}}{N_{Ri}} \tag{4.1}$$

where D represents a dimensionless index of fatigue damage, n_{Si} is the number of cycles at a given stress and amplitude level, and N_{Ri} is the number of cycles at failure for a given stress level. Values of index D vary from 0 for the intact material to 1 at failure (Ciavarella et al., 2018). However, the Palmgren-Miner rule does not consider the effect of load sequence and loading history. With increasing damage, the load is resisted only by the safe portion of the structure;

in practice the failure occurs when *D<1* (Brincker and Ventura, 2015). Fatigue failure can be classified according to the oscillation amplitude and the number of cycles to:

- low cycle fatigue $N_f \leq 10^3$with high oscillating stresses;
- large cycle fatigue $10^3 \leq N_f \leq 10^7$ with low oscillating stresses;
- very large cycle fatigue $N_f \geq 10^7$ with very low oscillating stresses.

An example of low cycle fatigue with a high amplitude is an earthquake, while the high-cycle fatigue can be caused by wind, waves, traffic, operation of machines, etc. Constant amplitude cycling loading affects micro-crack growth and thus the failure of concrete (Shah and Chandra, 1970). Micro-cracking fatigue damage is irreversible, the evolution of the *D* index during the life-time of the material can be phenomenologically described with an S-shaped curve presented in Fig. 4.5 (Destrebeco, 2004). The figure presents a simplified case of fatigue accumulation due to the constant amplitude cyclic load. The number of loading cycles on the *x* axis is represented

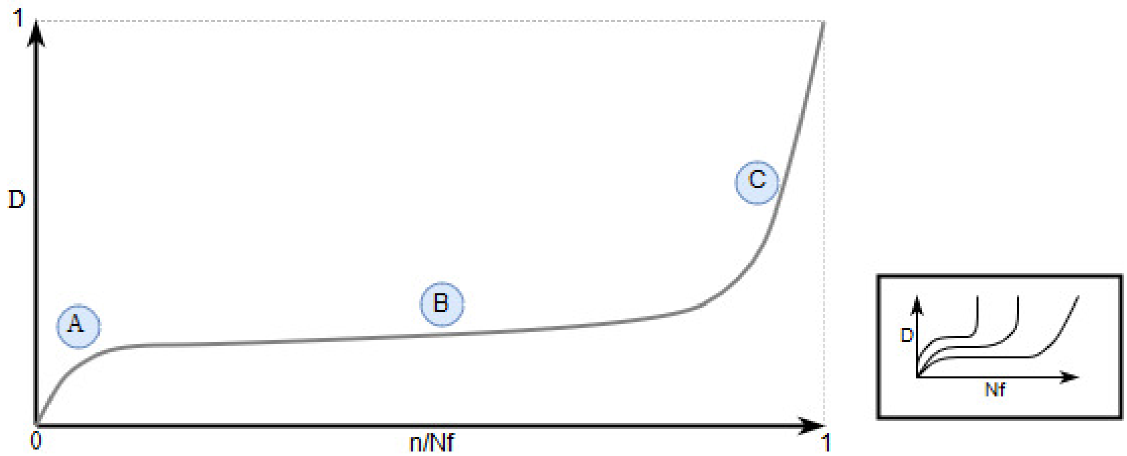

Slika 4.5: Kumulativni potek škode zaradi utrujanja v betonu ter raztros rezultatov. Prirejeno po: Destrebeco (2004) in ACI Committee 224 (2002).

Figure 4.5: Fatigue damage accumulation in concrete and scatter of damage accumulation. Adapted after: Destrebeco (2004) and ACI Committee 224 (2002).

with a normalised value with respect to the total number of cycles to failure N_f, while the *y* axis represents the fatigue damage index (*D*). The analogy between the fatigue deterioration and population growth curve is presented by Ray and Kishen (2010). The damage accumulation process consists of three distinct phases. Phase (A) represents the rapid growth of the bond micro-cracks in the 1st phase after the cycling loading is applied; in this phase 5–10% of the total number of loading cycles occur. This phase is followed by a long period where the rate of deterioration is stabilised (B). Cracks grow further at a very slow rate when the structure is subjected to elastic stresses substantially below the peak strength of the material. With the accumulation of damage, the load is resisted only by the remaining healthy part of the structure. After a certain amount of damage (with respect to the frequency and amplitude), the final phase of accelerated fatigue usually starts after the 80–90% of total number of cycles (C). At this stage, cracks propagate at an accelerated rate, damage is well visible and finally the material fails. Fatigue load can act as cycles of:

- alternate (tension-compression) stress,
- repeated (0 stress-stress (tension or compression)) stress, or
- undulated (only fraction of the load is cyclic) stress (Plizzari et al., 1997).

Fatigue strength can be defined as a portion of the static strength that can be repeatedly subjected to a given number of cycles. In practice, the stress level at $N_f = 2\times10^6$ cycles on the S–N curve defines the fatigue strength of the given material (Lantsoght et al., 2016). Fatigue tests have very scattered results; coefficients of variation typically show scatter of 30% or even more (Yao et al., 1986). The tested number of cycles to failure N_f can vary substantially due to the non-linear damage accumulation process and random characteristics of the tested material. The subject was extensively studied. Several authors proposed the use of probability when addressing the fatigue of material, furthermore, the use of Log-normal and Weibull distribution to describe concrete fatigue life as well as the use of S–N–P curves to describe the stochastic nature of the process were proposed. The basic constitutive law to describe the relationship between Cauchy stress σ, strain ε, initial Young modulus of concrete E_0, and damage parameter d can be written as (Liang et al., 2017):

$$\sigma = (1-d)E_0\varepsilon \tag{4.2}$$

In laboratory testing, the measured Young modulus at failure (E_f) was usually approximately at 60% of the E_0. If we define the change of damage as a ratio between the Young modulus in the undamaged state and the evolution of the modulus of elasticity during fatigue loading (E_d), we can describe the damage index as Destrebeco (2004):

$$d = 1 - \frac{E_d}{E_0} \tag{4.3}$$

Taking into account the laboratory testing of Thun et al. (2007), the value of damage index at failure therefore equals to:

$$d_f = 1 - \frac{E_f}{E_0} = 0.4. \tag{4.4}$$

Most of the research work considers only uni-axial fatigue loading scenarios, while real concrete structures are usually subjected to bi-axial (or also multi-axial), non-proportional fatigue loading, with fixed static load along one axis and cycling fatigue acting in the direction of the second axis. Wang and Song (2011) tested the performance of concrete cores subjected to cycles of compressive, tensile, and alternating stress, in biaxial stress condition. Three lateral confinement stress levels with respect to 28-day compressive strength *V* were considered $|\sigma_{lat}|/f_c = 0$, 0.25 and 0.5, respectively. The specimens were then subjected to sinusoidal cycles until failure. Based on the linear regression analysis, Wang and Song (2011) derived the following equations:

- A modified Aas-Jakobsen equation for fatigue under biaxial compressive condition.

$$\begin{aligned} \left|\frac{\sigma_{max}}{f_c}\right| &= \alpha - \beta(1-R)\log N_f \\ \alpha &= 1 + 0.83040\Big(\frac{|\sigma_{lat}|}{/f_c}\Big) \\ \beta &= 0.0638 + 0.115\Big(\frac{|\sigma_{lat}|}{/f_c}\Big) \\ 0 &\leq \left|\frac{\sigma_{lat}}{f_c}\right| \leq 0.5 \end{aligned} \tag{4.5}$$

Where $R = \sigma_{min}/\sigma_{max}$, α and β represent material constants correlated with the lateral stresses.

- Equation for tensile fatigue with constant lateral stress.

$$\log N_f = -12.87\frac{\sigma_{max}}{f_c} - 5.69\left|\frac{\sigma_{lat}}{f_c}\right| \tag{4.6}$$

Thun et al. (2007) performed uni-axial tensile fatigue tests on cylindrical concrete cores. They were unsuccessful to determine which factor has the prevailing influence on the fatigue life of specimens. The authors concluded that a sample will survive more than 1000 tensile load cycles if the deformation rate at 2 Hz loading cycle is under $0.05 \cdot 10^{-3}$ mm/cycle.

- Equation for alternate tensile-compressive fatigue with constant lateral stress.

$$\frac{\sigma_{max}}{f_t} = -0.5636\left|\frac{\sigma_{lat}}{f_c}\right| + 0.9818 - \left(0.0764 - 0.0458\left|\frac{\sigma_{lat}}{f_c}\right|\right)\log N_f \tag{4.7}$$

This experiment revealed the effect of lateral pressure to improve the compressive fatigue strength. However, in alternating stress-compression and tension fatigue scenario, the presence of lateral compression stress reduces the fatigue strength of the concrete. Moreover, a higher lateral stress reduces the fatigue strength of the concrete.

Keerthana and Kishen (2018) performed a study with variable amplitude fatigue loading on three different sizes of notched concrete beam specimens subjected to cycling loading with 1 Hz frequency, with a minimal load threshold at 0.2 kN and maximal load threshold in the first round of cycles at 0.25 kN and raised by additional 0.25 kN after every round of 250 cycles. Compressive strength and modulus of elasticity were determined on standard cubes poured at the same time as the test specimens; with the values of modulus elasticity 35305 MPa, compressive and tensile strength of 56 MPa and 3.6 MPa, respectively. When cycling loading was applied, specimens failed at the critical crack length of approximately 40% of the beam depth. The test also showed an instantaneous increase of crack length when the overload cycle is applied. Small, medium, and large specimens were all subjected to the same type of time-histories (the same initial load, level and gain). The small specimen failed first, then the medium one, and finally the large one after 2366, 4317, and 6581 cycles, respectively. A parametric study on the effect of maximum aggregate size with respect to specimen size confirmed that the size of the element affects the numerical result. Increasing the element size in the model causes numerical results of the fatigue life computation to deviate from the experimentally obtained values. The task of applying test results of laboratory specimens to the analysis of structures, where larger maximum aggregates are used, needs to be done with caution and conservatism, e.g. uni-axial tests usually have specimens with a maximum aggregate size of 40 mm.

Propagation of fully developed cracks can be described using the Paris law (Paris and Erdogan, 1963) where crack extension per cycle $\left(\frac{da}{dN}\right)$ is a function of crack length (a), stress range, and material properties (C_i):

$$\frac{da}{dN} = f(\sigma, a, C_i). \tag{4.8}$$

Ray and Kishen (2011) performed dimensional analysis to capture the size effect and validated their model with the data from different various experimental results in the literature. The process of crack extension per cycle is governed by 8 variables: ΔG - energy release rate range, G_f - fracture energy, σ_t - tensile strength, R - loading ratio, a - crack length, D - structural size, ω - loading frequency, and t - time.

$$\frac{da}{dN} = \Phi(\Delta G, G_f, \sigma_t, R, a, \omega, t) \tag{4.9}$$

After the application of the Π-theorem, Φ function contains five dimensionless terms and can be written as:

$$\frac{da}{dN} = \Big(\frac{G_f}{\sigma_t}\Big)\Phi\Big(\frac{\Delta G}{G_f}, \frac{\sigma_t}{G_f}a, \frac{\sigma_t}{G_f}D, R\Big). \tag{4.10}$$

After further reduction of the dimensions and calibration, the dimensionless parameter can be written as a function of $\frac{\sigma_t}{G_f}D$ and R and is considered a constant for a particular concrete with the same material mix and at constant loading ratio.

$$\log(\Phi) = 1.3963\Big(\log\Big(\frac{\sigma_t}{G_f}D\Big)\Big)^2 - 15.399\Big(\log\Big(\frac{\sigma_t}{G_f}D\Big)\Big) + 34.663 + 2.6R \tag{4.11}$$

And the fatigue life can be computed with:

$$N_f = \int_{a_0}^{a_c} \frac{da}{G_f^{1-\gamma_1-\gamma_2}\Delta G^{\gamma_1}\sigma_t^{\gamma_2-1}a^{\gamma_2}\Phi}. \tag{4.12}$$

where a_0 and a_c are the initial and critical crack length, γ_1 and γ_2 are material constants with values 5.4113 and 0.0648, respectively. The size independent fracture energy G_f value is 0.038 N/mm.

The response of the concrete to cyclic load can be represented in a σ-ϵ diagram or in Wöhler diagram that describes the relationship between the level of stress and the number of cycles to failure. Deterioration causes a change in mechanical properties, e.g. a drop in the modulus of elasticity and in residual strain. On a simplified σ-ϵ diagram in Fig. 4.6, a scheme of failure due to cycling fatigue loading occurs once the fatigue curve reaches the material envelope, obtained with static test (Plizzari et al., 1995). The moment of failure depends on amplitude, frequency, and mean value of the fatigue load. Goodman-Smith's diagram in Fig. 4.8 and

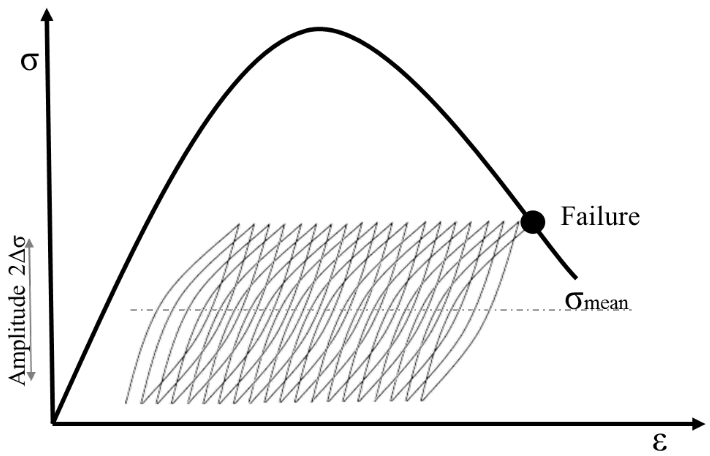

Slika 4.6: Odziv betona na ciklično obremenjevanje in razbremenjevanje. Prirejeno po: Destrebeco (2004).
Figure 4.6: Behaviour of concrete subjected to undulated cyclic load. Adapted after: Destrebeco (2004).

Haigh's diagram in Fig. 4.7 are based on a modified Aas-Jakobsen formula with β = 0.0685 in uni-axial compression. The formula is validated for frequency range from 0.1 to 150 Hz and to $2{\cdot}10^6$ cycles with loading up to value $S_{max} \leq 0.8$. The frequency of the loading has a dominant role when we deal with high *S* ratios; in these cases the equation 4.5 overestimates the number of cycles to failure. Haigh's diagram (Fig. 4.7) represents the influence of the loading amplitude (presented with ratio $R = \sigma_{min}/\sigma_{max}$) in each loading cycle to the overall fatigue strength (with the corresponding value of ratio $S = \frac{\sigma}{f_c}$). Higher fatigue load amplitude with respect to the strength of concrete results in failure after a lower number of cycles. On the other hand, concrete subjected to lower fatigue load and lower amplitudes can survive a high number of cycles. In Goodman-Smith's diagram (Fig. 4.8), the curves representing fatigue strength to a number of cycles to failure become linear in a semi-logarithmic plot. Goodman-Smith's diagram has been validated for *S* values below 0.8. This is marked with the red line in the graph. The number of cycles to failure will increase with lower *S* and *R* ratios. Whether the structure will survive is also conditioned by the loading frequency and the shape of the cycle as well (sinusoidal, triangular, square). Fatigue strength of material is influenced by many factors: aggregate type and its characteristics, mixture, grading, w/c ratio, porosity, methods and quality of placement, curing, age of the element, loading history, etc. Fatigue in concrete is a subject of extensive research, however, due to the heterogeneity of the material, this phenomenon is a lot less investigated than for instance in steel. Brittle material mostly possesses only elastic

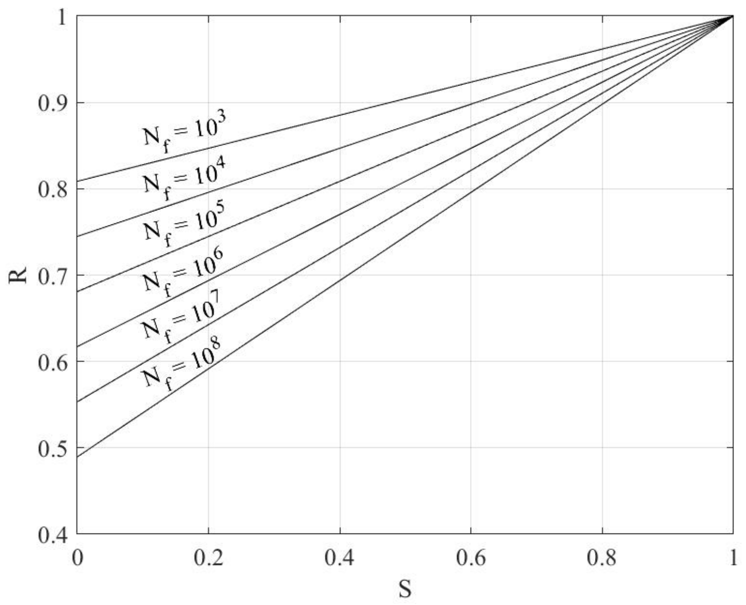

Slika 4.7: Razmerje ciklične obtežbe *R* v odvisnosti od odpornosti na utrujanje $S = \frac{\sigma}{f_c}$ pri danem številu ciklov do porušitve N_f. Prirejeno po: Destrebeco (2004).

Figure 4.7: The ratio between the fatigue strength $S = \frac{\sigma}{f_c}$ and the loading ratio *R* at a given number of cycles N_f. Adapted after: Destrebeco (2004).

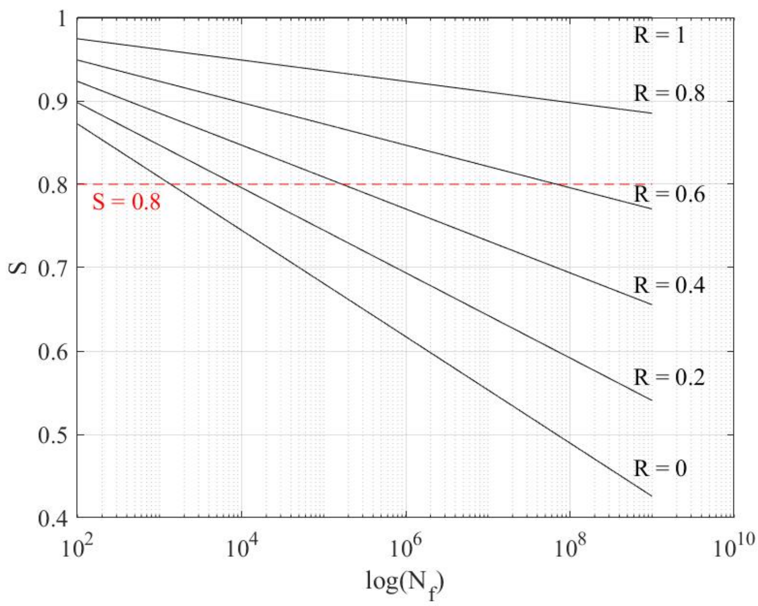

Slika 4.8: Odpornost na utrujanje $S = \frac{\sigma}{f_c}$ v odvisnosti od števila ciklov do porušitve N_f za dano razmerje R ciklične obtežbe. Prirejeno po: Destrebeco (2004).

Figure 4.8: The fatigue strength $S = \frac{\sigma}{f_c}$ with respect to the number of cycles to failure N_f at a given loading ratio R. Adapted after: Destrebeco (2004).

resistance to fatigue, while ductile material resistance is a sum of elastic and plastic resistance, as described in Courtney (2005). High amplitude fatigue load that leads to failure with a low number of cycles is mostly dependent on the plastic properties of the material, while a material able to develop higher plastic strain (more ductile material) will survive a higher number of cycles before it will fail. When subjected to low-amplitude and high-cycle loading, the elastic properties of the material are those which delegate the number of cycles before it fails. In general, brittle materials with their yield strength close to the fracture strength will last longer in low-amplitude, high-cycle fatigue compared to ductile ones. Measures to extend the longevity of the elastic material to limit the initial micro-cracking should be taken, e.g. measures to limit the initial damage supply in the young concrete, while the lower the supply of initial damage the longer the lifetime of the structure, since interior flaws accelerate crack initiation and shorten concrete immunity to fatigue. Concrete is a brittle material (in reality rather semi-brittle) and the initial cracking cannot be avoided, therefore, the sensitivity towards fatigue should be seriously considered, especially when we are dealing with concrete subjected to continuous cyclic load of low-amplitudes (ACI Committee 224, 2002; Courtney, 2005).

Almost all structures are prone to fatigue. Mass concrete is additionally vulnerable, because of the fatigue process being visible only when it is at a very advanced stage and also due to a common belief that concrete is able to last "forever". Fig. 4.9 presents a well-developed crack that has penetrated to the surface. We can notice an extensive damage area hiding behind the tip of the crack and new concentration areas forming inside the block, while the surface is in sound condition. In Eurocodes, the fatigue is placed in ultimate limit states since it results in structural

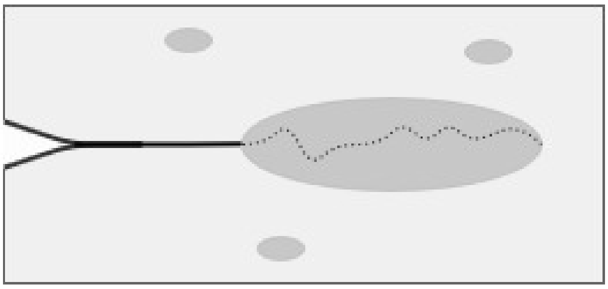

Slika 4.9: Vidni del razpoke, poškodovano območje za konico razpoke ter ostala žarišča poškodb v notranjosti.

Figure 4.9: Visible crack on the surface, extensive damaged zone at the tip of the crack and sources of macro cracking in the material.

failure; an endurance for shear and compressive fatigue for 10^6 cycles is required, the material safety factor for fatigue is 1.5 (CEN, 2010). For a powerhouse, being in operation over 50 years, $N_f = 10^6$ is a low value, since yearly, this value can be surpassed 20-times or greater. All concrete structures have a potential for fatigue damage, and even mass concrete when subjected to long-term cycling loading should be considered for deterioration and fatigue, especially in important infrastructure. Concrete dams are exposed to water, water pressure, and uplift. When cracks in a dam open, they are subjected to hydrostatic pressure and, in the worst-case scenario, to hydraulic fracture. Water related problems also include freezing, thawing, and chemical attacks (Ahmed et al., 2018; Sha and Zhang, 2017). In the reinforced concrete structures, most of the stiffness is contributed by the concrete; according to Friswell and Penny (1997), the corrosion and deterioration of the reinforcing steel has a minimal influence on natural frequencies of the structure. Therefore, by observing natural frequencies in mass concrete and minimally reinforced concrete in dams, we are observing the evolution of concrete.

4.2 Effects of Hydropower Operation

Turbines convert the power of water into rotational movement, while the generator transforms mechanical energy into electricity. Turbine are the heart of a HPP. Based on the site specificity, different types of turbines are installed. Generally, there are three basic groups of turbine types: Francis, Pelton, and Kaplan (Dorji and Ghomashchi, 2014). Kaplan and Francis turbines are the most common turbine type installed worldwide (Fu et al., 2016). In Slovenia out of 54 hydro units installed in total, 41 are Kaplan-type turbines; the biggest has a power of 60 MW, and the average power is 23.7 MW (Mikec, 2018). In this chapter we will focus only on Kaplan turbines with a vertical axis, since this is the type of the turbine installed at Brežice dam.

The scheme of the Kaplan unit is presented in Fig. 4.10. The vertically oriented unit has a generator positioned above the turbine. The turbine is in contact with the fluid while the mechanical rotation is transferred to the generator, which consists of a rotor and a stator, and where electricity is produced. The turbine consists of a runner, guide vanes, and runner vanes. The Kaplan turbine is a reaction type of turbine, where the pressure of water changes on its path while passing the rotor blades. In the reaction type of turbine, the runner is completely submerged. The Kaplan turbine has an axial water flow, meaning the fluid direction is parallel to the spinning axis. The drop of pressure and the change in fluid velocity cause the reaction of the rotor blades and spinning. The Kaplan turbine is categorised as an overpressure turbine, since the pressure on the upper side of the blade is higher than the pressure below the blades. Kaplan turbines are most suitable for lower design heads, usually in the range of 10–50 m, and high discharges (up to 500 m^3/s). Kaplan turbines are especially appropriate for run-of-the-river type of HPPs with partial retention capacity, while double regulated turbines, with manoeuvrable guide and runner vanes, provide possibilities for flexible operation in a wide range of operating points. Moreover, high nominal efficiency, above 90%, contributes to the popularity of Kaplan turbines (Wagner and Mathur, 2011). The cascading system of run-of-the river dams usually operates in a continuous chain and in these cases the propeller type of turbine is preferred. In Slovenia, due to the electricity demand, run-of-the-river dams operate as dams with partial retention and cover both base and peak loads; in this case double regulation turbines are more or less the only viable option.

We divide turbine operation into two groups:

- normal operation;
- emergency operation (Hočevar, 2015).

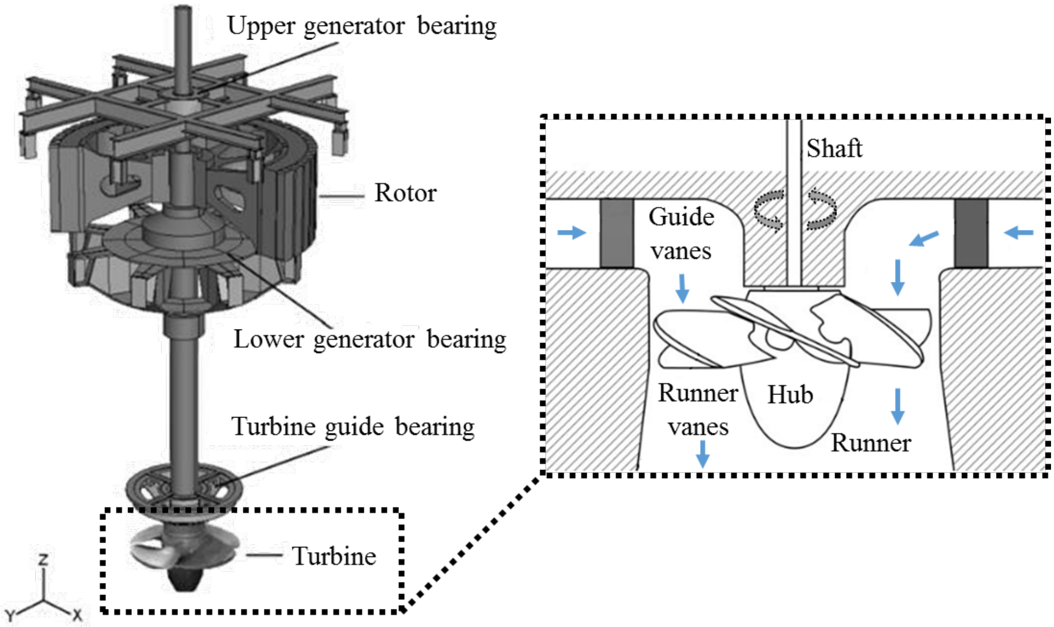

Slika 4.10: Shema vertikalne Kaplanove turbine. Prirejeno po: Wagner and Mathur (2011) in Nässelqvist et al. (2012).

Figure 4.10: Scheme of a vertical Kaplan turbine. Adapted after: Wagner and Mathur (2011) and Nässelqvist et al. (2012).

Normal operation covers all the steady-state and transient manoeuvres that regularly happen during the power production: starting and regular stopping of the turbine, power adjustment, load variations, no load rotation, and continuous operation at full or partial load. Emergency operation with turbines is initiated whenever the turbine needs to be protected from damage, in which case either mechanical or hydraulic brake is deployed. Damaging states happen due to hydrodynamic instabilities, off-design and dangerous transient operations, full or partial load rejection (Kougias et al., 2019). Off-design operation causes instabilities in operation and can cause damage to the turbine. The electricity grid needs to maintain a constant frequency of 50 Hz. In Slovenia the units connected to the grid have to be able to operate in a range of (-5%) 47.5 Hz to (+8%) 54 Hz; in the range 49–51 Hz permanently and up to 30 minutes in the extreme range (Official Gazette of the Republic of Slovenia 29/2016, 2016). Disruptions in the grid affect the turbines in operation and, vice versa, the disruptions in operation of turbines affect the stability of the grid as well. Hydropower turbines are, due to their fast response, the ones which are the first to feel any instabilities and need to react to them (Goyal and Gandhi, 2018; Fu et al., 2016). The lifetime of a turbine is linked with the operational conditions in which it operates. A more invasive operation will shorten its lifetime and, on the contrary, optimal conditions of operation will extend it. The effect of normal start-stop cycles was investigated by Trivedi et al. (2015). A turbine that covers a peak load, undergoes 3-5 start-stop cycles per day (Trivedi et al., 2013). Due to the regulation and providing balance between the production and demand, hydro units are constantly being regulated and operate in less favourable conditions (unsteady modes, transient actions). In the past, only a few predetermined units in the grid were sacrificed to cover the fluctuations and they operated in unsteady modes, but the rest of the units were exposed to optimal conditions of operations, since the turbines are designed to perform the best in the narrow area of operating conditions (optimal point +/-5%). This area is not only optimal in a sense of the utilisation rate but in a sense of the structural health as well (Deschênes et al., 2002).

The start of a turbine, with a synchronous generator, is initiated by disengaging the brakes and through gradual opening of the wicket gates. At first, the turbine is launched in a speed, no load position with runner accelerating to a near synchronous speed. The generator builds up voltage and starts with the synchronisation procedure. At first, the gate opening is fast until the unit reaches 80% of synchronisation speed. Then the gate opening is slowed down to achieve smooth coupling. Once the generator frequency is matched with the grid frequency, closing the circuit breakers connects the unit to the electrical grid. At the time of the coupling, the unit has a matching frequency in a no-load spinning position. At the moment the unit is coupled, the situation transits to a load spinning position, with an instant increase of the load on the turbine. This causes a drop of the runner speed but the grid demands a constant frequency; this transition is therefore connected with additional manoeuvring with the wicket and runner gates to prevent failure and damage. However, the generator sometimes fails to synchronise or a mismatch in the phase angle prevents a successful matching. Before the unit is connected to the grid, the load in the turbine shaft is minimal and the turbine runs close to the runaway speed. This is a very critical situation, since in case of a failure in the coupling procedure the unit can easily accelerate. That results in rapid fluctuations of torque and inlet pressure head, which can in extreme cases cause the rotating components of the generator and the turbine to fail. Out-of-phase synchronization also affects other neighbouring units in operation on the station, and can also cause extreme loading situations on them (Presas et al., 2019; Hočevar, 2015).

Total load rejection is the most invasive transient action turbines are subjected to. The runner starts to accelerate due to zero load situation after the load rejection. Turbines are very sophisticated machines that operate with minimal friction, the "brake" in the system is the load while the unit is connected to the grid (governor maintains the constant rotational speed). If the load is removed, we have a rotational system with practically no friction and strong inertia (moment and water inertia). This situation causes strong vibration and can lead to failure in case the movement is not contained. Causes for load rejection are various: servomotor failure, excessive vibration of the bearing/shaft, a rise of temperature, over-speed or under-speed of a turbine, shear pin failure, insufficient water flow, greasing system failure, etc. (Trivedi et al., 2013, 2015; Goyal and Gandhi, 2018; Fu et al., 2016).

Normal shut-down is conducted by slowly closing the guide vanes; the rotational speed of the runner is decreased, and subsequently the power output from the generator is gradually reduced. At roughly 30% of power, the generator is disconnected from the grid by opening the circuit breakers, the disconnection pushes the unit into a spin-no-load position. This transition causes the runner to start to accelerate, since the load was removed, therefore the unit is mechanically stopped using brakes. The phenomena of acceleration in no-load position is called speed overshot and it depends on the inertia of the rotating parts. Speed overshot causes imminent rise of pressure pulsations to the runner. Pressure measurements during start-ups and stops revealed that the shut-down is more damaging to the turbine than the start-up. During shut-down cycle, the turbine undergoes significant vibrations and unsteady pressure loading. Loads occurring during the stop manoeuvre are: dynamic loads from generator, change of vertical loads due to water action, and runner vibrations while it transitions through less-efficient rotating zones. It has been estimated that each cycle causes fatigue to the runner that equals 15–20 hours of normal operation (Trivedi et al., 2013, 2015; Goyal and Gandhi, 2018; Fu et al., 2016).

To prevent instantaneous pressure loading, water hammer, and damage to the conduits, the closing of the turbine is subjected to a predetermined closing law (Hočevar, 2015). However, whenever the turbine needs to be stopped instantaneously to prevent damage, different stopping manoeuvres are deployed (Presas et al., 2019). Mechanical brake is structurally less invasive than electrical brake and is therefore used in majority of emergency shut-downs (Trivedi et al., 2013). In this procedure, first the mechanical stopping of the turbine is activated and only seconds later the generator breakers are opened. An electrical brake is faster than a mechanical brake; the latter is activated only in cases when the turbine has to be immediately disconnected from the grid. By activating the electrical brake, at the same time the turbine is mechanically stopped and generator breakers are opened. Partial shut-down is applied when, due to electrical system faults, the unit is disconnected from the grid and off-loaded while mechanical spinning is preserved. By opening the generator breaker, the unit runs in a speed-no-load condition, ready to be synchronised and connected to the grid as soon as the system fault is resolved. Examples of normal and emergency operation of Kaplan turbines on the structure of Brežice dam are presented in Section 5.5.2. Researchers have investigated the effect of operation on the turbine and its components. Moreover, new operational regimes have been recognised to cause accelerated fatigue to the turbine and its constituent parts (Trivedi et al., 2013, 2015; Goyal and Gandhi, 2018; Fu et al., 2016; Deschênes et al., 2002; Presas et al., 2019). Turbines are the main source of excitation for the dam structure. The complex interaction between the generating systems and the supporting structure has not yet been fully investigated. Nevertheless, sources of turbine vibration can be divided into three groups: electrical, mechanical, and hydraulic, while vibrations happen on rotating and non-rotating parts as well (Mohanta et al., 2017). Malm et al. (2012), after the discovery of structural cracking on Swedish hydropower dams, investigated the cracking in the concrete foundations of hydropower stations. The analysis confirmed that the cracking in the generator foundation was caused by the combination of mechanical loads, temperature gradient, and drying shrinkage. The concrete gravity dam under investigation was built in 1941 and has three Kaplan turbines in the powerhouse. The investigation revealed that the structure is subjected to uneven drying shrinkage; the moisture content in the centre of the thick concrete parts was still 70%, while concrete close to the free surface had matching relative humidity as the environment. Therefore, uneven drying shrinkage contributes to the initial cracking. Thermal gradient also contributes to cracking. A mass concrete structure has a high heat storage capacity, therefore, the most unfavourable situation is a long operation followed by a long stop, while the ambient temperature is low. The study revealed that the dynamic forces caused by magnetic eccentricity introduced large stresses that locally exceeded tensile stresses and caused cracking in different regions.

Mohanta et al. (2017) prepared a review on the sources of vibration in HPPs and divided them into two groups, i.e. whether they occur on rotating or non-rotating parts. The turbine runner and rotor experience excessive vibration due to the following: mechanical, and hydraulic imbalance, cavitation, instabilities caused by the rub, hydraulic forces, operation away from the best efficiency point, poor lubrication of mechanical parts, defects in bearings, cracks in the blades and shaft and damage to the gates, defects on rotor rubs, and other. Non-rotating parts, i.e. draft tube, seals, penstock, transformer, and generator vibrate as well - their behaviour is influenced by electromagnetic forces, cavitation, water quality, power swings, and other.

The generator is usually the heaviest part of the power unit. Magnetic eccentricity of the generator causes unbalanced magnetic pull and excites the structure with a sinusoidal periodical loading with respect to the rotation of the unit (see Fig. 4.11). The eccentricity causes an imbalanced magnetic pull and the unbalanced rotor mass adds the dynamic eccentric force. The rotor and the stator are never perfectly cylindrical or centred to the turbine axis. The eccentricity of a rotor causes periodical load with respect to the rotation, while the eccentric placement of the stator is a source of constantly applied load (Malm et al., 2012). Every rotor and stator

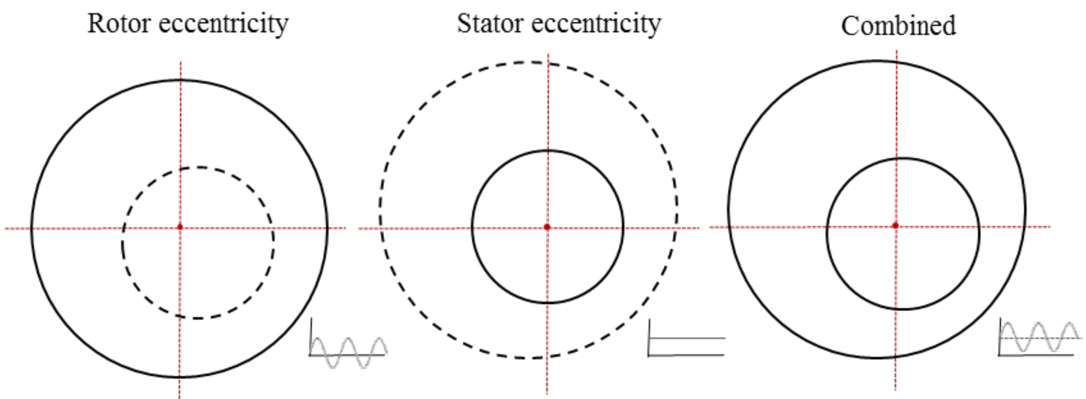

Slika 4.11: Vzroki za pojav ekscentričnosti magnetnega polja. Povzeto po: Malm et al. (2012).
Figure 4.11: Sources of magnetic eccentricity. Adapted after: Malm et al. (2012).

initially have minimal eccentricity within the design capabilities; with years of operation the initial imperfections increase (Gasch et al., 2013). In induction motors a maximum of 10% initial eccentricity is allowed and assumed as permissible (Tian et al., 2018). With operation, also other reasons for the imbalance become more distinct and cause excessive vibration, e.g. loose windings, high partial discharge, unequal loading of the generator, insulation failure, non-uniform air gap between the rotor and the stator. Once the eccentricity reaches 15% and remains unattended, it will lead to a structural failure (Mohanta et al., 2017; Choudhary et al., 2018).

The Kaplan runner is submerged in pressurised water current while operating. Vertical Kaplan turbines are reactive turbines and produce the majority of the excitation to the structure in the horizontal direction. However, double regulation allows manipulation of both, guide and wicket gates. During manoeuvres, gates are opened and closed, and especially during shut-down, the closing of the gates helps to slow down the turbine and subsequently the uplift force on the turbine changes. This change of the uplift causes additional excitation in the vertical direction. With the water passage, an axial force is created to the turbine which is absorbed by the thrust bearing; the load depends on the current operating mode and is connected to the pressure drop over the runner. The disruptions in the waterway are translated to the reactive turbine, e.g. unstable flow conditions, water hammer, large cavities, reversed water hammer, and cavitation. The major impact of the turbine to the structure is caused during faults; failure of a component (e.g. blade rupture), emergency stops, runaway, load rejection, or uncontrolled closing of guide vanes. The runner as well as the generator have design imperfections and are always unbalanced to some extent; the mechanical load caused by the eccentricity is estimated to be low with respect to the hydraulic loads (Gasch et al., 2013).

4.2.1 Identified potential failure modes due to the operational fatigue

Generally we can define four ultimate limit states that describe the loss of structural stability: loss of overall stability, sliding failure, overturning failure, and bearing capacity failure (de Wrachien and Mambretti, 2009). According to the literature, globally the dams built between 1900–1929 have the highest failure rate (34% of all failures), while the majority of failures of concrete dams happened in the first five years after the dams were in operation (12% in the 1st year and 11% in 2nd–5th year). The structural height of failed concrete dams was in 54% less than 15 m and in 20% 15–30 m. The main causes of failure were quality problems (40.8%), followed by overtopping (32.4%), disasters (5.6%), and poor management (2.8%), while in 18.4% the reason is unknown. Quality problems are further subdivided into: internal erosion, sliding/overturning, deficiency in spillway design and its construction, quality issues in culverts and embedded structures, and unknown quality issues. The most common quality reason is internal erosion, followed by the unknown reasons (Zhang et al., 2016a).

Potential fatigue failure modes do not represent an imminent threat to structural stability. However, due to the cumulative nature of the process, the identified failure modes affect the structural safety of the dams[3], while the slow mechanism substantially shortens the life expectancy of structural components and in the end leads to the loss of structural stability. Fatigue failure mode mechanisms are linked with the following:

- excessive vibrations caused by the loss of stiffness in the foundation concrete;
- large displacements in the concrete that cause a shift in the turbine axis which results in

[3] We discuss both serviceability and ultimate limit states, while the loss of operation is also an unfavourable condition.

the loss of production;

- dislodgement of the unit (lifting of the unit);
- fatigue failure of the concrete structure;
- breach of water;
- difficulties in operation with the hydro-mechanical equipment; fatigue failure of gates (de Wrachien and Mambretti, 2009; Zhang et al., 2016a; Colombo et al., 2016; Harris, 2002).

Power units are the main source of excitation for the dam structure. Structural cracks reduce the overall structural stiffness which results in larger loads on the remaining healthy part of the structure. Moreover, immunity to a chemical attack is reduced, while water penetration increases. This also affects the water tightness capability, cracks are subjected to the full uplift, the structure is more susceptible to freeze-thaw damage. Ageing and fatigue can cause difficulties in manoeuvring of the hydro-mechanical equipment, while the lack of maintenance can lead also to fatigue failure of gates. This failure is imminent and can cause flooding downstream; a textbook case of such failure is the Dunlap dam failure near New Braunfels, Texas. On a silent sunny day, the gates suddenly failed (May 21, 2019). Fortunately, the failure did not result in fatalities even though the evacuation of the reservoir caused flooding downstream. The moment of failure was caught on a surveillance camera and is therefore a live evidence of what can happen if ageing, fatigue, and maintenance are neglected (GeoEngineer, 2019).

Simultaneously, we are discussing two parallel categories: operation and processes that are linked with the loss of production, and structural stability issues related to the maintenance. Both categories have the same origin, where the operational issues develop on a shorter time-scale and the structural stability issues concern the same phenomena but on a longer time-scale. The fatigue process will be reflected at first in operational obstructions and more frequent service times. Moreover, if only the symptoms are treated while the cause remains, the fatigue in the end can result in permanent dislodgement of the unit, in accidents, and also in structural failure. The loss of stiffness in the concrete foundations results in excessive vibrations of the power units; the excessive vibrations cause larger load, which then causes further cracking, while the remaining healthy structure is the one that bears the load. The phenomena has a positive feedback loop; the accumulation of damage is slow and lasts for years and decades before it becomes critical. Unfortunately, the process is self-accelerating with an ever-increasing damage gain.

Cases with identified structural damage can be found in the literature. In his thesis, Hillgren (2011) prepared an overview on the incidents due to hydraulic pressure transients with Kaplan turbines that caused severe damage to the turbine and/or to the surrounding structure. The cases involve blade brakes, turbine dislodgement, lifting of the runner, etc. The accidents occurred during regular operating procedures and clearly demonstrate the brutal force of the water in the waterways. The most famous incident is undoubtedly the Sayano-Shushenskaya HPP accident in Russia in 2008 when during a regular operation, one of the units was suddenly destroyed and thrown out of its position (Bryksin et al., 2014). Lopez and Restrepo Velez (2003) in detail describe a case of Guadalupe-IV HPP, which after 10 years of operation, endured significant relative displacements between the first- and second-stage concretes surrounding the scroll case. Extensive investigation revealed that the cause of the damage was the transition in operation, from the designed 2 shut-downs per year to approximately 240 shut-downs yearly. An extensive rehabilitation works, consisting of anchor installation, injection and crack sealing, grouting of ducts after 15 years of operation, caused a disruption of operation (one month on each unit); the cost were estimated to be over 1/3 of a billion US dollars. Urquiza et al. (2014) describe a case of a turbine shaft failure after 12 years of operation. The cause of the failure was recognised to be high-frequency fatigue and actions caused by the load variations due to the continuous regulation during operation to meet the general demands of the grid. There are a few cases of accidents reported, while the actual number of cases must be more than can be accessed in public documents, since the responsible companies tend not to make the incident reports public (Hillgren, 2011). However, the majority of the cases accessible to public warn from the new operational patterns thet the already aged structures have been subjected to over the last decades.

4.2.2 Operational regimes on the Lower Sava River

To analyse operational regime characteristics, data from Brežice HPP and Krško HPP have been analysed. We obtained operational logs from both HPPs; for Krško station for the period from October 2012 to May 2018, and for Brežice HPP from October 2017 to May 2018. Krško HPP is the closest upstream HPP in the Sava River cascading system; it is located a few kilometres upstream and it is structurally very similar to Brežice HPP. In the powerhouse it also has three generating units (Kaplan-type, double regulated, vertical turbines) with a 39 MW of combined installed design-rated power. We included operational data from Krško HPP in this study due to the structural similarity and sequential placement in the HPP cascading system. It is expected that the operating schedule at both HPPs would be similar in a longer time period. Table 4.1 presents the basic statistics of turbine operation on both stations. The turbines on Brežice HPP have, on average, more start-stop cycles and a shorter duration of undisturbed operation than units within Krško HPP. This is to be expected, since the first year of operation has a lot of start-stop cycles due to the operational tests that need to be performed. The data from Krško HPP has been collected since 2012, which provides better insight into the operation of the scheme on the Lower Sava River. In total in the 5 years of operation there were 88 emergency operations and 806 start-stop cycles on Krško HPP, which are more or less evenly distributed among the three units (Unit 1, 0.3; Unit 2, 0.3; Unit 3, 0.4). The turbines have, in an average year, between 44 and 55 start-stop cycles of various lengths. The longest continuous operation recorded was on Unit 1 and it lasted for almost 82 days (1963 hours). The sum of working hours of all three units per year is 16492 h for Krško HPP and 15816 h for Brežice HPP. If we look at each unit at Krško HPP more closely (see Fig. 4.12), the sum of operating hours in a year per unit reveals that Unit 1 on HPP operates by more than 1500 h longer, compared to the other two units; this amounts to over 2 months of continuous operation. Unit 1 therefore operates 75% of the time per year, Unit 2 57%, and Unit 3 56%. Operational patterns can vary substantially; median for continuous operation is 40 h for Krško HPP and 15 h for Brežice HPP.

Preglednica 4.1: Obratovanje z agregati v enotah HE Brežice in HE Krško.
Table 4.1: Turbine operation within Brežice HPP and Krško HPP.

Unit	Median [h]	Longest [h]	Emergency operation [Total]	Start-stop [Total]	Start-stop [per year]	Emergency operation [per year]	Work hours [year]
Unit 1 Krško	67	1963	22	250	44	4	6573
Unit 2 Krško	34	1557	28	249	44	5	5009
Unit 3 Krško	23	1172	38	307	55	7	4911
$\sum$ Krško	40	1963	88	806	143	16	16492
Unit 1 Brežice	14	460	14	105	77	10	5447
Unit 2 Brežice	15	640	7	105	77	5	5270
Unit 3 Brežice	17	381	9	93	68	7	5098
$\sum$ Brežice	15	640	30	303	222	22	15816

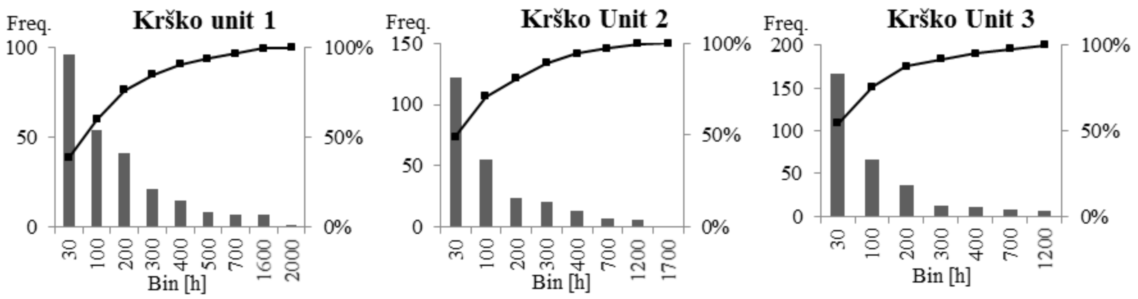

Slika 4.12: Histogram obratovanja agregatov na HE Krško.
Figure 4.12: Histograms of operation on Krško HPP power units.

Histograms of operation for each unit on Krško HPP are presented in Fig. 4.12. Only 2% of continuous operation is longer than 1000 h, while 90% of operation is of 300 h duration or less. To obtain characteristics of the start-stop cycles in a longer time scale, the data from Vrhovo HPP in the period 2008–2018 were analysed. Vrhovo HPP is the first HPP in Lower Sava cascading system (more on that in Chapter 5.1) built in 1993. Fig. 4.13 represents the dynamics of the number of start-stop cycles in the last decade. The mean number of cycles is 73 cycles/unit with a standard deviation of 20 cycles/unit. Statistically, Unit 2 has 1/3 more cycles compared to the remaining two. Over the years, the number of cycles varied; the minimum was reached in 2010 and the maximum in 2014, when the total number of cycles doubled with respect to the 2010 situation, otherwise the number of cycles is more or less stable. Unfortunately, we were not able to obtain also the data on the duration of the load cycles and therefore we were not able to estimate the working hours for Vrhovo HPP. Therefore, we assume that Krško HPP to gives representative data for the Lower Sava power scheme.

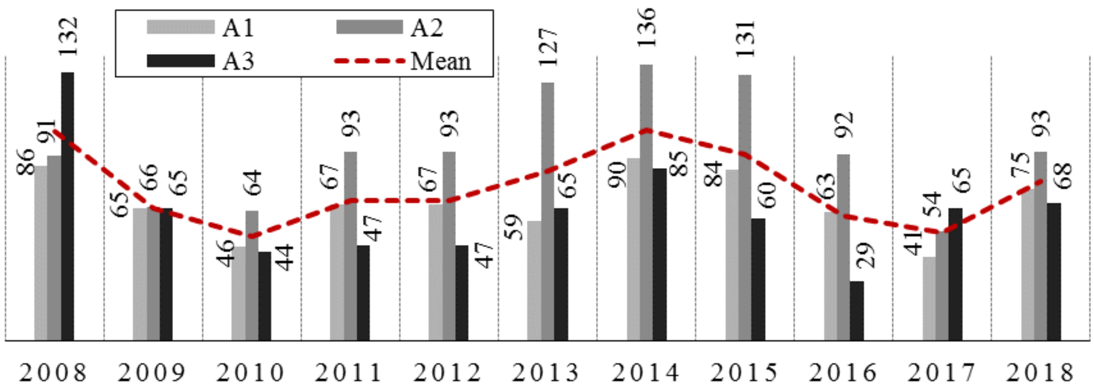

Slika 4.13: Število obratovalnih ciklov na HE Vrhovo v zadnjih 10 letih.
Figure 4.13: Number of start-stop cycles on Vrhovo HPP over last 10 years.

5 METHODOLOGY

The experimental work was in general divided into four stages:

- Vibration measurements on Brežice dam (during construction and during start-up tests).
- Data processing and numerical modelling.
- Research on application of a laser Doppler vibrometer as a new technique for vibration monitoring of dams.
- Proposal on inclusion of the vibration monitoring in regular monitoring activities on the dam.

The on-site experimental work presents the core of this research. Brežice dam was selected as the experimental site, since we were able to start the investigation of the dam already during the construction. Site specifics and locations of the experimental points are presented in section 5.1. Measurements were performed in three stages. The purpose of the 1st stage was to capture the reference state of the young structure, when we assume no damage has occurred yet. With measurements during start-up tests of the hydro-mechanical equipment (2nd stage), the structural response to typical operational manoeuvres was captured. The numerical model was built to support the identification of the structural eigenfrequencies and help us understand the structural behaviour. Data acquisition was done in time-domain while the Fast Fourier Transformation was used to transform data in frequency-domain, where structural eigenfrequencies were identified. We devoted a lot of efforts to the application of the laser Doppler vibrometer on the dam during regular operation (3rd stage measurements), using standing points that were subjected to vibrations as well. According to site specifics and the lessons learnt in the last chapter we propose a work methodology on how to upgrade the monitoring activities on Brežice dam and translate the knowledge gained at this site to other structurally similar dams, primarily on the Sava River.

5.1 Brežice Dam

Brežice dam, presented in Fig. 5.1, is a newly-built dam on the Sava River in Slovenia. An energy exploitation project that involves six structurally similar run-of-river cascading HPPs is underway on the Lower Sava River and Brežice HPP is the 5th in the chain. The dams upstream were built between 1993–2012: Vrhovo HPP (1993), Boštanj HPP (2005), Arto-Blanca HPP (2008), and Krško HPP (2012) (see Fig. 5.1). The construction of the last dam in the system, Mokrice HPP, is expected to start in the following years. Brežice dam is situated on a flat Krško-Brežice plain and it is designed as a run-of-river type of dam with limited water storage. Structurally it is a combined type of dam; it is a concrete gravity dam with two

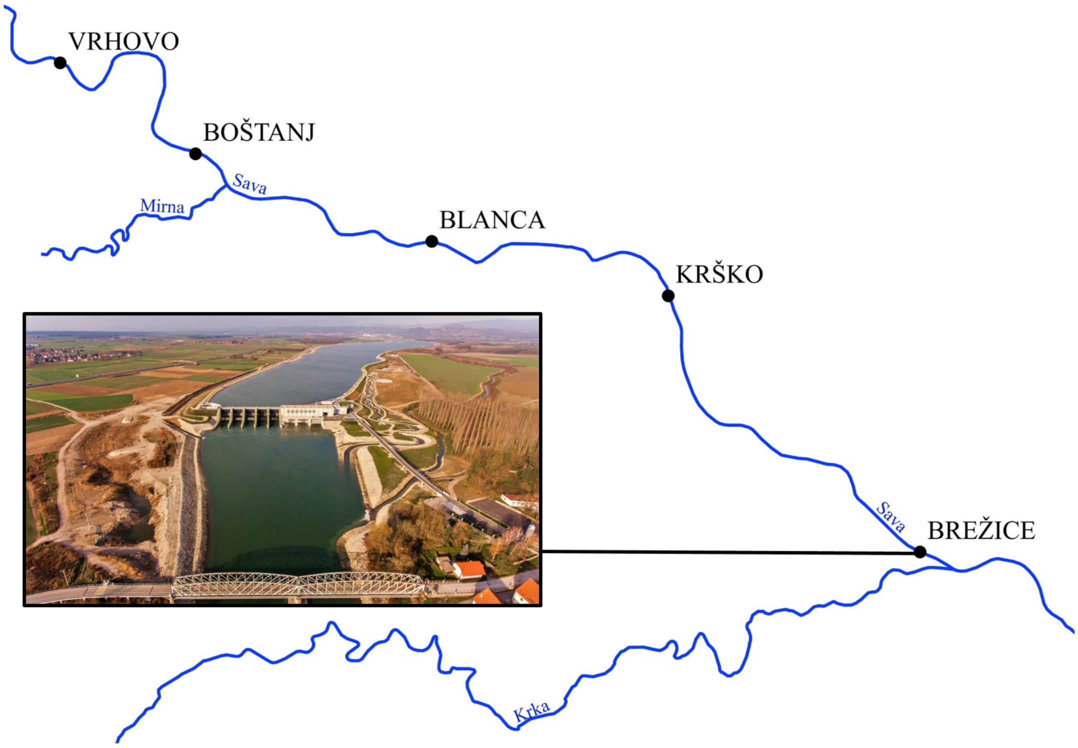

Slika 5.1: Lokacija že zgrajenih hidroelektrarn na spodnji Savi in pogled na pregrado Brežice iz zraka. Vir podatkov: http://www.he-ss.si/, GURS, SLOCOLD, Geopedia.
Figure 5.1: HPPs built on the Lower Sava River and Brežice Dam with the powerhouse. Data source: http://www.he-ss.si/, GURS, SLOCOLD, Geopedia.

embankments, with a total crest lengths of over 14 km. The concrete gravity part is connected with the embankments laterally confining the reservoir. The left embankment has a total length of 6.4 km and a varying height between 1.5–8.5 m. The right embankment is 7.5 km long, its height varies between 9.5–3.0 m. The concrete gravity part of the structure has a total length of 160 m and consists of an overflow section with 5 spillways and a powerhouse. Each spillway section is 15 m wide. The spillway piers are 3 m wide with a varying height, reaching the maximum of 15 m on the upstream end. Each spillway has a maximum discharge capacity of approximately 1000 m^3/s and is equipped with a segment gate with a flap for fine regulation. On the downstream side, the spillway chute continues into the stilling basin which enables efficient and safe operation of spillways in the majority of actual operating manoeuvres. The total width of the overflow section is approximately 91 m. An inspection gallery is built on the upstream side approximately 27 m below the highest point of the dam. The powerhouse is situated on the left-bank side and can be vertically divided into two distinct parts. The bottom part under the level of the generators is built with mass first-stage and second-stage concrete, with three large voids that connect the intake, penstock, spiral, and draft tube for each unit (see Fig. 5.2). This section is approximately 60 m wide in total. The upper part is a thin-walled cubus, surrounding the machine hall, and other control and ancillary rooms. The main bearing element is the support structure for the crane, consisting of a horizontal girder supported with beams. In the powerhouse, there are three double-regulated, vertical Kaplan-type turbines with a 500 m^3/s combined rated discharge and an 11 m hydraulic head installed. The technical details of the turbines and the generators are presented in Table 5.1. The estimated annual production of the power plant is 161 GWh. The joint between the powerhouse and the overflow section is dilated as well as the joint between the main powerhouse building section and the extension in the montage level. The extension of the powerhouse adds additional 16 m of total width to the powerhouse. The lowest elevation of the foundation under the turbine generator set is at 118.70 m a.s.l., while the highest elevation of the roof structure is at 155.20 m a.s.l., which gives a total height of the structure up to 36.5 m. The Brežice reservoir elevation equals to

Preglednica 5.1: Tehnični podatki o turbinah, nameščenih v strojnici HE Brežice. Vir podatkov: HESS.
Table 5.1: Technical details on the units installed at the Brežice powerhouse. Data source: HESS.

Name	Distance [m]
Turbine type	Kaplan
Rated power [MW]	15.2
Rated head [m]	10.16
Rated discharge [m^3/s]	166.7
Rotational velocity [min_{-1}]	107.14
Runaway velocity [min_{-1}]	300
Runner diameter [m]	4.9
Runner mass [t]	35
Number of runner vanes [no.]	4
Shaft tube length [m]	8.1
Generator rotor diameter [m]	6.4
Generator mass [t]	191.4
Generator rotor mass [t]	96.3

153.00 m a.s.l. which ensures an approx. 11 m of gross hydraulic head. The reservoir volume equals 19.3×10^6 m^3, from which 3.40×10^6 m^3 represents the utilizable volume, according to the concession agreement conditions (maximum of 1.1 m drawdown). The Sava River is a torrential river, the maximum discharge measured in 2010 in this section is 3680 m^3/s, while the evaluated mean yearly discharge is 231.2 m^3/s, and the discharge with a 100-year return period Q_{100} is 3750 m^3/s (Bombač, 2012; Rak et al., 2012). The dam design enables to lift the hydraulic gates above the highest level of flood water (with a sufficient safety margin), also the HPP does not operate with the discharges above 800 m^3/s, since due to the rise of the downstream water level there is an insufficient hydraulic head to produce power. This design enables the establishment of natural conditions during a flood, due to the lifted hydraulic gates during flood discharges (Rak et al., 2012; IBE, 2016; INFRA, 2012).

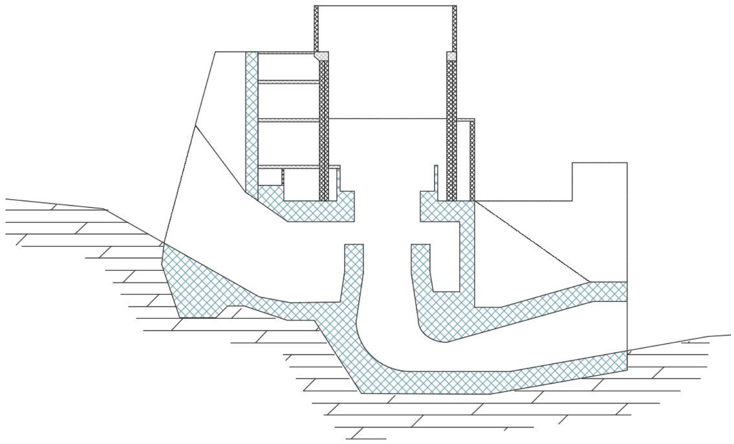

Slika 5.2: Prečni prerez strojnice preko enega izmed agregatov.
Figure 5.2: Powerhouse - transverse section across one of the units.

The construction of Brežice dam officially started on April 2, 2014, with the preparatory works. This phase concluded on February 2015 and the dam construction began. The concrete structure of the dam was built in roughly one year and on August 27, 2016, the Sava River was rerouted back from the bypass channel to the old river bed. The reservoir was slowly filled to the nominal height, which was reached on August 11, 2017, and after the provisional acceptance of all the power units, the start-up tests began. After the technical inspection and provisional acceptance of dam structure on September 27, 2017, the HPP was officially opened. On October 10, 2017, the one-year trial run operation period started, followed by regular operation when the operating license for HPP Brežice was obtained on October 11, 2018. The concession for the energy exploitation of the Lower Sava River was granted for a period of 50 years since the day of the validity of the building permit, with the possibility of an extension (Conditions of the Concession for Exploitation of the Energy Potential of the Lower Sava River Act (ZPKEPS-1), (Official Gazette of the Republic of Slovenia 87/2011, 2011)). During the commissioning period, regular monitoring is established on Brežice dam, since the dam falls in the category of large dams, where the legislation dictates monitoring. The monitoring program consists of automatic measurements and a regular frequency of field measurements and examination, defined in the measurements' program. In total, there are 114 monitoring locations located around the concrete dam body, of which there are 19 automated and 95 included in measurements' program. The program of displacement measurements of the dam's structure is established with the grid of stable geodetic points. All structural dilatations: the dilatation between the powerhouse and the spillway section, and the dilatation between the main structure and the two downstream and two upstream side walls, are equipped with dilatometers. Uplift is measured under the powerhouse and under the spillway section, in total in 27 points, but only 4 are automated. The program includes water level measurements (upstream and downstream), concrete temperature and air temperature measurements, and monitoring of physicochemical properties of the water in the reservoir. Seismological monitoring is connected to a grid of automatic measurements.

There are strong-motion accelerometers installed: two of them in the 3rd pier in the spillway section (one in the gallery and one in the crest) and a third one in the well on the right plateau. Accelerometers are active in trigger mode with 0.05g threshold (Partner Brežice, 2017; Mikro Medica, 2018).

5.2 Experimental Work

Experimental work on Brežice dam initiated in May 2016, roughly 2 years after the beginning of the construction works. At that time, the majority of the structure was already built. The construction site was still very active, which enabled us to measure the impact of the heavy machinery on the structural response. At that stage we used only the laser Doppler vibrometer for the in-situ, non-destructive, vibration measurements. Experimental points were chosen on representative locations following predefined criteria. The aim of the investigation is to observe the influence of the operational loads on the structural response and in the long-term to establish a methodology, where through vibration monitoring, the ageing of the structure or development of any other structural changes can be detected. The idea is to use non-contact measurement techniques; however, in reality we expect that a combination of various techniques will be used. Therefore, the experimental points were chosen on the representative structural parts, where we expect the effect of operation will have an impact. The locations have to enable the positioning of the tripod with LDV somewhere opposite, and within the measuring range of the device, preferably on a different type of structural member or/and on a more rigid foundation than the one under investigation. Special attention is devoted to the positioning of the vibrometer to ensure that the angle of incidence is 90° with minimal error. We also predicted that the measuring point would have to be accessed at least a few times, e.g. to mount reflective tiles for maintenance or to mount accelerometers or other devices. We identified eight experimental points in the powerhouse (see Fig. 5.6) and four in the spillway section (see Fig. 5.4). Table 5.2 summarises the basic information on the experimental points.

The experiment in the spillway section can only take place when the gates are closed or during low discharges. The dam is designed in a way so that during flood events the gates are lifted and natural flow is established. The downstream part of the piers gets over-flooded under these circumstances. Also in cases when the piers do not get submerged due to the non-stationary nature of the supercritical flow with a high Froude value, which can result in sudden fluctuations, the measurements are not performed due to safety reasons. This is the reason why even though high-discharge instances would provide interesting times to measure vibrations from the structural point of view, measurements were not performed at those times. Fig. 5.3 presents the situation at closed gates and during flood discharge. We can clearly see the piers being flooded, even though this is not a big flood and the discharge is managed with flaps, while the gates are only partially lifted (discharge of the Sava River was approximately 1200 m^3/s).

In the spillway section, all the experimental points were located on the piers dividing each

Preglednica 5.2: Eksperimentalne točke na pregradi Brežice; poimenovanje točk, opis nahajališča, absolutna višina ter merilna razdalja za uporabo vibrometra.

Table 5.2: Experimental points on Brežice dam; names, locations, vertical datum and stand-off distance when the vibrometer is used.

Name	Location	Distance [m]	Datum [m asl.]
P1	Spillway sect. (1st pier)	16	142.5
P2	Spillway sect. (1st pier)	16	142.5
P5	Spillway sect. (4th pier)	16	142.5
P6	Spillway sect. (4th pier)	16	142.5
ST1	Powerhouse	12	150
ST2	Engine room	12	144
S1	Powerhouse	12.5	150
S2	Powerhouse	12.5	144
A1	Powerhouse	3	141
A2	Powerhouse	3	141
A3	Powerhouse	3	141
StH,StV	Powerhouse	-	143.5

(a) Zaprte zapornice.

(a) Closed gates.

(b) Poplavne vode.

(b) A flood.

Slika 5.3: Situacija v prelivnem polju pri srednjem in povišanem pretoku.

Figure 5.3: Situation at Brežice dam during normal operational regime and during flood discharge.

spillway section. The most straightforward was the decision to observe the behaviour of the pier between the first and the second spillway section, while it satisfies all of the selection criteria. Each spillway section is 15 m wide (this means the stand-off distance is approximately 16 m). There is also a safe and more rigid standing point, while the mounting of both experimental points was not demanding and the measuring plateau is easily accessible. The pier was equipped with two reflecting tiles. Additional two points were in the later stages added on the pier number

4, located between the IV and V spillway sections, while often during normal operation there is a need for opening the gates, the last spillway section is activated. Under these circumstances, pier 4 can be measured from pier 3. The layout of the experimental points in the spillway section is displayed in Fig. 5.4. The odd numbered points are located approximately 2 m from the endpoint of the pier, and the even numbered 8 m. Fig. 5.5 displays the experimental point as viewed from the standing point from where the 1st pier is measured.

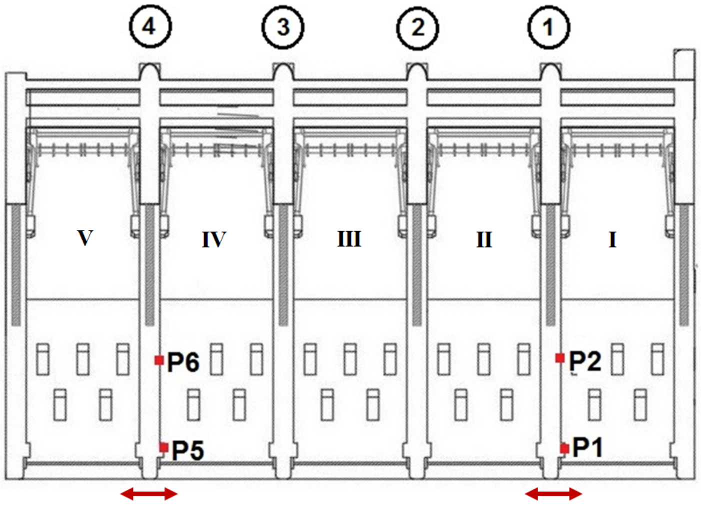

Slika 5.4: Razporeditev eksperimentalnih točk na prelivnih poljih ter številčenje stebrov. Z rdečimi puščicami je označena smer meritev vibracij. Prirejeno po: IBE (2016).
Figure 5.4: Locations of the experimental points in the spillway section and numbering of the piers. The red arrow demonstrates the direction in which the response was captured. Adapted after: IBE (2016).

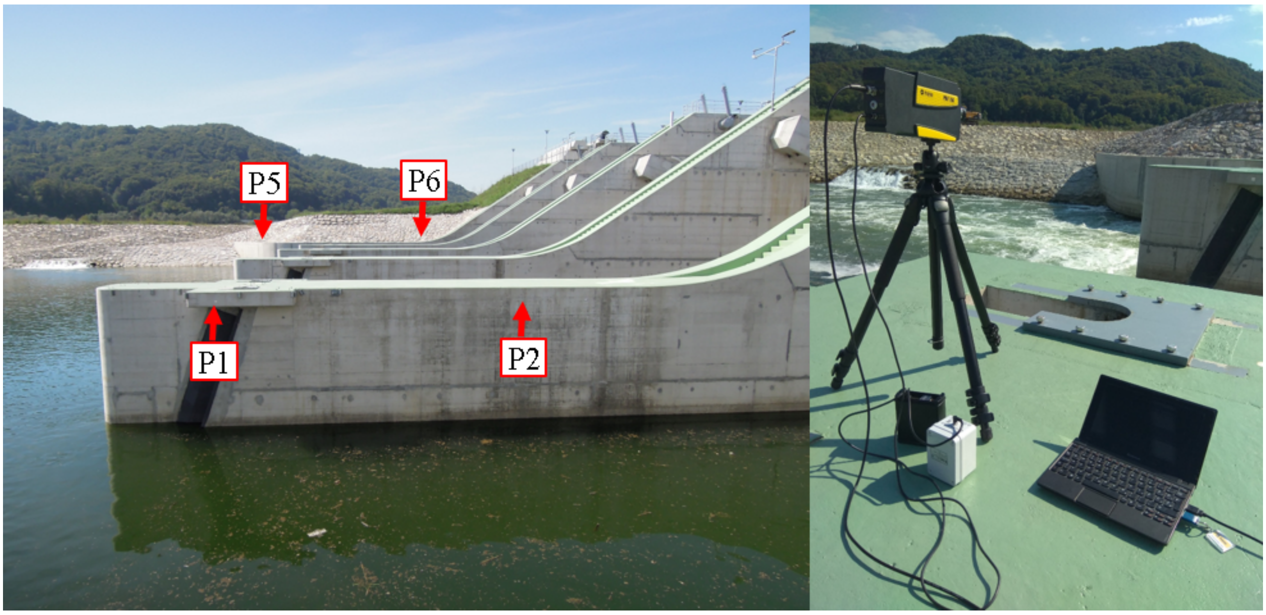

Slika 5.5: Eksperimentalne točke na prelivnih poljih, pogled s stojišča za meritve na stebru 1.
Figure 5.5: Experimental points in the spillway as they are visible from the standing plateau.

The majority of the experimental points is located in the powerhouse, where the operational loads have an effect. Due to the structural design, we assumed that the operational load is not transferred beyond the dilatation and the overflow section remains unaffected. Experimental work confirmed our assumption; with measurements in the spillway section, while the power house was operating, the influence of the operation with the turbines on the piers in the spillways was not detected.

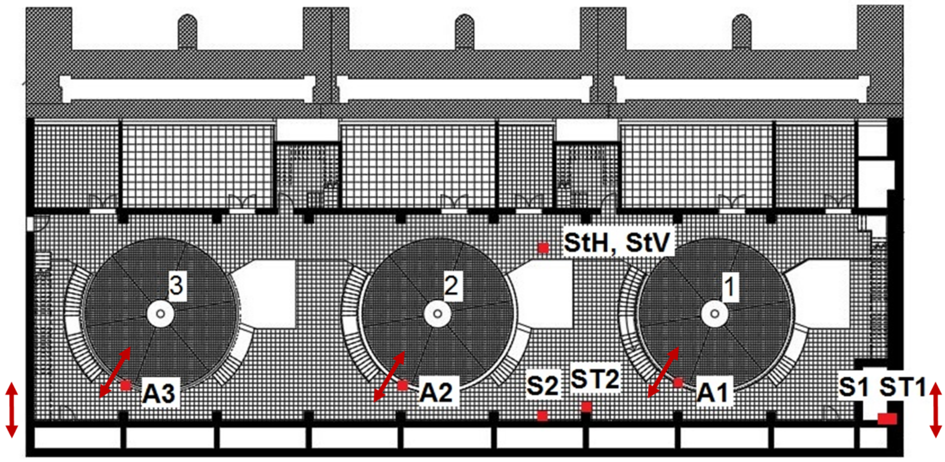

Slika 5.6: Razporeditev eksperimentalnih točk v strojnici ter številčenje turbin. Puščice označujejo smer meritev odziva. Prirejeno po: IBE (2016).
Figure 5.6: Layout of the experimental points in the powerhouse and the numbering of the turbines. The direction of the captured response is marked with red arrows. Adapted after: IBE (2016).

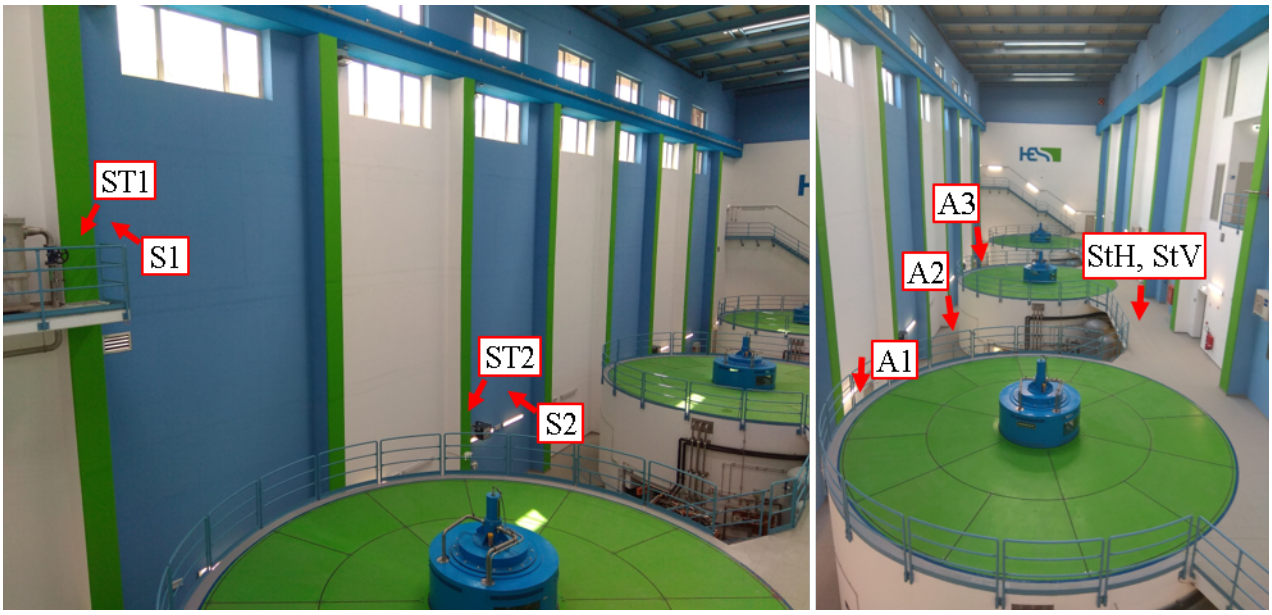

Slika 5.7: Merilna mesta v strojnici.
Figure 5.7: Experimental points in the powerhouse.

Experimental points in the powerhouse are located on different segments around the largest open space, i.e. the engine room hall. The situation is presented in Fig. 5.6; in total there are eight experimental locations, the majority of them (4) is located on the south wall of the powerhouse, each turbine shaft has one, and there is an additional point on the floor connecting all the turbine shafts (see Fig. 5.7)). The vertical datum of the points varies, the experimental points on the piers between the spillway sections have the lowest vertical datum. In the powerhouse, the lowest located experimental points are on the turbine shafts, and have an approximate vertical datum of 142.5 m a.s.l., while the highest located experimental points are on the left lateral end of the south wall in the engine room and are at 150 m a.s.l. On all points, horizontal vibrations were captured; the direction is marked in Figures 5.4 and 5.6. On the piers in the spillway sections, horizontal vibrations were captured in direction parallel to the upstream-downstream direction; in the powerhouse, on the points on the south wall, we captured the response in the upstream-downstream direction, while on the points on the turbine shafts we captured the response in the radial direction perpendicular to the measured surface. At location StV, also vertical vibration was measured. There are three turbines in the powerhouse and there is no predetermined operational schedule on how the units will be operated. The start-stop cycles are a consequence of the demand and the operators' decision. Therefore, the experiment was designed to enable data acquisition no matter what operation regime was underway. All experimental points were equipped with reflective tiles to enhance the intensity of the backscattered light.

The in-situ experiment was divided into different stages:

- stage 1: initial measurements and measurements prior to the first filling of the reservoir,
- stage 2: measurements during the start-up tests of the mechanical equipment,
- stage 3: measurements during regular operation.

The primary goal of stage 1 measurements was system identification, more precisely stage 1 provided the as-built baseline, while stage 2 provided system identification under various loading scenarios. Initial measurements captured the state of the structure shortly after the completion of the construction works. We identified this step as crucial, since this condition is required for the life-cycle structural health monitoring. However, this step is commonly missing, since structural diagnostics is usually performed after the structural damage is already visible and an intervention action is necessary. Stage 3 measurements included additional procedures to extend the applicability of the LDV to be used in non-stationary conditions, while during the 1st and 2nd stage measurements, we observed the need to develop procedures to reduce the noise in the LDV output.

5.3 Instrumentation

Vibration response is measured using accelerometers, velocity transducers, and a laser vibrometer. Various equipment was used in different stages. The specification of accelerometers are presented in Table 5.3. We used Dytran, A series, piezoelectric, uni-axial accelerometers; they were mainly used during stage 3 measurements. The devices are small and weigh only a few grams. They have a linear amplitude response within the entire frequency range, specification for the discrepancy at 100 Hz is 1%. Accelerometers can be mounted using a UNC pin, directly screwed-down, using a magnetic mounting base, or glued with beeswax. For our purposes it was necessary that they have a small footprint, which is also the reason why we chose this type instead of DC-type accelerometers. The cables used to connect the accelerometers to the DAQ have a Teflon cover and PVC to BNC plug-in connectors.

Preglednica 5.3: Tehnični podatki o pospeškomerih. Vir podatkov: Dytran (2019).
Table 5.3: Technical specifications of the accelerometers. Data source: Dytran (2019).

Weight	4.3	g
Frequency response (+-5%)	0.3–5000	Hz
Operating temperature	(-51)–82	°C
Sensitivity	10	mV/g
Broad band resolution	0.004	m/s^2 rms
Spectral noise[1]		
at 1 Hz	0.001	ms$^{-2}/\sqrt{\text{Hz}}$
at 100 Hz	0.0004	ms$^{-2}/\sqrt{\text{Hz}}$
at 1000 Hz	0–00002	ms$^{-2}/\sqrt{\text{Hz}}$

Preglednica 5.4: Tehnični podatki o vibrometru. Vir podatkov: Polytec (2016).
Table 5.4: Technical specifications of the vibrometer. Data source: Polytec (2016).

Laser type	Helium Neon	
Velocity range	500	mm/s
Frequency range	0.5–22000	Hz
Velocity resolution[1]	<0.1	μms$^{-1}/\sqrt{\text{Hz}}$
Laser wavelength	633	nm
Stand-off distance	0.09-30	m
Operating temperature	5–40	°C
Relative humidity	80	%
Weight	2.6	kg

The vibrometer we used is Polytec PDV-100 portable single beam vibrometer (Polytec, 2016). The technical details of the device are specified in Table 5.4. The vibrometer uses eye-safe HeNe class 2 laser, where the laser light does not cause irreversible damage, when direct eye contact

[1] RMS

with the laser beam is avoided. The device is portable, dust, and spray water safe. For operation, it needs power supply, also batteries can be used. Operating temperature of the vibrometer is in a range of +5 to +40°C and relative humidity must be below 80% and not condensing. It is also necessary that the temperature conditions during the measurement are constant. To achieve good results, we should guarantee there is at least a 15-minute warm-up time period with constant temperature prior to the beginning of the measurement, while at the same time it is crucial that the ambient temperature does not change during the measurement. In case a significant temperature drop/rise occurs during the measurement, the changed conditions of the medium (air) through which the laser beam travels will corrupt the measurement. The stand-off distance depends on the reflectiveness of the measured surface and the atmospheric conditions. Another challenge is the direct and strong sunlight, however, we combat this issue with the use of the retro-reflective tape and by placing the vibrometer in a shade or with the use of a visor to shade the lens of the vibrometer. A challenge for the operator is to focus the laser beam under these circumstances, while the visibility of the spot is affected by ambient light. Focusing in those conditions takes time and skill, while with the new generations of vibrometers with autofocus this is no longer a problem. Vibrometer has a broad frequency range up to 22 kHz and is linear in the entire frequency range. The velocity transducers used were HMB velocity pickups with the Hottinger amplifier and direct integration to velocity. The frequency range of the devices is from 0.7 to 1000 Hz (Fig. 5.8). In the last stage of the experimental work we used the Dewesoft Sirius that enabled simultaneous data acquisition from up to 8 analog channels at once (DEWESoft, 2019). We used only 4 channels connected with BNC connectors (see Fig. 5.9).

Slika 5.8: Hitrostna doza.
Figure 5.8: Velocity pickup.

Slika 5.9: Naprava za simultani zajem signala s pospeškomeri.
Figure 5.9: DAQ box with accelerometers.

5.4 Data Processing

Data acquisition is performed in time-domain. The sampling frequency was chosen at f_s = 2400 Hz. Considering the Nyquist-Shannon criteria to eliminate the effect of aliasing when sampling discrete-time signals, the sampling rate should be at least:

$$f_s > 2f_a \tag{5.1}$$

where f_a is the highest present frequency in the analogue signal (Brincker and Ventura, 2015). Such a sampling frequency was chosen due to the spectrum in the structural response lying in the range below 300 Hz. Since we expected longer time-series will have to be captured, we concluded 2400 samples per second is the optimal value to obtain good spectral resolution and not to waste computer memory while writing the data. We captured hours of data; the first step was revision and extraction of the events to analyse. Unfortunately, not all data series were appropriate for further work; we estimated that only 60% of extracted data were appropriate for further analysis. The main reason for some series not being appropriate was the loss of a sufficient backscatter and a change of the ambient temperature during the measurements. The majority of the experimental work was done in the cold time of the year, during regular work at the powerhouse. Whenever work demanded opening of the large entrance gate, a large mass of cold air entered in the powerhouse and the temperature instability obstructed the vibrometer measurements until the situation was stabilised and the instrument was again in equilibrium with the new conditions. Unforeseen events such as painting the reflective tiles during regular maintenance work caused the loss of data in the period before the tiles could be replaced. When the work caused the lifting of some fine dust and when the changes in the relative humidity and temperature caused the dust to glue to the tiles, again reducing the reflective capacity, this also caused the loss of data during some manoeuvres. Since this was a new experiment we anticipated that the unexpected loss of data can occur, while during the test many activities happen in the powerhouse and human factor can be unpredictable.

Signal post-processing of velocity channels was done using MATLAB software (Tervo, 2014; The MathWorks, 2018). We captured data sets of various lengths, the longest sets being 15 minutes long. In the first step the arrays of shorter segments of interest were selected. The shortest array contains information about only a few seconds during the start of a turbine and the longest one captures the entire start-up cycle, lasting for about 3 minutes. The usual segment is approximately 15 s long. DC offsets were removed by calculating the mean value of the signal blocks and subtracting them from the signal components. Instrumental drift is assumed to be linear over data blocks; if in a block a linear trend was evaluated, it was subtracted from the data block. Initial Fourier analysis revealed the presence of low frequency noise components. Digital filtering is done using ecliptic IIR band-pass filter. The use of elliptic filter minimised the number of poles, while the application of the zero-phase digital filter prevented phase distortion of the filtered signal. By processing the signal in both the forward and reverse directions, its phase remains unchanged. The filter is used to attenuate frequencies below the lower edge and upper edge passband frequencies at 1 Hz and 300 Hz, respectively. The band-pass ripple parameter is defined at 1 dB, and band-stop attenuation at 80 dB. The magnitude response of the used filter is presented in Figure 5.10. This filter was used as a default, however, in special cases filters with different specification had to be used, especially in cases where more of the low-frequency noise was present. These were the cases of changed circumstances during the measurement; for example in case of a temperature change we were able to further use the data set through specific filtering.

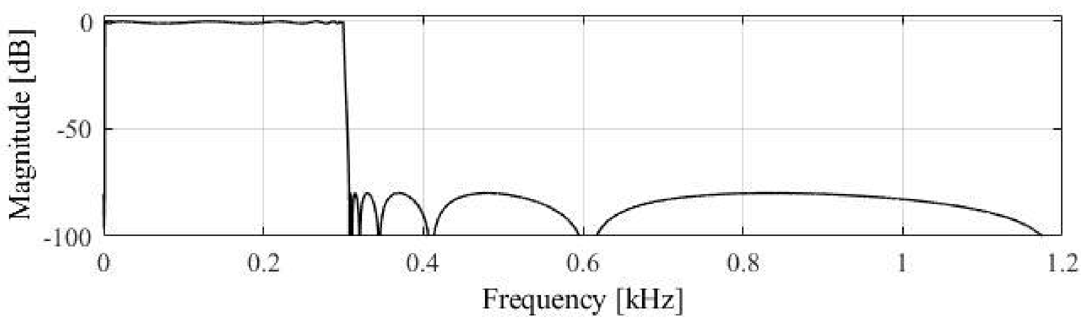

Slika 5.10: Karakteristika eliptičnega pasovno-prepustnega filtra.
Figure 5.10: Elliptic IIR band-pass filter.

The final step in the identification of the dominant frequencies of the system is the transformation into frequency-domain, using the Fast Fourier Transform (FFT):

$$P(f) = \int_{-N}^{N} x(t)e^{-j2\pi ft}dt \tag{5.2}$$

The prominent peaks in the spectrum were identified, using power spectral density to enhance the visibility of the peaks:

$$\hat{P}(f) = \frac{\Delta t}{N}\Big|\sum_{n=0}^{n-1} x_n e^{-j2\pi fn}\Big|^2, \qquad \frac{-1}{2\Delta t} < f < \frac{1}{2\Delta t}, \tag{5.3}$$

where Δt is the sampling interval, $\frac{1}{2\Delta t}$ is the Nyquist frequency: when the one-sided function is evaluated all the frequencies except 0 and Nyquist are multiplied by 2 in order to conserve the total power (Tervo, 2014).

5.5 Measurements

5.5.1 Stage 1 Measurements

Stage 1 measurements started on May 7, 2016, roughly two years after the beginning of the construction work. Fig. 5.11 presents the state of the structure on that day. The concrete works were mostly finished, however all the hydromechanics equipment was not installed yet and the Sava River was still re-routed in a diversion channel. On the day of the measurements, most of the work on the site was focused on installation of the components of the hydraulic gates and electrical equipment in the powerhouse. It was a sunny and clear day, with minimum wind. According to the Slovenian Environment Agency (ARSO), the nearest climate station in Cerklje recorded average daily temperature 15.4°C, average wind speed 2.5 m/s, relative humidity 68%, and estimated a 27% coverage of the sky with clouds. The experimental points investigated on that day were: P1 in the spillway, and S2 and ST2 in the powerhouse. The measurements on that day were intended to capture the stationary condition with the absence of any measurable external excitation force and under excitation with the construction works. Since the structure is never at rest and it vibrates at least to some extent, the term stationary state instead of rest state is used. Stationary condition is defined as the state when the statistical properties of the captured time-series over short time intervals do not vary significantly between consecutive intervals (Daniell and Taylor, 1999).

Pier in the Spillway

The 1st pier between the spillway sections I and II is measured from the opposite side from the pier annexed to the powerhouse. Under the influence of the construction works, the pier had vibrated significantly; the time-series of a one-minute recording is presented in Fig. 5.12(a). Short-term impacts result in a sudden rise of amplitudes, a maximum rise up to 0.08 m/s was

(a) Dolvodno lice pregrade.

(a) General view.

(b) Prelivno polje.

(b) Spillway section.

(c) Strojnica.

(c) Powerhouse.

(d) Vtok v turbinski trakt.

(d) Intake.

Slika 5.11: Izvedba prve faze meritev na HE Brežice.

Figure 5.11: 1st stage measurements at Brežice dam.

recorded, caused by a sudden burst in the construction site. A long-term excitement results also in higher modes. Fig. 5.12(b) presents a frequency spectrum of the measurement. We can notice three prominent peaks at 10.8 Hz, 16.8 Hz, and 33.6 Hz. In the late afternoon, when activities on the construction site came to an end, the stationary state of the pier was captured; amplitudes of the surface velocities were as low as $5{\cdot}10^{-5}$ m/s.

Powerhouse South Wall

Fig. 5.13 presents the surface velocities of the powerhouse south wall in a very short semi-stationary state during working hours on the construction site. Velocity oscillations are below $2.5{\cdot}10^{-4}$ m/s. When we repeated the measurement after the working hours on the same location, velocity amplitudes dropped even further, below $6{\cdot}10^{-5}$ m/s. The majority of the works on the day of the measurements took place near the stilling basin, and due to the dilated joint, the effects were not translating to the powerhouse section. The stationary state of the structure is presented in Fig. 5.13, while the response of the structure excited with construction works is

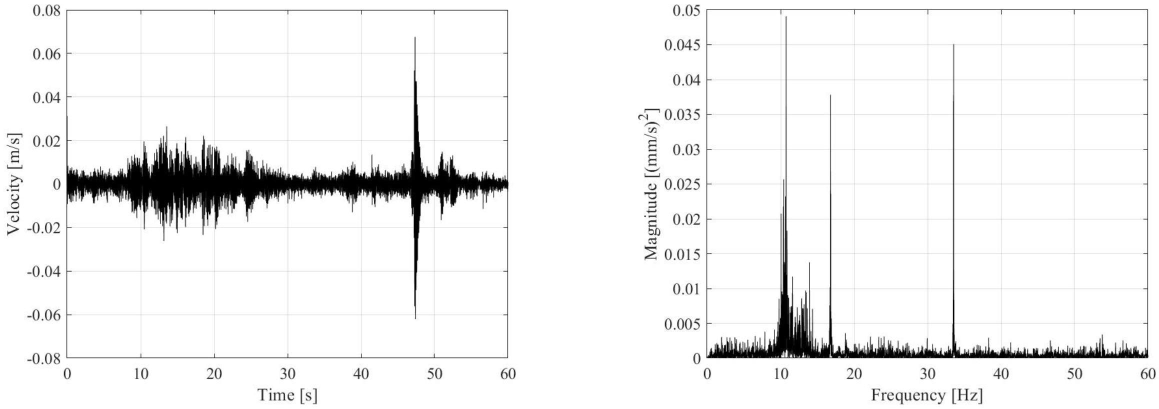

(a) Časovna serija. (b) Frekvenčni spekter.

(a) Time-series. (b) Frequency spectrum.

Slika 5.12: Odziv stebra v prelivnem polju na vzbujanje z aktivnostmi na gradbišču, meritev na merilnem mestu P1.

Figure 5.12: Response of the 1st pier in the spillway excited with the construction works, captured at location P1.

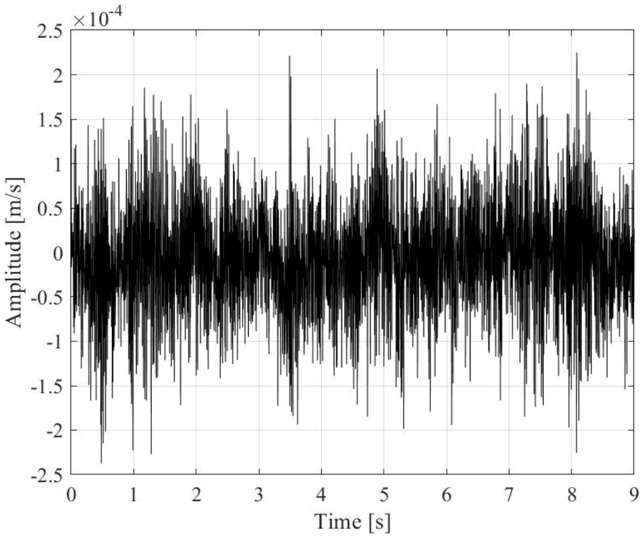

Slika 5.13: Meritev na južni steni strojnice v stacionarnem stanju, na mestu S2.

Figure 5.13: South wall in the powerhouse in the stationary state, measured at location S2.

presented in Fig. 5.14(a). The amplitudes are 10 times greater compared to the stationary state. However, in comparison, the amplitudes measured on the massive pier in the spillway are still one order of magnitude higher than those recorded in the powerhouse. The measurement had a lot of low-frequency noise below 1.2 Hz, the noise was removed using a high-pass filter with the cut-off frequency identified at 1.5 Hz. We were able to identify only one frequency at 40.5 Hz. The frequency spectrum is presented in Fig. 5.14(b).

The measurement revealed the amplitude of the structural vibration during stationary "rest" conditions. The excitation with the construction works caused the massive dam structure to response, with the amplitudes 10 times greater than in the stationary state. We have also noticed that long-term excitations provide better conditions to measure than short-term peak events. This observation was also confirmed during the re-routing of the Sava River back to the original river stream. The massive structure is very well damped and it needs longer excitation times to obtain qualitative experimental data. In other words, when peak events are expected to be measured, the use of accelerometers is advantageous to the use of a vibrometer.

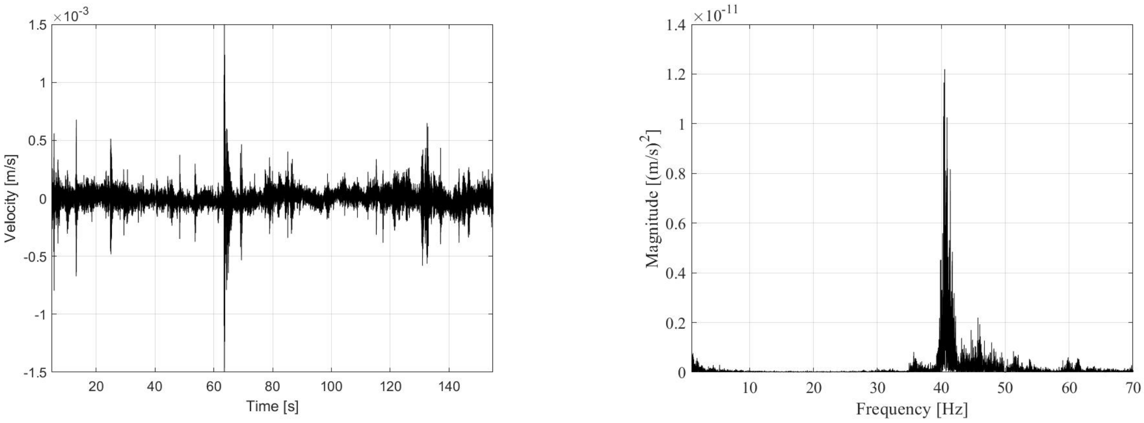

(a) Časovna serija.

(a) Time-series.

(b) Frekvenčni spekter.

(b) Frequency spectrum.

Slika 5.14: Odziv južne stene strojnice na vzbujanje z deli na prelivnih poljih, meritev na mestu S2.

Figure 5.14: South wall in the powerhouse excited with construction work in the overspilling section, measured at location S2.

5.5.2 Stage 2 Measurements

Stage 2 measurements aimed at detection of the operational loads and therefore concentrated on the powerhouse. The most extensive period of field investigations started in August 2017. The reservoir reached the nominal level on August 11, 2017, and a few days later the last stage of the start-up test of the hydro-mechanical equipment was scheduled. The stages of the test at this time included operation of the turbines at 0.25, 0.5, 0.75, and at full power, with tests of both electrical and mechanical emergency brakes. The last and the most invasive manoeuvre was the simultaneous load rejection on two units. The intention of the tests is to control the automation behind the operational procedures, whether the brakes deploy at the right time, whether flaps and the hydraulic gates follow, and if the emergency situations are automatically recognised. The tests are strongly conditioned with hydrology conditions, and unfortunately the conditions that year were very unfavourable, as the dry period was followed by extensive rainfall and flood water. In the first case, tests at full power were unobtainable while the level of water in the reservoir dropped below the nominal, since the outflow was a lot higher than the inflow in the reservoir. In the second case the rainfall caused the rise of the downstream level and the difference between the upstream and downstream level was again not sufficient to achieve full power. The tests were often aborted until the hydrology conditions improved and were basically a chase for optimal conditions. The tests were scheduled to be finished in two months. Due to the problems concerning hydrology the final stages of the tests were finishing as late as in January 2018. The tests were conducted in the following manner:

- test on Unit 3;
- test on Unit 1;
- test on Unit 2;
- simultaneous load rejection.

Experimental points were activated according to the unit where the tests were underway. Fig. 5.15 presents typical time-series during a unit's start-up procedure. The example presents the start of Unit 3. As it was previously explained in Section 4.2, the start of a unit happens in stages. At first with the opening of the guide vanes, when the water entering the blades of the runner causes rotation. By observing time-series in Fig. 5.15, the start of the turbine caused a rise in vibration amplitudes, the sudden acceleration of the turbine causes a sudden rise in amplitudes. In Fig. we see a 10 s period of elevated amplitudes, then the amplitude drops. The synchronization procedure lasts roughly 2 minutes. This is a period of unstable operation; the generator builds up voltage and matches the frequency to the grid frequency. Closing of the

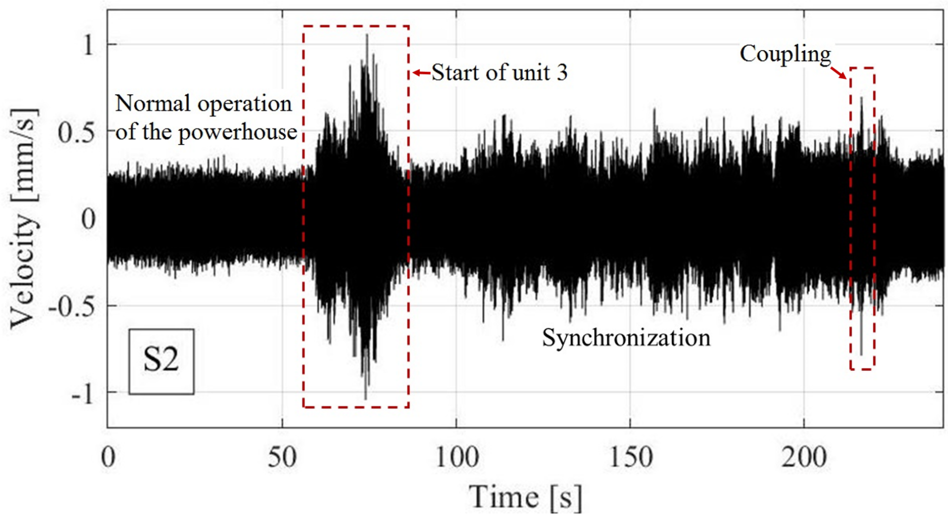

Slika 5.15: Zagon agregata 3 - časovna serija, zabeležena v točki S2. V času zagona elektrarna že obratuje, v mrežo se je vklapljal dodatni agregat.
Figure 5.15: Start of Unit 3 - time-series captured at location S2. The powerhouse was already in operation, the measurement captures the start of the additional unit.

circuit breakers connects the unit to the electrical grid, accompanied by a noise and a visible jump in the amplitude (in Fig. 5.15 the spike caused by the switch is marked with a dashed square). If the procedure is successful, in a few second the amplitudes drop and the production stabilises.

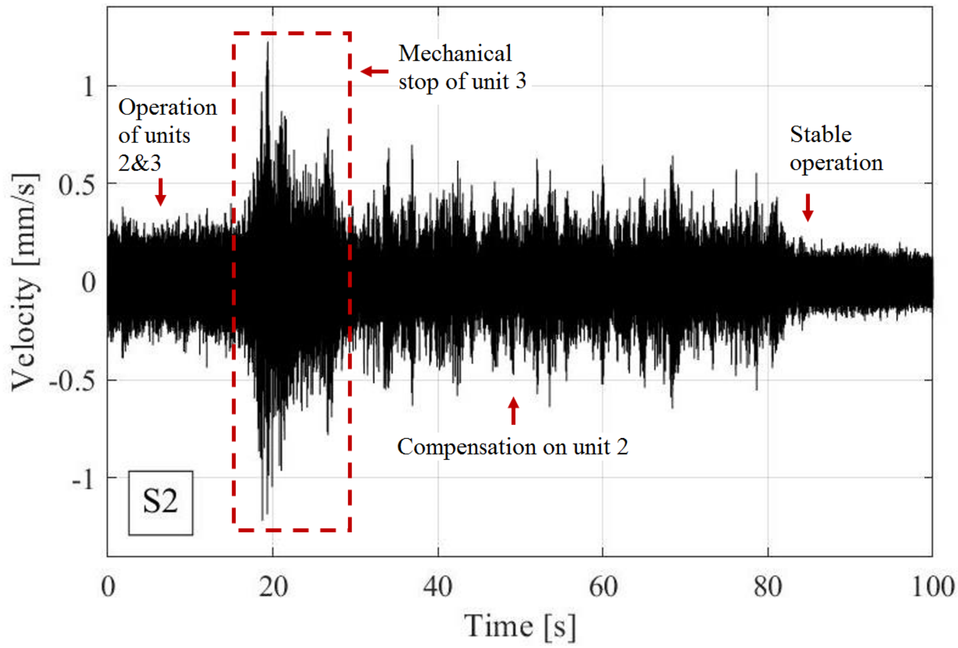

(a) Mehanska zapora agregata 3.

(a) Mechanical brake on Unit 3.

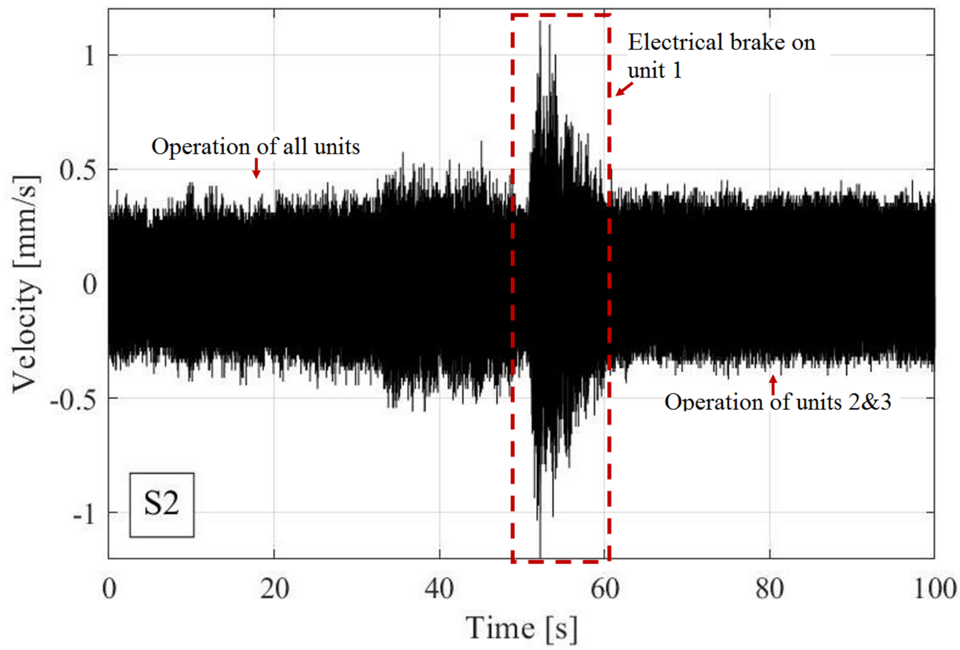

(b) Električna zapora agregata 1.

(b) Electrical brake on Unit 1.

Slika 5.16: Oba tipa zasilnih zapor, zabeležena na mestu S2.

Figure 5.16: Two types of emergency brakes and the time-series captured at S2.

In case the coupling to the grid would is unsuccessful, one of the emergency brakes is deployed. Examples of both are presented in Figures 5.16(a) and 5.16(b), where mechanical and electrical brakes are presented, respectively. Emergency braking is a very fast manoeuvre. The mechanical brake has two sequential actions; the stopping of the turbine is followed by opening of the circuit breakers, and the response of the structure also depends on how strong of a disturbance is caused by losing one unit to the remaining operating units. The case in Fig. 5.16(a) presents a case when operation of Units 3 and 2 is interrupted with the load rejection on Unit 3. If we look closely at the time-series, the rejection itself was not as intensive as we would expect, but it caused strong instabilities on the remaining unit in operation. After one minute, the operation again stabilises and amplitudes drop. The electrical brake on Unit 1 (Fig. 5.16(b)) had a similar impact on the structure. Typically the electrical brake reflects in a sharp triangular time-series, a sudden rise of amplitude and a quick drop. The transient action lasts for only a few seconds (10–12 s). In the case of Fig. 5.16(b), Unit 1 was stopped while all units were operating and were connected to the grid. The remaining two units did not try to compensate the loss of power, but only sustained their stable production with 15 MW output each. We have to emphasise as well that Unit 1, before being stopped, was trying to achieve the highest power in the given conditions. This is the reason why the time-series before the stopping manoeuvre does not show stable conditions. In the figure, it is evident that the operation was not stable, as elevated high-frequency oscillations are present in the time-series.

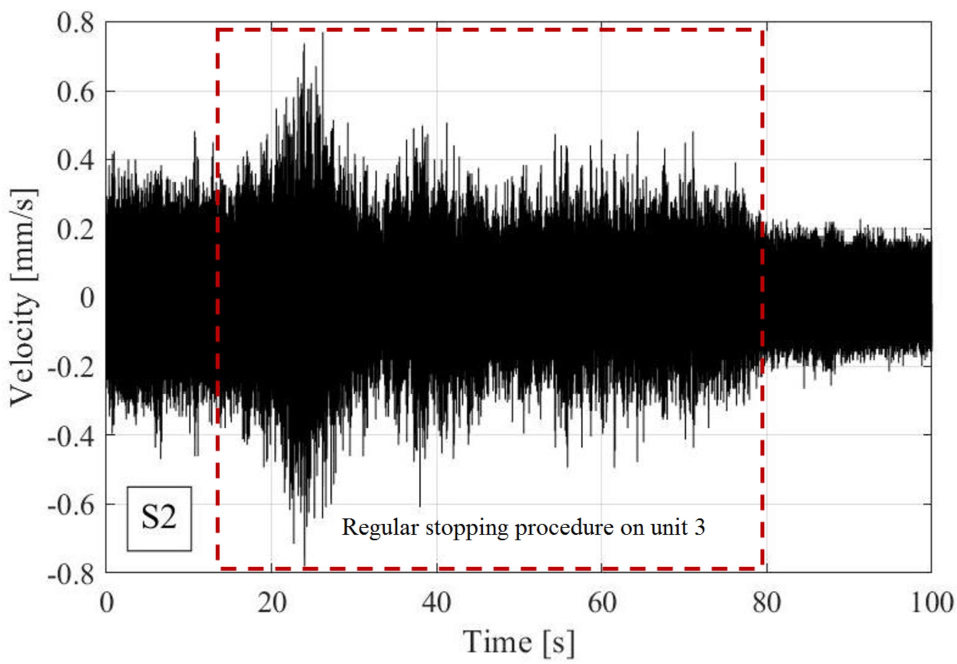

Slika 5.17: Zaustavitev agregata 3.
Figure 5.17: Regular stop of Unit 3.

A regular shut-down has a slower manoeuvre of stopping, guide vanes close slowly. The slow manoeuvre is designed to prevent damage to the electro-mechanical equipment, while the sudden closing causes water hammer and other hydraulic phenomena. Fig. 5.17 presents a case of a regular stop of Unit 3. A rise in amplitudes is caused by the closing of the guide vanes and opening the circuit breakers. Based on the structural response amplitudes, i.e. if we observe the peak values, the regular stop procedure is by about 1/3 less invasive compared to the emergency brakes. It takes around 1 minute for the unit to be off-loaded and stopped. During this time, the discharge is gradually stopped and the unit is eventually mechanically stopped from spinning.

Regular operation of turbines is a source of vibration for the dam structure. The measurements of the south wall in the powerhouse in stationary ("rest") condition revealed velocity oscillations in a magnitude range of a few 10^{-5} m/s. Regular operation of turbines rises the oscillations to reach the values of approximately 0.5 mm/s, and transient actions in rough estimation have double the amplitude.

Vertical Kaplan turbines are reactive turbines and produce the majority of the excitation in the horizontal direction. However, double regulation allows manipulation of both, guide and wicket gates. During manoeuvres, gates are opened and closed and, especially during shut-down, closing of the gates that helps to slow down the turbine subsequently changes the acting uplift force on the units. This change causes additional excitation also in the vertical direction. To detect the impact of the vertical actions, the experimental point StV on the floor connecting the turbine shafts was equipped with velocity pickups to measure vertical vibrations. The level of vibration in the vertical direction detected during transient actions was higher than expected, e.g. with a maximum amplitude more than 3 mm/s during the start manoeuvre of turbine 2. Influence of the turbine operation was detected on all experimental points located in the powerhouse.

The measurements also revealed that turbine 2 has a prevailing influence on the structural response, which was expected as it is located in the central part of the structure. In Tables 5.5–5.7 the maximum velocity amplitudes per specific manoeuvre are collated. Table 5.5 presents cases of normal operation manoeuvre start of a turbine, which according to available information occurs around 50 times in a year per unit. We have discovered that regardless of the unit and the manoeuvre the influence was detected through the structure of the powerhouse. Mechanical braking (Fig. 5.6) surprisingly results in lower peak amplitude velocities as for example the regular start; a similar situation occurs when the electrical brake is activated. However, the electrical brake causes a strong influence in the vertical direction as can be seen in Table 5.7. This is expected; the reactive type of turbine is susceptible to the sudden change in the uplift caused by the fastest manoeuvre and is expected to have the strongest vertical excitation force.

Simultaneous load rejection on two units was simulated twice, on Units 1 and 2, and 2 and 3 (presented in Figures 5.18(a) and 5.18(b)). This is a serious manoeuvre that causes a broader instability in the grid. The test was carefully planned and the grid operator was informed in advance, while compensation had to be provided. The procedure of the test was the following: all three units must operate at the highest possible power provided by hydrology at the time of the test and then mechanical brakes are manually activated in two units. The remaining unit needed to sustain an isolated operation procedure (island operation), and the rest of the automation had to prevent an upstream moving wave in the reservoir, with activation of gates and flaps in the spilling sections. The powerhouse needs to be able to sustain itself to keep one stable unit and to operate safely. Once the situation is stabilised, and as soon as possible, provided that the disconnected units are not damaged, they have to be synchronised again and connected back to the grid. The entire procedure is automatic. Load rejection on Units 2 and 3 had a stronger structural influence than the one on Units 1 and 2. The main reason for this is that in case of simultaneous load rejection on Units 1 and 2, there is a phase between the times that both brakes were deployed; an approx. 1 s time difference occurred. The brakes were deployed manually by counting down, and using this procedure, an error easily happens. If we look closely at Fig. 5.18(b), we can observe two peaks very close together, in comparison to one peak in Fig. 5.18(a). Instead of one cumulative push, the structure had two sequential events within 1 s, which resulted in lower peak amplitude values. After the procedure, a different type of automation was tested, the powerhouse needed to sustain the power, meaning the remaining Unit 3 that stayed on the grid had to compensate for the lost 2 units. By observing the time-series after the peak values, we can notice that that the operation was not stable, since Unit 3 had to remain operable and keep the balance while it was gradually building up load to the maximum power. The recordings in Figures 5.18(a) and 5.18(b) are until now noted as the most intense event occurring in the powerhouse since its construction.

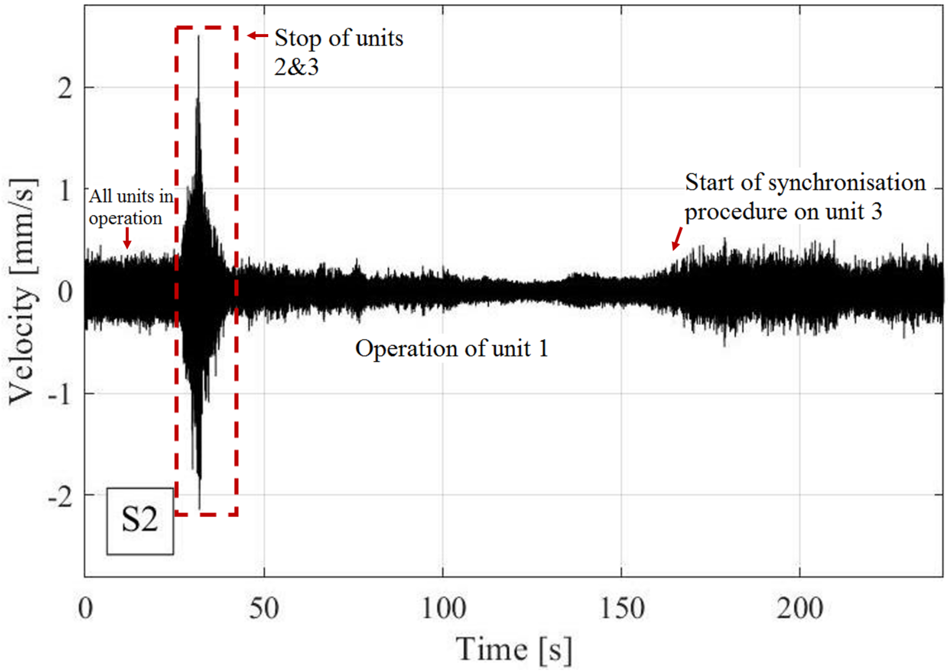

(a) Hitra zapora agregatov 2 in 3.

(a) Simultaneous load rejection on Units 2 and 3.

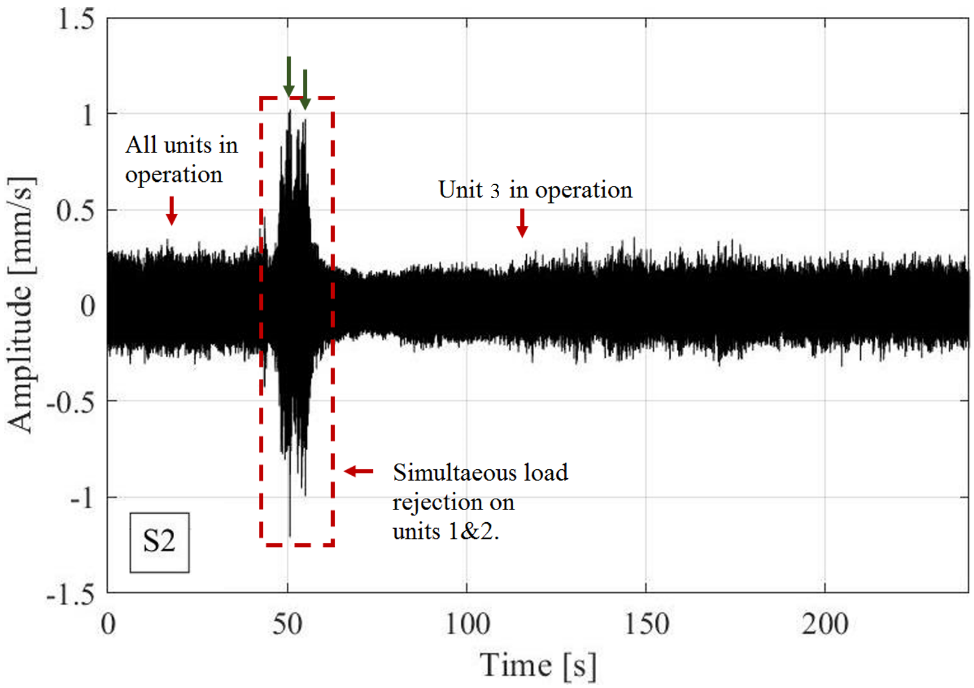

(b) Hitra zapora agregatov 1 in 2.

(b) Simultaneous load rejection on Units 1 and 2.

Slika 5.18: Hitra zapora dveh agregatov hkrati.

Figure 5.18: Simultaneous load rejection.

Other typical time-series captured during operation and corresponding frequency plots are presented in Appendix 1.

Preglednica 5.5: Maksimalne amplitude oscilacij v [mm/s], izmerjene pri zagonih turbin.
Table 5.5: Peak amplitudes (in [mm/s]) captured during starts of the units.

Location	Start of Unit 1	Start of Unit 2	Start of Unit 3
ST1	0.9	0.7	0.65
ST2	0.8	1.3	0.74
S2	1.1	1.7	0.95
StV	2.4	3.7	3

Preglednica 5.6: Maksimalne amplitude oscilacij v [mm/s], izmerjene pri proženju mehanske hitre zapore na posameznih agregatih.
Table 5.6: Peak velocity amplitudes (in [mm/s]) captured during mechanical brakes.

Location	Mechanical brake on Unit 1	Mechanical brake on Unit 2	Mechanical brake on Unit 3
ST1	0.55	0.65	0.45
ST2	0.7	1.0	0.45
S2	0.95	1.3	0.7
StV	2.2	2.8	1.8

Preglednica 5.7: Maksimalne amplitude oscilacij v [mm/s], izmerjene pri proženju električne hitre zapore ter pri hkratni razbremenitvi dveh agregatov.
Table 5.7: Peak velocity amplitudes (in [mm/s]) captured during the electrical brake on turbines and during simultaneous load rejection on two units.

Location	Electrical brake on Unit 1	Simultaneous load rejection on Units 1 and 2	Simultaneous load rejection on Units 2 and 3
ST1	0.5	0.62	1.3
ST2	0.65	0.68	1.5
S2	1.1	1.2	2.5
StV	4.2	2.6	3.7

Frequency spectrum

Our main interest is in the frequency spectrum of the captured response. The transformation of the time-series into frequency spectrum is done using the Fast Fourier Transform. One of the research questions was whether the effect of the turbine operation is limited only to the proximity of the turbine shaft or whether we can detect its influence through the structure. With the grid of measurement points we are able to experimentally prove that the influence of the system is uniform while the effect of operation is transferred and detected throughout the structure. As a rough estimate, the amplitudes at the south wall of the powerhouse are the highest at S2, while the values at location ST2 are approximately 30% lower and at location ST1 60% lower. The amplitudes in the vertical direction on the floor connecting the turbine shafts were surprising. Kaplan turbines are a known source of the vertical excitation force, however, we did not expect that the highest amplitudes would be measured at location StV and in vertical direction. Including the stator, each unit weights over 190 t and operates under 166 m^3/s of maximum discharge at full power. This presents a significant load at any type of transient action, while due to the transition from base to peak load operation, we can expect the turbines to operate under variable conditions more often and the number of start-stop cycles to even increase over time. Even during regular operation, the excitation of the water flow is substantial. The water enters the spiral which has a complex form in order to maximise the utilisation rate. A complex 3D flow of high velocity changes the direction of the flow by 90° to enter on the runner and it transforms its kinetic energy into rotation of the blades and then flows downstream to exit the conduit. During operation, the system is in a complex equilibrium and any flow disturbance is translated to the runner, while any rotating machinery disturbance is translated to the fluid. We have to emphasise that the runner rotation is practically not damped at all. The breaking force during operation is created with water inertia and the load of the grid. Therefore, any flow disturbance is directly felt by the runner. How this disturbance is translated further depends on the inertia of the rotating mass. This is also the reason why emergency brakes are installed, i.e. once the runner is in rotation it won't stop by itself. Even worse, once the load is removed, the blades are left with the initial push and subsequently the runner starts to accelerate. This is a very dangerous situation; in cases when the runner was not stopped in time, it resulted in failure.

Frequency plots presented in the following pages present the most prominent peaks captured during the manoeuvres. The response of experimental point S2 is presented, while the most prominent peaks on all experimental points have similar values. For example 7.1 Hz peak is recognised as one of the most prominent peaks throughout the structure. The structure is most susceptible to excitations in the lower frequency range. In the bounds from 7 Hz to 16 Hz, we can observe multiple peaks, then further to higher frequencies, prominent local peaks occur at 21 Hz and 43 Hz. The peak at 100 Hz is evident and very prominent. The 100 Hz peak is connected to the generator operation; researchers have identified that the eccentricity of the generator is recognised in the frequency spectrum as peaks close to the double of the frequency of the grid (Choudhary et al., 2018). Considering the large mass of the generator, it is expected that the effect is clearly visible, and can be identified on all experimental locations. We underline again that the eccentricity is normal, since every generator has some eccentricity, due to the manufacturer's and building margin of imperfections. The effect of turbine operation is clearly visible on the plots; for example, the excitation of the turbine with the blade-passing frequency is at 7.1 Hz. In this chapter, we present only some frequency plots, while more on the measurement results, from all test locations, including frequency plots, is given in Appendix 1.

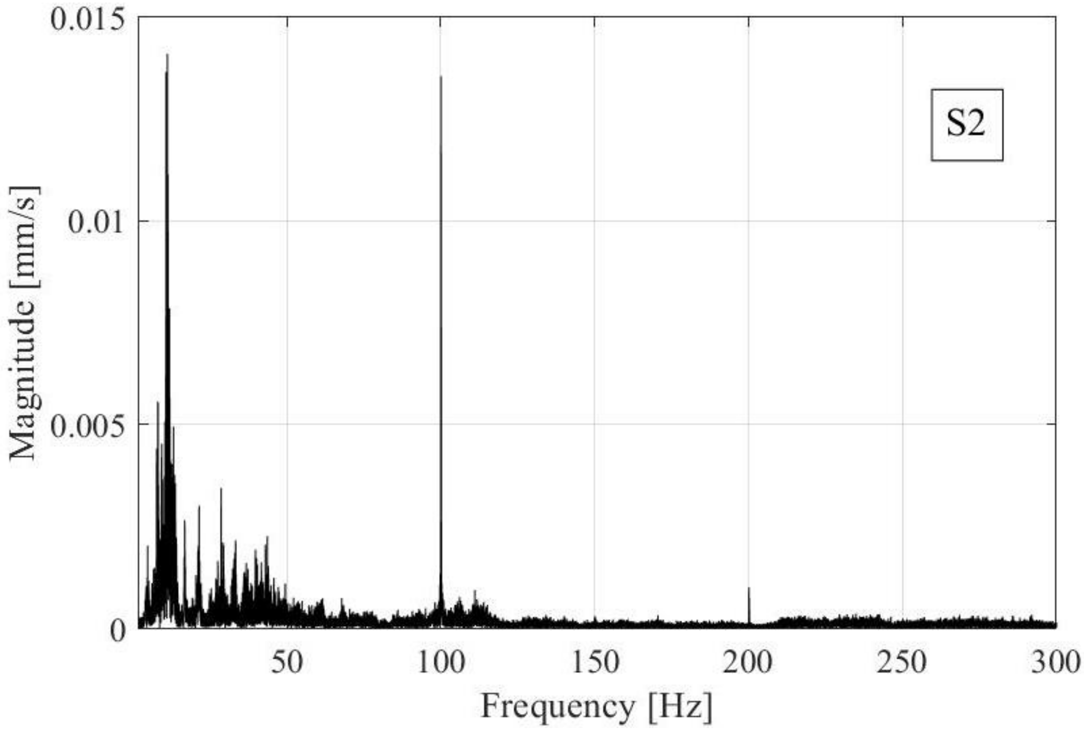

(a) Mehanska zapora agregata 3.

(a) Mechanical brake on Unit 3.

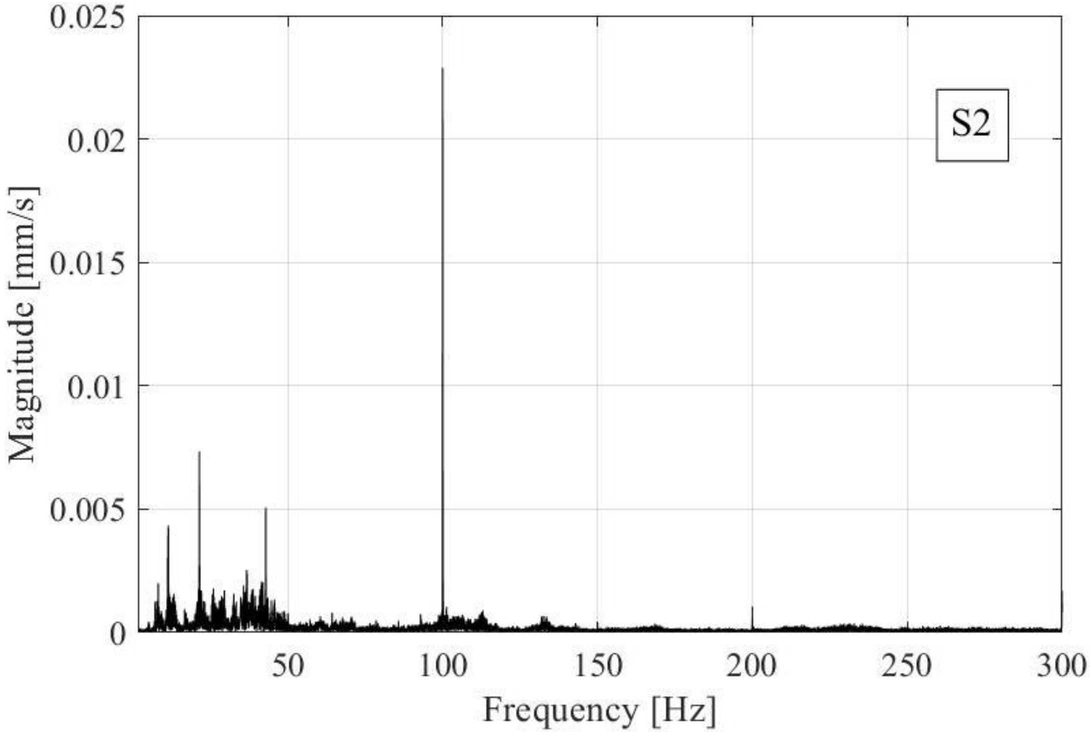

(b) Električna zapora agregata 1.

(b) Electrical brake on Unit 1.

Slika 5.19: Frekvenčni spekter obeh tipov zasilnih zapor, zabeleženih na mestu S2.

Figure 5.19: Frequency spectrum of two types of emergency brakes captured at S2.

Figures 5.19(a) and (b) present frequency domain during both types of emergency brakes, mechanical and electrical. We can observe that the electrical brake results in a high peak at 100 Hz, which is in accordance with the procedure, since the circuit breakers and the mechanical rotation are stopped at the same time. The rotor has a higher momentum than in the case of the mechanical brake, as a consequence a strong effect of the rotor mass is recognised in the structural response. In the lower frequency range, the 7.1 Hz effect of blade-passing frequency is recognised as well as the higher harmonics. The first recognizable peak in the frequency spectrum is, as expected, the rotational frequency at 1.8 Hz. Similar peaks are observed on the spectrum of the mechanical brake, where besides the frequencies that are linked to the mechanical equipment, a structural frequency at 10.6 Hz is evident as well. A similar frequency plot is revealed once we observe the regular stop of the unit. We need to emphasise that during the regular stopping manoeuvre, the structure is subjected to excitation for a longer time period, and due to the large mass, longer lasting phenomena are even less favourable from the structural point of view. The two cases of simultaneous load rejection are presented in Figures 5.20(a) and (b). We observed the two cases resulting in different time-series, due to the phase difference between the initiation of both brakes and also because two different units were activated. In the case of brakes on Units 1 and 2, when the stops were sequential within 1 s, the remaining unit covered the lost load. Again, we can observe the strong influence of the generator operation, while it was unstable due to the loss and needed to compensate during the load gain. The peaks in the low-frequency region are on the same locations and have similar magnitude values.

Start-stop cycles occur on a weekly basis; according to the statistical analysis of the operational regimes at Krško HPP, there are approximately 143 cycles/year. We identified the start of a turbine as a crucial manoeuvre, since the unloaded unit needs to gain speed and to synchronise phase and frequency to match the grid. After the mechanical start of the turbine, the first 20 s are the most active and produce the most excitation, which is further transferred to the structure. In Fig. 5.21 we present the spectrogram of the first 2-minute interval after the start of the turbine. The spectrogram is a time-frequency representation where we can visually observe frequency variability with time. In its essence it is a heat map where the intensity of the frequency content of the signal is represented with colour. In Fig. 5.21 the dark-blue-to-bright-yellow colour spectrum represents the intensity, the high-intensity signal is marked in yellow. The bright yellow ridges aligned with the time axis appear at frequencies of 7.1 Hz, 7.8 Hz, 11.2 Hz, 12.8 Hz, 21.4 Hz, 35.7 Hz, 42 Hz, and 100 Hz. These ridges are prominent, stable through the entire start-up sequence and easily recognised. In the first 20 s after the start-up we can observe the vertical noise spreading in the vertical direction. This indicates the instability in the signal. If we correlate the vertical noise with the excitement caused with the turbine, the spectrogram confirms that in the first 20 s after the start-up, the turbine accelerates to a near synchronous speed, and after that it rotates with more or less constant rotational speed. The acceleration in the first 20 s reflects in the added frequency noise, which drops drastically after the turbine reaches synchronous speed.

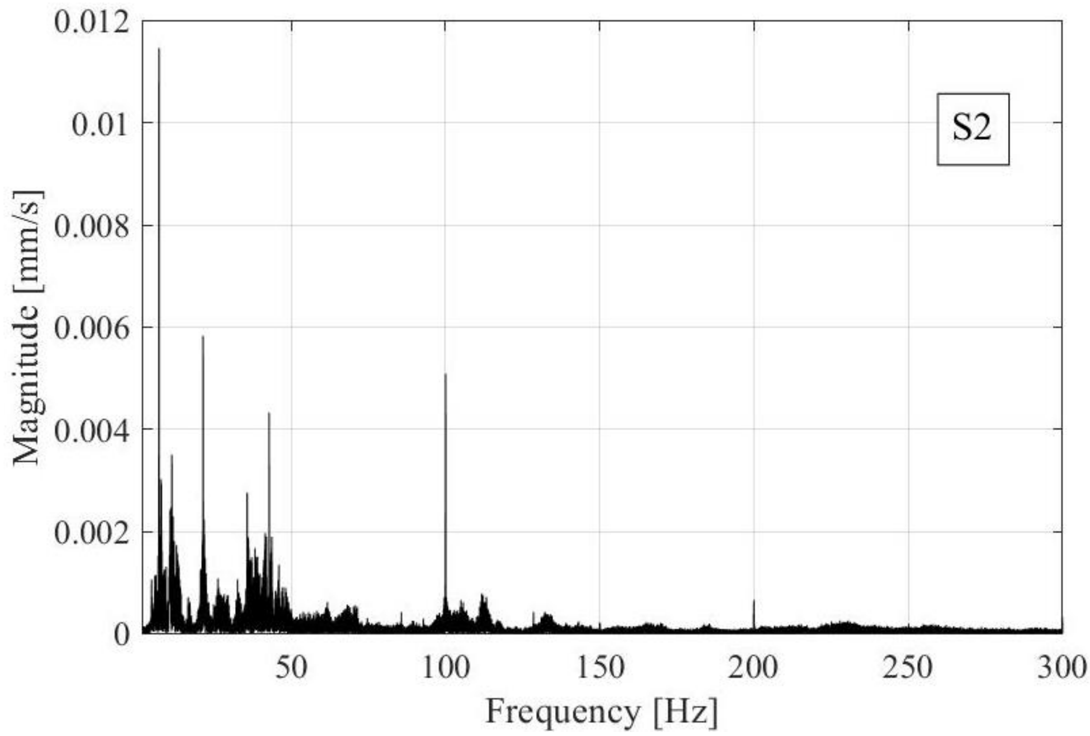

(a) Hitra zapora agregatov 2 in 3.

(a) Simultaneous load rejection on Units 2 and 3

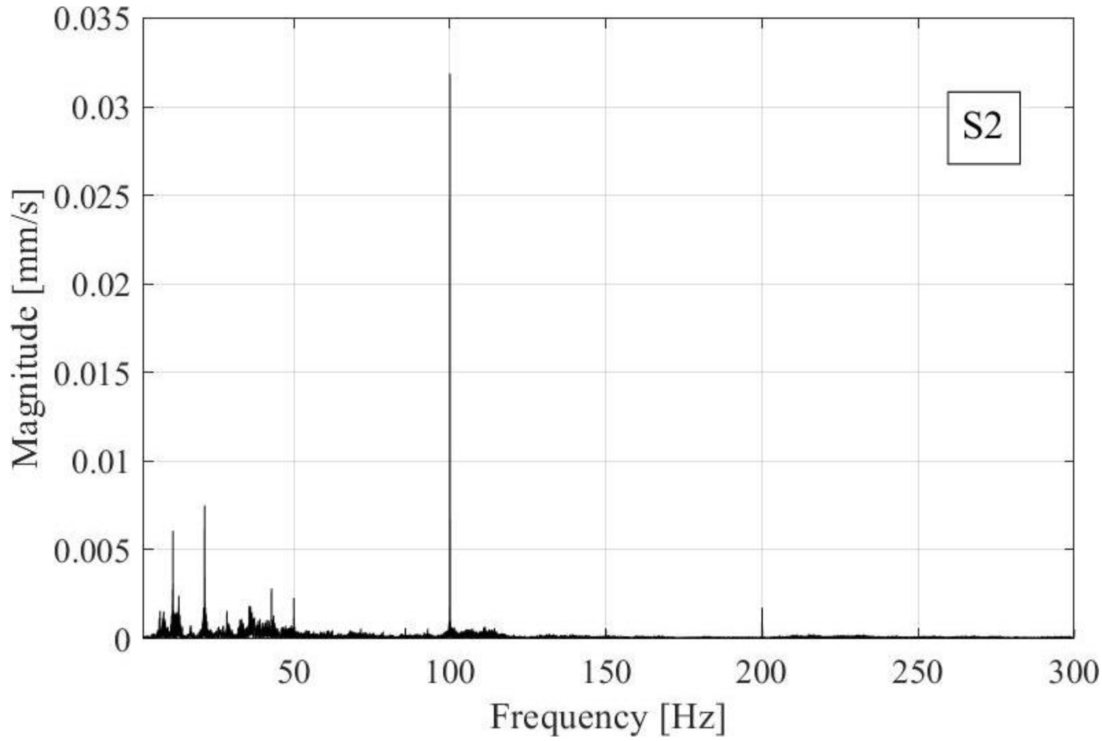

(b) Hitra zapora agregatov 1 in 2.

(b) Simultaneous load rejection on Units 1 and 2

Slika 5.20: Frekvenčni spekter odziva med proženjem hitrih zapor na dveh agregatih hkrati.

Figure 5.20: Frequency spectrum of the recordings of simultaneous load rejection.

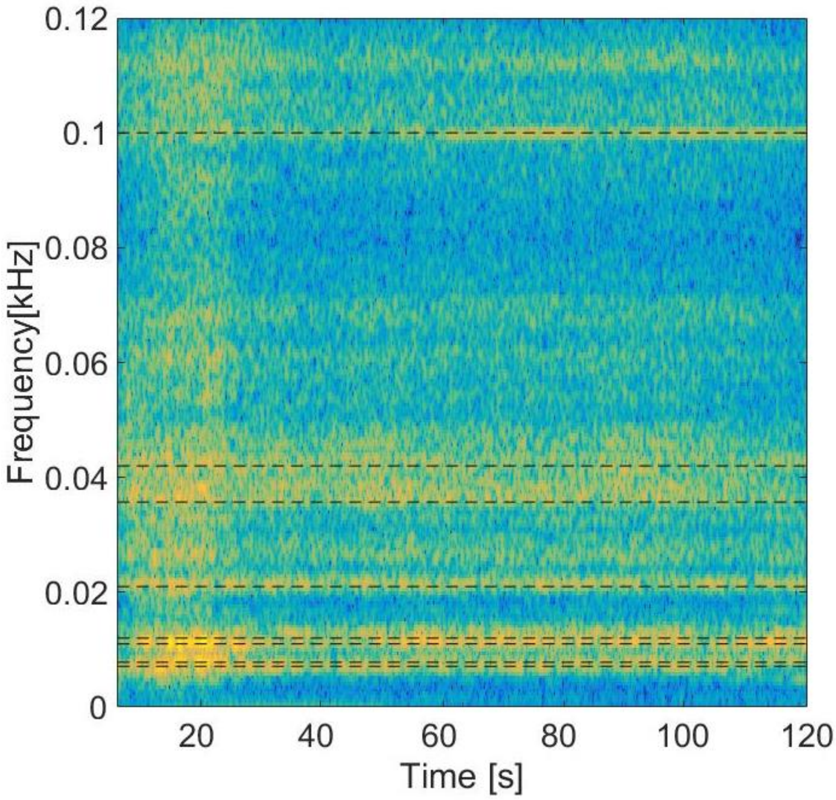

Slika 5.21: Spektrogram zagona turbine.
Figure 5.21: Spectrogram of turbine start.

In Tables 5.8–5.10, the first five peaks in the frequency spectrum are listed in a descending order of magnitude; only the first five are listed, but also others are clearly visible in the frequency spectrum.

Preglednica 5.8: Izstopajoči vrhovi v frekvenčnem spektru odziva [Hz] v padajočem velikostnem redu, zabeleženi med zagoni turbin.
Table 5.8: Most prominent peaks in the frequency spectrum captured during starts of the units in [Hz] in a descending order.

Location	Start of turbine 1	Start of turbine 2	Start of turbine 3
ST1	21.4, 100, 11.5, 13.5, 8.0	7.1, 100, 11.7, 13.5, 21.4	7.1, 11.4, 21.4, 100, 16.8
ST2	21.4, 11.5, 12.8, 100, 7.6	11.3, 13.2, 42.9, 8.1, 21.5	7.1, 11.4, 13.1, 42.9, 8.4
S2	100, 21.4, 42.9, 11.5	100, 11.3, 12.2, 8.1, 21.4	100, 11.4, 7.1, 21.4, 13.1
StV	100, 200, 27.9, 21.4, 42.9	100, 28.1, 65.6, 13.5, 7.1	100, 200, 28.2, 7.1, 65.6

Preglednica 5.9: Izstopajoči vrhovi v frekvenčnem spektru odziva [Hz] v padajočem velikostnem redu, izmerjeni pri proženju mehanske hitre zapore na posameznih agregatih.
Table 5.9: Most prominent peaks in the frequency spectrum captured during mechanical brakes on the units in [Hz] in a descending order.

Location	Mechanical brake on Unit 1	Mechanical brake on Unit 2	Mechanical brake on Unit 3
ST1	100.1, 11.5, 21.7, 49.4, 45.1	12.6, 21.4, 8.0, 100.1, 4.7	100, 8.4, 9.4, 11.4, 21.4
ST2	11.5, 21.5, 47.9, 13.2, 26.7	12.6, 11.3, 21.4, 8.0, 25.6	9.4, 11.2, 8.4, 12.7, 21.4
S2	100.1, 11.5, 42.8, 21.5, 36.8	100.1, 12.6, 21.4, 11.3, 8.0	100, 9.4, 11.4, 21.4, 43
StV	100.1, 200.1, 28.0, 65.9	100.1, 200.1, 28, 65.6	100, 27.9, 200, 9.4, 65.1

Preglednica 5.10: Izstopajoči vrhovi v frekvenčnem spektru odziva [Hz] v padajočem velikostnem redu, izmerjeni pri proženju mehanske hitre zapore na posameznih agregatih ter pri hkratni razbremenitvi dveh agregatov.
Table 5.10: Most prominent peaks in the frequency spectrum captured during electrical brakes and during simultaneous load rejection on two units in [Hz] in a descending order.

Location	Electrical brake on Unit 1	Simultaneous load rejection on Units 1 and 2	Simultaneous load rejection on Units 2 and 3
ST1	99.9, 21.4, 25.6, 8.2, 199.9	100, 21.4, 42.9, 11.2, 200	21.5, 8, 16.6, 100, 13.1
ST2	21.4, 11.4, 25.6, 42.9, 199.9	42.9, 21.4, 11.3, 13.1, 27.8	11.3, 21.5, 7.9, 13.1, 6.1
S2	100, 21.4, 42.9, 11.4, 36.7	100, 21.4, 11.3, 42.3, 36.1	100, 11.3, 21.5, 7.9, 6.1
StV	100, 199.9, 28.3, 65.6, 42.9	100, 200, 28,3, 65.2, 25	27.7, 100, 200.1, 66, 25

5.5.3 Stage 3 Measurements

In stage 3 measurements, we focused on the turbines and on improving the capabilities of the laser Doppler vibrometer. Our investigation revealed the effect of operation on the structural response. The broader aim of this investigation is to establish a methodology to monitor vibration on a regular basis to be able to detect the process of ageing or any other structural changes using non-contact measurements. To gain reliable data we used a combination of various measuring devices. After completing the start-up test, we extended our research to develop a methodology to use only one piece of equipment, the non-contact LDV in all cases. This means we have to be able to mount the LDV on a tripod and also on a moving ground and be able to measure real structural response with sufficient accuracy. A robust methodology should enable measurements during all operating regimes and also on active standing points. LDV has not been used yet for such a purpose. However, after a literature review, we discovered there were research groups trying to mount a LDV on an unmanned aerial vehicle and there has already been a successful application of vibration measurements on an object out of line-of-sight of a laser beam, diverted with a prism mounted on a vibrating object (Halkon and Rothberg, 2017a, 2018). Authors also present a methodology where laser measurements are corrected using two accelerometers mounted on a LDV (Halkon and Rothberg, 2017b). The basic assumptions for the derived equations are:

- LDV and any additional sensor mounted on the device move as a rigid body;
- the accelerometer's output is automatically integrated into velocity.

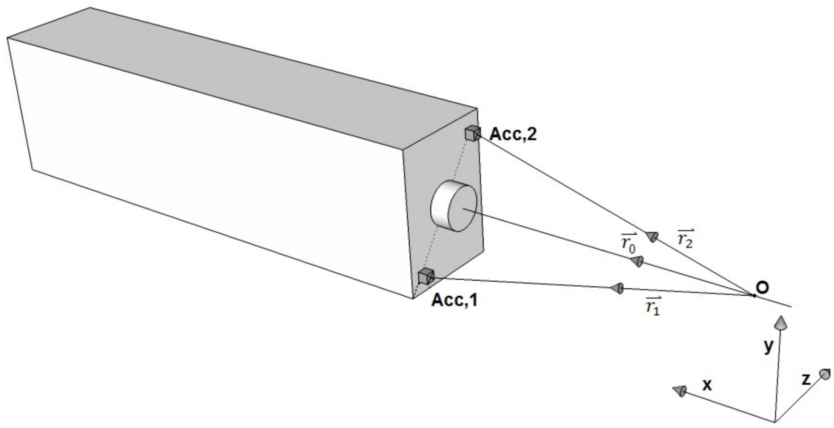

Slika 5.22: Shema namestitve dveh enoosnih pospeškomerov na LDV z občutljivo osjo, usmerjeno v smeri žarka, ter na diagonalnih pozicijah na enakih oddaljenostih od osi žarka.
Figure 5.22: Scheme of the mounting of the accelerometers on LDV with its sensitive axis in the direction of the laser beam and equal but opposite (y,z) location coordinates.

The arbitrary velocity of the accelerometer mounted on LDV, $\vec{v_i}$, can be written as a sum of velocity at reference point *O* on the beam path, $\vec{v_0}$, and angular motion around that point, $\vec{\theta}$. The position of the accelerometer is described with position vector $\vec{r_i}$.

$$\vec{v_i} = \vec{v_0} + \vec{r_i} \times \vec{\theta} \tag{5.4}$$

The correction component of the velocity is a fraction of the total velocity component in the direction of the beam and can be written as:

$$\vec{u_0} = \vec{e_i} \cdot \vec{v_0} \tag{5.5}$$

where $\vec{e_i}$ is the unit vector. If we introduce Eq. 5.4, the Eq. 5.5 can be written as:

$$\vec{e_i} \cdot \vec{v_0} = \vec{e_i} \cdot \vec{v_0} - \vec{e_i} \cdot (\vec{r_i} \times \vec{\theta}). \tag{5.6}$$

The angular motion around the reference point in the laser beam path $\vec{\theta}$ is unknown. By mounting two accelerometers on the LDV, summing and averaging their output we get:

$$\vec{v_1} = \vec{v_0} + \vec{r_1} \times \vec{\theta} \qquad \vec{v_2} = \vec{v_0} + \vec{r_2} \times \vec{\theta} \tag{5.7}$$

$$\frac{\vec{e_i} \cdot \vec{v_1} + \vec{e_i} \cdot \vec{v_2}}{2} = \vec{u_0} + \frac{\vec{e_i} \cdot (\vec{r_1} \times \vec{\theta}) + \vec{e_i} \cdot (\vec{r_2} \times \vec{\theta})}{2} \tag{5.8}$$

We would like that the second term on the right-hand side in Eq. 5.8 vanishes. This can be achieved when the accelerometers are mounted at locations where their cross-products will be zero:

$$\vec{e_i} \cdot (\vec{r_1} \times \vec{\theta}) + \vec{e_i} \cdot (\vec{r_2} \times \vec{\theta}) = (\vec{r_1} + \vec{r_2}) \cdot (\vec{\theta} \times \vec{e_i}) = 0. \tag{5.9}$$

The cross product $(\vec{\theta} \times \vec{e_i})$ only has y and z components. For the term 5.9 to be zero, the sum $(\vec{r_1} + \vec{r_2})$ needs to have zero y and z components. Practically this means the accelerometers have to be mounted on positions with equal but opposite y and z location components. However, the precise installation is very important; a 1 mm imperfection in the position causes an error of $\frac{\pi}{360}$ mm/s and an angle misalignment causes a 1% error per degree of misalignment. With respect to the works of Halkon and Rothberg (2017a,b, 2018), we applied the methodology to mount two single-axis accelerometers on LDV to perform corrective measurements. We have designed an interface to be mounted on the PDV-100. The aluminium interface has a design tolerance of 0.02 mm to precisely rest on the frontal face of the vibrometer (see Fig. 5.23(a)). Exact positioning is done using a total station and geodetic measuring, and fixed with three bolts. The circular interface is a 10 mm thick metal plate with 12 sensory cavities, on a 97 mm

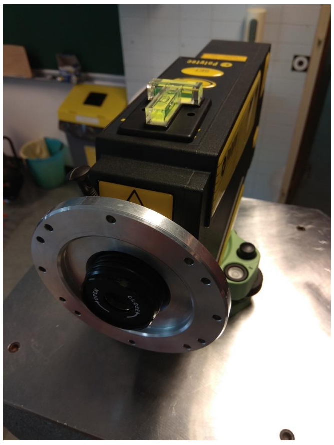

(a) Namestitev nastavka na vibrometer.

(a) Aluminium interface positioned on the LDV.

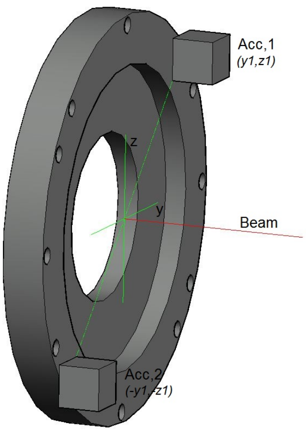

(b) Nameščanje pospeškomerov na vmesnik.

(b) Accelerometers placed on the interface.

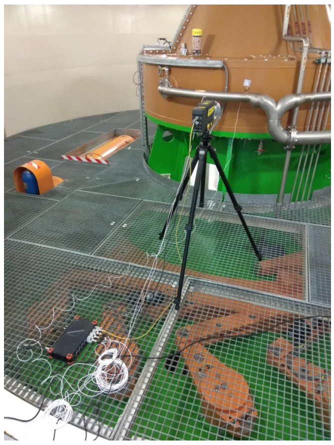

(c) Meritev na turbini.

(c) Measurement on the turbine.

Slika 5.23: Lega nastavka na napravi ter namestitev pospeškomerov na nastavek.

Figure 5.23: The interface mounting, scheme of the accelerometers positioning, and the measurement on the turbine in Brežice HPP.

circumference with the origin in the centre of the lens. The primary orientation of the vertical axis is through the centre of the lens, other sensory points are graduated with a 45° and 60° phase step enabling variable positioning of the accelerometers on the interface. The coupling of the accelerometers with the interface is implemented using UNC bolts compatible with the coaxial connector on the accelerometers. The placement of the corrective accelerometers has to be precise, and in order to smooth the error caused by the rigid body tilt of the vibrometer, accelerometers have to be placed on one of the diagonals and perfectly symmetrically to the origin of the laser beam, i.e., mirrored where the y, z location components should be $(y_1, z_1) = -(y_2, z_2)$ and also $y_1 = z_1$ and $y_2 = z_2$, where $y = 0$ and $z = 0$ represent the origin of the laser beam (see Fig. 5.24). Practically this means pairing an accelerometer positioned with a 45°

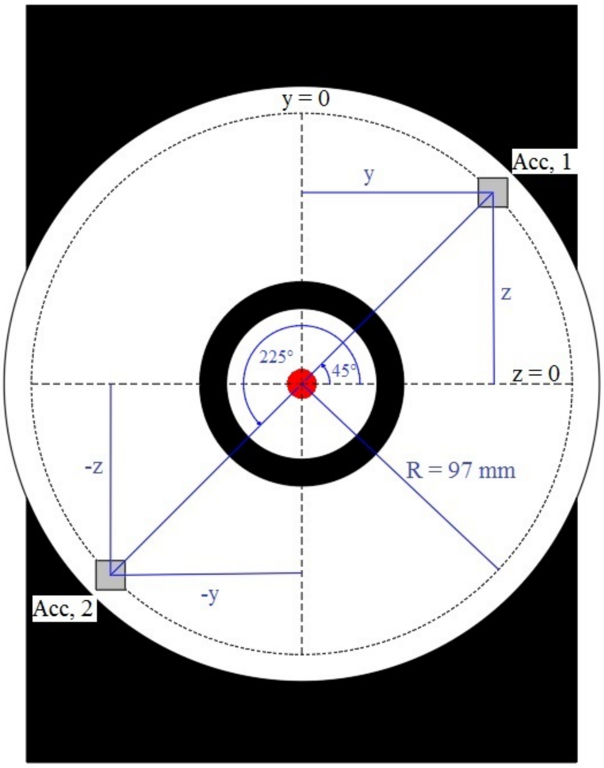

Slika 5.24: Pravilna namestitev popeškomerov.
Figure 5.24: Installation of the accelerometers on the front mask of a vibrometer.

angle from the vertical axis with an accelerometer positioned on 225° from the same origin (a schematic example of the placement is presented in Fig. 5.23(b)).

Our setup was tested during normal operation of turbine 1 at Brežice HPP. Polytec PDV-100 was equipped with two Dytran piezoelectric accelerometers. Simultaneous data acquisition was done using the DEWESoft Sirius data acquisition box. Our set-up required four sensor spots: PDV-100 and three accelerometers; two were mounted on the interface measuring vibrometer movements and one was mounted on the turbine housing at the location where the laser beam illuminated the surface. Additional accelerometer on the turbine was placed to perform a control measurement. The experimental setup is presented in Fig. 5.23(c) and the scheme of the channels is provided in Fig. 5.25. Channel 1 represents the vibrometer signal, and channels 2 and 3 are the corrective accelerometers mounted on the LDV. Data acquisition was done in time domain, and since we were interested in the velocity signal, all accelerometer signals were directly integrated, using DEWESoft software, which enables direct integration and definition of the acquisition parameters (DEWESoft, 2019). Integration was done following the middle Riemann sum rule. The sampling frequency was high, i.e., 20 kHz, and the low-pass filter with the cut-off frequency at 1 kHz was applied. Considering the Nyquist criteria a lower sampling

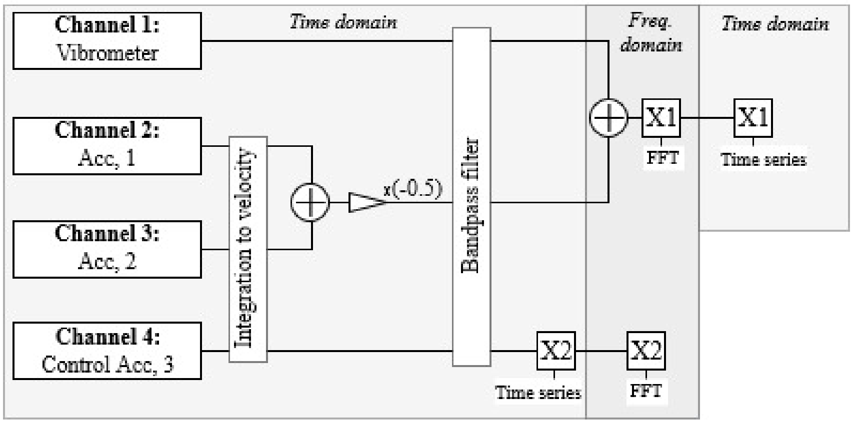

Slika 5.25: Shema računskih operacij na signalih.

Figure 5.25: Scheme of mathematical operations on the output of sensor channels. Channel 1 represents the raw vibrometer velocity signal. Channels 2 and 3 represent the integrated velocity signal from accelerometers mounted on the vibrometer, while Channel 4 represents the control measurement of an accelerometer mounted directly on the turbine housing where the vibrometer light illuminates the surface.

rate would be sufficient; we decided to oversample and filter high frequencies in order to reduce the broadband noise floor of the system. Signal post-processing of velocity channels was done using MATLAB software (The MathWorks, 2018). To determine the phase lag between the vibrometer and the accelerometers signals, the cross-correlation function was used (Brincker and Ventura, 2015):

$$R_{xy}(\tau) = \frac{1}{T}\int_0^\infty x(t)y(t+\tau)dt \tag{5.10}$$

Cross-correlation function $R_{xy}(\tau)$ can be used as a measure of similarity between two discrete signals where τ represents the time delay and T the size of the data segment. Phase delay can occur even with a simultaneous data acquisition, e.g., when different technologies are used, filters are applied, and while cable lengths differ. A rough estimate of a phase delay due to the variable cable length is that 1 m of cable adds approximately $5 \cdot 10^{-9}$ s (an estimate when the speed of light is assumed to be c = $3 \cdot 10^8$ m/s, since signal velocity propagation in the cable is 2/3·c, which equals to $2 \cdot 10^8$ m/s, and 1m/($2 \cdot 10^8$ m/s) = 5ns). Integration turns the phase by $\pi/2$, meaning that integrated velocity signal will lag behind the acceleration signal. The maximum value of the cross-correlation function is in position where the signal similarity is the strongest, hence the indicator of the phase delay between the signals. The time delay between the LDV and the accelerometer channels is 1.35 ms, where accelerometers lag behind the LDV signal. The output of the function is plotted in Fig. 5.26, where we can observe local maxima at 1.35 ms indicating the accelerometer signal lags behind the LDV signal. Fig. 5.25 represents the scheme of 4 channels during the measurements on the turbine after the alignment and integration of accelerometer signals. The first step in data manipulation is averaging of Channels 2 and 3 to omit the error caused by the tilt of the rigid body. Signals are then further transformed in the

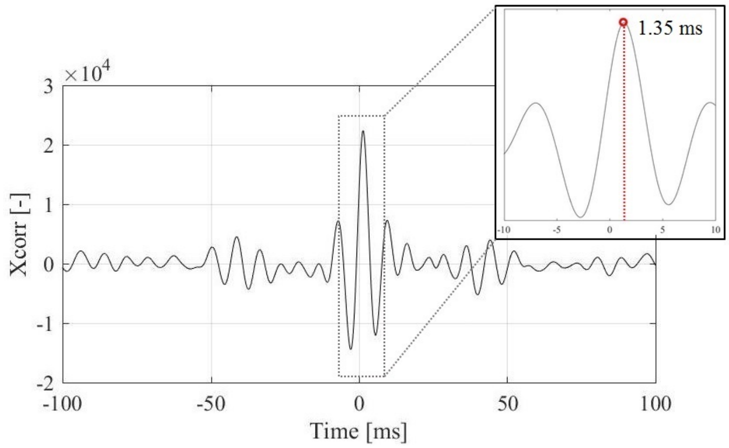

Slika 5.26: Rezultat križne korelacije med signalom vibrometra in pospeškomera.
Figure 5.26: Cross-correlation value of LDV and accelerometer signals.

frequency domain using the Fast Fourier Transformation (FFT), Signals are de-trended (linear trend is assumed), and the DC component is removed. The frequency content of interest lies within 1—300 Hz. All signals were filtered with this 1-300Hz band-pass filter, including the control signal. Furthermore, the averaged signal from Channels 2 and 3 was deducted from the original vibrometer signal. Using reverse FFT, the corrected time-series were constructed. The result presents a corrected velocity signal of the turbine. The vibration is captured on the turbine housing on the location of the main turbine bearing. The units rotate at 107.14 revolutions per minute. Including the stator, each unit weights over 190 t and operates under 166 m^3/s of rated discharge, the runner with 4 blades weights 35 t and the rotating part of the generator 96.3 t. The vibrometer is placed a few metres away from the experimental point on an active ground, excited with the turbine operation. The raw vibrometer velocity output contains summation of the turbine vibration and error due to the movement of the standing point. Due to this additional movement the measured amplitudes are larger than the true vibration of the machine. Fig. 5.27 presents the original vibrometer time-series, the control accelerometer output, and the final, corrected velocity signal. Amplitudes of the raw vibrometer signal are larger than the control signal indicates, while after the corrective procedure, the output amplitudes are in the range of the control amplitudes. The raw amplitudes exceed control measurements amplitudes by 80% or even more; the amplitude correction is therefore substantial. The correction is further discussed in the frequency plots in Fig. 5.28. All signals in Fig. 5.28 were subjected to the same filtering and signal processing, e.g., the band-stop filter (that we discuss in section 5.5.3) was used also on the LDV signal. Signals X1 and X2 present the corrected and the control signal, respectively. Fig. 5.28(c)(d) presents the final result: the corrected (X1) and control signal (X2). We can notice that the behaviour of the standing point is similar to the point under observation; the dominant frequencies are observed at 100 Hz, 42.9 Hz, 14.3 Hz, and 11.2 Hz (see Fig. 5.28(a)(b)). The highest magnitude is at 100 Hz with magnitude approx. $2{\cdot}10^{-3}$ mm, the velocity magnitudes of the correction signal are at least one order of magnitude smaller than the vibration of the observed structure. Even though the turbine was at full operation,

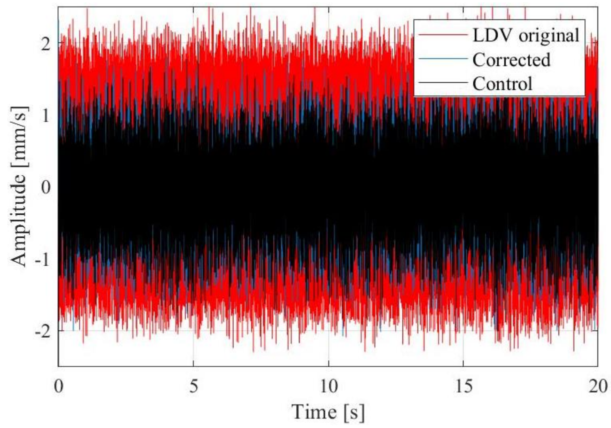

Slika 5.27: Časovne serije korigiranega signala (črno), signala s kotrolnega psopeškomera (modro) in začetnega signala vibrometra (rdeče).
Figure 5.27: Comparison of the time-series of the original vibrometer signal (red), control signal from the accelerometer (black), and the corrected vibrometer signal (blue) after the mathematical procedure is applied.

the standing point was not as active as we would expect. The corrective frequency peaks also coincide with the structural frequency peaks. In Table 5.11 we summarise the most prominent frequencies in the power-spectrum in the range from 1–100 Hz; they are listed in the decreasing order in the spectrum and not by the order of magnitude. The three frequencies with the most energy during this measurement were 21.4 Hz, 42.9 Hz, and 100 Hz. The lowest peak in the frequency spectrum is at 1.8 Hz, which is a reflection of the rotational speed of the runner. Turbines rotate with 107.14 revolutions per minute. This is represented with the first peak in the frequency spectrum at 1.78 Hz. We can notice higher harmonics as well, e.g. the second peak at 3.6 Hz. The runner has four blades; the blade passing frequency at 7.2 Hz is recognised in the frequency spectrum as well. The higher harmonics are visible up to 200 Hz; however, the 100 Hz, 150 Hz, and 200 Hz peaks are not considered to be structural. In the accelerometer output they are considered as higher harmonics of the ripple, caused by the power supply of the electronic processing equipment, converting the AC mains power to the lower voltage DC power. With the corrective mathematical procedure, where the main signal manipulation is

Preglednica 5.11: Močnostni spekter obratovanja turbine.
Table 5.11: Power spectrum of turbine operation.

Frequencies in power spectrum [Hz]	1.8, 3.6, 7.2, 21.4, 35.7, 42.9, 85.7, 100

done in the frequency domain, we were able to improve signal similarity. We used the value of normalised cross-correlation to be the measure of signal similarity, where the function from Eq.

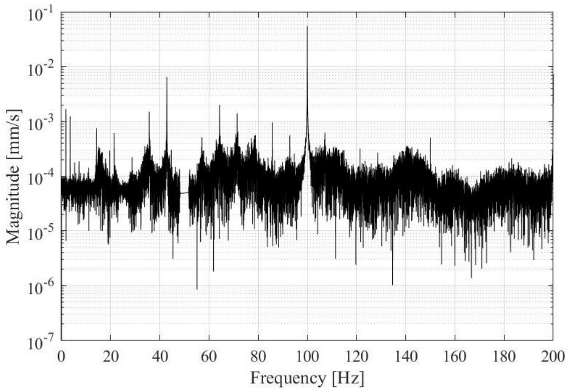

(a) Originalni LDV signal.

(a) Uncorrected vibrometer signal.

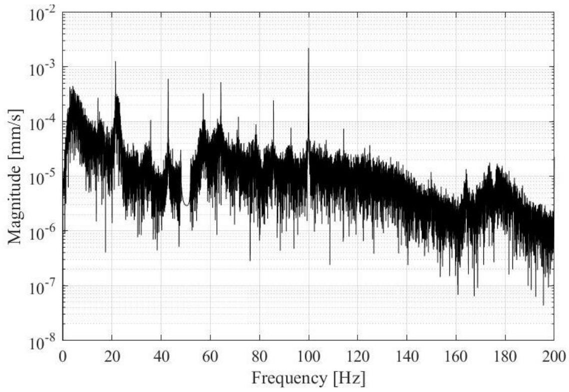

(b) Korekcijski signal.

(b) Correction signal.

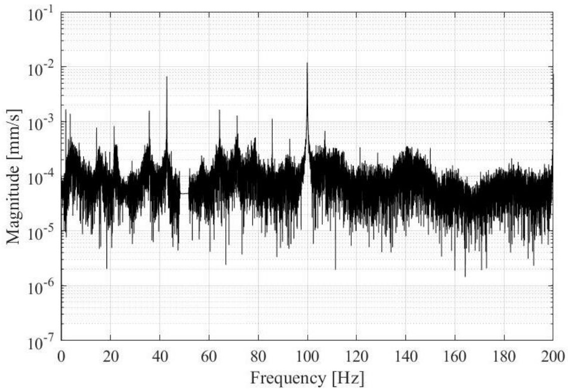

(c) Končni rezultat - X1.

(c) Corrected signal X1.

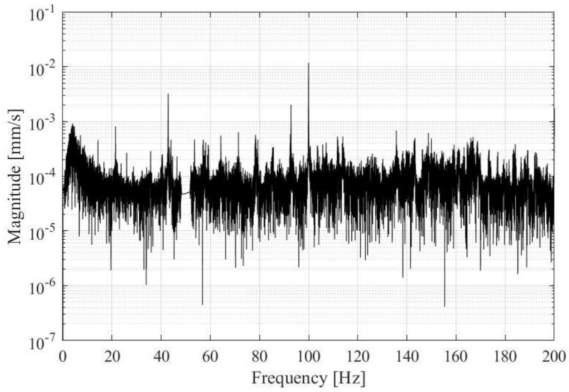

(d) Kotrolni signal X2.

(d) Control signal X2.

Slika 5.28: Prikaz frekvenčnega spektra surovega LDV signala (a), korekcijske meritve (b), signala po matematičnih operacijah (c) in kontrolnega signala (d).
Figure 5.28: Frequency spectrum of the uncorrected vibrometer signal (a), the correction signal from accelerometers 2 and 3 (b), corrected output signal (c), and the control signal that has been filtered and transformed in frequency spectrum (d).

5.10 is normalised by the multiplication of the standard deviations $\sigma_x\sigma_y$.

$$R_{norm}(\tau) = \frac{\frac{1}{T}\int_0^\infty x(t)y(t+\tau)dt}{\sqrt{\sigma_x\sigma_y}} \tag{5.11}$$

Normalised cross-correlation is a simple method to determine signal similarity and can range from values -1 to +1, where -1 means we are comparing two mirrored signals and +1 that we are comparing two exactly the same signals. The starting signal similarity ranged from values from 0.4 to 0.8 and after we applied the mathematical procedure the value was 0.9, which is a substantial improvement. However, at this stage we do not recommend for this technology to be used for blast loadings but rather for measurements during regular loading regimes. The LDV is not very suitable for shock vibration measurements of well-damped structures. This disadvantage was mentioned in the literature and has been confirmed during the field work, when the diversion dykes were blasted to reroute the Sava River back to the original river bed. The sudden blast caused only a minimal effect on the structure, however, only uniform movement occurred and with relative measurements and a lot of noise, the true response was hidden well below the noise threshold. Blast loading scenarios have not yet been tested enough; the tripod on the stating point can move permanently, either to pivot or translate.

Challenge of non-contact vibration monitoring during full operation of the powerhouse

The investigation revealed some advantages as well as disadvantages of the used technologies. The challenge of on-site measurements in comparison to laboratory measurements is the noise of the environment. In laboratory, we are able to control ambient conditions, while on site we have limited options; basically the conditions are given and we have to adapt to them (Das et al., 2016). Measurements using LDV are limited to surfaces that provide a sufficient amount of reflected light. HeNe laser light has a wavelength of 630 nm. This means that the majority of the surfaces in civil engineering is at least to some extent optically rough with respect to the laser light wavelength. When laser light is reflected from a rough surface, coherent waves of the incident laser beam are dephased and speckles are formed (Martin and Rothberg, 2008b). The measurement is possible when a speckle has sufficient intensity to be recognised on the photo detector. The amount of the backscattered light is also affected by atmospheric conditions (humidity, temperature), laser beam propagation, focus, and alignment (Castellini et al., 2006; Agostinelli et al., 2010; Agostinelli and Paone, 2012). The laser speckle is classified as a fundamental measuring uncertainty, while the laser signal can be a carrier of surface motion information unrelated to normal surface motion, known as pseudo-vibration (Martin and Rothberg, 2011). An in-depth analysis of the origin of speckle noise is presented by Rothberg (2006). The use of a retro-reflective tape helps to increase the intensity of the light in the backscatter. The retro-reflective tape is also optically rough on the scale of the laser light; however, it is designed to concentrate the scattered light up a narrow cone, which provides for a brighter concentrated speckle. The use of the retro-reflective tape increases the intensity of the light in the backscatter. However, it does not guarantee a signal clear of drop-outs, while it provides for a wider range of where acceptable levels of the signal can be obtained (Martin and Rothberg, 2009). In practical cases, it was shown that a coherent laser beam sufficiently scatters from rough surfaces on the scale of laser light while the roughness is smaller than the size of the beam (Martin and Rothberg, 2011).

All commercial vibrometers have a limited range. The maximum stand-off distance is limited with the product limitations. Special attention is devoted to the positioning of the vibrometer to ensure that the angle of incidence is 90° with minimal error. Another significant noise reduction measure is temperature; vibrometers have a wide temperature range where they operate, e.g. our equipment can operate in the range from 5 to 40°C with 80% maximum relative humidity (non-condensing). There are numerous reasons why the temperature can change during an experiment on site. In case a significant temperature drop/rise occurs during the measurement, the changed conditions of the medium (air) through which the laser beam travels will corrupt the measurement. Another challenge is direct and strong sunlight; we can easily combat this issue with the use of the retro-reflective tape and the placing vibrometer in a shade or with the use of a visor to shade the lens of the vibrometer. A challenge for the operator is to focus the laser beam under these circumstances, while the visibility of the spot is affected by ambient light. Measurements with LDV are relative. This is something we have to consider when measuring outside of the laboratory. Preparation of the experimental work is crucial, with identification of all the influencing factors, where we can minimise or completely eliminate their effect. The effect of ambient noise can be minimised following a few simple rules:

- we recommend to always use the reflective tape (unless we have a clear reason why it cannot be used);
- whenever possible, the standing point should be on a structurally different member than the surface under observation;
- the standing point should be on a structurally more rigid member than the point under observation;
- when measurements are done in strong sunlight, the visor of the instrument must be shaded;
- methods to enhance the signal-to-noise ratio should be applied together with an adequate anti-aliasing method with a proper measurement resolution.

During the experiment we confirmed that the LDV does not suffer from magnetic field disturbances.

Challenges for contact technologies

The piezoelectric accelerometers, used in this study, were chosen for their small footprint and light mass for easy and reliable attachment. The accelerometer on the turbine was mounted with a magnet, while the accelerometers on the LDV interface were mounted with bolts. During turbine measurements, we noticed a parasitic frequency at 50 Hz being present in the output of the accelerometers. The parasitic frequency was more evident on the accelerometers mounted on the vibrometer than on the accelerometer placed directly on the turbine housing. The first suspicion was of course electrical noise and the effect of the magnetic field that develops in the powerhouse while the generators are operating, since it is known that accelerometers can be susceptible to the magnetic field excitation (Cristalli et al., 2006). The output with the parasitic frequency is presented in Fig. 5.29; in this specific case the amount of the noise dominates the measurement output. In the powerhouse, due to electricity generation, also magnetic field is formed. To confirm if the magnetic field is responsible for the noise in the measurements and to determine all possible sources of the parasitic frequency, a detailed inspection was carried out in the laboratory of company DMS, Data merilni sistemi, where they helped us with the diagnostic work to discover the sources of the parasitic frequency. All components were tested for magnetic properties and exposed to the influence of a strong electromagnetic coil, designed

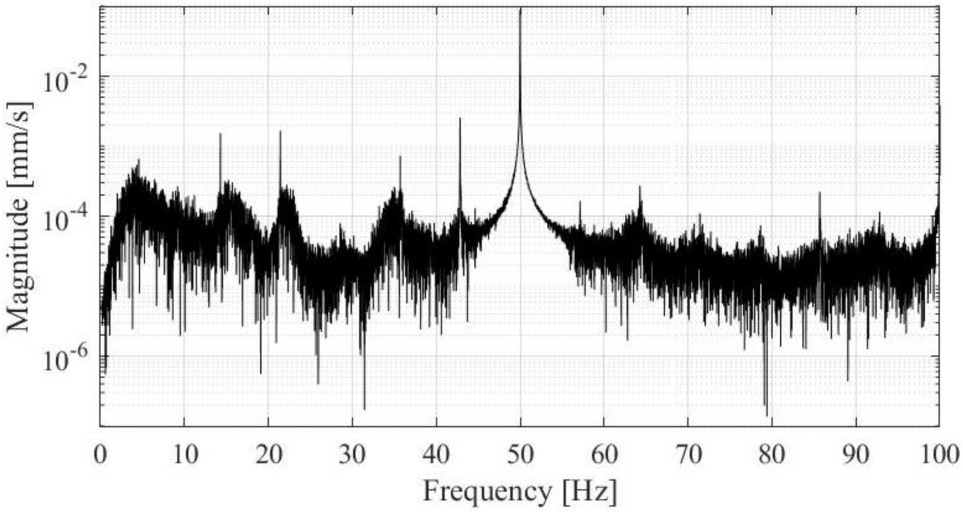

Slika 5.29: Šum v meritvi pospeškomera.
Figure 5.29: Noise at 50 Hz in the accelerometer output (output of channel 1).

for medical purposes. The coil induces a strong EM field with a frequency of 50 Hz. During the test, at first the output of one accelerometer was monitored while the accelerometer was positioned on different surfaces (metallic, fabric, concrete) and on different distances from the magnetic core. The electronic noise at 50 Hz appeared in the measurement as soon as the electromagnetic coil was turned on. The closer the mounting of the accelerometer, the higher the spike in the frequency output. The accelerometer itself is mechanically moved by the EM field and the movement is so strong that it can be felt if we hold the accelerometer in our hand. The intensity of the movement reduces if the magnet used for mounting is removed, however, the reduction is minimal.

The Teflon covered cable is also a little bit magnetic: the magnetism is barely detectable, but over the long length of the cable (15 m) the contribution is substantial. The effect can be minimised if the cable is always fully unrolled, while the rolled cable behaves like an electromagnetic coil itself. Furthermore, the vibrometer's sensitivity to the EM effect was tested. Turning on the EM coil did not affect the vibrometer's output. In the second step, the accelerometers were added in the scheme. When the whole scheme was in operation, a parasitic frequency at 50 Hz appeared in the accelerometer output even before the EM coil was on; the effect barely rises above the white noise threshold. We added an isolation transformer in the scheme to introduce galvanic isolation in the system (see Fig. 5.30). A galvanic isolation is used also to suppress the electrical noise and isolate the plugged equipment from the original power-source. The transmission of the DC component is blocked while the AC components are allowed to pass. This prevents the formation of a ground loop between two circuits (devices). The ground loop that forms between LDV-Sirius DAQ box-computer and affects the accelerometer readings was successfully suppressed with the introduction of the insulation. Based on the laboratory test, we can conclude that the detected parasitic frequency consisted of the effect of the magnetic field and the ground loop. The latter is successfully eliminated with the introduction of the isolation transformer. Moreover, by applying a digital band-stop filter, the parasitic frequency is completely eliminated.

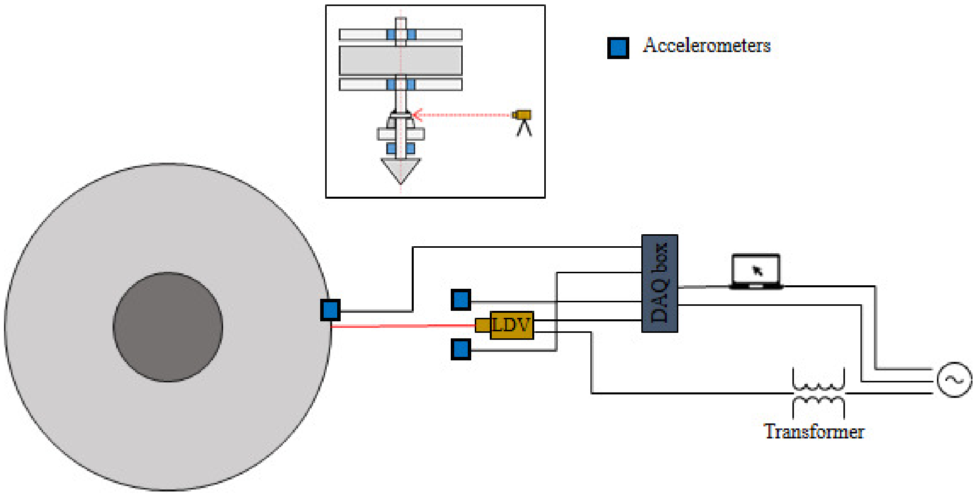

Slika 5.30: Shema meritve vibracij na turbini z vpeljavo ločilnega transformatorja.
Figure 5.30: Layout of the instruments during vibration measurements, where the vibrometer is plugged into the isolation transformer. Vibrations are measured on the housing of the main bearing.

We use the band-stop IIR Elliptic filter with attenuation bandwidth from 49 Hz to 51 Hz and 1 Hz transition band on the lower and upper edge frequency, pass-stop parameter 80 dB and peak pass-band ripple limited to 1 dB (see Fig. 5.31). The 50 Hz parasitic frequency is not near any system eigenfrequencies, therefore filtering can be applied. With the presence of the magnetic field during the regular operation, the power plant environment once more proved to be a challenging environment for the measurements. The investigation confirmed the cause for

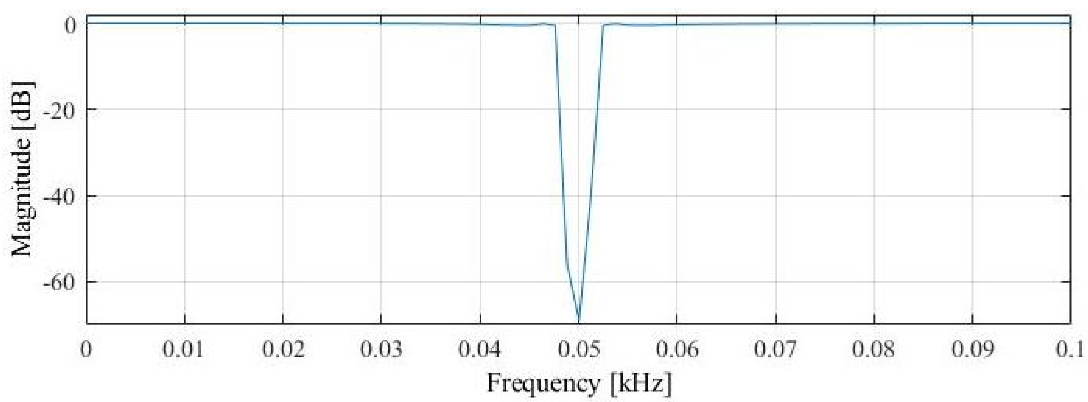

Slika 5.31: Digitalni eliptični pasovno-zaporni filter.
Figure 5.31: Band-stop IIR Elliptic digital filter.

the parasitic frequency. However, since the effect of the magnetism is translated onto accelerometers, the cable, and in the ground loop between LDV-Sirius DAQ box-computer at this point cannot be to completely eliminated. This will require the work of magnetism experts and redesigning of the DAQ box, which is beyond the scope of this work. Fortunately, the parasitic frequency is only one and is there where our system under observation does not have an eigenfrequency. Therefore by applying a digital band-stop filter, this frequency is filtered before the signal is further analysed.

During the test on the mechanical equipment, also velocity transducers were used, since they are often used in vibration monitoring of buildings. The velocity transducers that were used proved to be impractical due to their size and the lack of linearity in the frequency response. Measurements done with velocity transducers that showed linearity problems were dismissed. In our opinion, accelerometers are a more suitable alternative to the velocity transducers, they are smaller, weigh less, and are linear in the entire frequency response. Especially when contact sensors are planned to be permanently installed, the velocity traducers that we used are not appropriate. Indeed, the common practice in dam monitoring is the installation of accelerometers. We should underline that permanently installed sensors are expected to operate for the lifetime of the infrastructure that may be as long as 50 or even 100 years.

5.6 Numerical Modelling

We modelled the structure in Diana 10.2 environment. Separately, two 3-dimensional models were built: one for the spillway section and a separate model for the powerhouse. Both are presented in Fig. 5.32. For the purpose of our analysis, structural, groundwater flow, and fluid-structure interaction modules were activated.

The overflow section was modelled considering symmetry criteria. In order to save computational time, only one half of the section was modelled (Fig. 5.32(a)). The entire section consists of five spillway sections, divided by piers: 2.7 m wide and 51.15 m long, with varying height; the highest are on the upstream side (22.9 m) and the lowest on the downstream side (15 m). The width of each spillway segment is 15 m. The fixed part of the spillway section is in the highest point 11.3 m above the lowest point in the stilling basin. The radial gates were not modelled directly as elements, only by introducing boundary conditions. Baffle blocks were not included in the model nor was the gallery located on the upstream side of the dam, below the spillway crest level. Following the symmetry criteria, and to decrease the size of the model, the entire spillway section was divided into two using the centreline in the global X direction as the symmetry plane. In the symmetry plane, translations in the global Y direction were restrained. We defined a phased model to be able to analyse the structure with and without the fluid-structure interaction. We used the linear material model for concrete with Young modulus $E = 3.1 \cdot 10^{10}$ N/m^2, Poisson ratio $\nu = 0.2$ and mass density 2500 kg/m^3. Concrete structural parts are meshed with 3D isoperimetrical solid brick elements and fluid with 3D brick potential flow element coupled with fluid-structure interaction plane interface elements. The fluid medium is modelled as an incompressible fluid. By applying the zero pressure boundary condition, zero dynamic water pressure at semi finite and surface boundaries of the fluid, neither radiation nor surface effect in the fluid domain were considered. The reservoir in the model has a significant contribution to the mass matrix. We clamped the spillway at the bottom. Due to symmetry criteria, the supports in the global Y-direction were also applied at the lateral surfaces in the middle of the whole spillway section. The interface with the powerhouse is also supported with pinned supports in the global Y-direction.

The model of the powerhouse was built separately (see Fig. 5.32(b)). To reduce the size of the model and to save computational time, only a section of the entire powerhouse cross-section was modelled, while structurally it can be divided into two segments. As can be seen in Fig. 5.2, the bottom part is built with mass concrete and the upper part is much more slender. We are interested in the behaviour of the structure encasing the turbines and in the natural frequencies of the upper section, therefore only this part was modelled and we assumed it is clamped to the ground. We used the same properties for concrete that were used in the model of the overflow section, while for the structural steel (HEA and I profiles supporting the roof) the linear model with modulus of elasticity $E = 21 \cdot 10^{10}$ N/m^2, Poisson ratio $\nu = 0.3$, and mass density 7850 kg/m^3 was used. The HEA 500 and IPE 200 steel profiles support the roof; they were modelled as 2D line elements with a prescribed geometry and the corresponding properties. The mass bottom concrete in the model has three large voids presenting the turbine shafts with the radius of 3.5 m. The annex was not modelled since it is also located behind the structural joint. The effect of annex and of the overflow section is presented with lateral supports in the global Y-direction. The ground plan of the modelled area has a dimension of 58.2×24.1 m and a maximum height of 23.1 m. The turbine hall is the main feature in the model. The entire south wall in the powerhouse has nine piers supporting the crane transverse, located 15.7 m above the floor level. The thickness of the wall is 40 cm and the piers add an additional 60 cm. The transverse has a rectangular 100×100 cm cross section. The wall extends above the line to the final height of 20.5 m above the floor level. The north wall has symmetric features to the south wall, only the width of the wall is thicker.

The applied loads were dead load and the load of water at the nominal operating levels for the model of the spillway. Fluid domain was not included in the powerhouse model.

5.6.1 Meshing

The preferred elements for discretization and meshing were elements with quadratic interpolation and on shape adoption to curvatures. The fluid elements were modelled using elements with linear interpolation, since we were not interested in the fluid phenomena and while the fluid-structure interface elements (FSI) transfer fluid load only via the corner nodes and the load is then further interpolated to intermediate nodes in the structural domain. By using linear elements, also the total number of nodes in the model reduces, which has a direct effect on the computational times. Pyramid and brick shape general 3D potential flow elements with linear interpolation are used to discretize fluid domain. Fluid structure-plane interface elements are

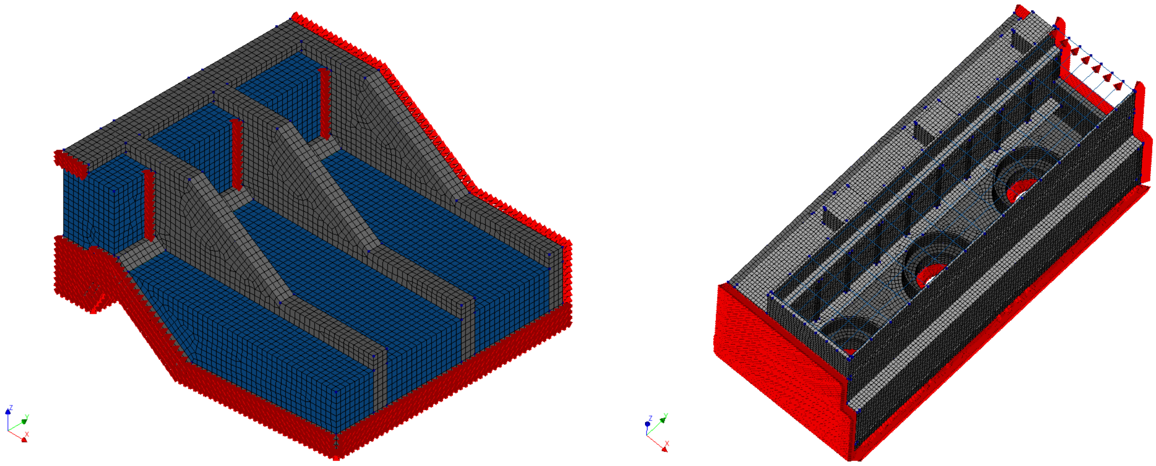

(a) Model polovice prelivnega polja.
(a) Spillway model.

(b) Model strojnice.
(b) Powerhouse model.

Slika 5.32: Numerični model strojnice in prelivnih polj.
Figure 5.32: Numerical model of the overflow section and the powerhouse.

placed between the fluid and the structural domain. Quadrilateral and triangular elements with isoparametric linear interpolation for the displacements and linear interpolation for pressures are used. FSI elements provide continuity between the normal displacements in the structural domain and pressure in the fluid domain. 15-node quadrilateral and pyramid nodes with quadratic interpolation finite elements are used to discretize structural concrete, while for the steel roof beams, 3-node 3D class-III beam elements are used. Typical types of finite elements in the model are presented in Fig. 5.33. The meshing seed was done by limiting the maximal element size and by prescribing the number of divisions on critical edges. The spillway model has a li-

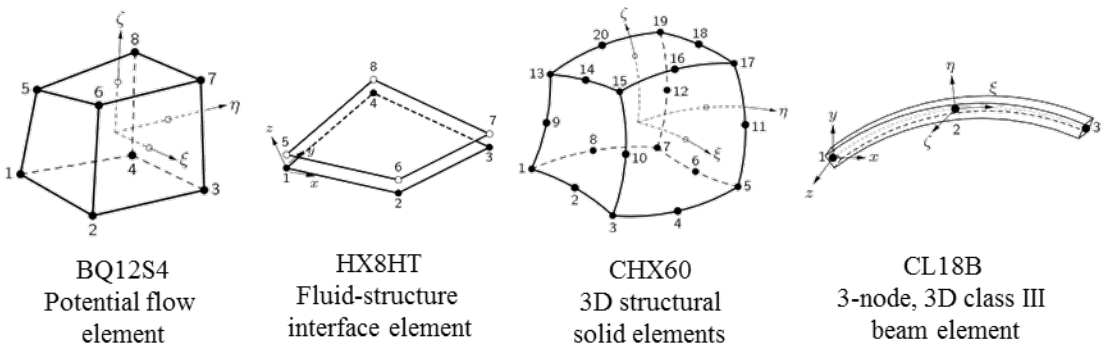

Slika 5.33: Uporabljeni končni elementi (DIANA FEA, 2017).
Figure 5.33: Used finite elements (DIANA FEA, 2017).

mited element size of $1 \times 1 \times 1$ m, with additional mesh seeds on the imprinted pier edges on the interface with the bottom mass concrete to keep the uniform shape of the mesh without distorted elements. Structural elements in the spillway have a mesh seed of $1 \times 1 \times 1$ m maximum element size with quadratic interpolation. The powerhouse model has a mesh seed of $0.5 \times 0.5 \times 0.5$ m quadratic elements, additional mesh seeds were applied to the intersecting edges to prevent distortion. Structural FE elements must be quadratic to prevent hourglass modes, even though quadratic interpolation significantly increased the cpu-time.

5.6.2 Analysis

Phased analysis was defined, therefore one model can be used to evaluate the structure with and without the participation of the reservoir. The following analyses were defined: structural linear static and structural eigenvalue. The first 100 and 200 eigenfrequencies were evaluated in the spillway model and in the powerhouse model, respectively. This corresponds to have a 90% of the total mass contributing in the evaluation, which is considered among the criteria to have a representative model.

To simulate the ageing phenomena, the reduced values of the concrete's Young modulus were assumed. We estimated that a global 10% reduction in the modulus of elasticity is a realistic estimation, which can occur in the following years. Python scripts were used to automate the calculations. Meshed models in .dat format were exported then in every file, the modulus of elasticity of concrete was replaced with a corresponding reduced value, then the model was evaluated under the new material condition. With this procedure, we omitted the need to re-mesh the updated model.

5.6.3 Results

In the model of the powerhouse, the following nodes agree with the measured experimental points:

- node 4726 (ST2) is located on the pier number 10, approximately 4.7 m above the turbine floor level;
- node 177476 (S2) is located on the wall between piers 10 and 12, approximately 4.7 m above the turbine floor level;
- node 225011 representing points StH and StV is located on the floor connecting turbine shafts opposite point S2, 3.7 m above the turbine floor level;
- nodes 147237 and 176776 represents experimental points ST1 and S1, respectively.

For better visualisation, the nodes are presented graphically in Fig. 5.34. The nodes 4627 (ST2) and 177476 (S2) are approximately 2.7 m apart and are situated in the central part of the south wall. Nodes 147237 (ST1) and 176776 (S1) are approximately 10.7 m above the turbine floor level.

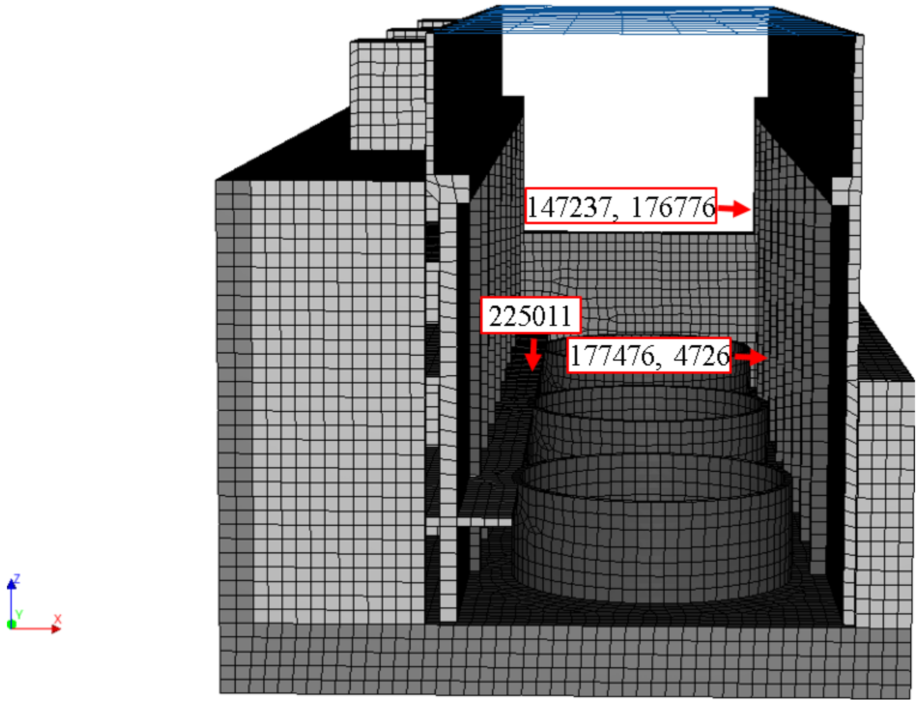

Slika 5.34: Vozlišča v modelu.
Figure 5.34: Nodes in the numerical model.

The numerical model provided information on the location of the experimental points. It is important that the points are not located on the structure's stationary points for any of the representative mode shapes. We observed the displacement amplitudes of the experimental points. Vibration amplitude of the south wall increases with wall height and is the highest in the range from 1/2 to 3/4 of the total height span. All experimental points fulfilled the criteria, they are not on any stationary points, and all the representative modes can be detected on them.

The stress levels in the structure were examined as well to check whether there are locations in the structure where compressive stresses develop, and no critical locations were observed. The numerical model did not show any locations where tensile stresses develop. The maximum compressive stress develops at the foundation of the turbine shaft and has the value of 10.9 MPa. According to SIST EN 1992-1-1 we verified resistance to fatigue. Resistance is determined with respect to the stress levels of the fatigue load, number of cycles, designed value of ultimate concrete fatigue strength under compression of shear, and maximum stress level in the structure. We estimated that the first cycle of fatigue load has been applied to the structure roughly one year after it was constructed (as an estimation t_0=400 was chosen). The stress amplitude is minimal, estimated at 0.0001. Using the equation for normal strength concretes, the ratio between the maximum compressive stress and the designed fatigue compression strength must be below 0.91. The design value of concrete strength under compression or shear fatigue for concrete type C25/30 under given conditions is 15.3 MPa. We have estimated a ratio of 0.71, the value is below the threshold value. At this point it is still important to emphasise, that this is a basic model, and further more detailed study can confirm the actual state with respect to the fatigue loading.

The numerical model also confirmed the measured frequencies. The numerical values of the first two eigenfrequencies of the pier between the first and the second spillway section are summarised in Table 5.12. The Table is divided into two parts. In the first part, we present the result of the model where water elements are turned off, i.e. the structural response without the presence of the reservoir, and in the second part we present the full model with the contribution of the reservoir. As we can notice, the contribution of the added body of water is lowering the eigenfrequencies; the first mode drops from 10.9 Hz to 10.6 Hz and the second from 15.8 Hz to 14.9 Hz for the case of the sound (healthy) concrete. The same deduction of the eigenfrequencies is present for the reduced Young modulus values indicating structural ageing. The table presents the eigenfrequencies with the maximum mass contribution in the global Y-direction, in which the response is also experimentally measured, the values are in accordance with the experimental results. Fig. 5.35 presents the modal shapes of the measured pier, between the 1st and 2nd overflow sections, for the first two eigenfrequencies and also the outlook of the half of the spillway model at the first eigenfrequency. The comparison between the numerical results and the experimental values of the pier in the spillway is presented in Fig. 5.36. The discrepancy between the numerical and measured values is only 3% for the first eigenfrequency while 6% and 8% for the second and third, respectively.

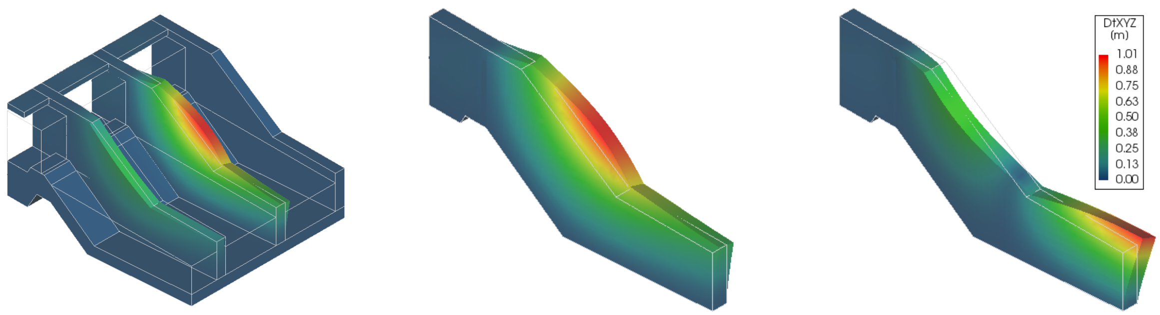

(a) 1 LF - polovični model prelivnih polj.
(a) 1st eigfr. - half of the spillway.

(b) 1 LF; 10.9 Hz.
(b) 1st eigfr.; 10.9 Hz.

(c) 2 LF; 15.8 Hz.
(c) 2nd eigfr.; 15.8 Hz.

Slika 5.35: Rezultati modela prelivnih polj.
Figure 5.35: Results of the spillway section model.

Preglednica 5.12: Rezultati modela prelivnih polj s predpostavljenim staranjem.
Table 5.12: Results of the spillway section model under the influence of ageing.

Young modulus [$\cdot 10^7$ kN/m^2]	3.1	3.07	3.03	2.99	2.96	2.92	2.89	2.85	2.82	2.79
Only structural										
1st eigfr. [Hz]	10.98	10.93	10.85	10.78	10.72	10.65	10.6	10.53	10.48	10.42
2nd eigfr. [Hz]	15.81	15.73	15.63	15.52	15.45	15.34	15.26	15.16	15.08	14.99
Fluid-structure interaction										
1st eigfr. [Hz]	10.58	10.53	10.46	10.39	10.34	10.27	10.22	10.15	10.09	10.04
2nd eigfr. [Hz]	14.86	14.78	14.69	14.59	14.52	14.42	14.34	14.25	14.17	14.09

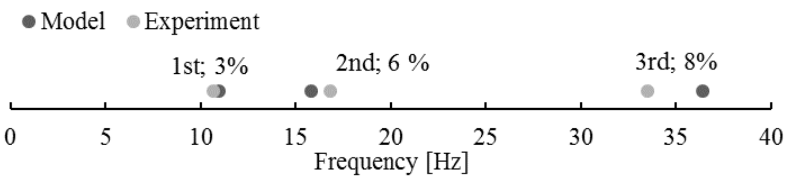

Slika 5.36: Primerjava numeričnih vrednosti modela prelivnih polj z eksperimentalnimi.
Figure 5.36: Measured eigenfrequencies of the pier in the spillway with respect to the numerical values.

Fig. 5.37 summarises experimental and numerical results captured on the south wall of the powerhouse. In representation the results from the experimental points ST2 and S2 are averaged. Averaging is done on the dataset of the experimental points, where only the cases with emergency brakes on one of the units at a time were deployed. These cases were chosen while in general the peaks we are interested in are in these cases the most prominent (in general the experimental points S2 and ST2). Numerical results present the eigenfrequencies that contribute the most in the global X-direction of the model, that is the direction of the measurement on the south wall. If we compare the results of the numerical model and the experimental value in the powerhouse we need to limit numerical values solely to the results in the X-direction, where the first 5 eigenfrequencies are the following: 5.8 Hz, 8.2 Hz, 10.6 Hz, 14.1 Hz, and 20.1 Hz. Numerical and experimental results agree well; the discrepancy for the first eigenvalue is 5%, the 2nd only 1.3%, at the 3rd mode the model shows the most difference to the measured values, where the discrepancy is almost 9%. We present the values for the first 5 modes, while overall the discrepancies are in the range of 1–9%. The results of the model of the powerhouse for the 5 eigenfrequencies are presented on Fig. 5.38. We were also interested in the displacement envelopes in the experimental points. The displacement amplitude of the experimental point StV, with respect to the frequency, is presented in Fig. 5.39. This part of the structure is mainly susceptible to excitation in the vertical direction which have the most effect during the transient actions of the turbines. The main effect has the excitations in the frequency range above 40 Hz. With on-site measurements, the frequencies at 42.9 Hz and 28 Hz were recognised among the

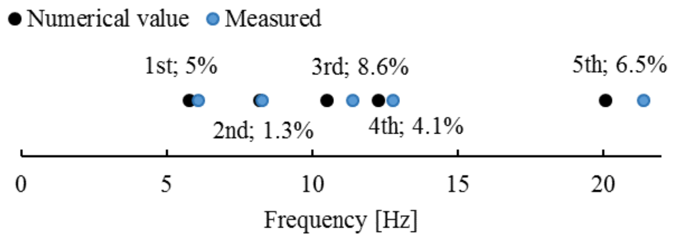

Slika 5.37: Primerjava numeričnih vrednosti modela strojnice z eksperimentalnimi (v smeri globalne osi X).
Figure 5.37: Measured eigenfrequencies (in the X-direction) on the south wall with respect to the numerical values.

five most prominent peaks with others in that range to follow (39 Hz, 48 Hz, etc.). Those peaks are also in accordance with the numerical results.

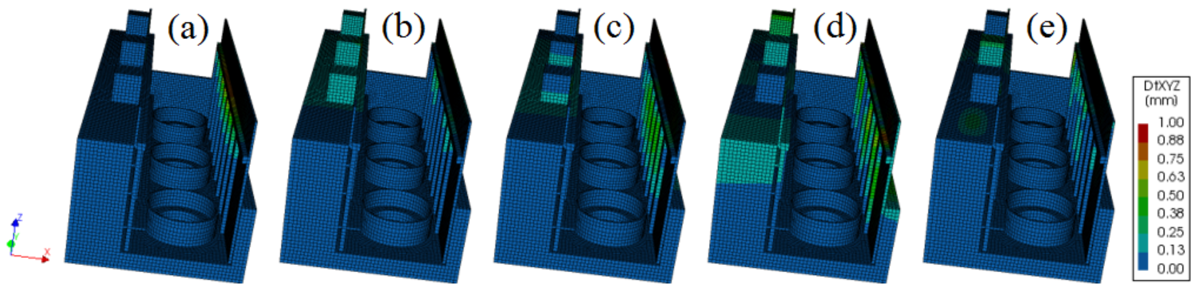

Slika 5.38: Prvih 5 modalnih oblik modela strojnice (a) 5.8 Hz, (b) 10.6 Hz, (c) 14.1 Hz, (d) 20.1 Hz, (e) 29.8 Hz.
Figure 5.38: The first 5 eigenfrequencies (a) 5.8 Hz, (b) 10.6 Hz, (c) 14.1 Hz, (d) 20.1 Hz, (e) 29.8 Hz.

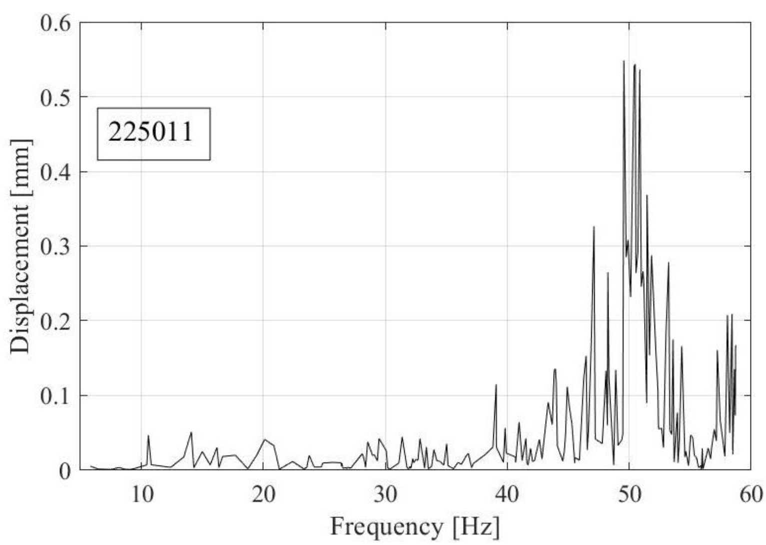

Slika 5.39: Vozlišče 225011 (StV).
Figure 5.39: Node 225011 (StV).

The variable modulus of elasticity is considered in the model. Ageing phenomena are modelled with the values of the Young modulus ranging from 31000–27900 N/mm^2. The change in the first five eigenfrequencies (that contribute the most in the global X direction) is observed. For a better visualisation, the results were normalised to the value at the intact state. The intact state is assumed with the Young modulus value at E = 31000 N/mm^2. The normalised value (f_{norm}) of the modulus of elasticity is determined using the following formula:

$$f_{norm} = \frac{f_i}{f_0} \tag{5.12}$$

where f_i represents the value of the eigenfrequency at the reduced value of the Young modulus and f_0 is the eigenfrequency in the sound state. In Fig. 5.40 the results of the analysis are presented, the initial value of the eigenfrequency is marked in the legend, while the relative change with respect to the reference state is presented with the curve. The drop in the modulus of elasticity caused a drop in the eigenfrequencies. An almost 12% drop in the modulus of elasticity causes a 6% drop in the values of the individual eigenfrequencies. Table 5.13 summarises the initial values and the value of the drop at the final step of the analysis.

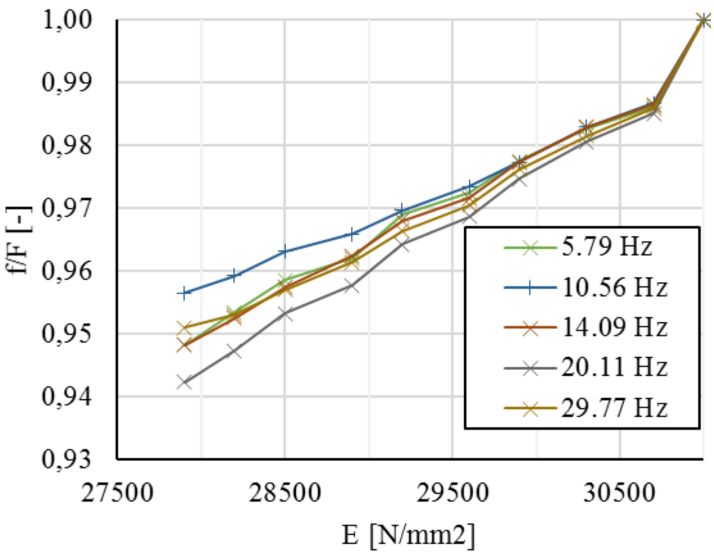

Slika 5.40: Padec vrednosti lastnih frekvenc zaradi staranja betona.

Figure 5.40: Drop in the eigenfrequencies when ageing of concrete is assumed.

Preglednica 5.13: Sprememba prvih pet lastnih frekvenc z maksimalnim prispevkom v globalni X-smeri.

Table 5.13: The drop of the first five eigenfrequencies with the maximum contribution in the global X direction.

Eigenfrequency [Hz]	5.8	10.6	14.1	20.1	29.8
Total drop [Hz]	0.33	0.49	0.80	1.25	1.52

With the numerical model we were able to confirm the suitability of the experimental points; they are appropriate for observations of the frequency response of the dam. Since the selected locations are not near any critical (stationary) points, all the representative eigenfrequencies can be captured. Moreover, the measured frequencies were numerically confirmed. The eigenfrequencies in the model agree with the measured values. The results confirm our hypothesis, i.e. that the effect of the turbine operation is directly translated to the entire bearing structure, while some frequencies of interest are close to the structural response. Also the susceptibility to the excitation in the vertical direction is confirmed. The ageing of concrete was modelled with the global drop of modulus of elasticity. Both models, the model of the overflow section and the model of the powerhouse, confirmed susceptibility of the eigenfrequencies to the change of the values of the Young modulus. The long-term effect of the operation should be seriously considered in the following studies on this dam and other structurally similar ones.

6 PROPOSAL FOR THE DYNAMIC MONITORING OF RUN-OF-THE-RIVER DAMS

The recommendations in this chapter are based on the review of the state-of-the-art practice in the literature and the study cases with respect to the on-site observations during this research. The aim of this chapter is to introduce dynamic monitoring, with minimal additional costs and, if possible, with the extension of the use of the equipment already installed, to monitor the behaviour of a dam. Dynamic monitoring should be applied considering all the basic criteria discussed in Chapter 3.1. The system should be designed by having the seven fundamental axioms of structural health monitoring in mind (Worden et al., 2007). The basic steps are to decide which technology to use, how much of it, and where. The following question is whether we need real time on-line assessment or whether discrete intervals will suffice. Data acquisition, processing and storage strongly depend on these criteria. What are the prognosis intervals? We have to establish the warning and alarm limit values. The procedures to be followed in case if any of the threshold values is reached, need to be defined to support the decision on the measures to take to prevent the predefined potential failure modes to develop further. And before this step, the definition of the threshold values is far from being a trivial task.

6.1 Upgrade of the Existing Monitoring System

Generally the extension of the current system would include:

- the use of the existing accelerometers in continuous mode;
- installation of additional accelerometers in the powerhouse;
- additional measurements of temperature, humidity, joint opening, dilatation behaviour, seepage data, and storage of data on manoeuvring with the hydro-mechanical equipment;
- additional prognostic (vibration) measurements once a year;
- establishment of the statistical and numerical models;
- storage and analysis of data;
- interpretation.

The existing monitoring system in Slovenia requires that on all large dams, seismic monitoring needs to be established as well. For dams between 30–60 m in height, it consists of at least three accelerographs, where one has to be placed in the foundation of the dam, one in the dam body above the foundation, and one on the free surface. Induced seismicity needs to be monitored only on dams higher than 60 m. Large dams lower than 30 m need to have two accelerographs installed, one in the foundation of the dam and one on the free surface (Official Gazette of the Republic of Slovenia 58/16, 2016). The equipment is installed in trigger mode with at least 5 s of pre-event memory.

During our research, we obtained data from the nearest station in the Seismic network of the Republic of Slovenia, Gornji Cirnik (GCIS) (Slovenian Environment Agency (ARSO), 2018). We asked for data on all seismic events with the epicentre location on Krško-Brežice plain and within a radius of 50 km from Brežice, during 2017–2018, and a magnitude of 1 or higher. The CGIS station is equipped with GURALP CMG-40T seismometer and records in directions: east-west, north-south, and vertical with sampling frequency of 200 Hz. We collected time-series of 15 recorded events with epicentre depths from 4 to 25 km and magnitudes from 1.1 to 2.9. The events were from 9 s to 40 s long and have a low-frequency signature; dominant frequencies appear in the range of 4–20 Hz. However, even though the seismic monitoring on Brežice dam was already established, these events did not cause the devices to trigger. That is very unfortunate, since the data from local seismic events could be of benefit for structural diagnostics. The two accelerometers mounted on Brežice dam are located in the 3rd pier in the overflow section, where the effect of turbine manoeuvring does not have any effect, while due to the inaccessibility during high waters, there is a lack of situations when diagnostic measurements are performed. According to the seismic observations data of the Republic of Slovenia, there are at least five local earthquakes occurring per year in our area of interest. If the events would be captured also on the dam, they could serve as an excellent diagnostic tool. The first improvement of the existing system is to set the mounted accelerometers to operate in a continuous mode (or at least with very low threshold trigger values), so they will be able to record the local earthquakes. According to the specification of instruments, as stated in the regulations on seismicity observations on large dams in Slovenia (Official Gazette of the Republic of Slovenia 58/16, 2016), the installed accelerometers could be appropriate. Similar recommendations for implementation on Russian dams is also presented by Antonovskaya et al. (2017). Moreover, in the next step, the grid of seismic observation points on the dam should be extended. Additional accelerometers should be installed. To observe the impact of the turbine operation, each turbine shaft should be equipped with one accelerometer. Vibration measurements should be accompanied with the temperature measurements of the surrounding concrete, while ageing of the concrete is affected by the constant vibration, while in order to have solid long-term prognosis the influence of temperature gradient should be considered as well. Moreover, air temperature and humidity should be monitored. There should be at least three more accelerometers mounted in the powerhouse: one in the bottom gallery, one on the south wall, and one on the floor connecting the turbine shafts. In the overflow section, pier number one should be further investigated. The general observations of the dam state should include continuous measurements of the amount of seepage, opening and closing of the joints. Manoeuvring of the hydro-mechanical equipment is already registered, however, this data should be linked with the structural observation. All recordings should be stored and archived in the same manner. These data are necessary to provide diagnostic and prognostic work, since a dam is a complex structure. Ageing monitoring should be supplemented with in-depth vibration measurements at the established experimental points. These points should be analysed at least once a year, preferably at the end of the cold part of the year. This can be done using non-contact technologies by observing ambient vibrations. In this case the test is fast and in the case of the Lower Sava River cascading system, all the dams could be tested in one day. Moreover, the operation of the equipment should be analysed, i.e. what is the amount of bad data, site specifics, etc. The last step is the analysis of the data using statistical and finite element modelling. The raw data must be cleaned, analysed, and included in the report. It is recommended that the analysis is done simultaneously with in-depth vibration measurements and both of these included in the overall report of the dam state. The results must be interpreted.

6.2 Archives and Evaluation

It is not necessary to provide an on-line evaluation. However, a protocol for data storage, where the events, times, and the triggering cause are written, should be established. The data should be evaluated and interpreted once a year together with the interpretation of other monitored parameters and operational logs. The existence of dynamic monitoring data provides the possibility to transform time-based data into condition-based information. The reference state of Brežice dam has been recorded with the measurement right after the completion of the construction work. However, we were not able to obtain the data on the concrete installed in the dam. With respect to the dam safety, the owner is advised to gain the information on the concrete built in the dam, for this dam and the ones upstream (and for all dams in Slovenia where this information is also missing) and to properly archive this information, to prevent a further similar loss of data. For other dams, where the reference state is not recorded, we advise to include numerical modelling in the near-future surveillance activities. In case a new dam will be built, we advise the initiation of the surveillance activities in parallel with the design stage and construction, since the obtained information in these stages is indispensable and directly linked to the overall dam safety in the future. Finally, a carefully planned monitoring system provides a more reliable operation which will reflect in the quantity and quality of the data.

6.3 Future Work

There is a lot of work to be done to establish a system of dam safety in accordance with the safety standards of the society today. The disadvantages of Slovenian dam surveillance activities and safety are discussed in the reports of the VODPREG project (Kryžanowski and Humar, 2014). The dam community has transitioned from the phase of building and designing the dams, to the phase of maintaining and extending their exploitation stage. A broad approach, including the provision of an appropriate legislative framework, is necessary, which should include the following dam surveillance activities: personnel training, installation and maintenance of sensors, assessment of the potential failure modes and failure analysis of these modes, establishment of statistical and numerical models with multivariate condition assessment analysis with the inclusion of the data from dynamic monitoring. It is important that in case of building new dams, the activities of structural health monitoring are introduced already in the design phase.

7 CONCLUSIONS

In this dissertation, we have analysed and investigated the possibilities of including vibration based techniques in the framework of regular structural health monitoring of dams. The core of our work was organized around the experiment on Brežice dam. We have formulated three research hypotheses, which were evaluated during the research work: (*i*) dynamic loading, present throughout regular or exceptional operating, regimes has a significant impact on mechanical properties of concrete gravity dams; (*ii*) state-of-the-art on non-contact ambient vibration testing provide for a more efficient monitoring of dam ageing; and (*iii*) state-of-the-art experimental techniques can be used for a more efficient monitoring of dam ageing.

The main challenge that the dam community is faced with are ageing dams, built in times of different safety standards and economic regimes, while many of them are already extending their designed exploitation period. The role of the turbines installed in run-of-the-river dams is nowadays indispensable as the provide a fast reserve and ancillary services to the grid. The HPPs' operational regimes follow the demand on the market; hydropower is used to cover a variable part of the production (intermediate and peak load) and provides compensation for base load production in times of surplus of power in the system. Hydropower plants are paying the highest toll of this type of operation. Units that were in general designed to operate continuously in conditions of optimal utilisation are being controlled on-line with multiple start-stop cycles and operate in off-design regimes. The sacrifice of turbines is already recognized in their shorter life expectancy; it was estimated that each start and stop procedure causes fatigue equal to 15–20 h of operation (Trivedi et al., 2013). Moreover, the warning signs of fatigue on the bearing concrete structure are recognized by some dam operators as well. In this research, the full scale issue of operational loads is adequately addressed for the first time, by observing a dam's dynamic response right after the completion of the construction work, by the analysis of the operational patterns, and by implementing the measures gained by experience from similar structures, operating for years, where signs of an accelerated fatigue are discovered.

The analysis of operational logs from the HPPs on the Lower Sava River show that the median of their continuous turbine operation is 40 h, while the longest operation is longer than 80 days and the shortest only a few minutes. Emergency operation regimes occur quite frequently; statistically more than one per month. According to the data from Vrhovo HPP, the operational regimes remain more or less the same throughout the last decade of operation. The sum of working hours of turbines accounts for more than 60% of the time of the year - around 5500 h of operation per unit per year. This contributes to the cumulative effect of low-amplitude, high-frequency excitation load present on those dams. In the particular case of the Lower Sava River scheme, this accumulates to 3 times 5500 h of operation in random order dictated by the demand, since every HPP has three units installed.

The dynamic monitoring of HPP Brežice started in 2016 with the first recordings before the mechanical equipment was installed and when the Sava River was still flowing in a diversion channel. These measurements were crucial for further diagnostic work, since they represent the reference (as-built) state of the dam. This state is assumed as the state of the dam in sound conditions with the initial latent condition, i.e. with the initial micro-cracking supply, where the effects of placement, curing, and hydration of concrete are captured. The information on a dam's initial state is crucial for any SHM; unfortunately in the majority of cases, it is unobtainable. The first recordings were performed in the powerhouse and in the 1st pillar in the overflow section. The dynamic properties of the structure were determined from the response to the excitation by the construction activities. In the next stage, the start-up tests of the mechanical equipment provided for the most extensive experimental phase. Various operating regimes on each unit were tested during this period, including normal and emergency manoeuvres:

- regular start-stop cycles;
- emergency braking (mechanical and electrical);
- regulation;
- simultaneous load rejection on two units.

The response of the structure was measured in eight experimental points located at different structural parts in the powerhouse. The observation of the structural response has confirmed the hypothesis of the massive dam structure being sensitive to the loading caused by the operation of the turbines. We discovered that Unit 2 has the prevailing influence on the structural response; this outcome was suspected due to the design of the dam. We also confirmed the assumption that the effect of turbine operation is not reaching beyond the dilatation and further into the spillway section of the dam. At the same time, this information confirms the high quality of the constructed dilatation joint. The response of the structure to the transient actions with turbines revealed that regular starts and stops of the turbine have a larger effect than expected, while peak velocity values are comparable with the emergency manoeuvres. This is not unexpected, since regular manoeuvres last longer than emergency ones, which provide for longer excitation times, and a massive structure is more prone to longer excitation than to short impacts. Another important finding is the measured response to the excitation in the vertical direction. The double regulation of Kaplan turbines provides better utilisation rates, and at the same time the reactive machine responds to the changes in the uplift. These fluctuations are directly transferred to the bearing structure and were measured in location StV in vertical direction. The highest amplitudes were measured at that location, and the frequency response in the same location is directly linked to the frequency signature of the unit. The experimental findings were confirmed with the numerical model as well.

An extensive effort was devoted to the use of laser Doppler vibrometry as an alternative to traditional contact measurements. Laser technology is well developed, however, it has long been believed that it cannot be used on active experimental grounds. Following the developments in peer literature, we developed the interface, which is mounted on the vibrometer. The interface enables placement of corrective accelerometers on the face of the vibrometer. With the use of two correctly placed accelerometers, we are able to extract the pseudo-vibration caused by the movement of the LDV. When the proper methods to enhance the signal-to-noise ratio, filtering, and mathematical operations between the signal channels were applied, we were able to extract the pure structural response. We confirmed the result using parallel control measurements on the turbine housing, where an additional accelerometer was mounted in close proximity to the laser beam illumination spot. At this stage, we can confirm the applicability of the LDV, which can be used inside the powerhouse on an active standing point during regular operation of the powerhouse. This work provided the first step in the implementation of non-contact vibration measurements on dams. A substantial amount of work to continue this research remains. We have provided the recommendation on how condition monitoring should be included on run-of-the-river dams, with minimal extension of the existing monitoring system on dams. We believe this implementation will help to improve the safety of the dams, minimise repair costs, and help to extend the expected lifetime of the existing dams. With continuation of the investigation, we will be able to provide an exact answer on how many fatigue cycles the structure can experience before reaching the critical condition. This has not been possible so far, since the structures under investigation are always already heavily damaged and the information on the latent condition is unknown. Moreover, Brežice dam is structurally similar to the upstream dams on the Lower Sava River. The experience gained here can primarily be used on other structures on the Sava River and indirectly on other run-of-the river dams beyond the Sava River as well. While the issue of ageing dams is not unique to Slovenia, this information, together with the experience of other researchers, will have a broader impact on the safety of dams.

“Blank page.”

8 RAZŠIRJENI POVZETEK

8.1 Uvod

Ko zbolimo, se nam zdi povsem samoumevno, da se odpravimo k zdravniku. Vsi se tudi zavedamo, da je skrb za naše zdravje zelo pomembna, ter da je bolje preprečevati kot zdraviti. Misel, da je treba stanje mehanske opreme redno preverjati in opremo vzdrževati, nam je tudi še nekoliko blizu. Običajno pa pozabimo, da se tudi konstrukcije in veliki infrastrukturni objekti spreminjajo s časom (da se starajo), da tudi ti zahtevajo stalno vzdrževanje ter da je za njihovo pravilno vzdrževanje potrebna tudi dobra diagnostika. Analogijo z zdravniškim delom lahko še razširimo. Zdravniki za spremljanje pacientovega zdravja uporabljajo specializirano opremo in če na primer ugotovijo, da ima pacient povišano temperaturo, predpišejo ustrezno zdravljenje ali naročijo dodatne teste, vse pa zabeležijo v pacientov karton. Z rednimi sistematskimi pregledi pa pacienta spremljajo od rojstva in beležijo njegovo stanje, kar jim pomaga pri diagnostiki v času bolezenskih stanj. Podobnega načina dela se lotevajo inženirji pri spremljanju objektov. Z beleženjem in rednimi analizami podatkov s senzorjev, ki so nameščeni na primernih mestih na konstrukciji, je mogoče dobro načrtovati redne in izredne posege v objekt. Če imamo na objektu na primer nameščene senzorje za spremljanje pomikov in če njihovi podatki kažejo na povečane pomike, lahko s pomočjo podatkov z drugih senzorjev primerno diagnosticiramo vzroke za pojav neobičajnih vrednosti pomika in se odločimo o ukrepih. Vzroki za nastalo situacijo so lahko zelo različni. Morda je prišlo do poslabšanja lastnosti vgrajenega materiala, sprememb v okolju ali povečane obtežbe. Ob podpori informacij, ki jih pridobimo s spremljanjem posameznih parametrov na objektu, lahko pravočasno in preventivno ukrepamo, preprečimo drage sanacije ali v skrajnem primeru preprečimo porušitev. Z dobrim gospodarjenjem pa izboljšamo stanje konstrukcij in podaljšamo njihovo življenjsko dobo. S takšnim preventivnim delom vsekakor tudi optimiziramo ekonomiko vzdrževanja objekta. In nenazadnje, mar ni tudi v primeru objektov bolje preprečevati kot zdraviti (Aktan et al., 2000)?

Ideja spremljanja stanja objektov je pravzaprav zelo stara. V najpreprostejši obliki se pojavlja že iz časov prvih gradbenih dosežkov v zgodovini. Inženirji in arhitekti so opazovali svoje objekte, njihovo obnašanje in iskali znake poškodb v želji, da razširijo svoje znanje in v prihodnosti izboljšajo njihovo zasnovo. Prvi inženirski objekti, ki so jih pričeli sistematično spremljati, so mostovi. Že starodavni graditelji so opazovali svoje konstrukcije in beležili vzorce razpok. Začetki so predstavljali zelo osnovne občasne vizualne preglede na terenu. Kasneje se je ob pregledih izvedlo tudi kakšen osnovni test z merilno opremo, ki jo je bilo mogoče prinesti s seboj. Sledilo je obdobje nameščanja merilnih naprav v objekte, vendar so te naprave še vedno zahtevale ročno odčitavanje. Kasneje so se pričeli razvijati sistemi za avtomatsko beleženje meritev. V zadnjem obdobju pa se trend pomika k uporabi sodobnih merilnih tehnik, ki temeljijo na laserski tehnologiji, ultrazvoku in lastnostih optičnih kablov. Želja je, da se vse meritve beležijo v enotnih informacijskih sistemih, ki omogočajo vpogled v dogajanje brez odhoda na teren (Ansari, 2005).

Trenutni izziv zgodnjega odkrivanja poškodb preko meritev vibracij je zmožnost zaznavanja zelo zgodnjih poškodb, ko so te minimalne. To pa bo mogoče z razvojem robustne metode, ki bo brez lažnih alarmov omogočala zaznavo poškodb (sprememb konstrukcije) neodvisno od sprememb v okolju (Balageas et al., 2006).

8.2 Spremljanje kondicijskega stanja pregrad

Spremljanje kondicijskega stanja pregrad je interdisciplinarno področje, kjer se srečajo gradbeništvo, mehanika, elektrotehnika, teorija signalov, znanost o materialih in druge vede. Gre za relativno novo znanstveno področje, ki se je začelo razvijati po letu 1990 iz potreb po se sistematični obravnavi problematike identifikacije, vzdrževanja in dolgoročnih napovedi obnašanja opazovanih sistemov (Balageas et al., 2006; Chang et al., 2002; Mufti, 2011). Osnovna shema aktivnosti, ki jih naj vsebuje uspešen sistem kondicijskega spremljanja, je prikazana na Sliki 8.1. Osnovo predstavljajo vizualni pregledi, saj z nameščanjem senzorjev ne moremo na-

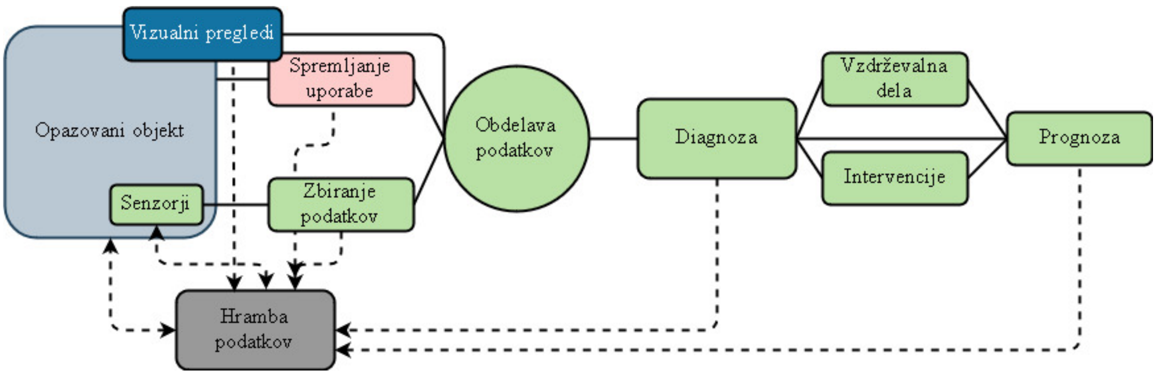

Slika 8.1: Zasnova sistema spremljanja kondicijskega stanja.
Figure 8.1: Principle of a SHM system.

domestiti kritične zaznave izkušenega inženirja. Celotni sistem pa sestoji iz: objekta z vsemi pripadajočimi senzorskimi mesti (to so predhodno identificirana mesta, kjer je mogoče namestiti senzorje in na katerih je mogoče spremljati točno določen porušni mehanizem), sistema spremljanja obratovanja objekta ter sistema za obdelavo in hrambo podatkov. Za izdelavo prognoz je nujno spremljanje t. i. latentnih parametrov, ki ponudijo informacijo o skritih stanjih. Spremljanje vibracij in njihova analiza omogočata na primer ugotavljanje kondicije (poškodovanosti, mikrorazpok) vgrajenega materiala. Takšen celoviti pristop k spremljanju objekta je tudi močno orodje za napovedovanje vzdrževalnih ukrepov in gospodarjenja.

Monitoring pregrad ima zelo dolgo tradicijo, vendar le v svoji osnovni obliki, torej v meritvah. Intenzivnost gradnje pregrad je bila v preteklosti precej večja, kot je dandanes. Trenutno se v svetovnem merilu na leto zgradi približno 200 pregrad različnih tipov, v preteklosti pa je bila ta številka precej višja (Bernstone, 2006). V času pred letom 1990 je bila večina pregrad vodena lokalno, s stalno prisotno posadko. Nato je sledila postopna optimizacija z daljinsko vodenimi elektrarnami, krčenjem števila članov posadk in z zmanjševanjem časa, ko je posadka prisotna na posameznem objektu. Intenziteta gradnje pregrad je upadala in tako so se začeli krčiti tudi gradbeni oddelki. Znanje in naloge gradbenih inženirjev so se tako spotoma prenesli na posadko za vodenje proizvodnje električne energije, ki prihaja večinoma iz elektroinženirskih vrst. Dandanes je vloga gradbenih inženirjev precej marginalna, čeprav govorimo o gradbenih objektih, kar pa žal tudi pomeni, da je gradbeni del nekoliko na stranskem tiru. Sem pa sodi tudi vzdrževanje kondicije objekta, ki je v primerjavi z elektromehansko opremo precej bolj trajen, ni pa večen.

8.3 Staranje pregrad

Staranje pregrad lahko opišemo kot kateri koli časovno odvisni vpliv, ki vodi do sprememb v materialu ter ima vpliv na varnost objekta (Zenz, 2008). Sodeč po razlagi ICOLD Tehničnega komiteja za staranje pregrad lahko o staranju govorimo po preteku prvih petih let obratovanja, poškodbe, ki se pojavijo prej, pa so povezane z napakami pri zasnovi in vgradnji ter jih uvrščamo v latentno stanje (ICOLD Committee on Dam Ageing, 1994). Po podatkih Slovenskega nacionalnega komiteja za velike pregrade (SLOCOLD) imamo v Sloveniji 42 velikih pregrad, od tega tri zgodovinske (klavže). Povprečna starost pregradnih objektov je bila leta 2019 že 43 let, najstarejša sodobna pregrada je stara 105 let (Fala) in najnovejša 2 leti (Brežice). Dinamika gradnje po letih je predstavljena na Sliki 4.1, na strani 35. Najbolj običajen tip pregrade v Sloveniji je kombinirani tip pretočnih rečnih pregrad, ki so pretežno namenjene hidroenergetski izrabi (glej Sliko 4.2, na strani 36). Tudi v tujini je situacija podobna. Več kot 80 % vseh pregrad v ZDA je bilo zgrajenih pred letom 1979, v Avstraliji več kot 50 % pred letom 1969. Celo na Kitajskem, kjer je gradnja pregrad tudi dandanes v razcvetu, so večino pregrad zgradili v letih 1950–1970 (Su et al., 2013; SLOCOLD, 2018; USBR, 2018; ANCOLD, 2018).

Glavni vzroki za staranje betonskih pregrad so naslednji:

- alkali-agregatna reakcija;
- kemični napad (sulfati, kloridi);
- abrazija in kavitacija;
- pronicanje vode;
- krčenje in raztezanje betona;
- temperaturni cikli;
- obratovalna obtežba.

Alkali-agregatno reakcijo povzroča uporaba reaktivnih agregatov. Kemični napad povzročijo sulfidi in kloridi, prisotni v vodi. Abrazija in kavitacija sta težavi na površinah, kjer je beton v stiku z vodo in vodnim tokom. Temperaturni cikli so posledica sezonskih izmenjav letnih časov, spremenljivega sončnega sevanja ter izmenjave dneva in noči. Izpostavljenost cikličnim obtežbam zaradi obratovanja hidromehanske opreme predstavlja vir visokocikličnega in nizkoamplitudnega vzbujanja z velikim kumulativnim učinkom. Utrujanje namreč lahko razdelimo v 3 skupine:

- utrujanje z nizkim številom ciklov $N_f \leq 10^3$ in visokimi amplitudami napetosti;
- utrujanje z velikim številom ciklov $10^3 \leq N_f \leq 10^7$ in nizkimi amplitudami napetosti;
- utrujanje z zelo velikim številom ciklov $N_f \geq 10^7$ z zelo nizkimi amplitudami napetosti (Shah et al., 1970).

Primer utrujanja z nizkim številom ciklov z visoko amplitudo je potres, medtem ko obtežbo z velikim številom ciklov lahko predstavljajo: veter, promet ali delovanje strojev. Utrujanje z obratovalnimi obtežbami, ki je prisotno na hidroenergetskih pregradah, sodi v skupino, kjer ima prisotna obtežba zelo veliko ciklov z zelo nizkimi amplitudami. Takšna obtežba je zelo primerna za razvoj in rast mikrorazpok (Shah et al., 1970).

8.3.1 Staranje betona

Beton je kompozitni material, ki ga sestavlja agregat, cementno vezivo in voda. Lastnosti betona so odvisne od lastnosti posameznih gradnikov, njihovega razmerja in stanja ob vgradnji, kvalitete vgradnje in nege mladega betona. Hidrotehnični betoni so posebna vrsta betona, saj morajo kljubovati drugačnim pogojem kot običajni, konstrukcijski betoni. Zaradi posebnosti pri vgradnji je pri hidrotehničnih betonih premer maksimalnega zrna precej večji kot pri konstrukcijskih betonih in je običajno med 80–150 mm. Delež cementa v mešanici je zaradi zmanjšanja hidratacijske toplote nižji. Nizko je tudi vodo-cementno razmerje. Tudi popolno vgrajeni in optimalno negovani beton razvije začetno stanje mikrorazpok, ki so posledica pojava notranjih napetosti med strjevanjem (Ortiz, 1985). Te razpoke se lahko, glede na zunanje dejavnike, s časom povečujejo. Pri običajnih konstrukcijskih betonih prisotnost mikrorazpok ni problematična, če njihova velikost ne preseže dopustnih vrednosti. Pri hidrotehničnih betonih pa je pojav razpok bolj problematičen, saj vpliva na vodoprepustnost. Hkrati pa je na hidroenergetskih objektih rast razpok še pospešena zaradi cikličnih obremenitev konstrukcije zaradi obratovanja elektrarne (Japan Society of Civil Engineers, 2007; Lamond et al., 2006; USBR, 1988).

Ločimo med tremi vrstami začetnega stanja mikrorazpok: razpoke na stiku cementne paste in agregata, razpoke v cementnem vezivu in razpoke v agregatu. Zrna agregata so bolj toga od cementne paste in omejijo prosto krčenje paste med strjevanjem ter hidratacijo cementa – tako se tvori začetni vzorec mikrorazpok (Wicke et al., 1999; Ortiz, 1985). Nadaljnja rast mikrorazpok je dolgotrajen in počasen proces. Tudi ta sestoji iz treh osnovnih faz, ki so predstavljene na Sliki 4.5, na strani 41, kjer prikazujemo vrednost indeksa poškodovanosti (0–intakten material, 1–porušen) glede na normirano vrednost ciklov. Začetna faza (A) predstavlja tvorjenje začetne zaloge mikrorazpok in njihovo začetno rast, ki je posledica reoloških procesov v fazi strjevanja betona. Sledi faza (B), kjer je konstrukcija izpostavljena cikličnim zunanjim obremenitvam. Rast razpok je v tej fazi, glede na predhodno fazo, zelo upočasnjena. Proces tvorbe razpok v tej fazi je počasen in se povečuje z izpostavljenostjo konstrukcije cikličnim obremenitvam. Na površini pa so poškodbe vidne šele takrat, ko je proces že dobro napredoval. Z nadaljnjo izpostavljenostjo konstrukcije, v fazi (C), je proces tvorbe razpok že zelo intenziven in se z nadaljnjimi cikli deformacije naglo povečujejo. Ko je presežena kritična točka trdnosti materiala, postane rast razpok nestabilna in vodi do porušitve. V naši raziskavi smo posvetili pozornost vplivu cikličnih obremenitev na konstrukcijo hidroenergetskih objektov, za katere poskušamo dokazati, da dolgoročna izpostavljenost konstrukcije pregrade dinamičnim obtežbam vpliva na varnost konstrukcije.

8.4 Eksperimentalno delo

Eksperimentalno delo na pregradi Brežice predstavlja jedro te raziskave. Pregrada Brežice je bila zgrajena leta 2017 in danes predstavlja zadnjo zgrajeno pregrado na Slovenskem. Sistemsko je vključena v sistem šestih pregrad na spodnji Savi, ki bo dokončan z izgradnjo Mokric v prihodnjih letih (Na Sliki 5.1, na strani 59 je prikazana shema spodnjesavske verige). Pregrada je po tipu kombinirana težnostna pregrada, ki jo sestavljajo osrednja betonska pregrada, na katero se priključujeta visokovodna nasipa, ki omejujeta območje zadrževalnika. Betonsko pregrado, skupne dolžine 160 m in z maksimalno konstrukcijsko višino 36,5 m, sestavljajo strojnica in pet prelivnih polj. V strojnici so nameščene tri vertikalne, dvojno regulirane, Kaplanove turbine s posamično močjo 15,2 MW in s planirano srednjo letno proizvodnjo 161 GWh.

Z eksperimentalnim delom na pregradi Brežice smo pričeli maja 2016, približno 2 leti po pričetku gradbenih del. Do takrat je že bila zaključena večina betonerskih del, gradbena jama pa je bila še vedno suha. Gradbišče je bilo še vedno zelo živo, zato smo s prvimi meritvami lahko izmerili odziv masivne konstrukcije na vzbujanje z gradbenimi deli. Za meritve smo uporabili laserski vibrometer PDV-100 (Polytec, 2016). Eksperimentalne točke smo izbrali na mestih, ki smo jih lahko z laserjem osvetlili tudi kasneje, ko je objekt že obratoval. Odločili pa smo se za mesta, do katerih je mogoče varno dostopati, saj smo pričakovali, da jih bomo občasno vseeno želeli tudi fizično doseči. Iskali smo mesta, kjer je nasprotno stojišče na drugačnem tipu strukturnega elementa, po možnosti bolj togem, na oddaljenosti znotraj merilnega dosega naprave, ki je v optimalnih pogojih 30 m, ter da zagotavlja čim bolj pravokotno usmerjenost laserskega žarka glede na merjeno površino. Za izboljšanje odboja so bila vsa mesta opremljena z odbojnim trakom, ki ga je treba vsakih nekaj mesecev očistiti, na mestih v prelivnih poljih pa zamenjati po vsaki visoki vodi. Skupno je bilo aktiviranih 12 eksperimentalnih točk (glej Sliko 8.2).

Meritve v prelivnem polju lahko potekajo le pri zaprtih zapornicah in nizkih pretokih. Pregrada je namreč zasnovana tako, da je v času visokih voda spodnji del stebrov poplavljen. V strojnici smo v času zagonskih testov merili odziv konstrukcije v osmih točkah. Pri meritvah smo upora-

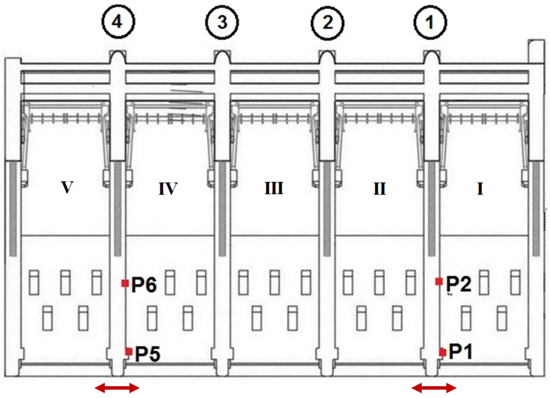

(a) Overspilling section.

(a) Prelivna polja.

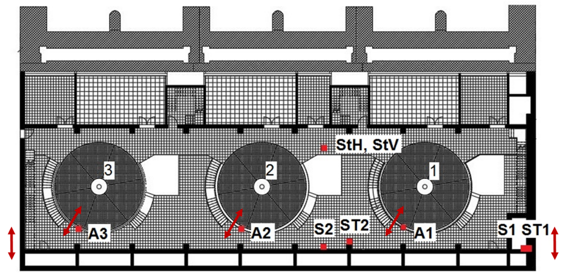

(b) Powerhouse.

(b) Strojnica.

Slika 8.2: Merilna mesta na objektu.

Figure 8.2: Experimental points on Brežice dam.

bili laserski vibrometer, hitrostne doze in pospeškomere. Zasnovali smo metodologijo merjenja odziva konstrukcije z uporabo vibrometra tudi v pogojih, ki so veljali za neprimerne za uporabo laserske tehnologije. Težava pri relativnih meritvah je, da v primeru gibanja instrumenta merimo vsoto, obnašanje merjene ploskve in napako zaradi gibanja instrumenta v smeri laserskega žarka. V ta namen smo izdelali aluminijasti vmesnik, ki se namešča na prednje lice vibrometra, nanj pa se namestita dva pospeškomera, ki ju uporabimo za korigiranje napake, nastale zaradi gibanja instrumenta. Dva enoosna pospeškomera, nameščena simetrično glede na smer žarka na eni izmed diagonal, zadoščata za izolacijo napake, ki jo povzroči gibanje naprave. Metodologijo smo testirali s kontrolnimi meritvami, kjer smo namestili kontrolni pospeškomer na turbino, v to mesto usmerili laserski žarek ter merili vibracije turbine med njenim obratovanjem. Stojalo vibrometra je bilo nameščeno znotraj turbinskega jaška, kar pomeni, da se je vibrometer med meritvijo prav tako tresel. Z uporabo filtrov in matematičnih operacij smo uspeli izolirati napako in izmeriti pravi odziv turbine (glej Sliko 5.27, na strani 93).

Izmerili smo odziv konstrukcije pri različnih obratovalnih manevrih in analizirali njihov frekvenčni spekter. Analize so pokazale, da je v odzivu konstrukcije zaznati vpliv obratovanja turbin. Tipične časovne serije in prikaz frekvenčnega spektra so prikazani v poglavju 5 in v Prilogi 1.

8.5 Numerični model

Za pomoč pri interpretaciji smo izdelali dva ločena numerična modela: model strojnice in model prelivnih polj (glej Sliko 5.32 na strani 101). Pri izgradnji modela prelivnih polj smo upoštevali simetrijo in modelirali zgolj polovico segmenta, kjer simetrijsko os predstavlja sredinska črta v smeri gorvodno-dolvodno (v modelu v smeri globalne osi X po sredini 3. prelivnega polja). Celotna prelivna sekcija je sestavljena iz petih prelivnih polj razdeljenih s stebri širine 2,7 m, dolžine 51,15 m ter spremenljive višine, ki je najvišja na gorvodni strani (22,9 m) in najnižja na skrajno dolvodni točki (15 m). Vsako prelivno polje je široko 15 m. Fiksni del prelivnega praga je v najvišji točki 11,3 m nad najnižjo točko globine podslapja. Vpliv segmentnih zapornic smo modelirali preko robnih pogojev. Razbijačev in galerije nismo vključili v model. V modelu smo definirali tudi fluidni medij in stični element na mestu kontakta fluidnega elementa s strukturnimi. Za beton smo predpostavili linearni materialni model, vodo smo modelirali kot nestisljivo in preprečili smo pojav površinskih valov. Na spodnjem robu modela so preprečeni pomiki v smeri osi X, Y in Z, vpliv objekta strojnice je na boku nadomeščen s podporami v smeri osi Y. Definirali smo fazni model, ki je omogočal na enem modelu izračune z dodano vodo v akumulaciji in podslapju ter brez nje.

Model stojnice obsega tlorisno 58,2 m $\times$ 24,1 m ter 23,1 m visok izsek. Temeljnih masivnih betonov nismo modelirali, na spodnjem robu smo zato predpostavili togo vpetje v podlago. Model predstavlja masivni betonski blok na nivoju turbinske etaže z upoštevanimi odprtinami turbinskih traktov, ter vse vertikalne elemente do nivoja jeklene strehe. Južna stena, na kateri je bilo precej eksperimentalnih točk, je debela 40 cm z dodatnimi 9 stebri, dimenzij 60 $\times$ 60 cm, ki podpirajo žerjavno progo. Streho smo modelirali z linijskimi elementi, ki smo jim pripisali geometrijo profilov HEA in IPE, ter materialne lastnosti jekla S235. Za beton smo predpostavili linearno-elastično obnašanje, za materialne lastnosti smo privzeli projektne vrednosti betona C25/30.

Za delitev na končne elemente smo predpisali maksimalno velikost stranice elementa (1 m v prelivnem polju; 0,5 m v strojnici). Predhodno smo poskrbeli še za odtise stičnih ploskev na soležnih elementih in izbrali kubusno obliko končnih elementov s kvadratno interpolacijo. Za fluidne elemente smo se odločili za linearno shemo diskretizacije. Izvedli smo modalno analizo; zanimale so nas lastne nihajne oblike. Izračun smo izvedli za 200 lastnih vrednosti pri modelu strojnice in 100 pri modelu prelivnih polj. Kot pogoj smo postavili, da pri računu sodeluje vsaj 90 % mase v modelu. Obtežba v modelu je zgolj lastna teža.

Staranje objekta smo simulirali s spreminjanjem vrednosti elastičnega modula betona. Predpostavili smo globalno znižanje vrednosti elastičnega modula v območju do približno 10 %, nato smo izvedli večje število analiz z različnimi vrednostmi. Izačune smo avtomatizirali s pomočjo skript v Pythonu.

Z modelom smo preverili primernost eksperimentalnih točk, da se ne nahajajo na mestu t. i. stacionarnih točk. Preverili smo računske vrednosti lastnih frekvenc. Uspeli smo potrditi izmerjene frekvence z numeričnimi vrednostmi. Pokazali smo, da sprememba elastičnega modula povzroči padanje prvih dveh lastnih frekvenc stebra med 1. in 2. prelivnem poljem, enako potrditev smo dobili tudi za model strojnice.

8.6 Rezultati

Z meritvami neposredno na turbini smo prepoznali frekvence vzbujanja konstrukcije, te so pri: 1,8 Hz, 3,6 Hz, 7,2 Hz, 21,4 Hz, 35,7 Hz in 42,9 Hz. Prva lastna frekvenca je povezana z vrtenjem turbine, ta obratuje s 107 obr/min. Pojavljajo pa se tudi višje harmonične oblike; najbolj izrazite so pri 21,4 Hz in 42,9 Hz. Prepoznali smo tudi lastne frekvence konstrukcije in numerično preverili vpliv staranja na njihove vrednosti. Na Sliki 5.35, na strani 104, sta prikazani prvi dve lastni frekvenci stebra 1 med prelivnima poljema I in II. Njuni vrednosti sta 10,98 Hz in 18,8 Hz. Primerjava eksperimentalnih vrednosti z računskimi pa je prikazana na Sliki 5.36, na strani 105, pri prvi lastni vrednosti je odstopanje 3 %, 6 % pri drugi in 8 % pri tretji. Na Sliki 5.38, na strani 106, je prikazanih prvih pet nihajnih oblik modela strojnice ter na Sliki 5.37, na strani 106, primerjava numeričnih vrednosti z merjenimi. Odstopanja so 5 % pri prvi, 1,3 % pri drugi in 9 % pri tretji lastni frekvenci. Staranje smo v modelu predstavili z zmanjšanjem vrednosti elastičnega modula. Padec elastičnega modula za 12 % povzroči padec lastnih frekvenc za približno 6 %.

8.7 Predlog za vključitev dinamičnega monitoringa pretočnih pregrad

Priporočila za vključitev dinamičnega monitoringa v obseg rednih aktivnosti spremljanja pregrad temeljijo na pregledu literature, na dognanjih stroke in na izkušnjah pri eksperimentalnem delu na pregradi Brežice. V tem poglavju predstavimo način, kako z minimalnimi razširitvami obstoječega, zakonsko obveznega sistema spremljanja pregrad vključiti meritve vibracij in spremljanje kondicijskega stanja v program rednega opazovanja. Poudariti je treba, da mora biti sistem spremljanja vibracij prav tako zasnovan ob upoštevanju osnovnih kriterijev spremljanja objektov, ki so podrobno predstavljeni v poglavju 3.1, ter ob upoštevanju sedmih osnovnih načel kondicijskega spremljanja objektov, predstavljenih v Worden et al. (2007). Osnovna vprašanja, na katera moramo odgovoriti, so: katero tehnologijo bomo uporabili, koliko in kje, ali potrebujemo kontinuirano in avtomatizirano beleženje, ali bodo zadostovali diskretni intervali, kako pogosti naj bodo ti intervali? Zajem podatkov ter njihova obdelava in arhiviranje so odvisni od odgovorov na zgornja vprašanja. Sledi identifikacija opozorilnih vrednosti merjenih parametrov ter postopkov, ki sledijo ob zaznanih, potencialno alarmantnih vrednostih.

Obstoječi sistem opazovanja pregrad v Sloveniji od upravljalca zahteva, da se na vseh velikih pregradah vzpostavi sistem seizmičnega opazovanja. Za pregrade višine 30–60 m ta sestoji iz vsaj treh akcelerografov, kjer je eden nameščen v temelju pregrade, eden v telesu ter eden na prostem površju v bližini pregrade (Uradni list RS 58/16, 2016). Naprave so nameščene v prožilnem načinu z vsaj 5 s predogodkovnega pomnilnika.

Za potrebe preiskave smo pridobili podatke z najbližje seizmične opazovalnice iz državne mreže, Gornji Cirnik (GCIS) (ARSO, 2018). Zanimali so nas vsi lokalni dogodki z epicentrom v radiju do 50 km s središčem v Brežicah v letih 2017 in 2018 ter z magnitudo potresa vsaj 1.

Postaja GCIS je opremljena s seizmomerom tipa GURALP CMG-40T. V omenjenem obdobju so na njej zaznali 15 lokalnih potresov z magnitudami od 1,1 do 2,9. Potresi so trajali 9–40 s in imajo prevladujoče frekvence v območju 4–20 Hz. Kljub že vzpostavljenemu seizmološkemu monitoringu na Brežicah se pospeškomeri ob teh dogodkih žal niso prožili. Dva pospeškomera sta nameščena v 3. stebru prelivnega polja, torej sta odmaknjena od vpliva turbin. Glede na podatke seizmološkega opazovanja ozemlja RS je območje izpostavljeno lokalnim potresom. Ocenjujemo, če bi bila nameščena pospeškomera aktivirana v kontinuiranem načinu ali pa vsaj z zelo nizkimi mejami proženja, bi lahko vsako leto pridobili vsaj pet zapisov, ki bi jih lahko uporabili za izdelavo ocene kondicijskega stanja. Poleg obstoječih pospeškomerov priporočamo namestitev dodatnih pospeškomerov v strojnici objekta, in sicer po enega v vsak turbinski jašek, ter še vsaj tri na konstrukciji: v temeljne masivne betone, na južno steno in na podest, ki povezuje vse tri turbinske jaške. Pospeškomeri pa morajo nujno delovati kontinuirano in ne v prožilnem načinu. Poleg meritev vibracij bi bilo treba izvajati meritve temperatur betona v turbinskih jaških, saj imajo tudi te vpliv na staranje, ter spremljati vlažnost in temperaturo zraka. Ostali parametri, ki bi se na konstrukciji morali kontinuirano beležiti, so: odpiranje in zapiranje dilatacij ter konstrukcijskih stikov, rast razpok ter meritve količine precedne vode. Hkratno je potrebno tudi beleženje obratovanja hidromehanske opreme, saj se vpliv obratovalnih manevrov prenaša na konstrukcijo. Nenazadnje pa bi bilo treba v program vključiti periodične meritve vibracij na že vzpostavljenih mestih za spremljanje staranja, in to vsaj enkrat letno, na primer ob koncu hladnega dela leta. Priporočamo uporabo brezkontaktnih metod, saj je z njihovo uporabo mogoče z eno napravo v enem dnevu preiskati vse objekte v spodnjesavski verigi. Nujni dodatni koraki pri izvajanju opazovanja objektov pa so: analiza merjenih parametrov, izdelava statističnih in numeričnih modelov, ter kvalitativni pregled in interpretacija rezultatov meritev. Obdelave podatkov ni treba opravljati v realnem času; zadostuje beleženje časovnih serij z natančno označenim začetnim časom, ter povezava zabeleženih serij z obratovalnim dnevnikom. Enkrat letno priporočamo izdelavo interpretacije meritev ob upoštevanju referenčnih vrednosti, ki smo jih izmerili z meritvami v letu 2016. Poleg tega priporočamo pridobitev podatkov o betonu, ki je vgrajen v pregrado, saj odsotnost teh podatkov na dolgi rok ogroža varnost pregrade. Če gre za manjkajoče arhivske podatke pri pregradah gorvodno, priporočamo ureditev tudi teh.

Na kratko upravljalcem priporočamo naslednje:

- uporabo že nameščenih pospeškomerov na pregradah v kontinuiranem načinu;
- namestitev dodatnih pospeškomerov v strojnici;
- vključitev meritev vlažnosti, temperature betona, dilatacij, količine izcedne vode, spremljanje razpok, temperature zraka, beleženje obratovalnih manevrov;
- dodatno prognostično meritev enkrat letno;
- izdelavo statističnih in numeričnih modelov pregrade;
- poenoteno hrambo podatkov;
- letne interpretacije kondicijskega stanja.

V primeru gradnje novih pregrad priporočamo pričetek aktivnosti, povezanih z opazovanjem v fazi planiranja in gradnje. Vsekakor pa priporočamo vpeljavo dinamičnega monitoringa že v času gradnje, tudi z uporabo brezkontaktnih metod.

Precej dela pa je še na strani zakonodajalca. Nujni ukrepi so: pravna ureditev področja pregrad v Sloveniji ter ureditev zahtev, kdo sme izdelovati ocene kondicijskega stanja teh objektov, ter postavitev zahtev o neodvisnih pregledih, podobno, kot je to urejeno v drugih državah. Glavne pomanjkljivosti sistema varnosti pregrad so bile izpostavljene že v poročilu projekta VODPREG (Kryžanowski in Humar, 2014).

8.8 Zaključek

V delu smo obravnavali možnosti spremljanja vibracij na pregradah ter vzpostavitve sistema spremljanja kondicijskega stanja v redno prakso aktivnosti zakonsko predpisanega monitoringa. Glavnino našega dela je predstavljalo eksperimentalno delo na pregradi Brežice na spodnji Savi. Pri delu so nas vodile tri raziskovalne hipoteze: (*i*) vseskozi prisotne dinamične obremenitve v sklopu rednih in izrednih obratovalnih režimov lahko pomembno vplivajo na mehanski odziv betonskih težnostnih pregrad; (*ii*) laserski vibrometer je ustrezno orodje za spremljanje dinamičnega odziva pregrad; in (*iii*) s sodobnimi merilnimi tehnikami je mogoče proces staranja pregrad spremljati bolje kot le z uporabo tradicionalnih metod, in na ta način bolje gospodariti in zagotavljati obratovalno varnost objekta.

Glavni izzivi, s katerimi se sooča pregradno inženirstvo, so staranje objektov, podaljševanje njihove življenjske dobe ter nadaljnje pokrivanje potreb po energiji in preostalih sistemskih storitvah. Glede na intenzivnost gradnje v preteklosti lahko sklepamo, da je večina objektov, ki bodo obratovali v prihajajočih desetletjih ali stoletjih, že zgrajenih. Večina pa je bila zgrajena v drugačnem političnem in ekonomskem okolju ter z zasnovo, ki ni predvidela današnjih obratovalnih režimov in podnebnih sprememb. Vloga pretočnih elektrarn dandanes se je povsem spremenila. Njihova hitra odzivnost in zmožnost zagotavljanja sistemskih rezerv in storitev jih postavlja med najbolj fleksibilne vire energije. Posledično sprejemajo tudi vlogo žrtve pri zagotavljanju stabilnosti v sistemu in vzdrževanju ravnovesja med porabo in proizvodnjo energije. Takšna njihova vloga v preteklosti vsekakor ni bila predvidena, saj so pretočni sistemi zasnovani, da bodo obratovali predvsem v pasu blizu optimalnih pogojev. Posledice, ki jih trpijo turbine, so že znane; vsak zagon in zaustavitev povzročita utrujanje, ki je enakovredno 15–20 uram rednega obratovanja (Trivedi et al., 2013). Nekateri upravljalci pa prav tako opažajo prve znake utrujanja nosilne betonske konstrukcije. Namen te raziskave je prva podrobna in celovita obravnava problema. Objekt smo pričeli opazovati takoj po zaključku gradbenih del ter izvedli smo analizo obratovalnih vzorcev in obtežb. Pri svojem delu smo upoštevali izkušnje iz drugih konstrukcijsko sorodnih objektov, ki so v obratovanju že dlje časa in kažejo znake staranja, z ne povsem pojasnjenim vzrokom.

Z analizo obratovalnih dnevnikov pregrad spodnjesavske verige smo določili statistične parametre obratovanja. Mediana neprekinjenega obratovanja tako znaša 40 ur, medtem ko je bilo najdaljše neprekinjeno obratovanje kar 80 dni in najkrajše le nekaj minut. Manever zasilnega obratovanja se v povprečju zgodi več kot 1-krat mesečno oz. približno 16-krat letno. Sodeč po podatkih, pridobljenih s HE Vrhovo, so obratovalni režimi v zadnjem desetletju bolj ali manj nesprejemljivi. Vsota obratovalnih ur je preko 60 % razpoložljivih ur v letu na enoto in znaša približno 5500 ur/leto. Ta vrednost predstavlja trajanje dinamičnega cikličnega utrujanja, ki nanese na spodnjesavski verigi trikratnik te vrednosti, saj so v vsakem objektu vgrajeni po trije agregati, ki obratujejo razmeroma uravnoteženo.

S spremljanjem vibracij na pregradi Brežice smo pričeli v letu 2016. Prva meritev je potekala pred vgraditvijo hidromehanske opreme, v času, ko je bila Sava še preusmerjena v obvodni kanal. Ta meritev je bila ključnega pomena, saj smo z njo zabeležili začetno referenčno stanje. Ta meritev predstavlja odziv konstrukcije v zdravem stanju, vendar pa že z izhodiščno zalogo mikrorazpok, ki nastajajo kot posledica načina vgradnje betona, strjevanja, nege in poteka hidratacije. Ta prvi, ključni korak uspešnega sistema spremljanja kondicijskega stanja pa običajno na konstrukcijah žal ni izveden. V okviru te prve akcije smo izmerili odziv stebra v prelivnem polju ter južne stene v strojnici na vzbujanje z ambientalno obtežbo, ki so jo povzročale aktivnosti na gradbišču. Zagonski testi hidromehanske opreme so predstavljali najbolj obsežno eksperimentalno obdobje. V tem času so bili preizkušeni različni obratovalni režimi:

- običajni zagon in zaustavitev;
- varnostni hitri zapori (mehanska in električna);
- krmiljenje turbin;
- simultana razbremenitev dveh enot.

Odziv konstrukcije smo spremljali na osmih mestih v strojnici. Izmerjeni odziv je v prvi vrsti potrdil hipotezo, da so tudi masivne betonske pregrade občutljive na obremenitve, ki jih povzroča obratovanje s turbinami. Izkazalo se je, da ima agregat št. 2 prevladujoči vpliv na konstrukcijo, kar je glede na zasnovo konstrukcije povsem smiseln rezultat. Potrdili smo tudi domnevo, da se vpliv obratovanja elektrarne ne prenaša preko dilatiranega stika na prelivna polja, kar priča tudi o kvaliteti izdelave stika. Analiza odziva konstrukcije ob različnih manevrih je pokazala, da običajni manevri povzročijo večji odziv kot bi morda pričakovali. Njihov učinek namreč lahko primerjamo z učinkom izjemnih obratovalnih manevrov. Po premisleku tudi ta ugotovitev ni tako presenetljiva, saj je masivni objekt bolj dovzeten na vplive z daljšim trajanjem kot na hitre dogodke. Pomembna ugotovitev je povezana z vzbujanjem v vertikalni smeri. Dvojno regulirane Kaplanove turbine omogočajo dobre izkoristke, hkrati pa se spremembe v vzgonu ob krmiljenju z lopaticami prenašajo na nosilno konstrukcijo. Ob zapiranju predvodilniških lopatic turbina sili navzgor – učinek je pulzirajoč. Z meritvami vibracij v vertikalni smeri na mestu StV med zaustavljanjem turbin smo se lahko prepričali o razsežnostih tega vpliva. To merilno mesto je pravzaprav lokacija z največjimi izmerjenimi amplitudami hitrosti, frekvenčni spekter izmerjenega odziva pa je direktno povezan s frekvenčnim odzivom, ki smo ga izmerili na agregatu.

Uporabi laserske vibrometrije smo namenili precej časa. Brezkontaktne meritve ponujajo privlačno alternativo tradicionalnim kontaktnim metodam. Laserska tehnologija je zelo napredovala in se dandanes uporablja v številnih inženirskih disciplinah. Vendar zaradi relativne narave meritev velja, da je ni mogoče uporabljati na aktivnih stojiščih. Po pregledu literature in izdelavi vmesnika za nameščanje pospeškomerov na instrument smo z uporabo dveh dodatnih pospeškomerov, filtrov in matematičnih operacij med signali uspeli izolirati čisti konstrukcijski odziv in gibanje instrumenta. Na tak način smo uspeli izločiti psevdovibracije v merilnem doprinosu, ki jih je povzročilo gibanje instrumenta, ter izmeriti pravi odziv konstrukcije. Meritve smo izvajali na turbini med rednim obratovanjem. Za kontrolno meritev smo na ohišje turbine, na mestu, ki ga je osvetljeval laserski žarek, namestili dodatni pospeškomer. Ta meritev predstavlja prvo aplikacijo vibrometra v strojnici elektrarne med rednim obratovanjem, kjer je stojišče izpostavljeno enakemu vzbujanju kot točka, ki jo merimo. Vrednost križne korelacije med kontrolnim signalom in signalom z vibrometra je 0,9, kar potrjuje uporabnost vibrometra na pregradi med njenim rednim obratovanjem. Raziskava predstavlja prvi korak pri vpeljavi brezkontaktnih meritev v sistem spremljanja pregrad. Delo še zdaleč ni končano in pušča možnosti za nadaljnjo raziskovalno delo in aplikacije. Na podlagi novih spoznanj smo sestavili priporočila za vključitev dinamičnega monitoringa na pretočnih pregradah, z uvedbo minimalnih razširitev obstoječega zakonsko določenega sistema opazovanja pregrad. Po našem mnenju bi imela uvedba dinamičnega monitoringa pregrad pozitiven vpliv na varnost objektov, poleg tega pa lahko informacije kondicijskega opazovanja objektov služijo kot instrument v procesu vzdrževanja in tako vplivajo na zmanjšanje stroškov in podaljševanje življenjske dobe pregrad. Z nadaljevanjem raziskovalnega dela na pregradi Brežice ter ob pridobljenem znanju in z informacijami začetnih meritev bo v prihodnosti mogoč odgovor na vprašanje, koliko ciklov je objekt zmožen prenesti, preden pride do kritične stopnje poškodb. Tega namreč sedaj še ni mogoče napovedati, saj je v preteklosti prihajalo do meritev in raziskav na objektih šele po pojavu obsežnih poškodb, brez informacij o latentnem stanju po vgradnji. Ob odsotnosti teh podatkov pa takšne napovedi niso možne. Pregrada Brežice je po zasnovi sorodna ostalim objektom na spodnji Savi. Izkušnje, pridobljene na tem objektu, bodo lahko direktno uporabljene na gorvodnih pregradah, posredno pa na pretočnih pregradah podobnega tipa. Problematika staranja pregrad in vpliva obratovalnih manevrov ni aktualna samo v Sloveniji, zato lahko ob kombinaciji dognanj drugih raziskovalcev pričakujemo širši vpliv tega dela na izboljšanje varnosti betonskih pregrad.

REFERENCES

FIB Task group 5.1, 2003. Monitoring and Safety Evaluation of Existing Concrete Structures. State-of-Art Report. FIB Bulletion No. 22. Technical report, Internternational Federation for Structural Concrete (FIB), Lausanne, Switzerland.

Abruzzese, D., Angelaccio, M., Giuliano, R., Miccoli, L., Vari, A., 2009. Monitoring and Vibration Risk Assessment in Cultural Heritage via Wireless Sensors Network. In L., Bello, L., Iannizzotto, G., Eds., 2nd Conference on Human System Interactions, 568–573. IEEE, Catania, Italy. doi:10.1109/HSI.2009.5091040.

ACI Committee 207, 2009. Guide to Mass Concrete ACI 207.1R-05. Technical report, American Concrete Institute, Farmington Hills, MI.

ACI Committee 224, 2002. Control of Cracking in Concrete Structures Report. Technical report, American concrete institute.

Agostinelli, G., Cristalli, C., Paone, N., Serafini, S., 2010. Drop-Out Noise of Laser Vibrometers Measuring on Varnished Steel Surfaces of Appliance Cabinets for Industrial Diagnostics. AIP Conference Proceedings 1253: 298–312. doi:10.1063/1.3455469.

Agostinelli, G., Paone, N., 2012. Uncertainty of Diagnostic Features Measured by Laser Vibrometry: The Case of Optically Non-Cooperative Surfaces. Optics and Lasers in Engineering 50, 12: 1804–1816. doi:10.1016/j.optlaseng.2012.06.014.

Ahmed, L., Guarin, A., Ghafars, A. N., 2018. Crack Propagation Under Water Pressure, Experimental and Computed Tomography Investigation. Technical report, Energiforsk AB.

Aiwina, H., Zhang, S., Tan, A. C. C., Mathew, J., 2009. Rotating Machinery Prognostics: State of the Art, Challenges and Opportunities. Mechanical Systems and Signal Processing 23, 3: 724–739. doi:10.1016/j.ymssp.2008.06.009.

Aktan, A. E., Catbas, F. N., Grimmelsman, K. A., Tsikos, C. G., 2000. Issues in Infrastructure Health Monitoring for Management. Journal of Engineering Mechanics 126, 7: 711–724. doi:10.1061/(ASCE)0733-9399(2000)126:7(711).

Aktan, E. A., Catbas, N. N., Grimmelsman, K. A., Pervizpour, M., 2003. Development of a Model Health Monitoring Guide for Major Bridges. Technical report, Federal Highway Administration Research and Development.

Alessandro, A. D., Ubertini, F., Materazzi, A. L., Laflamme, S., Porfiri, M., 2015. Electromechanical Modelling of a New Class of Nanocomposite Cement-Based Sensors for

Structural Health Monitoring. Structural Health Monitoring 14, 2: 137–147. doi:10.1177/1475921714560071.

Allemang, R. J., 2003. The Modal Assurance Criterion-Twenty Years of Use and Abuse. Sound and Vibration 1: 14–21.

ANCOLD, 2018. Register of Large Dams in Australia. Website: https://www.ancold.org.au/?page{_}id=24. Accessed: 12. 6. 2018.

Ansari, F., Ed., 2005. Sensing Issues in Civil Structural Health Monitoribng. Springer The Netherlands., University of Illinois, Chicago, IL, U.S.A.

Antonovskaya, G. N., Kapustian, N. K., Moshkunov, A. I., Danilov, A. V., Moshkunov, K. A., 2017. New Seismic Array Solution for Earthquake Observations and Hydropower Plant Health Monitoring. Journal of Seismology 21, 5: 1039–1053. doi:10.1007/s10950-017-9650-8.

Balageas, D., Fritzen, C.-P., Guemes, A., 2006. Structural Health Monitoring. 1 edition. ISTE Ltd, Chippenham, Wiltshire.

Bandara, R. P., Chan, T. H. T., Thambiratnam, D. P., 2014. Structural Damage Detection Method Using Frequency Response Functions. Structural Health Monitoring 13, 4: 418–429. doi:10.1177/1475921714522847.

Begg, R. D., Mackenzie, A. C., Glasgow, U., Dodds, C. J., Loland, O., 1976. Structural Integrity Monitoring Using Digital Processing of Vibration Signals. In Offshore Technology Conference, 305–311. Houston, TX. doi:10.4043/2549-MS.

Bernstone, C., 2006. Automated Performance Monitoring of Concrete Dams. Doctoral Thesis, Lund University., Lund.

Boller, C., 2001. Ways and options for Aircraft Structural Health Management. Smart Materials and Structures 10, 3: 432–440.

Bombač, M., 2012. Hydraulic Research of the Construction Pit of HPP Brežice on a Physical Model. Acta Hydrotechnica 25, 42: 1–16.

Brincker, R., Ventura, C., 2015. Introduction to Operational Modal Analysis. John Wiley & Sons, Ltd, 372 p.

Bryksin, A. A., Liseikin, A. V., Gromyko, P. V., Seleznev, V. S., 2014. What Caused the Accident at the Sayano–Shushenskaya Hydroelectric Power Plant (SSHPP): A Seismologist's Point of View. Seismological Research Letters 85, 4: 817–824. doi:10.1785/0220130163.

Bukenya, P., Moyo, P., Beushausen, H., Oosthuizen, C., 2014a. Health Monitoring of Concrete Dams: a Literature Review. Journal of Civil Structural Health Monitoring 4, 4: 235–244. doi:10.1007/s13349-014-0079-2.

Bukenya, P., Moyo, P., Oosthuizen, C., 2014b. Long Term Ambient Vibration Monitoring of Roode Elsberg Dam – Initial Results. In International Symposium on Dams in a Global Environmental Challenges. ICOLD - CIGB, Bali, Indonesia.

Carden, E. P., Fanning, P., 2004. Vibration Based Condition Monitoring: A Review. Structural Health Monitoring 3, 355: 355–377. doi:10.1177/1475921704047500.

Castellini, P., Martarelli, M., Tomasini, E. P., 2006. Laser Doppler Vibrometry: Development of Advanced Solutions Answering to Technology's Needs. Mechanical Systems and Signal Processing 20, 6: 1265–1285. doi:10.1016/j.ymssp.2005.11.015.

Castellini, P., Paone, N., Tomasini, E. P., 1996. The Laser Doppler Vibrometer as an Instrument for Nonintrusive Diagnostic of Works of Art: Application to Fresco Paintings. Optics and Lasers in Engineering 25, 4-5: 227–246. doi:10.1016/0143-8166(95)00073-9.

CEN, 2010. Eurocode 2: Design of Concrete Structures - Part 1-1 : General Rules and Rules for Buildings.

Chanda, P., Suparna, M., 2016. Energy Systems in Electrical Engineering Operation and Maintenance of Thermal Power Stations Best Practices and Health Monitoring. Springer. doi: 10.1007/978-81-322-2722-9.

Chang, F.-K., Prosser, W. H., Schulz, M. J., 2002. Editorial : Letter of Introduction from the Editors of Structural Health Monitoring. Structural Health Monitoring 1, 1: 3–4.

Chang, P. C., Flatau, A., Liu, S. C., 2003. Review Paper: Health Monitoring of Civil Infrastructure. Structural Health Monitoring 2, 3: 257–267. doi:10.1177/1475921703036169.

Chen, H., Spyrakos, C., Venkatesh, G., 1995. Evaluating Structural Deterioration by Dynamic Response. ASCE Journal of Structural Engineering 121, 8: 1197–1204. doi:/10.1061/(ASCE)0733-9445(1995)121:8(1197).

Cheng, L., Zheng, D., 2013. Two Online Dam Safety Monitoring Models Based on the Process of Extracting Environmental Effect. Advances in Engineering Software 57: 48–56. doi: 10.1016/j.advengsoft.2012.11.015.

Chopra, A. K., 2012. Dynamics of Structures Theory and Applications to Earthquake Engineering. 4 edition. Prentice-Hall, Berkley, California, 980 p.

Choudhary, A., Goyal, D., Shimi, S. L., Akula, A., 2018. Condition Monitoring and Fault Diagnosis of Induction Motors: A Review. Archives of Computational Methods in Engineering 20, 4: 719–729. doi:10.1007/s11831-018-9286-z.

Chowdhury, M., Ramirez, M., 1992. A Comparison of the Modal Responses for Defective Versus Nondefective Concrete Test Beams. In Proceedings of the 10th International Modal Analysis Conference, 508–515.

Ciavarella, M., Papangelo, A., Bari, P., 2018. On the Connection Between Palmgren-Miner Rule and Crack Propagation Laws. Fatigue & Fracture of Engineering Materials & Structures 41, 7: 1469–1475. doi:10.1111/ffe.12789.

Clough, R. W., Chang, K.-T., Stephen, R. M., Wang, G.-L., Ghanaat, Y., 1984. Dynamic Response Behavior of Xiang Hong Dian Dam. Technical report, Earthquake Engineering Research Center University of California.

Colombo, M., Domaneschi, M., Ghisi, A., 2016. Existing Concrete Dams: Loads Definition and Finite Element Models Validation. Structural Monitoring and Maintenance 3, 2: 129–144. doi:10.12989/smm.2016.3.2.129.

Courtney, T. H., 2005. Mechanical Behaviour of Materials. 2 edition. Waveland press, Inc., Long Grove, Illinois, 733 p.

Cristalli, C., Paone, N., Rodríguez, R. M., 2006. Mechanical Fault Detection of Electric Motors by Laser Vibrometer and Accelerometer Measurements. Mechanical Systems and Signal Processing 20, 6: 1350–1361. doi:10.1016/j.ymssp.2005.11.013.

Dainty, J. C., 1975. Laser Speckle and Related Phenomena, volume 9. 286 p.

Daniell, W. E., Taylor, C. A., 1999. Effective Ambient Vibration Testing for Validating Numerical Models of Concrete Dams. Earthquake Engineering and Structural Dynamics 28, 11: 1327–1344. doi:10.1002/(SICI)1096-9845(199911)28:11<1327::AID-EQE869>3.0.CO;2-V.

Darbre, G. R., Proulx, J., 2002. Continuous Ambient-Vibration Monitoring of the Arch Dam of Mauvoisin. Earthquake Engineering Structural Dynamics 31, 2: 475–480. doi:10.1002/eqe.118.

Das, S., Saha, P., Patro, S. K., 2016. Vibration-Based Damage Detection Techniques Used for Health Monitoring of Structures: A Review. Journal of Civil Structural Health Monitoring 6, 3: 477–507. doi:10.1007/s13349-016-0168-5.

De Roeck, G., Peeters, B., Maeck, J., 2000. Dynamic Monitoring of Civil Engineering Structures. In Papadrakakis, M., Samartin, A., Onate, E., Eds., Computational Methods for Shell and Spatial Structures IASS-IACM 2000, 79–85. Athens, Greece. doi:10.1109/EXPAT.2015.7463219.

De Sortis, A., Paoliani, P., 2007. Statistical Analysis and Structural Identification in Concrete Dam Monitoring. Engineering Structures 29, 1: 110–120. doi:10.1016/j.engstruct.2006.04.022.

De Sousa, H. F. M., 2012. Data-Based Engineering Techniques for the Management of Concrete Bridges. Phd thesis, University of Porto.

Deinum, P. J., Dungar, R., Ellis, B. R., Jeary, A. P., Reed, G. A. L., Severn, R. T., 1982. Vibration Tests on Emosson Arch Dam, Switzerland. Earthquake Engineering & Structural Dynamics 10, 3: 447–470. doi:10.1002/eqe.4290100308.

Derucher, K. N., 1978. Application of the Scanning Electron Microscope to Fracture Studies of Concrete. Building and Environment 13, 2: 135–141. doi:10.1016/0360-1323(78)90031-8.

Deschênes, C., Fraser, R., Fau, J.-P., 2002. New Trends in Turbine Modelling and New Ways of Partnership. In Proceedings of International Conference on Hydraulic Efficiency Measurement-IGHEM, 1–12. Toronto, Ontario, Canada.

Destrebeco, J.-F., 2004. Cyclic and Dynamic Loading Fatigue of Structural Concrete. In Torrenti, J.-M., Pijaudier-Cabot, G., Reynouard, J.-M., Eds., Mechanical Behavior of Concrete, 151–181. John Wiley & Sons.

DEWESoft, 2019. DEWESoft Measurement Innovation User Manual. DEWESoft.

DIANA FEA, 2017. User's Manual - Release 10.2. Diana FEA BV, Delft, Netherlands. URL https://dianafea.com/manuals/d102/Diana.html.

Doebling, S., Farrar, C., Prime, M., 1998. A Summary Review of Vibration-Based Damage Identification Methods. The Shock and Vibration Digest 30: 91–105.

Doebling, S. W., Farrar, C. R., Prime, M. B., Shevitz, D. W., 1996. Damage Identification and Health Monitoring of Structural and Mechanical Systems From Changes in their Vibration Characteristics: A Literature Review. The Shock and Vibration Digest doi:10.2172/249299.

Donges, A., Noll, R., 2015. Laser Measurement Technology: Fundamentals and Applications (Springer Series in Optical Sciences). 427 p. doi:10.1007/978-3-642-01237-2.

Dorji, U., Ghomashchi, R., 2014. Hydro Turbine Failure Mechanisms: An Overview. Engineering Failure Analysis 44: 136–147. doi:10.1016/j.engfailanal.2014.04.013.

Dytran, 2019. Dytran Accelerometer 3097A2 Data Sheet. Technical report.

Farfan, J., Breyer, C., 2017. Ageing of European Power Plant Infrastructure as an Opportunity to Evolve Towards Sustainability. International Journal of Hydrogen Energy 42, 28: 18081–18091. doi:10.1016/j.ijhydene.2016.12.138.

Farrar, C. R., Lieven, N. A. J., 2006. Damage Prognosis: The Future of Structural Health Monitoring. Philosophical Transactions of the Royal Society a Mathematical, Physical and Engineering Sciences 365: 623–632. doi:10.1098/rsta.2006.1927.

Fassois, S. D., Sakellariou, J. S., 2007. Time-Series Methods for Fault Detection and Identification in Vibrating Structures. Philosophical Transactions of the Royal Society A 365: 411–448. doi:10.1098/rsta.2006.1929.

Fenves, G., Chopra, A. K., 1986. Simplified Analysis for Earthquake Resistant Design of Concrete Gravity Dams. Technical report, Earthquake Engineering Research Center University of California, Berkeley, Berkeley, California.

Friswell, M. I., Penny, J. E. T., 1997. Is Damage Location Using Vibration Measurements Practical? In EUROMECH365 international workshop: damas 97, Structural Damage Assessment using Advanced Signal Processing Procedures, June/July, 1–6. Sheffield, UK.

Fritzen, C.-P., 2006. Vibration-Based Techniques for Structural Health Monitoring. In Balageas, D., Fritzen, C.-P., Guemes, A., Eds., Structural Health Monitoring, 45–208. ISTE Ltd, Chippenham, Wiltshire.

Fu, T., Deng, Z. D., Duncan, J. P., Zhou, D., Carlson, T. J., Johnson, G. E., Hou, H., 2016. Assessing Hydraulic Conditions Through Francis Turbines Using an Autonomous Sensor Device. Renewable Energy 99: 1244–1252. doi:10.1016/j.renene.2016.08.029.

Gaftoi, D., Abdulamit, A., Stematiu, D., 2016. Assessment of Gura Raului Dam Safety Using Measurements of Structural Response to Ambient Vibrations. Procedia Engineering 161: 722–728. doi:10.1016/j.proeng.2016.08.751.

Gamse, S., Zhou, W.-H., Tan, F., Yuen, K.-V., Oberguggenberger, M., 2018. Hydrostatic-Season-Time Model Updating Using Bayesian Model Class Selection. Reliability Engineering and System Safety 169: 40–50. doi:10.1016/j.ress.2017.07.018.

Gardner-Morse, M. G., Huston, D. R., 1993. Modal Identification of Cable-Stayed Pedestrian Bridges. ASCE Journal of Structural Engineering 119, 11: 3384–3404. doi:10.1061/(ASCE)0733-9445(1993)119:11(3384).

Gasch, T., Nässelqvist, M., Hansson, H., Malm, R., Gustavsson, R., Hassanzadeh, M., 2013. Cracking in the Concrete Foundation for Hydropower Generators Part II Elforsk Rapport 13:64. Technical report, ELFORSK, Stockholm, Sweden.

GeoEngineer, 2019. Texas Lake Dunlap Dam Collapse. URL https://www.geoengineer.org/news/texas-lake-dunlap-dam-collapse. Accessed: 1. 6. 2019.

Gillich, G.-R., Praisach, Z.-I., 2014. Modal Identification and Damage Detection in Beam-Like Structures Using the Power Spectrum and Time – Frequency Analysis. Signal Processing 96: 29–44. doi:10.1016/j.sigpro.2013.04.027.

Gladiné, K., Muyshondt, P. G. G., Dirckx, J. J. J., 2017. Human Middle-Ear Nonlinearity Measurements Using Laser Doppler Vibrometry. Optics and Lasers in Engineering 99: 98–102. doi:10.1016/j.optlaseng.2017.03.001.

Goyal, R., Gandhi, B. K., 2018. Review of Hydrodynamics Instabilities in Francis Turbine During Off-Design and Transient Operations. Renewable Energy 116, Part A: 697–709. doi:10.1016/j.renene.2017.10.012.

Halkon, B. J., Rothberg, S. J., 2017a. Restoring High Accuracy to Laser Doppler Vibrometry Measurements Affected by Vibration of Beam Steering Optics. Journal of Sound and Vibration 405: 144–157. doi:10.1016/j.jsv.2017.05.014.

Halkon, B. J., Rothberg, S. J., 2017b. Taking Laser Doppler Vibrometry Off the Tripod: Correction of Measurements Affected by Instrument Vibration. Optics and Lasers in Engineering 91: 16–23. doi:10.1016/j.optlaseng.2016.11.006.

Halkon, B. J., Rothberg, S. J., 2018. Towards Laser Doppler Vibrometry From Unmanned Aerial Vehicles. Journal of Physics: Conference Series 1149. doi:10.1088/1742-6596/1149/1/012022.

Halliwell, N., 1996. The Laser Torsional Vibrometer: A Step Forward in Rotating Machinery Diagnostics. Journal of Sound and Vibration 190, 3: 399–418. doi:10.1006/jsvi.1996.0071.

Hansteen, O. E., Bell, K., 1979. On the Accuracy of Mode Superposition Analysis in Structural Dynamics. Earthquake Engineering & Structural Dynamics 7, 5: 405–411. doi:10.1002/eqe.4290070502.

Harris, D. W., 2002. Investigation of the Failure Modes of Concrete Dams - Physical Model Tests Report No. DSO-02-02. Technical report, US Bureau of Reclamation, Springfield, Virginia.

Harris, D. W., Travers, F., 2006. Investigation of the Failure Modes of Concrete Dams - Physical Model Tests Report DSO-06-03. Technical report, US Bureau of Reclamation, Denver, Colorado.

Hattingh, L., Moyo, P., Mutede, M., Shaanika, S., le Roux, B., Muir, C., 2019. The Use of Ambient Vibration Monitoring in the Behavioral Assessment of an Arch Dam With Gravity Flanks and Limited Surveillance Records. In Tournier, J.-P., Bennett, T., Bibeau, J., Eds., ICOLD 2019 Sustainable and Safe Dams Around the World, 2819–2831. CRC Press, Ottawa, Canada.

Hillgren, N., 2011. Analysis of Hydraulic Pressure Transients in the Waterways of Hydropower Stations. Doctoral Thesis, University of Uppsala.

Hočevar, M., 2015. Hidroenergetski sistemi učbenik za predmet Hidroenergetski sistemi. Univerza v Ljubljani Fakulteta za strojništvo Laboratorij za vodne in turbinske stroje, Ljubljana, 138 p. (In Slovenian language).

Hong, Y. U., Zhongru, W. U., Tengfei, B. A. O., Lan, Z., 2010. Multivariate Analysis in Dam Monitoring Data With PCA. Science China Technological Sciences 53, 4: 1088–1097. doi:10.1007/s11431-010-0060-1.

Hsieh, K. H., Halling, M. W., Barr, P. J., 2006. Overview of Vibrational Structural Health Monitoring with Representative Case Studies. Journal of Bridge Engineering II, 6: 707–715. doi:10.1061/(asce)1084-0702(2006)11:6(707).

Humar, J., Bagchi, A., Xu, H., 2006. Performance of Vibration-Based Techniques for the Identification of Structural Damage. Structural Health Monitoring 5, 3: 215–241. doi:10.1177/1475921706067738.

IBE, 2016. Projektna dokumentacija HE Brežice (Interno gradivo HESS). Technical report, Ljubljana. (In Slovenian language).

ICOLD Committee on Dam Ageing, 1994. Bulletin 93: Ageing of Dams and Appurtenant Works Review and Recomendations. ICOLD - CIGB, Paris.

ICOLD Committee on Monitoiring of Dams and Their Foundations, 1988. Bulletin 60: Dam Monitoring - General Considerations. ICOLD - CIGB, Paris, 74 p.

ICOLD Committee on Monitoring of Dams and their Foundations, 1989. Bulletin 68: Monitoring of Dams and Their Foundations State-of-the-Art. ICOLD - CIGB, Paris.

ICOLD Technical Committee on Dam Surveillance, 2009. Bulletin 138: Surveillance: Basic Elements in a Dam Safety Process. ICOLD - CIGB, Paris.

ICOLD Technical Committee on Dam Surveillance, 2018. Bulletin preprint 180: Dam surveillance Lessons learnt from Case Histories. ICOLD - CIGB, Paris.

ICOLD Technical Committee on Dams for Hydroelectric Energy, 2019. Dams for Hydroelectric Energy (PREPRINT). ICOLD - CIGB, Paris.

INFRA, 2012. Program izvedbe objektov vodne, državne in lokalne infrastrukture ter objektov Vodne in energetske infrastrukture v nedeljivem razmerju za izgradnjo Novelacija št. 1 HE Brežice. Technical report, Brežice. (In Slovenian language).

Japan Society of Civil Engineers, 2007. Standard Specifications for Concrete Structures Dam Concrete. Japan Society of Civil Engineers (JSCE).

Jardine, A. K. S., Lin, D., Banjevic, D., 2006. A Review on Machinery Diagnostics and Prognostics Implementing Condition-Based Maintenance. Mechanical Systems and Signal Processing 20, 7: 1483–1510. doi:10.1016/j.ymssp.2005.09.012.

Jennings, P. C., Kuriowa, J. H., 1968. Vibration and Soil-Structure Interactions Tests of a Nine-Story Reinforced Concrete Building. Bulletin of the Seismological Society of America 58, 3: 891–916.

Jennings, P. C., Matthiesen, R. B., Hoerner, J. B., 1971. Forced Vibration of a 22-Story Steel Frame Building. Technical report, California Institute of Technology, Pasadena, California.

Juneja, V., Haftka, R., Cudney, H., 1997. Damage Detection and Damage Detectability Analysis and Experiments. ASCE Journal of Aerospace Engineering 10, 4: 135–142. doi:10.1061/(ASCE)0893-1321(1997)10:4(135).

Karbhari, V., 2005. Health Monitoring, Damage Prognosis and Service-Life Prediction – Issues Related to Implementation. In Ansari, F., Ed., Sensing Issues in Civil Structural Health Monitoring, 301–310. Springer.

Karbhari, V. M., Ansari, F., Eds., 2009. Structural Health Monitoring of Civil Infrastructure Systems. CRC Press. doi:10.1533/9781845696825.

Kashangaki, T. A., Weaver S., S., Lim, T. W., 1992. Underlying Modal Data Issues for Detecting Damage in Truss Structures. In 33rd Structures, Structural Dynamics and Materials Conference. National Aeronautics and Space Administration, Langley Research Center. doi:10.2514/6.1992-2264.

Kashangaki, T. A.-L., 1991. On-Orbit Damage Detection and Health Monitoring of Large Space Trusses – Status and Critical Issues. Technical report, NASA National Aeronautics and Space Administration, Hampton, Virginia.

Kato, M., Shimada, S., 1986. Vibration of PC Bridge During Failure Process. ASCE Journal of Structural Engineering 112, 7: 1692–1703.

Keerthana, K., Kishen, J. M. C., 2018. An Experimental and Analytical Study on Fatigue Damage in Concrete Under Variable Amplitude Loading. International Journal of Fatigue 111: 278–288. doi:10.1016/j.ijfatigue.2018.02.014.

Klun, M., Kryžanowski, A., Schnabl, S., 2016. Uporaba metode odzivnih ploskev pri analizi hidrotehničnih objektov Application of Response Surface Method in Analysis of Hydraulic Structures. Acta Hydrotechnica 29, 51: 103–123.

Kong, X., Cai, C.-s., Hu, J., 2017. The State-of-the-Art on Framework of Vibration-Based Structural Damage Identification for Decision Making. MDPI Applied Sciences 7, 5. doi:10.3390/app7050497.

Kougias, I., Aggidis, G., Avellan, F., Deniz, S., Lundin, U., Moro, A., Muntean, S., Novara, D., Pérez-Díaz, J. I., Quaranta, E., Schild, P., Theodossiou, N., 2019. Analysis of Emerging Technologies in the Hydropower Sector. Renewable and Sustainable Energy Reviews 113: 109257. doi:10.1016/j.rser.2019.109257.

Kryžanowski, A., Humar, N., 2011. Dam Safety Practice in Slovenia. In Proceedings: Hydrovision International 2011, 1–10. Sacramento, USA.

Kryžanowski, A., Humar, N., 2014. Kako lahko z minimalnimi organizacijskimi ukrepi izboljšamo varnost pregrad v Sloveniji. In Zbornik referatov posvetovanja 25. Mišičev vodarski dan, 172–179. Maribor. (In Slovenian language).

Kyžanowski, A., Humar, N., 2018. Dam Construction in Slovenia. In Mitovski, S., Ed., Proceedings Tribune on topic: 80 Years of Dam Engineering in Republic of Macedonia, 15–25. Macedonian Committee on Large Dams, Skopje, Republic of Macedonia.

Lamond, J. F., Pielert, J. H., Eds., 2006. Significance of Tests and Properties of Concrete and Concrete-Making. ASTM International, Bridgeport, NJ, 664 p.

Lantsoght, E. O. L., Van Der Veen, C., De Boer, A., 2016. Proposal for the Fatigue Strength of Concrete Under Cycles of Compression. Construction and Building Materials 107: 138–156. doi:10.1016/j.conbuildmat.2016.01.007.

Léger, P., Leclerc, M., 2007. Hydrostatic, Temperature, Time-Displacement Model for Concrete Dams. Journal of Engineering Mechanics 133, 3: 267–277. doi:10.1061/(ASCE) 0733-9399(2007)133:3(267).

Li, G.-Q., Hao, K.-C., Lu, Y., Chen, S.-W., 1999. A Fexibility Approach for Damage Identification of Cantilever-Type Structures With Bending and Shear Deformation. Computers and Structures 73, 6: 576–572. doi:10.1016/S0045-7949(98)00295-8.

Liang, J., Ding, Z., Li, J., 2017. A Probabilistic Analyzed Method for Concrete Fatigue Life. Probabilistic Engineering Mechanics 49: 13–21. doi:10.1016/j.probengmech.2017.08.002.

Lima, H. F., Vicente, S., Nogueira, R. N., Abe, I., Sérgio, P., André, D. B., Fernandes, C., Rodrigues, H., Varum, H., Kalinowski, H. J., Costa, A., Pinto, J. D. L., 2008. Structural Health Monitoring of the Church of Santa Casa da Misericórdia of Aveiro Using FBG Sensors. IEEE Sensors Journal 8, 7: 1236–1242.

Loh, C.-H., Wu, T.-S., 1996. Identification of Fei-Tsui Arch Dam From Both Ambient and Seismic Response Data. Soil Dynamics and Earthquake Engineering 15, 7: 465–483. doi: 10.1016/0267-7261(96)00016-4.

Lopez, F., Restrepo Velez, L., 2003. Assessment and Structural Rehabilitation With Post-Tensioning and CFRP of a Mass Concrete Structure Subjected to Dynamic Loading. In FIB Symposium Concrete Structures in Seismic Regions. Athens, Greece.

Malm, R., Hassanzadeh, M., Gasch, T., Eriksson, D., Nordstrom, E., 2012. Cracking in the Concrete Foundation for Hydropower Generators Analyses of Non-Linear Drying Diffusion, Thermal Effects and Mechanical Loads Elforsk Rapport 13:63. Technical report, Elforsk, Stockholm.

Martin, P., Rothberg, S., 2008a. Laser Vibrometry and the Secret Life of Speckle Patterns. In Eighth International Conference on Vibration Measurements by Laser Techniques: Advances and Applications. Ancona, Italy. doi:10.1117/12.803156.

Martin, P., Rothberg, S., 2008b. Laser Vibrometry and the Secret Life of Speckle Patterns. In Eighth International Conference on Vibration Measurements by Laser Techniques: Advances and Applications. Ancona, Italy. doi:10.1117/12.803156.

Martin, P., Rothberg, S., 2009. Introducing speckle noise maps for Laser Vibrometry. Optics and Lasers in Engineering 47, 3-4: 431–442. doi:10.1016/j.optlaseng.2008.06.010.

Martin, P., Rothberg, S. J., 2011. Pseudo-Vibration Sensitivities for Commercial Laser Vibrometers. Mechanical Systems and Signal Processing 25, 7: 2753–2765. doi:10.1016/j.ymssp.2011.02.009.

Mata, J., De Castro, A. T., Da Costa, J. S., 2013. Time-Frequency Analysis for Concrete Dam Safety Control: Correlation Between the Daily Variation of Structural Response and Air Temperature. Engineering Structures 48: 658–665. doi:10.1016/j.engstruct.2012.12.013.

Mata, J., Leitão, N. S., Castro, A. T., Sá, J., 2014. Construction of Decision Rules for Early Detection of a Developing Concrete Arch Dam Failure Scenario. A Discriminant Approach. Computers and Structures 142: 45–53. doi:10.1016/j.compstruc.2014.07.002.

Mazurek, D. F., Dewolf, J. T., 1991. Experimental Study of Bridge Monitoring Technique. ASCE Journal of Structural Engineering 116, 9: 2532–2549. doi:10.1061/(ASCE)0733-9445(1990)116:9(2532).

Mendes, P., 2006. Development of a Cabril Dam Finite Element Model for Dynamic Analysis Using Ambient Vibration Tests. In Mota Soares, C., Martins, J., Rodrigues, H., Ambrosio, J., Pina, C., Pereira, E., Folgado, J., Eds., III European Conference on Computational Mechanics Solids, Structures and Coupled Problems in Engineering, 788. Springer Netherlands, Lisbon, Portugal. doi:10.1007/1-4020-5370-3.

Mendes, P., Oliveira, S., 2009. Influence of the Intake Tower Dynamic Behaviour on Modal Identification of Cabril Dam. In 3rd International Operational Modal Analysis Conference (IOMAC 2009), 803. Portonovo, Italy.

Mendes, P., Oliveira, S., Guerreiro, L., Baptista, M. A., Costa, A. C., 2004. Dynamic Behaviour of Concrete Dams Monitoring and Modeling. In 13th World Conference on Earthquake Engineering: Conference Proceedings, 1–9. WCEE Secretariat, Vancouver, Canada.

Mesquita, E., Antunes, P., Coelho, F., André, P., Arêde, A., Varum, H., 2016. Global Overview on Advances in Structural Health Monitoring Platforms. Journal of Civil Structural Health Monitoring 6, 3: 461–475. doi:10.1007/s13349-016-0184-5.

Mihashi, H., Leite, J. P. D. B., 2004. State-of-the-Art Report on Control of Cracking in Early Age Concrete . Journal of Advanced Concrete Technology 2, 2: 141–154. doi:10.3151/jact.2.141.

Mikec, S., 2018. Prehodnost vodnih turbin tipa Kaplan za dolvodne ribje migracije - Passibility of Kaplan Turbine for Downstream Fish Passage. (In Slovenian language).

Mikro Medica, 2018. Seizmično opazovanje pregrade letno poročilo 2017, Pregrada HE Brežice (Interno gradivo družbe HESS). Technical report, Puconci. (In Slovenian language).

Mohanta, R. K., Chelliah, T. R., Allamsetty, S., Akula, A., Ghosh, R., 2017. Sources of Vibration and Their Treatment in Hydro Power Stations – A Review. Engineering Science and Technology, an International Journal 20, 2: 637–648. doi:10.1016/j.jestch.2016.11.004.

Mottershead, J., Friswell, M., 1993. Model Updating In Structural Dynamics: A Survey. Journal of Sound and Vibration 167, 2: 347–375. doi:10.1006/jsvi.1993.1340.

Moyo, P., Oosthuizen, C., 2009. Dynamic Testing of a Concrete Arch Dam. In IOMAC 2009 -3rd International Operational Modal Analysis Conference, 95–100. Portonovo.

Mufti, A., 2011. Editorial to the First Issue. Journal of Civil Structural Health Monitoring 1, 1: 1. doi:10.1007/s13349-011-0007-7.

Nässelqvist, M., Gustavsson, R., Aidanpää, J., 2012. Bearing Load Measurement in a Hydropower Unit Using Strain Gauges Installed Inside Pivot Pin. Experimental Mechanics 52, 4: 361–369. doi:10.1007/s11340-011-9495-y.

Nie, Z., Hao, H., Ma, H., 2012. Using Vibration Phase Space Topology Changes for Structural Damage Detection. Structural Health Monitoring 11, 5: 538–557. doi:10.1177/1475921712447590.

Niezrecki, C., Avitabile, P., Chen, J., Sherwood, J., Lundstrom, T., Leblanc, B., Hughes, S., Desmond, M., Beattie, A., Rumsey, M., Klute, S. M., Pedrazzani, R., Werlink, R., Newman, J., 2014. Inspection and Monitoring of Wind Turbine Blade-Embedded Wave Defects During Fatigue Testing. Structural Health Monitoring 13, 6: 629–643. doi:10.1177/1475921714532995.

Niwa, A., Clough, R. W., 1980. Shaking Table Research on Concrete Dam Models. Technical report, University of California, Earthquake Engineering Research Center, Berkeley, California.

Norman, C. D., Stone, H. E., 1981. Comparison of Vibration Test Results for a Model and Prototype Gravity Dam. Technical report, U. S. Army Engineer Waterways Experiment Station Structures Laboratory, Vicksburg, Mississipi.

Official Gazette of the Republic of Slovenia 29/2016, 2016. Sistemska obratovalna navodila za prenosni sistem električne energije Republike Slovenije (In Slovenian language).

Official Gazette of the Republic of Slovenia 58/16, 2016. Pravilnik o opazovanju seizmičnosti na območju velike pregrade. (In Slovenian language).

Official Gazette of the Republic of Slovenia 87/2011, 2011. Conditions of the Concession for Exploitation of the Energy Potential of the Lower Sava River Act (ZPKEPS-1).

Oliveira, S., Alegre, A., 2019. Seismic and Structural Health Monitoring of Dams in Portugal. In Limongelli, M. P., Çelebi, M., Eds., Seismic Structural Health Monitoring, 2002, 87–113. Springer. doi:10.1007/978-3-030-13976-6_4.

Oliveira, S., Rodrigues, J., Mendes, P., Costa, A., 2004. Damage Characterization in Concrete Dams Using Output-Only Modal Analysis. In Proceedings of IMAC XXII. Detroit.

Ortiz, M., 1985. A Constitutive Theory for the Inelastic Behavior of Concrete. Mechanics of Materials 4, 1: 67–93. doi:10.1016/0167-6636(85)90007-9.

Paine, T., 2002. Shaking Table Study to Investigate Failure Modes of Arch Dams Report No. DSO-02-01. Technical report, US Bureau of Reclamation, Springfield, Virginia.

Pandey, A. K., Biswas, M., Samman, M. M., 1991. Damage Detection From Changes in Curvature Mode Shapes. Journal of Sound and Vibration 145, 2: 321–332. doi: 10.1016/0022-460x(91)90595-b.

Pappa, S., James, H., Zimmerman, C., 1997. Autonomous Space Shuttle Modal Identification of the Tail Rudder. Technical report, National Aeronautics and Space Administration Langley Research Center, Hampton, Virginia.

Paris, P., Erdogan, F., 1963. A Critical Analysis of Crack Propagation Laws. Journal of Basic Engineering 85, 4: 528–533. doi:10.1115/1.3656900.

Partner Brežice, 2017. Tehnično in okoljsko opazovanje HE Brežice med polnenjem akumulacisjkega bazena - Poročilo pred tehničnim pregledom (Interno gradivo družbe HESS). Technical report, HESS d.o.o., Brežice. (In Slovenian language).

Peeters, B., Maeck, J., De Roeck, G., 2001. Vibration-Based Damage Detection in Civil Engineering: Excitation Sources and Temperature Effects. Smart Materials and Structures 10, 3: 518–527. doi:10.1088/0964-1726/10/3/314.

Plizzari, G., Waggoner, F., Saouma, V. E., 1995. Centrifuge Modeling and Analysis of Concrete Gravity Dams. Journal of Structural Engineering 121, 10: 1471–1479. doi:10.1061/(ASCE) 0733-9445(1995)121:10(1471).

Plizzari, G. A., Cangiano, S., Alleruzzo, S., 1997. The Fatigue Behaviour of Cracked Concrete. Fatigue & Fracture of Engineering Materials & Structures 20, 8: 1195–1206. doi:10.1111/j. 1460-2695.1997.tb00323.x.

Polytec, 2016. PDV-100 Portable Digital Vibrometer Truly Portable Laser Vibration Measurement Datasheet. Technical report, Polytec.

Presas, A., Luo, Y., Wang, Z., Guo, B., 2019. Fatigue Life Estimation of Francis Turbines Based on Experimental Strain Measurements: Review of the Actual Data and Future Trends. Renewable and Sustainable Energy Reviews 102, July 2018: 96–110. doi:10.1016/j.rser.2018.12.001.

Proulx, J., Paultre, P., Rheault, J., Robert, Y., 2001. An Experimental Investigation of Water Level Effects on the Dynamic Behaviour of a Large Arch Dam. Earthquake Engineering Structural Dynamics 30, 8: 1147–1166. doi:10.1002/eqe.055.

Pytharouli, S. I., Stiros, S. C., 2005. Ladon Dam Greece Deformation and Reservoir Level Fluctuations: Evidence for a Causative Relationship From the Spectral Analysis of a Geodetic Monitoring Record. Engineering Structures 27, 3: 361–370. doi:10.1016/j.engstruct.2004.10.012.

Raghavendrachar, M., Aktan, A. E., 1992. Flexibility by Multireference Impact Testing for Bridge Diagnostics. ASCE Journal of Structural Engineering 118, 8: 2186–2203. doi:10.1061/(ASCE)0733-9445(1992)118:8(2186).

Rak, G., Müller, M., Šantl, S., Steinman, F., 2012. Use of Hybrid Hidraulic Models in the Process of Hydropower Plants Design on the Lower Sava. Acta Hydrotechnica 25, 42: 59–70.

Ray, S., Kishen, J. M. C., 2010. Fatigue Crack Propagation Model for Plain Concrete – an Analogy With Population Growth. Engineering Fracture Mechanics 77, 17: 3418–3433. doi:10.1016/j.engfracmech.2010.09.008.

Ray, S., Kishen, J. M. C., 2011. Fatigue Crack Propagation Model and Size Effect in Concrete Using Dimensional Analysis. Mechanics of Materials 43, 2: 75–86. doi:10.1016/j.mechmat.2010.12.002.

Rea, D., Liaw, C. Y., Chopra, A. K., 1972. Dynamic Properties of Pine Flat Dam. Technical report, University of California, Berkeley, California.

Rothberg, S., 2006. Numerical Simulation of Speckle Noise in Laser Vibrometry. Applied Optics 45, 19: 4523–4533. doi:10.1364/AO.45.004523.

Rothberg, S., Baker, J., Halliwell, N., 1989. Laser Vibrometry: Psuedo-Vibrations. Journal of Sound and Vibration 135, 3: 516–522. doi:10.1016/0022-460X(89)90705-0.

Rothberg, S. J., Allen, M. S., Castellini, P., Di Maio, D., Dirckx, J. J., Ewins, D. J., Halkon, B. J., Muyshondt, P., Paone, N., Ryan, T., Steger, H., Tomasini, E. P., Vanlanduit, S., Vignola, J. F., 2017. An International Review of Laser Doppler Vibrometry: Making Light Work of Vibration Measurement. Optics and Lasers in Engineering 99: 11–22. doi:10.1016/j.optlaseng.2016.10.023.

Rücker, W., Hille, F., Rohrmann, R., 2006. SAMCO Final Report 2006 Guideline for Structural Health Monitoring. Technical report, Federal Institute of Materials Research and Testing (BAM), Berlin, Germany. URL http://www.samco.org.

Rytter, A., 1993. Vibrational Based Inspection of Civil Engineering Structures. Fracture and dynamics, no. 44, vol. r9314 general, Aalborg University.

Saed Mirza, M., Ferdiani, O., Hadi-Arab, A., Joucdar, K., Khaled, A., RazaQpur, A. G., 1990. An Experimental Study of Static and Dynamic Responses of Prestressed Concrete Box – Girder Bridges. Canadian Journal of Civil Engineering 17, 3: 481–493. doi:10.1139/l90-052.

Safiuddin, M., Kaish, A. B. M. A., Woon, C. O., Raman, S. N., 2018. Early-Age Cracking in Concrete: Causes, Consequences, Remedialmeasures, and Recommendations. Applied Sciences 8, 10: 1730. doi:10.3390/app8101730.

Saitoh, M., Takei, B. T., 1996. Damage Estimation and Identification of Strucutral Faults Using Modal Parameters. In Proceedings of the 14th International Modal Analysis Conference, 1159–1164.

Salane, H. J., Baldwin Jr., J. W., Duffield, R. C., 1981. Dynamics Approach for Monitoring Bridge Deterioration. In 60th Annual Meeting of the Transportation Research Board, 21–28. Transportation Research Board, Washington District of Columbia, United States.

Salawu, O. S., 1997. Detection of Structural Damage Through Changes in Frequency: A Review. Engineering Structures 19, 9: 718–723. doi:10.1016/S0141-0296(96)00149-6.

Salazar, F., Morán, R., Toledo, M., Oñate, E., 2017. Data-Based Models for the Prediction of Dam Behaviour: A Review and Some Methodological Considerations. Archives of Computational Methods in Engineering 24, 1: 1–21. doi:10.1007/s11831-015-9157-9.

Severn, R. T., Jeary, A. P., Ellis, B. R., 1980. Forced Vibration Tests and Theoretical Studies on Dams. Proceedings of the Institution of Civil Engineers 69, 3: 605–634. doi:10.1680/iicep.1980.2367.

Sha, S., Zhang, G., 2017. Modeling of Hydraulic Fracture of Concrete Gravity Dams by Stress-Seepage-Damage Coupling Model. Mathematical Problems in Engineering 15. doi:doi.org/10.1155/2017/8523213.

Shah, S. P., Chandra, S., 1970. Fracture of Concrete Subjected to Cyclic and Sustained Loading. ACI Materials Journal 67, 10: 816–827.

Shirole, A. M., Holt, R. C., 1991. Planning for a Comprehensive Bridge Safety Assurance Program. In Third Bridge Engineering Conference: Papers Presented at the Third Bridge Engineering Conference. Transportation Research Board, Denver, Colorado.

Slastan, J., Pietrzko, S., 1993. Changes of RC Beam Modal Parameters Due to Cracks. In Proceedings of the 11th International Modal Analysis Conference (IMAC), 70–76. Kissimmee, Florida.

SLOCOLD, 2018. List of Large Dams in Slovenia. Website: http://www.slocold.si/e{_}pregrade{_}seznam.htm. Accessed: 6. 1. 2018.

Slovenian Environment Agency (ARSO), 2018. Seismic Network of the Republic of Slovenia. International Federation of Digital Seismograph Networks. Dataset/Seismic Network. doi: 10.7914/SN/SL.

Smoak, G. W., 1996. Guide to Concrete Repair. US Bureau of the Interior, Denver, Colorado, 168 p.

Sodnik, J., Kogovšek, B., Mikoš, M., 2014. Vodna infrastruktura v Sloveniji: Ali vemo kaj moramo vzdrževati? In Mišičev vodarski dan 2014, 24–31. (In Slovenian language).

Sohn, H., Farrar, C. R., Hemez, F. M., Shunk, D. D., Stinemates, D. W., Nadler, B. R., Czarnecki, J. J., 2004. A Review of Structural Health Monitoring Literature: 1996–2001, Los Alamos National Laboratory Report, LA-13976-MS, 2004. Massachusetts Institute of Technology, Los Alamos National Laboratory. doi:LA-13976-MS.

Sriravindrarajah, R., Swamy, R. N., 1989. Load Effects on Fracture of Concrete. Materials and Structures 22, 1: 15–22. doi:10.1007/BF02472690.

Stevanovic, N., Corbetta, M., Dervilis, N., Worden, K., 2017. On the Structural Health Monitoring of Operational Wind Turbine Blades. In Proceedings of the 11th International Workshop on Structural Health Monitoring. Stanford. doi:10.12783/shm2017/14151.

Strean, R., Mitchell, L., Barker, A., 1998. Global Noise Characteristics of a Laser Doppler Vibrometer 1. Theory. Optics and Lasers in Engineering 30, 2: 127–139. doi:10.1016/S0143-8166(98)00014-1.

Su, H., Hu, J., Wen, Z., 2013. Service Life Predicting of Dam Systems with Correlated Failure Modes. Journal of Performance of Constructed Facilities 27, 3: 252–269. doi:10.1061/(ASCE)CF.1943-5509.0000308.

Tang, J., Soua, S., Mares, C., Gan, T.-h., 2016. An Experimental Study of Acoustic Emission Methodology for in Service Condition Monitoring of Wind Turbine Blades. Renewable Energy 99: 170–179. doi:10.1016/j.renene.2016.06.048.

Tekie, P. B., Ellingwood, B. R., 2003. Seismic Fragility Assessment of Concrete Gravity Dams. Earthquake Engineering & Structural Dynamics 32, 14: 2221–2240. doi:10.1002/eqe.325.

Tervo, R. J., 2014. Practical Signals Theory With MATLAB Applications. Wiley, Hoboken, (NJ), 451 p.

The MathWorks, 2018. MATLAB Release 2018a. Natick, Massachusetts, USA.

Thun, H., Ohlson, U., Eklfgren, L., 2007. Tensile Fatigue Capacity of Concrete. Nordic Concrete Research 36, 1-2: 48–64.

Tian, K., Zhang, T., Ai, Y., Zhang, W., 2018. Induction Motors Dynamic Eccentricity Fault Diagnosis Based on the Combined Use of WPD and EMD-Simulation Study. Applied Sciences 8, 10: 1709. doi:10.3390/app8101709.

Trifunac, M. D., 1970. Wind and Microtremor Induced Vibrations of a Twenty-Two Story Steel Frame Building. Technical report, California Institute of Technology, Pasadena, California.

Trifunac, M. D., 1972. Comparisons Between Ambient and Forced Vibration Experiments. Earthquake Engineering and Structural Dynamics 1, 2: 133–150. doi:10.1002/eqe.4290010203.

Trivedi, C., Gandhi, B., Michel, C. J., 2013. Effect of Transients on Francis Turbine Runner Life: A Review. Journal of Hydraulic Research 51, 2: 121–132. doi:10.1080/00221686.2012.732971.

Trivedi, C., Gandhi, B. K., Cervantes, M. J., Dahlhaug, O. G., 2015. Experimental Investigations of a Model Francis Turbine During Shutdown at Synchronous Speed. Renewable Energy 83: 828–836. doi:10.1016/j.renene.2015.05.026.

Turner, J. D., Pretlove, A. J., 1988. A Study of the Spectrum of Traffic-Induced Bridge Vibration. Journal of Sound and Vibration 122, 1: 31–42. doi:https://doi.org/10.1016/S0022-460X(88)80004-X.

Urquiza, G., García, J. C., González, J. G., Castro, L., Rodríguez, J. A., Basurto-pensado, M. A., 2014. Failure Analysis of a Hydraulic Kaplan Turbine Shaft. Engineering Failure Analysis 41: 108–117. doi:10.1016/j.engfailanal.2014.02.009.

USBR, 1988. Concrete Manual A Water Resources Technical Publication. Technical report, USBR, Denver, Colorado.

USBR, 2018. National Inventory of Dams Dataset. Website: http://nid.usace.army.mil/. Accessed: 12. 6. 2018.

Vandiver, J. K., 1977. Detection of Structural Failure on Fixed Platforms By Measurement of Dynamic Response. Journal of Petroleum Technology 29, 3: 305–310. doi:10.2118/5679-PA.

Vanlanduit, S., Dirckx, J., 2017. Editorial Special Issue on Laser Doppler Vibrometry. Optics and Lasers in Engineering 99: 1–2. doi:10.1016/j.optlaseng.2017.09.007.

VODPREG, 2012. Razvojno raziskovalni projekt Zemeljske in betonske vodne pregrade strateškega pomena v RS VODPREG Končno poročilo. Technical report. (In Slovenian language).

Wagner, H.-J., Mathur, J., 2011. Hydraulic Turbines: Types and Operational Aspects, 71–93. Springer Berlin Heidelberg, Berlin, Heidelberg. doi:10.1007/978-3-642-20709-9_5.

Wang, H. L., Song, Y. P., 2011. Fatigue Capacity of Plain Concrete Under Fatigue Loading With Constant Confined Stress. Materials and Structures 44, 1: 253–262. doi:10.1617/s11527-010-9624-6.

Wicke, M., Randl, N., Foraboschi, P., Siviero, E., Schiessl, A., Tewes, R., 1999. Structural Concrete Textbook on Behavior, Design and Performance, volume 1.

Wolff, T., Richardson, M., 1989. Fault Detection in Structures From Changes in Their Modal Parameters. In Proceedings of the 7th International Modal Analysis Conference, 87–94. Las Vegas.

Worden, K., Farrar, C. R., Manson, G., Park, G., 2007. The Fundamental Axioms of Structural Health Monitoring. Proceedings of the Royal Society a Mathematical, Physical and Engineering Sciences 463: 1639–1664. doi:10.1098/rspa.2007.1834.

de Wrachien, D., Mambretti, S., Eds., 2009. Dam-break Problems, Solutions and Case Studies. WIT Press, Southampton, UK, 368 p.

Xia, Y., Hao, H., Zanardo, G., Deeks, A., 2006. Long Term Vibration Monitoring of an RC Slab: Temperature and Humidity Effect. Engineering Structures 28, 3: 441–452. doi:10.1016/j.engstruct.2005.09.001.

Yao, J. T. P., Kozin, F., Wen, Y.-K., Yang, J.-N., Schuëller, G., Ditlevsen, O., 1986. Stochastic Fatigue, Fracture and Damage Analysis. Structural Safety 3, 3-4: 231–267. doi:10.1016/0167-4730(86)90005-6Get.

Ye, X. W., Su, Y. H., Han, J. P., 2014. Structural Health Monitoring of Civil Infrastructure Using Optical Fiber Sensing Technology: A Comprehensive Review. The Scientific World Journal 2014: 1–11. doi:10.1155/2014/652329.

Yeh, Y., Cummins, H. Z., 1964. Localized Fluid Flow Measurements With an HeNe Laser Spectrometer. Applied Physics Letters 4, 10: 176–178. doi:10.1063/1.1753925.

Zenz, G., 2008. Long Term Behaviour of Dams – Earthquake Loading Design. In Yueming, Z., Ed., Proceedings of the 1st International Conference on Long Time Effects and Seepage Behavior of Dams, 1–13. Hohai University Press, Nanjing, China.

Zhang, L., Peng, M., Chang, D., Xu, Y., 2016a. Dam Failure Mechanisms and Risk Assessment. Wiley, Singapore, 476 p.

Zhang, L. M., Peng, M., Chang, D., Xu, Y., 2016b. Dam Failure Mechanisms and Risk Assessment. John Wiley & Sons Singapore Pte. Ltd.

Zhang, Z., Aktan, A. E., 1995. The Damage Indices for the Constructed Facilities. In Proceedings of SPIE - The International Society for Optical Engineering, 2460, 1520– 1529.

Zhou, L., Yan, G., Wang, L., Ou, J., 2013. Review of Benchmark Studies and Guidelines for Structural Health Monitoring. Advances in Structural Engineering 16, 7: 1187–1207. doi:10.1260/1369-4332.16.7.1187.

Zucca, S., Di Maio, D., Ewins, D. J., 2012. Measuring the Performance of Underplatform Dampers for Turbine Blades by Rotating Laser Doppler Vibrometer. Mechanical Systems and Signal Processing 32: 269–281. doi:10.1016/j.ymssp.2012.05.011.

Appendices / Priloge

9 APPENDIX 1: Brief report from measurements on Brežice Dam - ONLY REPRESENTATIVE CASES

Time series and frequency plots are displayed.

9.1 Simultaneous load rejection on Units 1 and 2

Units 1 and 2 are simultaneously off-loaded using mechanical brake (1 s phase). All units were in operation, after the brake, Unit 3 only sustained operation.

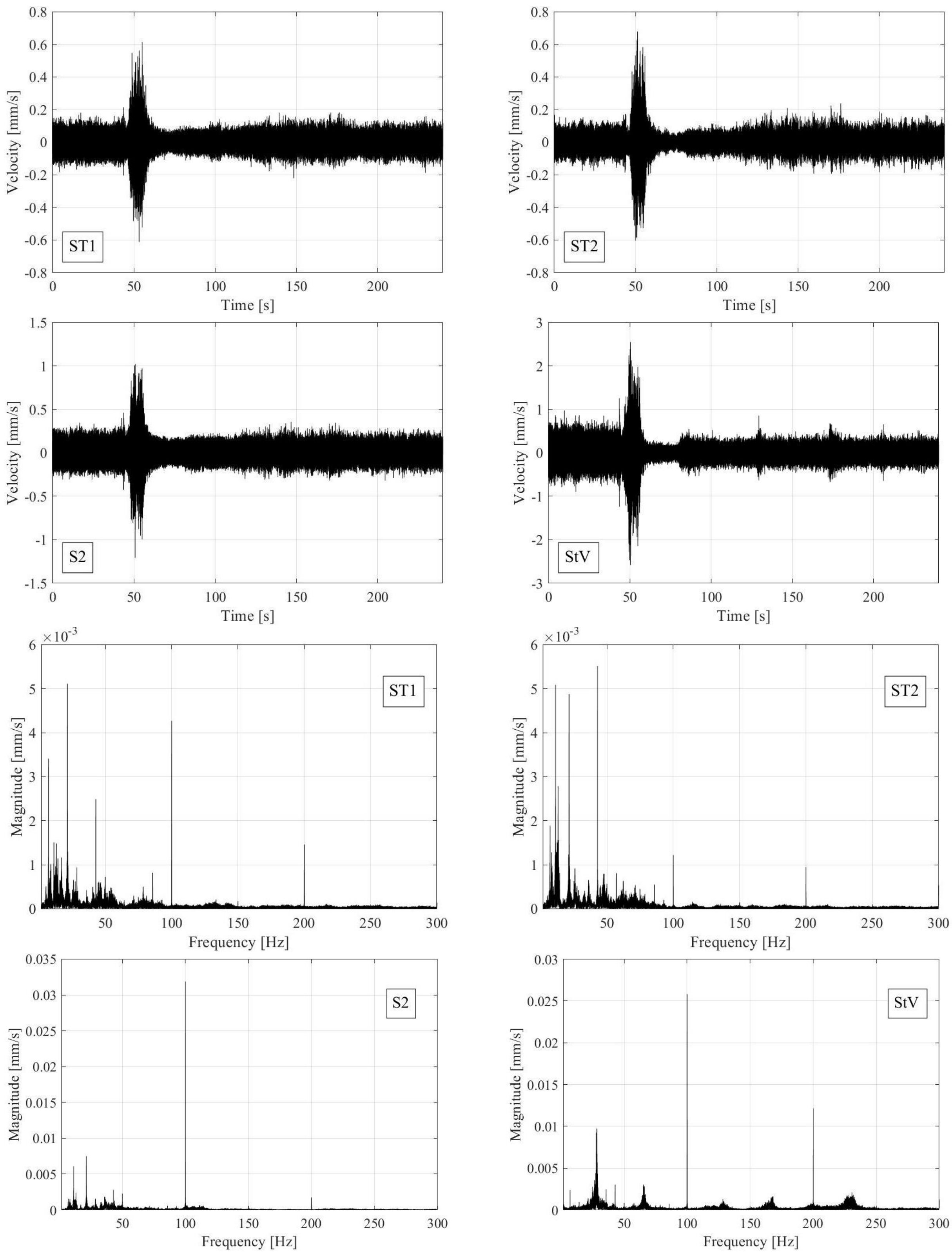

9.2 Simultaneous load rejection on Units 2 and 3

During the measurement the Units 2 and 3 are simultaneously off-loaded using mechanical brake. The brakes were deployed manually. Before the break, all 3 units were in operation, after the brake, Unit 1 sustains island operation.

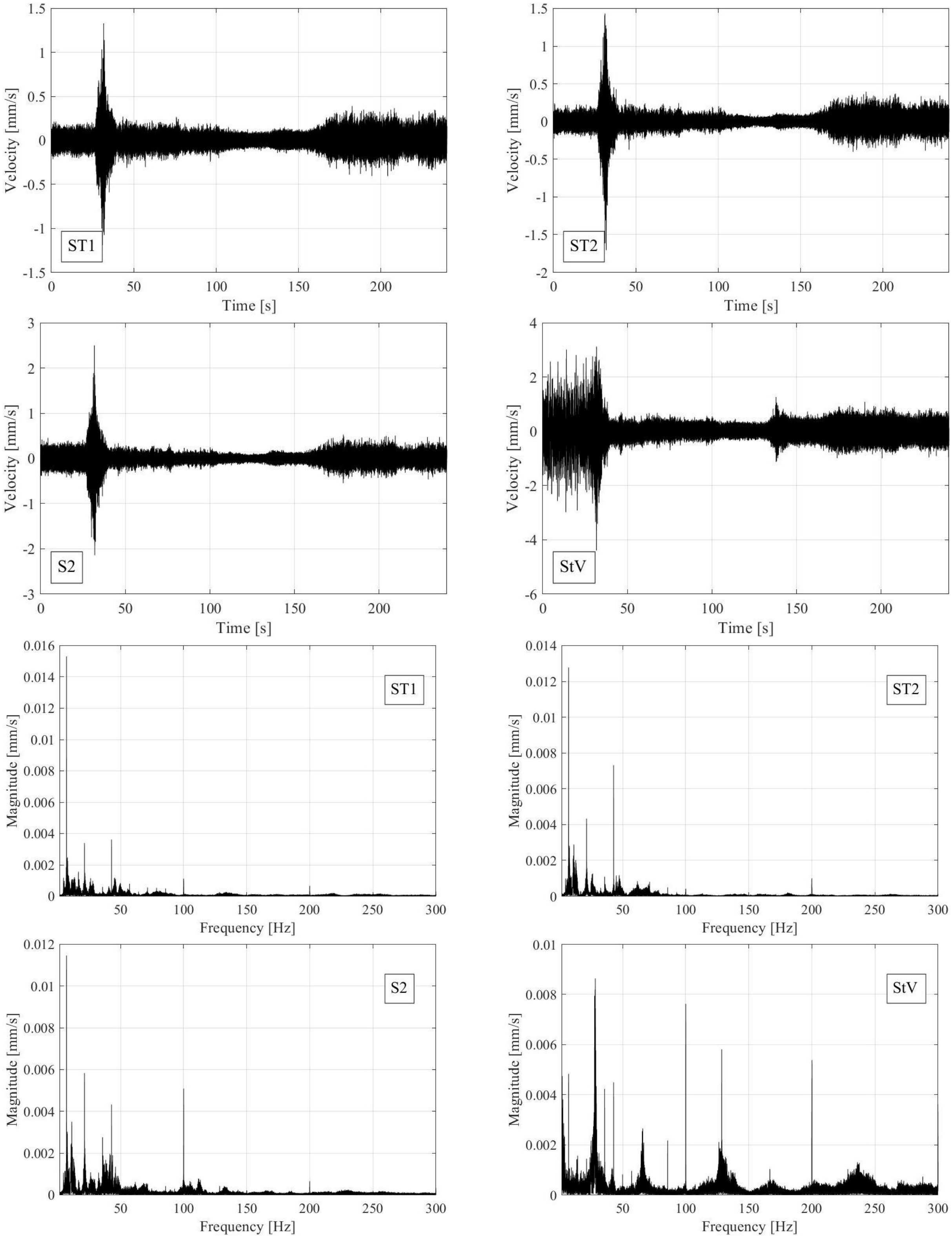

9.3 Electrical brake on Unit 1

Unit one was stopped using electrical brake, once it reached 10 MW of power, before the shut down the unit was not operating in a continuous mode but it was building power from 4–10 MW.

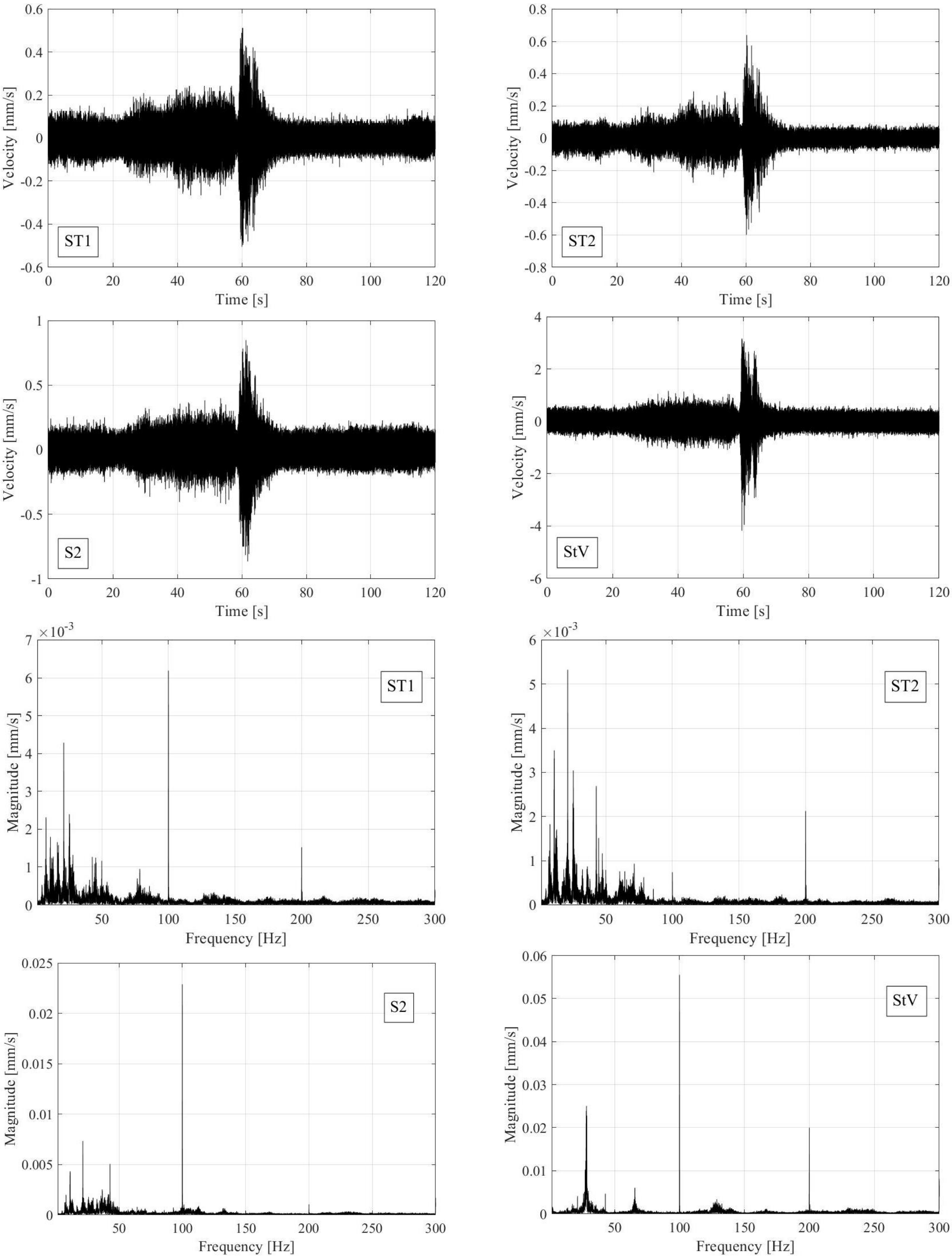

9.4 Mechanical brake on Unit 1

Operation of Units 1 and 2 (joint power of 23 MW) is interrupted with the mechanical brake on Unit 1.

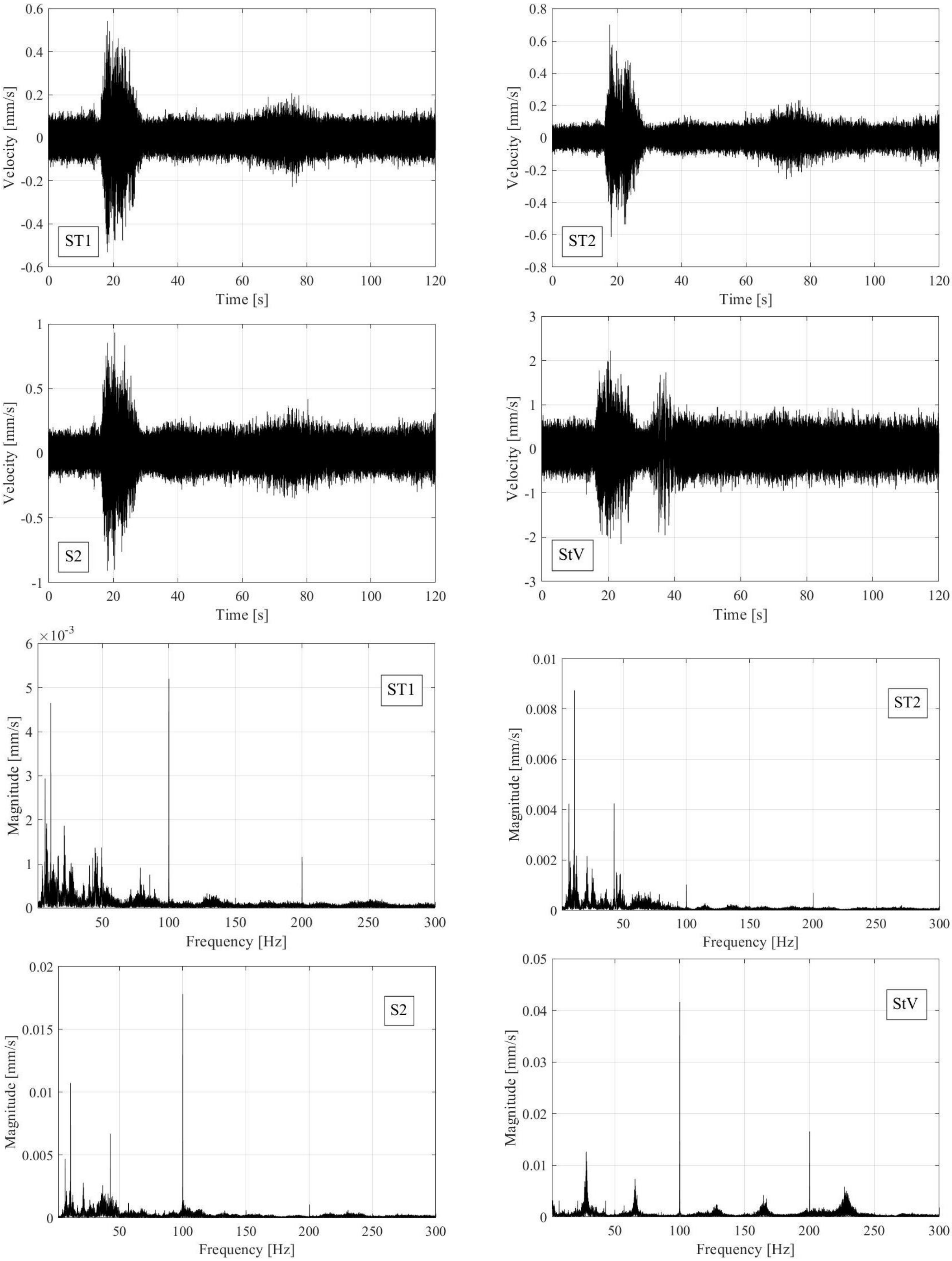

9.5 Start of Units 1 and 3

Unit 2 operates, after 40 s Unit 1 starts, and one minute later Unit 3 starts as well.

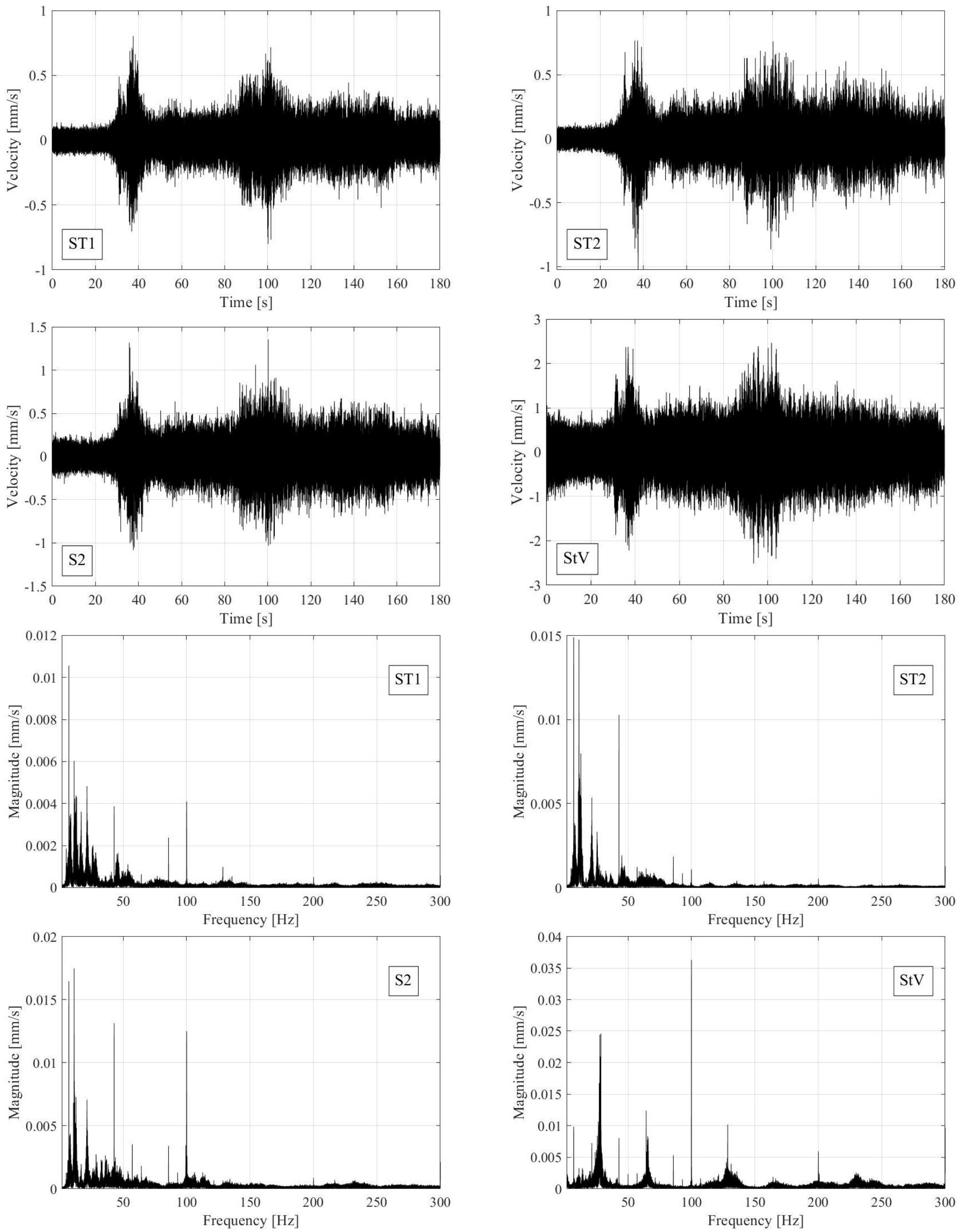

9.6 Regular stop of Unit 2

All units operate (joint power 20 MW), and then Unit 2 is stopped.

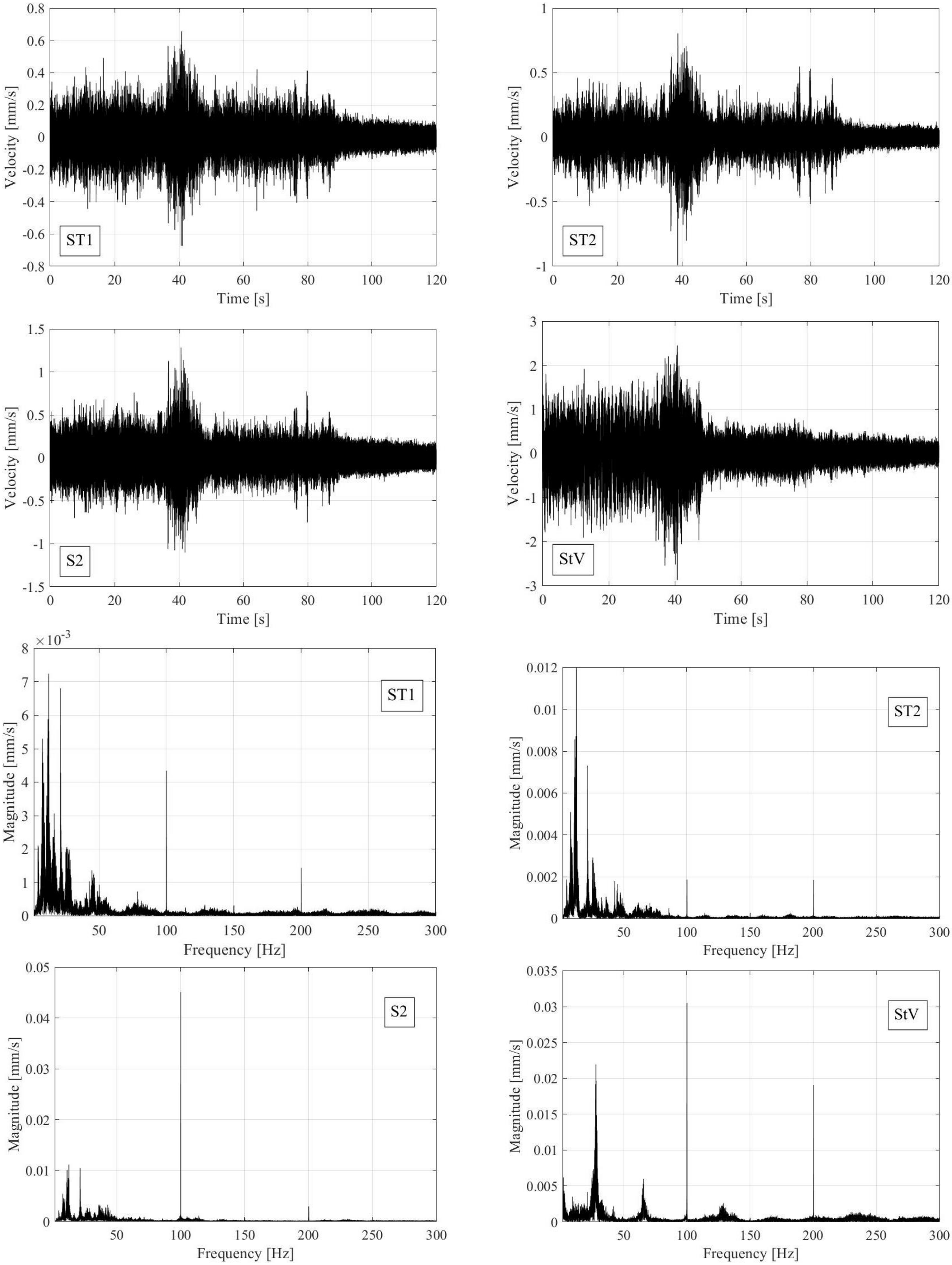

9.7 Start of Unit 2

Unit 2 starts, while Unit 3 already operates.

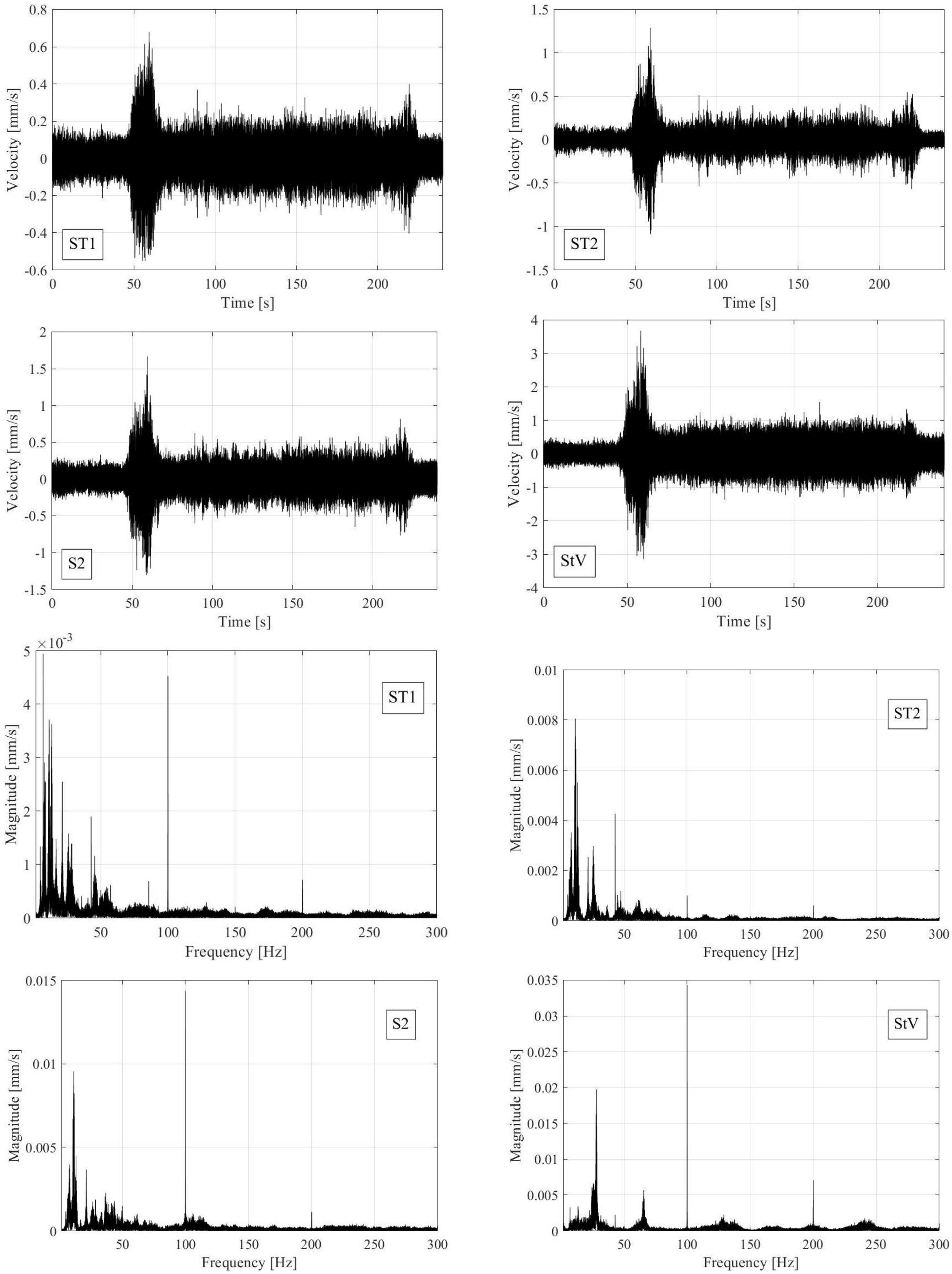

9.8 Mechanical break on Unit 3

Unit 3 is stopped using mechanical break from operation with 10 MW.

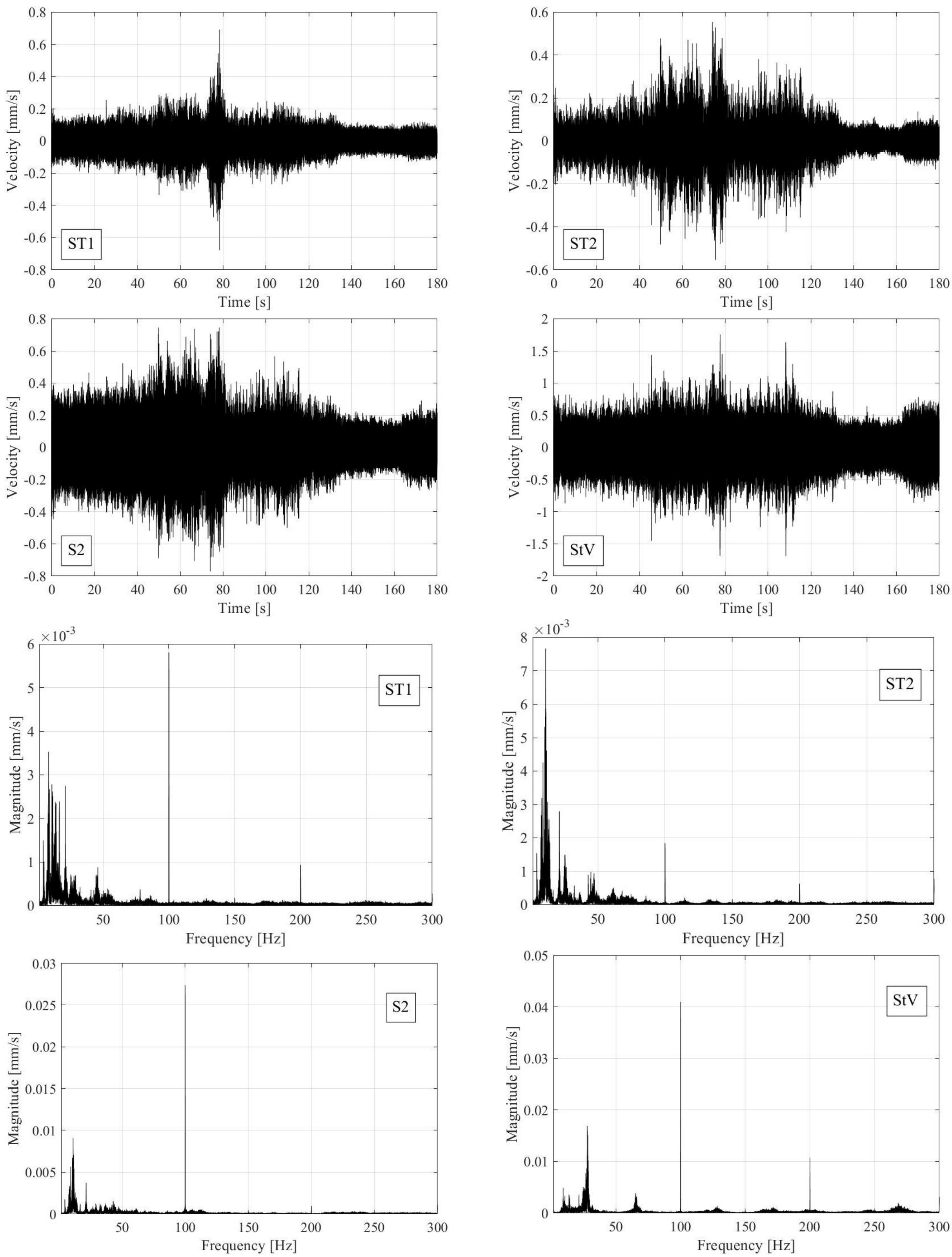

9.9 Start of Unit 3

Unit 3 starts, while Unit 2 already operates.